CONTEMPORARY NEUROLOGY SERIES

MOLECULAR PHYSIOLOGY AND METABOLISM OF THE NERVOUS SYSTEM

A CLINICAL PERSPECTIVE

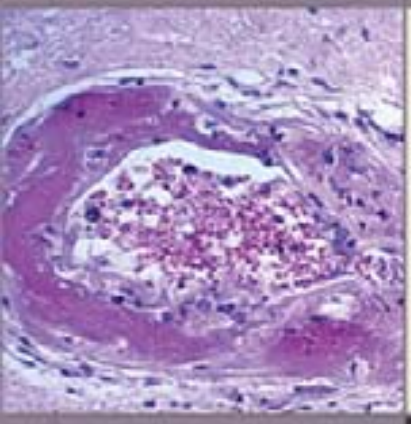

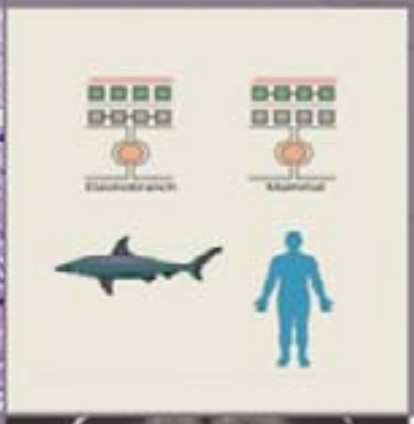

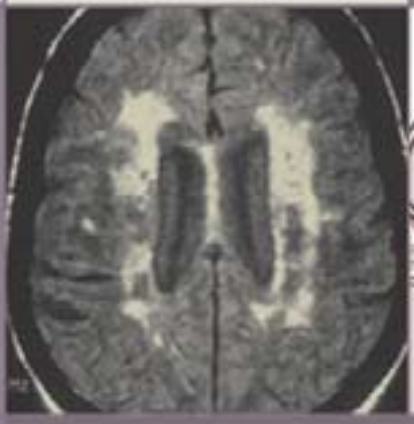

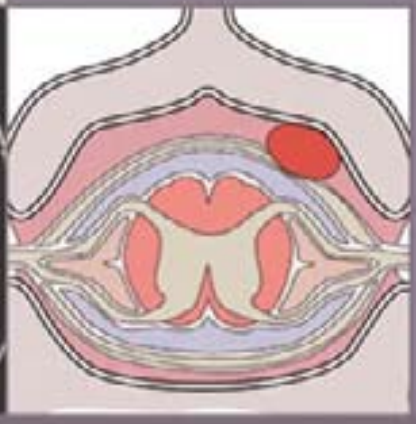

GARY A. ROSENBERG

OXFORD

MOLECULAR PHYSIOLOGY AND METABOLISM OF THE NERVOUS SYSTEM

SERIES EDITOR
Sid Gilman, MD, FRCP
William J. Herdman Distinguished University Professor of Neurology
University of Michigan

Contemporary Neurology Series

61 HIV NEUROLOGY
Bruce James Brew, MBBS, MD, FRACP

62 ISCHEMIC CEREBROVASCULAR DISEASE
Harold P. Adams, Jr., MD, Vladimir Hachinski, MD, and John W. Norris, MD

65 MIGRAINE: MANIFESTATIONS, PATHOGENESIS, AND MANAGEMENT, Second Edition
Robert A. Davidoff, MD

67 THE CLINICAL SCIENCE OF NEUROLOGIC REHABILITATION, Second Edition
Bruce H. Dobkin, MD

68 NEUROLOGY OF COGNITIVE AND BEHAVIORAL DISORDERS
Orrin Devinsky, MD and Mark D'Esposito, MD

69 PALLIATIVE CARE IN NEUROLOGY
Raymond Voltz, MD, James L. Bernat, MD, Gian Domenico Borasio, MD, DipPallMed, Ian Maddocks, MD, David Oliver, FRCGP, and Russell K. Portenoy, MD

70 THE NEUROLOGY OF EYE MOVEMENTS, Fourth Edition
R. John Leigh, MD, FRCP and David S. Zee, MD

71 PLUM AND POSNER'S DIAGNOSIS OF STUPOR AND COMA, Fourth Edition
Jerome B. Posner, MD, Clifford B. Saper, MD, PhD, Nicholas D. Schiff, MD, and Fred Plum, MD

72 PRINCIPLES OF DRUG THERAPY IN NEUROLOGY, Second Edition
Michael V. Johnston, MD and Robert A. Gross, MD, PhD, Editors

73 NEUROLOGIC COMPLICATIONS OF CANCER, Second Edition
Lisa M. DeAngelis, MD and Jerome B. Posner, MD

74 NEUROLOGIC COMPLICATIONS OF CRITICAL ILLNESS, Third Edition
Eelco F.M. Wijdicks, MD, PhD, FACP

75 CLINICAL NEUROPHYSIOLOGY, Third Edition
Jasper R. Daube, MD and Devon I Rubin, MD, Editors

76 PERIPHERAL NEUROPATHIES IN CLINICAL PRACTICE
Steven Herskovitz, MD, Stephen N. Scelsa, MD, and Herbert H. Schaumburg, MD

77 CLINICAL NEUROPHYSIOLIOGY OF THE VESTIBULAR SYSTEM, Fourth Edition
Robert W. Baloh, MD, FAAN and Kevin A. Kerber, MD

78 THE NEURONAL CEROID LIPOFUSCINOSES (BATTEN DISEASE), Second Edition
Sara E. Mole, PhD, Ruth D. Williams, MD, and Hans H Goebel, MD, Editors

79 PARANEOPLASTIC SYNDROMES
Robert B. Darnell, MD, PhD, and Jerome B. Posner, MD

80 JASPER'S BASIC MECHANISMS OF THE EPILEPSIES
Jeffrey L. Noebels, MD, PhD, Massimo Avoli, MD, PhD, Michael A. Rogawski, MD, PhD, Richard W. Olsen, PhD, and Antonio V. Delgado-Escueta, MD, Editors

81 MYASTHENIA GRAVIS AND MYASTEHNIC DISORDERS, Second Edition
Andrew G. Engel, MD, Editor

MOLECULAR PHYSIOLOGY AND METABOLISM OF THE NERVOUS SYSTEM

Gary A. Rosenberg, MD
Chairman of Neurology
Professor of Neurology, Neurosciences, Cell Biology and Physiology, and Mathematics and Statistics
University of New Mexico Health Sciences Center
Albuquerque, NM

OXFORD
UNIVERSITY PRESS

OXFORD
UNIVERSITY PRESS

Oxford University Press, Inc., publishes works that further
Oxford University's objective of excellence
in research, scholarship, and education.

Oxford New York

Auckland Cape Town Dar es Salaam Hong Kong Karachi
Kuala Lumpur Madrid Melbourne Mexico City Nairobi
New Delhi Shanghai Taipei Toronto

With offices in
Argentina Austria Brazil Chile Czech Republic France Greece
Guatemala Hungary Italy Japan Poland Portugal Singapore
South Korea Switzerland Thailand Turkey Ukraine Vietnam

Published by Oxford University Press, Inc.
198 Madison Avenue, New York, New York 10016
www.oup.com

Oxford is a registered trademark of Oxford University Press

Library of Congress Cataloging-in-Publication Data

Rosenberg, Gary A.
Molecular physiology and metabolism of the nervous system : a clinical perspective / Gary A. Rosenberg.
p. ; cm. — (Contemporary neurology series ; 82)
Includes bibliographical references and index.
ISBN 978-0-19–539427-6 (hardcover : alk. paper)
I. Title. II. Series: Contemporary neurology series ; 82. 0069–9446
[DNLM: 1. Cerebrospinal Fluid—physiology. 2. Blood-Brain Barrier—physiology.
3. Brain Diseases—physiopathology. 4. Cerebrospinal Fluid—metabolism. 5. Cerebrovascular
Circulation—physiology. W1 CO769N v. 82 2012 / WL 203]

612.8'042—dc23 2011044062

---

9 8 7 6 5 4 3 2 1
Printed in the United States of America
on acid-free paper

To Evelyn

This page intentionally left blank

Preface

The neurosciences and clinical neurology have undergone dramatic changes in the past 25 years brought about by major advances in molecular biology and neuroimaging. Clinical practice has remained grounded in ideas and concepts that were first enunciated decades ago, but the advances made in the laboratory are beginning to impact the clinician. In the 1970s, the invention of mathematical equations for tomography opened an era of neuroimaging using x-rays for computed tomography (CT), radionuclear isotopes for positron emission tomography (PET), and magnetic resonance for magnetic resonance imaging (MRI). This ability to visualize brain pathology prior to autopsy profoundly changed the practice of neurology. At around that same time, advances in molecular biology began to penetrate the neurosciences, and have now exploded with the elucidation of the human genome, gene chip technology, and, more recently, the findings of proteomics and metabolomics.

Clinicians and neuroscientists beginning to grapple with this profusion of information are faced with the need to learn older physiological concepts that are relevant to patient care. But knowing the physiology, which used to be sufficient, is no longer adequate. It must be combined with the molecular biology to form a new science of molecular physiology. To be successful in clinical care as well as in clinical or basic neurosciences, multiple concepts and techniques need to be mastered. No longer is it sufficient to be well versed only in one of the major branches of neuroscience, such as neuroanatomy, neurophysiology, neuropathology or neurochemistry; it is now necessary to combine and use them all at some point. To do this successfully, scientists and clinicians need to work as a team; each person in the collaboration brings a unique skill to the project. Each person on the team has a set of skills and a group of words that he or she understands best, but it remains mainly one person's work, and for that individual to lead the effort, an understanding of the others' areas of expertise is required. Learning to do that person's part of the project usually is possible, and having a common language is the key to true teamwork. This is true not only for the complex scientific project but even more so for the clinician, who on a daily, even hourly, basis is involved in a large team.

Working with residents and graduate students over the past years has taught me the importance of incorporating the newer molecular insights into the care of patients. While we now know the patterns of most neurological diseases from intensive work of neuroimagers, along with many of the genes involved, we remain far behind in developing treatments. The challenge we now face is to relate the imaging to the molecular studies and to understand the underlying physiological role of the specific molecules in the injury cascades. Once that knowledge is available, we will need to translate it into novel therapies.

Translational research attempts to accelerate the movement of information from the basic sciences to the clinic and to take the insights gained from caring for patients back to the laboratory for further study. Drug screening can be done with high-throughput systems; blood tests can identify arrays of genes; clinical trials can be done by large consortia; information learned on one continent can be quickly conveyed to another group far away by the Internet. This acceleration of information transfer has resulted in remarkable advances in treatment. For that to occur, a new type of investigator is needed, one who is equally comfortable working in the worlds of brain physiology and molecular neurochemistry. My goal in writing this book is to combine the important insights into brain physiology gained by early investigators with the new knowledge being obtained on genes and proteins in order to understand the impact of these substances in the living animal.

The goal of this book is explain the basic physiological concepts about the brain fluids, cerebral blood flow, and the blood-brain barrier and the quantitative approaches to their study. This is the topic of the first part of the book. The second part is more concerned with metabolic pathways and aspects of transport. Pathological aspects of the brain fluids and metabolism are introduced where

appropriate in both of these parts but are more extensively discussed in the final part on hypoxia, ischemia, brain edema, and inflammation. I have tried to emphasize the commonalities among the various aspects of fluid balance and metabolism in the different diseases.

The information in this book will aid students, trainees in neurology and neurosurgery and research neuroscientists in the understanding of the basic concepts of physiology and molecular biology that apply to clinical practice and translational medicine.

— G. A. R
Albuquerque, New Mexico 2011

Acknowledgments

Paul Akmajian skillfully made the original drawings in the book. Craig Panner of Oxford University Press and Sid Gilman of the Contemporary Neurology Series provided much appreciated assistance. The American Heart Association and the National Institute of Neurological Disorders and Stroke provided research support.

This page intentionally left blank

Contents

PART 1

Physiology of Brain Fluids and the Blood-Brain Barrier

This page intentionally left blank

Chapter 1

Anatomy of Fluid Interfaces that Protect the Microenvironment

HISTORICAL PERSPECTIVE

Brain fluid studies entered the modern era with the work begun at the beginning of the twentieth century by the physiologist Louis Weed and the neurosurgeon Harvey Cushing. They understood that the brain, lacking lymphatics, used the cerebrospinal and interstitial fluids (CSF and ISF) as lymph, calling this a *third circulation*[1] (Figure 1–1). At around the same time, there was growing awareness that the brain was sequestered from the systemic circulation. Ehrlich was the first to show this in 1885; he injected a blue dye into the blood, which stained all organs except the brain. In 1913, Goldmann observed that trypan blue dye injected into the CSF stained brain tissue. These two experiments were a dramatic demonstration that proved that the brain was isolated from the blood but that, once inside the skull, fluids had free access to brain parenchyma via CSF/ISF. This isolation became known as the *blood-brain barrier* (BBB).

Camillo Golgi discovered the method of silver staining. Cajal used this method to describe the close relationship between astrocytes and cerebral blood vessels in the human brain. Silver staining shows only a small population of astrocytes, which fortuitously provided a clearer picture of the connections between glial cells and blood vessels, showing that the astrocytic foot processes expanded as they contacted the cerebral vessels. This prescient observation lost favor for many years as the endothelium assumed the dominant role as the site of the BBB. Recent studies have revived the concept of a functional unit including vessels and astrocytes as the regulator of permeability. Golgi's illustrations were remarkably accurate considering the state of neuroanatomy at the beginning of the twentieth century (Figure 1–2). Comparison of a recent confocal micrograph of astrocytes attached to capillaries and one of Golgi's hand-drawn figures demonstrates this accuracy.[2]

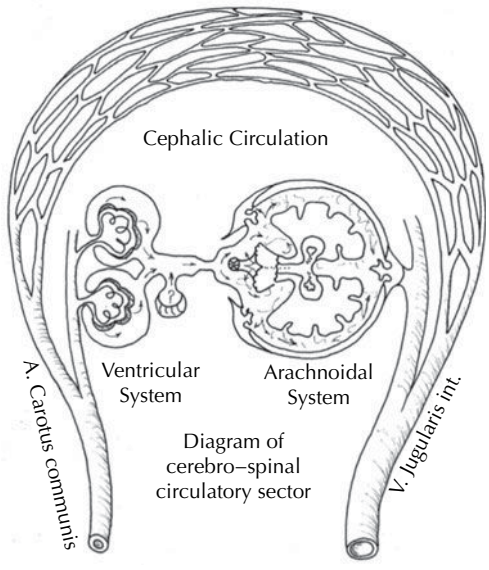

Figure 1–1. Drawing of the third circulation. Blood and lymph are the first and second circulations. Fluid leaving the capillaries and the choroid plexuses moves into the brain's extracellular space and the cerebral ventricles. Removal of CSF and ISF is across the arachnoid granulations. (From Ref. 1.)

CEREBRAL MICROENVIRONMENT

Normal cellular function depends on the microenvironment created around brain cells by the ISF, which is contiguous with CSF (Figure 1–3). Cerebrospinal fluid fills the cerebral ventricles, the subarachnoid space over the brain, and the fluid spaces around spinal cord and pools in the lumbar sac below the ending of the cord at L1-L2. Cerebral ventricles contain about 20 mL, with the remainder of the 140 mL over the brain, around the spinal cord, and in the lumbar sac, where it can be removed by lumbar puncture. Several important neurological illnesses require examination of the CSF for diagnosis. Infection, Guillain-Barré syndrome, central nervous system vasculitis, idiopathic intracranial hypertension, multiple sclerosis, and, more recently, Alzheimer's disease are examples of diseases in which the CSF is an important diagnostic aid (Table 1–1). An imaging study should be performed prior to lumbar puncture to rule out a mass lesion or obstructive hydrocephalus. Occasionally, in critically ill patients suspected of having meningitis or when imaging is difficult, lumbar puncture can be done after careful examination of the fundi to rule out papilledema and close observation after the test to assess for possible herniation. Examination of the CSF should always be considered in the diagnostic workup when infection, subarachnoid hemorrhage or idiopathic increased intracranial pressure is suspected because it is cost-effective and ultimately can contain costs by reducing the need for more expensive tests.

Cerebrospinal fluid and ISF are separated by the ependyma in the ventricles and by the pia in the subarachnoid space. Substances in the CSF can enter the brain across these cell layers because they have gap junctions rather than tight junctions. Continuity of the CSF and ISF means that substances that would be excluded from the brain after injection into the blood can be injected intrathecally where they can access brain cells. Drainage of metabolic products from the brain into the CSF via the ISF provides a lymph-like function, which solves the problem created when the brain tissues were isolated from the body during evolution. Fluids of the third circulation are formed at the cerebral endothelial cells and the ependymal cells of the choroid plexus. At both sites, adenosine triphosphatase (ATPase) pumps provide the energy to create the osmotic gradients that pull water into brain extracellular space and cerebral ventricles. Newly formed ISF from the capillaries and CSF from the choroid plexuses join together in the ventricles before draining back into the blood.

Proteins in the blood circulate into tissues through fenestrations in systemic capillaries. Acting as passive sieves, pores in the capillaries permit these large molecules to move into the tissue to be drained back to the blood by the lymphatic vessels. This essential lymphatic function prevents protein accumulation in the tissues, which would create oncotic pressure, resulting in edema.

By contrast, cerebral vessels restrict transport between the blood and the brain of most substances except lipophilic molecules. Specialized proteins that self-assemble to form tight junctions fill the clefts between cerebral capillaries. Tight junction proteins restrict the movement of charged or large protein molecules. Another unique feature of the brain capillary is the requirement for an energy source to power sodium-potassium ATPase exchange pumps, which maintain a constant flow of ISF

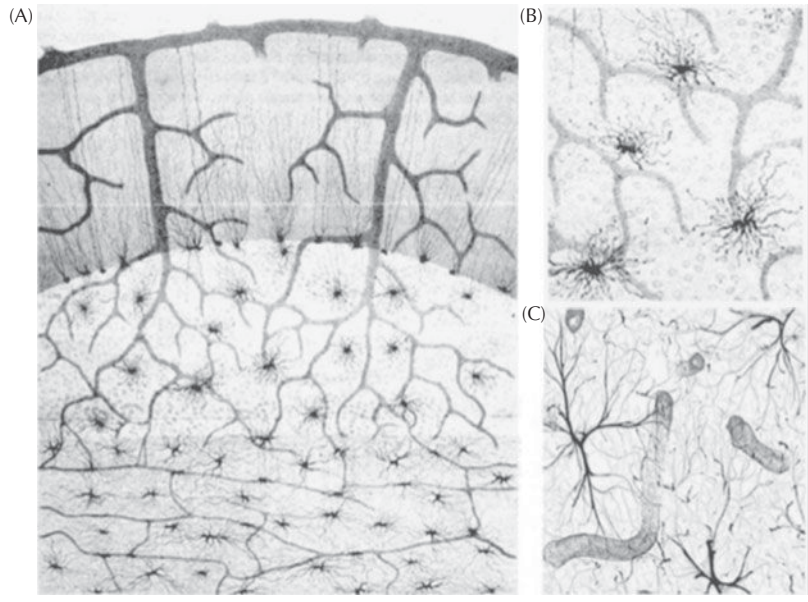

Figure 1–2. Camillo Golgi (1843–1926) described the close relationship between astrocytes and cerebral blood vessels in the human cerebellum as follows: "the connection between glia and vessels is either direct, the cell bodies being applied on the vessel walls, of which they seem to be part of, or occurs through protrusions more or less pronounced, which exhibit a small expansion at the point of contact." (**A**) Drawing from table XII of Golgi's book. (**B**) Enlargement of (**A**) showing the relationships between astrocytes and blood vessels. (**C**) Confocal image in which astrocytes were double-labeled with aquaporin 4 and glial fibrillary acidic protein (GFAP). The similarities between Golgi's drawing and the confocal image obtained more than a century later are striking. (From Ref. 2.)

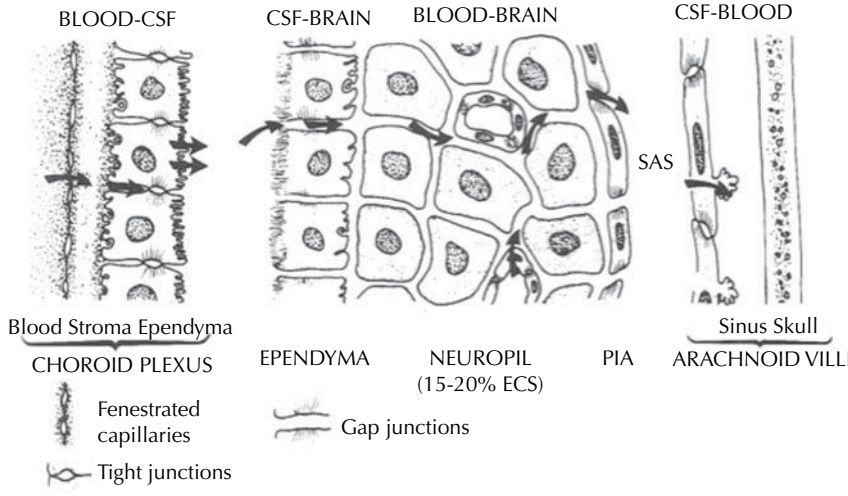

Figure 1–3. Illustration of the third circulation with the regions of tight and gap junctions. In the choroid plexus, substances in the blood leave fenestrated capillaries to enter the stroma beneath the ependyma, where apical tight junctions prevent them from entering the CSF. Once in the CSF, molecules can pass through the gap junctions of the nonchoroid plexus ependyma. Extracellular space makes up 15% to 20% of the brain, and ISF delivers substances to the cells in the neuropil. Interstitial fluid leaves the neuropil to enter the subarachnoid space before returning to the blood across the arachnoid villa. The arachnoid has tight junctions. Within the brain, the capillaries also have tight junctions.

Table 1–1 **Cerebrospinal Fluid Examinations Essential in the Diagnosis of Several Neurological Disorders**

CSF test for central nervous system infection
Cellular and protein content of CSF are helpful in distinguishing the various types of meningitis
Protein elevation without cells is diagnostic of Guillain-Barré syndrome
CSF pressure is diagnostic test for idiopathic intracranial hypertension
Large number of cells in central nervous system vasculitis, which can separate it from multiple sclerosis
Demyelinating profile in multiple sclerosis diagnosis (myelin basic protein, oligoclonal bands, IgG synthesis)

that leaves the capillaries along osmotic gradients created by ion pumps on the abluminal surface. Similar mechanisms of fluid formation are found at the choroid plexus.

Water can readily cross membranes, which is anomalous behavior that was poorly understood until the recent discovery of a family of pore-forming molecules called *aquaporins*. These molecules form channels through which water molecules move passively along pressure and osmotic gradients.[3] Astrocytic endfeet are rich in aquaporin molecules, and when edema fluid forms from movement of water out of the capillaries into the extracellular space, the astrocytic endfeet swell. The flow of ISF that is formed by capillaries occurs through the extracellular spaces by either passive diffusion or bulk flow. White matter tracts permit the unidirectional movement of ISF, while gray matter has random flow through a dense neuropil.

Table 1–2 **Circulation of Brain Fluids Controlled by Types of Junctions Between Cells**

Blood and lymph form the first and second circulations
CSF and ISF form the third circulation
CSF and ISF are formed at the choroid plexuses and cerebral capillaries
CSF and ISF are contiguous across ependymal and pial surfaces
Drainage back into the blood occurs at arachnoid granulations

Fluid formed by brain capillaries and choroid plexus flows through interstitial spaces, delivering nutrients and removing waste, eventually draining into the ventricles for removal over the convexities via the arachnoid granulations in the superior sagittal sinus and down along the spinal cord, where arachnoid granulations located in the nerve root sleeves perform a similar function (Table 1–2).

DEVELOPMENT OF THE BRAIN-FLUID INTERFACES

Neural Tube, Ependymal Cells, and Stem Cells

The nervous system develops from a region in the middorsal line of the embryo. A thickened plate of ectoderm folds in to form the neural groove, which, once closed, becomes the neural tube (Figure 1–4). The cephalic part begins to dilate to form the brain and the ventricular system, while the caudal segment that will be the spinal cord maintains a uniform diameter. An internal limiting membrane on the inner surface forms next to the cells that will become the ependyma. At the outer surface is mesenchyma that is separated from the ectoderm by an external limiting membrane. Germinal cells are found between the inner and outer membranes. The mantle layer becomes the gray matter, composed of glia and neurons, and the marginal layer becomes white matter. Ciliated epithelial cells line the neural tube, and cilia persist in some regions of the adult human ependyma.

The neural tube is formed from neuroepithelial cells that extend from the internal to the external limiting membranes.[4] Nuclei synthesizing DNA are found near the external limiting membrane and migrate toward the inner limiting membrane. Once DNA synthesis is complete, these cells become the neuroblasts that form the mantle layer. When neuroblasts mature into the neuronal cells of the adult, they lose their ability to divide. Neurons establish synapses with specific nuclear groups, probably on the basis of chemical affinities (Figure 1–5). After neuroblast differentiation has ceased, future glial cells are formed from neuroepithelial cells that have differentiated with glioblasts. Ependymal cells are formed along

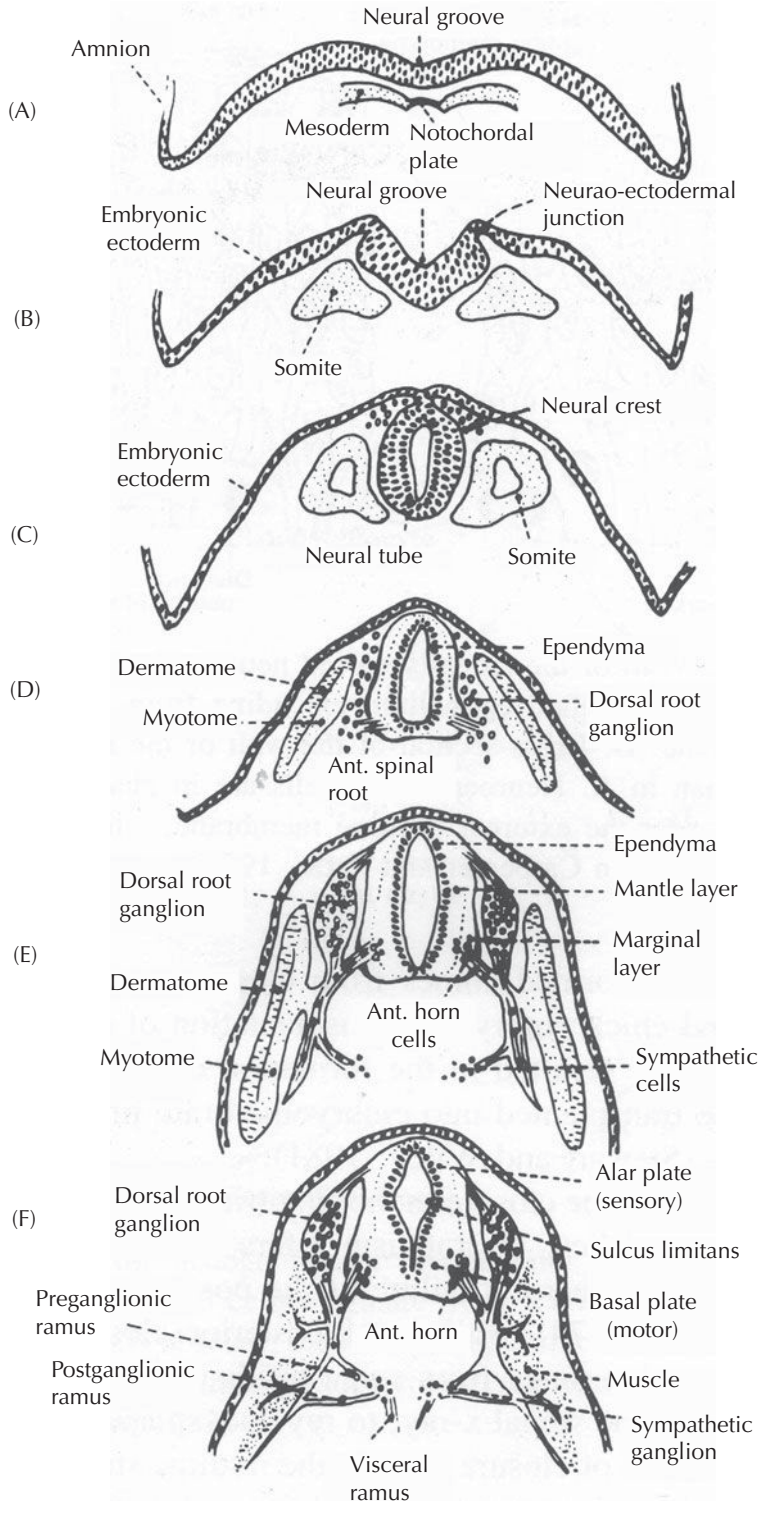

Figure 1–4. Stages in the development of the neural tube from the neural plate with subsequent formation of the spinal cord. (From Ref. 29.)

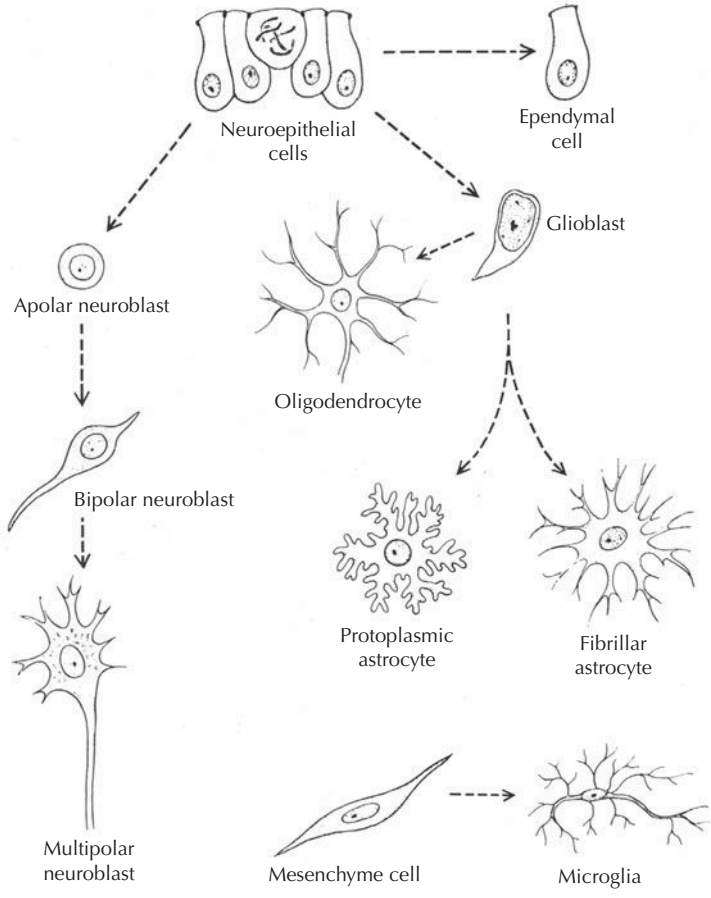

Figure 1–5. Diagram of the histogenesis of neurons and neuroglial cells. Neuroblasts, glioblasts, and ependymal cells originate from neuroepithelial cells. The origin of the oligodendrocyte is obscure, but both protoplasmic and fibrillary astrocytes are derived from glioblasts. The microglia are considered to arise from mesenchyme. (From Ref. 30.).

with glioblasts. Ependymal and subependymal cells form a separate unit loosely attached to the outer limiting membrane.

Cells in the subependymal zone of the lateral wall of the lateral ventricles continue to divide throughout life and proliferate after an injury to participate in the repair process. Stem cells differentiate into a wide variety of cells but mainly form glial cell types including astrocytes and oligodendroglial cells.[5] The hippocampus is another region that has plasticity based on stem cells. The discovery that there is continued growth of brain cells in adults was made by studies of patients dying of terminal cancer who had been injected with a molecule incorporated into dividing cells prior to death; their brains were studied after death. Human brain tissue was obtained postmortem from patients who had been treated with the thymidine analog bromodeoxyuridine (BrdU), which labels DNA during the S phase. Using immunofluorescent labeling for BrdU and for one of the neuronal antigens, that is, a marker for mature neurons—NeuN (neuronal nuclei), calbindin, or neuron specific enolase—the researchers demonstrated that new neurons, as defined by these markers, are generated from dividing progenitor cells in the dentate gyrus of adult humans, showing that human hippocampus retains its ability to generate neurons throughout life.[6] The field of stem cell biology has grown dramatically since this seminal observation.[7,8]

Cilated Ependymal Cells and CSF Movement

Ependymal cells that line the walls of the ventricular system in the adult brain are ciliated epithelial cells. These polarized epithelial cells are

thought to propel CSF through the ventricles by the action of the cilia. Early in neurodevelopment, the embryonic ventricles are lined by a germinal epithelium. This embryonic neuroepithelium has planar polarity that drives morphogenetic movements essential for neural tube closure. Radial glial cells contain both spatial and temporal patterning that determines the fate and position of the cells in the developing brain, and a subpopulation of radial glia transform into ependymal cells.[9] Ependymal cells extend multiple motile cilia from their apical surface into the ventricles. Planar-polarized beating of these cilia generates directed CSF flow and helps maintain CSF homeostasis. Ependymal-generated CSF flow establishes gradients of chemorepellents that guide the migration of young neurons in the adult mammalian subventricular zone.[10] Radial glia in the embryo have a translational polarity that predicts the orientation of mature ependymal cells, which suggests that ependymal planar cell polarity is a multistep process initially organized by primary cilia in radial glia and then refined by motile cilia in ependymal cells.[11]

Choroid Plexuses, Arachnoid, and Capillaries

The choroid plexuses are formed in specialized regions where underlying blood vessels grow and push out the ependyma (Figure 1–6). Blood vessels in the choroid plexus lack tight junctions, allowing substances from the blood to pass through the vessels' pores, as in the systemic circulation. Ependymal cells provide the barrier, and the tight junctions have shifted to the apical surface of the ependymal cells that line the choroid plexus. For reasons that are unclear, there is a sharp demarcation between the type of ependymal cell that lines the ventricles and those that form the choroid plexuses.

Mesenchyme outside the outer limiting membrane condenses to become the outer covering layers of the brain, namely, periosteum, dura, and arachnoid. Fine trabeculi join the arachnoid to the pia, and CSF fills the space between the two membranes. The dura thickens into a tough connective tissue, and the space between the dura and arachnoid is absent except in pathological situations, such as a subdural hematoma or empyema.

The mechanisms involved in the expansion of the ventricles are poorly understood. It is suggested that the large amount of protein, albumin, in the fluid in the ventricles of the newborn, which is formed by the choroid plexus, may in fact participate in the expansion of the ventricles by creating high oncotic pressure inside the ventricles of the newborn.[12]

Development of the cerebral capillaries depends on trophic factors secreted by brain tissue. Proof that the brain has trophic factors that determine the type of vessel formed comes

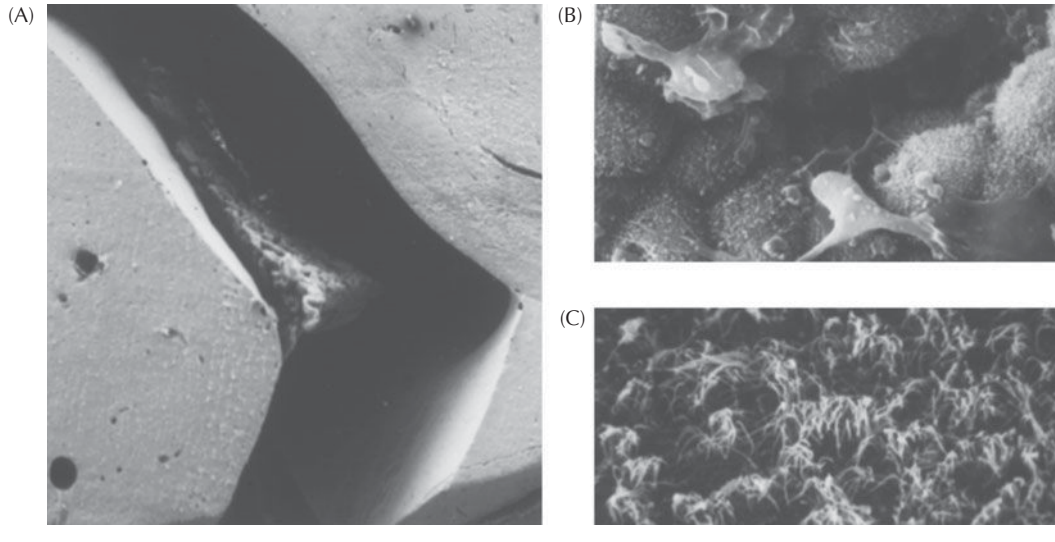

Figure 1–6. (**A**) Scanning electron micrograph of the ventricular system of the adult cat. (**B**) Choroid plexus with microvilla. (**C**) Third ventricle with cilia. (Courtesy of Dr. Linda Saland.)

from elegant transplant experiments between quail and chick embryos. Transplantation of quail brain into embryonic chick cultures resulted in the formation of systemic vessels, while nonbrain tissue transplanted into embryonic brain produced capillaries with tight junctions.[13]

Failure of neural tube closure in the first trimester of embryonic life results in congenital anomalies. *Dysraphism* refers to a group of congenital malformations in which the posterior part of the neural tube fails to close.[14,15] Failure of posterior closure produces developmental disorders that range from spina bifida occulta, an incidental finding discovered on routine spinal x-ray, to myelodysplasia, a severe deformation that involves failure of closure of both the midline structures in the posterior fossa of the brain and the central canal of the spinal cord and can lead to death. Commonly encountered dysraphic syndromes include absence of cerebral hemisphere development (anencephaly), failure of vertebrae and skull to close (spina bifida and cranium bifidum), and the combined spinal and nervous tissue abnormalities of the Chiari malformations. In Chiari type I malformation there is a protrusion of an elongated cerebellar tonsil into the foramen magnum. When these patients begin to have symptoms, usually in adult life, they have signs of lower brainstem dysfunction. Patients with type II Chiari malformation have meningomyelocele; hydrocephalus is often present at birth or becomes manifest when the spinal defect is repaired. Chiari type III and type IV are more extensive malformations of the cerebellum and brainstem, which are generally incompatible with life (Table 1–3).

EXTRACELLULAR SPACE AND EXTRACELLULAR MATRIX

Physiological studies demonstrated the presence of a significant extracellular space that is necessary for flow of the CSF/ISF through brain tissue. Rall and colleagues performed ventriculocisternal perfusions with an inert substance, inulin, that remained in the extracellular space. By sampling tissues surrounding the ventricles, they found an extracellular space of 15% to 20%, which was consistent with a third circulation.[16] In other organs, the cells are embedded in a connective tissue matrix that contains collagen fibers. However, the extracellular matrix of the brain has very little collagen, and the neurons are embedded in a matrix of extracellular matrix molecules with glial cells. Better definition of the glial cell membranes has shown the presence of a space that contains complex carbohydrates, such as the glycosaminoglycans, heparin sulfate, chondroitin sulfate, dermatan sulfate, and hyaluronic acid.[17]

Extracellular matrix can inhibit neural cell migration. Schwann cell migration is integrin-dependent and is inhibited by astrocyte-produced aggrecan. Transplantation of Schwann cells is suggested as a potential treatment for spinal cord injury. However, following

Table 1-3 **Common Dysraphic Syndromes Involving Developmental Malformations of the Cerebellum, Fourth Ventricle, and Posterior Fossa**

Posterior Fossa Malformations	Anatomical Features	Clinical Features
Chiari Type I	Protrusion of an elongated cerebellar tonsil into the foramen magnum	Symptoms usually begin in adult life with signs of lower brainstem dysfunction
Chiari Type II	Meningomyelocele	Hydrocephalus is often present at birth or becomes manifest when the spinal defect is repaired
Chiari Types III and IV	Extensive malformations of the cerebellum and brainstem	Generally incompatible with life
Dandy-Walker Syndrome	Agenesis of the cerebellar vermis, cystic dilatation of the fourth ventricle, and enlargement of the posterior fossa	Hydrocephalus and other anomalies of the brain

transplantation Schwann cells show limited migratory ability, and they are unable to intermingle with the host astrocytes. Aggrecan produced by astrocytes is involved in the inhibition of Schwann cell motility on astrocytic monolayers. Knockdown of this proteoglycan in astrocytes using interfering RNA (RNAi) that blocks the action of the normal RNA molecules or digestion of glycosaminglycan chains on aggrecan improves Schwann cell migration. Aggrecan acts by disrupting integrins on Schwann cells.[18]

Injury to the adult central nervous system increases the levels of extracellular matrix molecules, which inhibit repair of injured axons. Chondroitin sulfate chains on proteoglycans and enzymes necessary for their synthesis are expressed after an injury. Microglial cells at the injury sites express both keratan sulfate and chondroitin sulfate. Transforming growth factor-β (TGF-β) induces the expression of the enzymes involved in the synthesis of keratan sulfate and chondroitin sulfate as well as the expression of the chondroitin/keratan sulfate proteoglycan aggrecan. Transforming growth factor-β induces basic fibroblast growth factor (bFGF) expression in microglia, and bFGF induces TGF-β expression in astrocytes. Thus, the biosynthesis of keratan sulfate and chondroitin sulfate is upregulated in common by TGF-β in microglia.[19]

Success of the stem cell transplantation procedures depends to a large extent on the ability of the transplanted cells to disrupt the extracellular matrix and move toward the site of injury. Under normal conditions, movement of cells within the extracellular matrix is difficult, but when injury is present and there is secretion of extracellular molecules by the reactive astrocytes and microglia, the task becomes almost impossible. Altering the conditions of the extracellular matrix by enzymes, such as hyaluronidase and chondroitinase, facilitates cellular mobility.

BRAIN-FLUID INTERFACES

Anatomy of the Cerebral Blood Vessels

Specialized cell-to-cell junctions occur at each of the sites of contact between brain fluids. Tight junctions are present at the major interface of the endothelial cells, as well as at the interface of the choroid plexus and the arachnoid (Table 1–4). At the ependymal and pial cells, gap junctions separate the CSF and ISF.

Table 1-4 **Types of Cell Junctions at Major Sites of Brain Interfaces**

Tight Junctions
Choroid plexus ependymal cells (apex)
Arachnoid
Cerebral endothelial cells
Gap Junctions
Ependymal cells
Pia cells

Blood vessels have evolved to internalize the delivery of nutrients to cells. In single and simple multicell organisms the cell surface was adequate, but as the complexity increased, another solution was needed. A system of tubes formed inside the organs that need the nutrients and a fluid to carry them gradually evolved. The process of blood vessel formation, which is called *vasculogenesis* for new vessel formation and *angiogenesis* for sprouting from existing vessels, is critical for normal development and for repair of tissues after an injury. The end result of these processes is a densely packed network of arteries, arterioles, capillaries, venules, and veins.

Observations of the vessels on the brain's surface suggested that there were anastomoses between the arteries and the veins. Ernst Scharrer made the important observation that arteries rarely form anastomoses with veins and that the arteries are more numerous than the veins.[20] Arteries enter the brain separately from the surfaces, giving off branches in the layers of the cortex, joining the draining veins through a network of capillaries. This was a seminal observation based on a relatively simple technique that reversed decades of erroneous observations. The finding that cerebral arteries end in capillaries without anastomoses eliminated the confusion about the vulnerability of the brain to ischemia since it was now clear that the brain had end arteries with poor collateralizations. These early observations have been confirmed with studies that utilize colored plastics to show arteries (red plastic) and veins (blue plastic). Plastic casts of the blood vessels revealed dense networks of vessels that were necessary to ensure adequate perfusion of the entire brain (Figure 1–7). Elegant images of

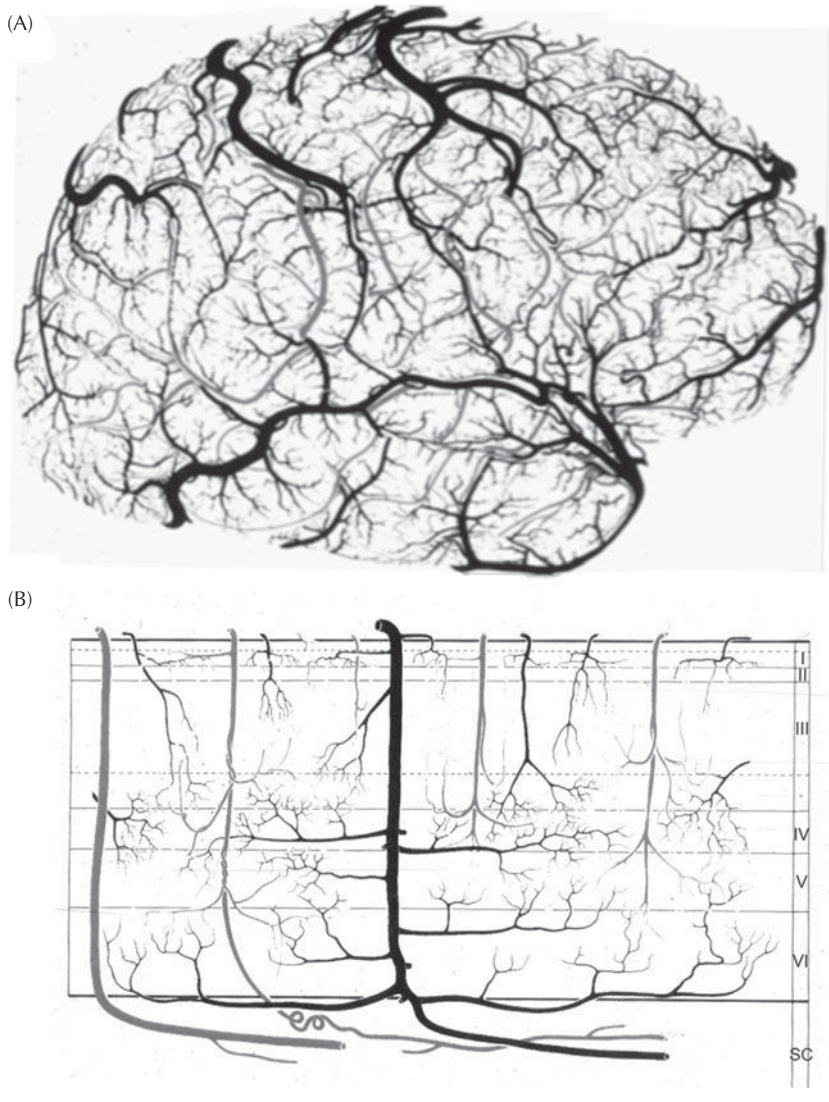

Figure 1–7. Blood vessels in the human brain. (**A**) Brain vasculature on the surface of the brain. Red plastic fills the arteries and blue plastic fills the veins. There are no anastomoses of the arteries and the veins since the arteries are end arteries. (**B**) This schematic drawing demonstrates that the arteries pass from the surface to the deep white matter, traversing the six layers of the cortex. Arterioles give off branches as the arteries pass through the cortex. The capillaries that join the arterioles and the veins are not seen. (From Ref. 31; See also the color insert.)

the surfaces of the brain confirmed the relationships of the arteries to the veins shown earlier, with the added benefit of indicating the extensive branching of the arteries in the layers of the cortex. Layers of the cortex with large neurons received the greatest number of arterial branches, as would be expected due to their greater metabolic need.

As a consequence of the poor collateralization and the flow of blood from the cortex to deeper structures, the deep white matter, which is at the end of the arterial supply, is vulnerable to either changes in blood flow or oxygenation of the blood. Patients with hypoxic/ischemic injury due to loss of cerebral blood flow often have damage to the white matter with death of the oligodendrocytes. Deep white matter is a frequent site for hypoxic/ischemic damage in the newborn.

Increased cerebral blood flow to the inner layers of the cortex can be seen with functional

magnetic resonance imaging, which shows the subtle changes in blood oxygenation related to metabolic activity. When a region in the cortex is activated, a fall in the oxygenation of the blood vessels produces a change in the nuclear magnetic resonance signal that can be visualized when very fast scans are made.

Endothelial cells line the cerebral blood vessels. Except in a few specialized regions, these vessels are joined together by self-assembling proteins that form the tight junctions. Around the vessels is a basal lamina with pericytes. Astrocytic endfeet surround the capillaries. Close by, but separate from the vessels, are the neurons and microglia (Figure 1–8).

Brain Cell Interfaces with CSF at Ependyma and Pia

A heterogeneous layer of epithelial cells lines the ventricular surface and choroid plexuses. Over the choroid plexuses the epithelial cells are cuboidal in shape and have microvilli on the apical surface next to the CSF; the microvilli are short protrusions from the surface of the cells that increase the surface area. Choroid plexus epithelial cells have nuclei in the basal region, a large number of mitochondria in the cytoplasm, and a high energy requirement. Tight junctions join their apical surfaces. These cells have features in common with those in the kidney that are also involved in active transport.[21]

Cerebrospinal fluid has two major sources: the choroid plexuses in the ventricles and the cerebral capillaries. Choroid plexuses are outpocketings that contain fenestrated blood vessels, a stroma, and a layer of epithelial cells that have tight junctions and actively secrete CSF (Figure 1–9). The ependymal cells of the choroid plexus have microvilla but lack cilia. Cerebrospinal fluid absorption occurs at the arachnoid through arachnoid granulations in the sagittal sinus. The arachnoid is one of the tight junction sites except in the region of the arachnoid granulations where CSF absorption takes place across one-way valve structures. The collapsing of the one-way valves when blood pressure increases prevents the backflow of red blood cells into the CSF.

In the region of the floor of the third ventricle, called the *median eminence* or *infundibulum*, specialized cells called *tanycytes* connect the hypothalamic nuclei with the ventricular surface. On electron micrographs these tanycytes appear to extend to the surface of the ependyma. The ventricular surface of the

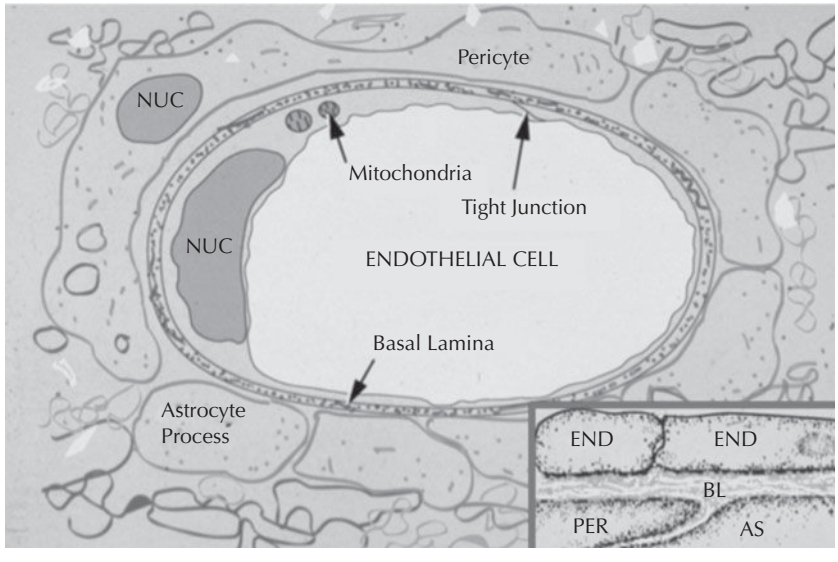

Figure 1–8. Schematic from electron micrograph of an endothelial cell. Note the large number of mitochondria, the tight junctions, and the surrounding basal lamina and astrocyte foot processes. Nucleus (NUC), Inset: higher magnification of two endothelial cells (END) with a basal lamina (BL) containing an embedded pericyte (PER) and an adjacent astrocyte foot process (AS). (Adapted from Ref. 32.)

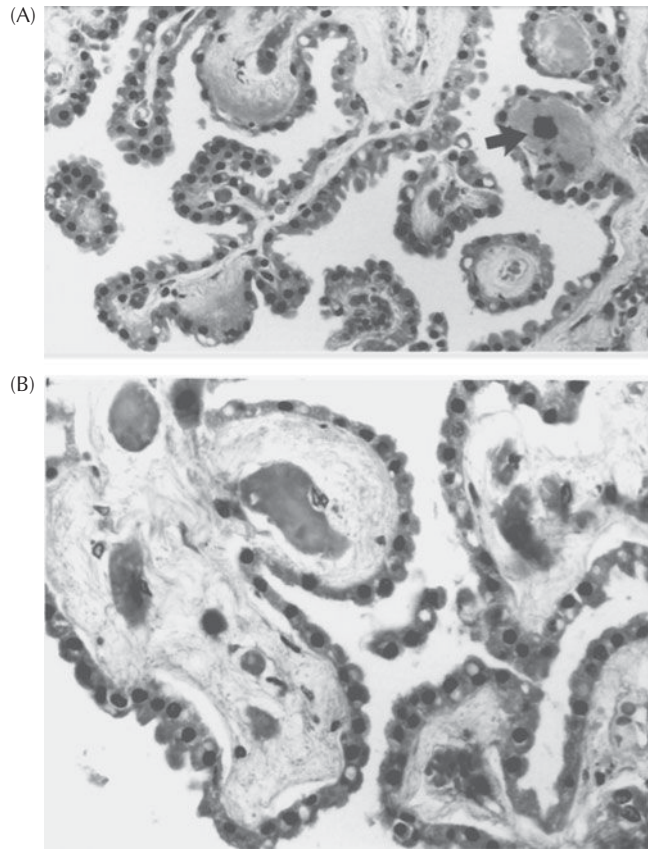

Figure 1–9. (**A**) Choroid plexuses showing the ependymal cells with dark nuclei and a cuboidal shape. Beneath the ependymal cells are the stroma with embedded blood vessels. A rare calcereous deposit is seen in the cores (arrow). (**B**) Higher power image. (Courtesy of Dr. Mario Kornfeld.)

tanycytes has microvilli rather than cilia. The tanycytes are connected by tight junctions forming a diffusion barrier at the ependyma that restricts the movement of molecules from the CSF to median eminence structures. As the tanycyte processes pass through the median eminence, they end on capillaries. The anterior region of the third ventricle contains the circumventricular organs, including the median eminence, organum vasculorum of the lamina terminalis, subfornical organ, subcommissural organ, neural lobe, pineal gland, and area postrema. The BBB is lacking here, exposing hypothalamic cells to the circulating blood, which is important since nuclei in these areas can act as chemical sensors.[22] The extracellular space of the median eminence is exposed to substances in the blood that can modulate release of the hypothalamic releasing factors. To compensate for the absence of the BBB, the ependyma over the hypothalamic region of the third ventricle has tight junctions that limit the movement of substances between the hypothalamic nuclei and the CSF. Thus, substances that enter the brain in the hypothalamic region are restricted from moving into the CSF and confined within the brain.

The surfaces of the choroid plexuses are covered with microvilli. Clefts between cells are seen to extend from the basal surface up to the apical tight junctions. The choroid plexuses are similar to other secretory epithelia. The fully developed choroid plexus cell has numerous mitochondria, a Golgi complex, an endoplasmic reticulum, and small vesicles.[21] Occasional cilia protrude from between the microvilli on the surface, which may expand the secretory components.

The final site where the blood and the CSF come into contact is at the arachnoid villi. As at other interfaces, the arachnoid cells covering the brain's surface are joined by tight

junctions.[23] Over the sagittal sinus, the arachnoid cells form villi that protrude into the dural sinuses. Electron microscopy of the arachnoid villi suggests that there are continuous channels through them.[24] An important function of the arachnoid villi is to prevent blood from the venous sinus from entering the CSF. The valve-like channels that collapse when pressure is applied from the blood side and open when the CSF pressure increases accomplish this. Even when the sinus pressure exceeds that in the CSF, there is no reversal of flow. Thus, the arachnoid villi act as one-way valves that open with pressure to allow CSF to drain into the sinuses but close when sinus pressure exceeds that in the CSF to prevent backward flow of blood. An unresolved issue is whether these villi are actual channels or merely a series of vesicles that can coalesce to form pseudochannels. Arachnoid cells with the capacity to drain into veins have been found along the spinal cord at the interface of the arachnoid with the spinal roots.[25]

Electron microscopic studies of the arachnoid reveal a multilayered structure in humans.[26] Five or six layers of cells form the subdural mesothelium. Directly below this layer is the central portion formed from closely opposed polygonal cells joined by desmosomes and tight junctions; this is the barrier layer. The inner layers consist of more loosely packed cells that are separated by bundles of collagen fibers. Finally, a very thin layer of leptomeningeal cells is found. Traversing the subarachnoid space are sheets of trabeculae that are formed from collagen fibers and contain small blood vessels. The collagen bundles of the trabeculae are continuous with those in the subpial space.

DURA, ARACHNOID, AND PIAL LAYERS

Directly beneath the skull is the dura, a tough membrane and an important structure that prevents the spread of infection from the skull into the brain and contains the CSF. Tears in the dura can occur when the skull is fractured or during surgery. Once the dura is damaged, the CSF can leak out; this leads to symptoms of headache from low CSF pressure or from the introduction of infection into the central nervous system with meningeal irritation.[27]

Beneath the dura is the arachnoid, whose cells are joined together by tight junctions. Subarachnoid spaces are filled with CSF. Over the surface of the brain is a layer of pial cells that are bathed by CSF. The pia is joined together by gap junctions, and similar to the ependymal cells, substances injected into the CSF can cross the pial surface and enter brain tissue.

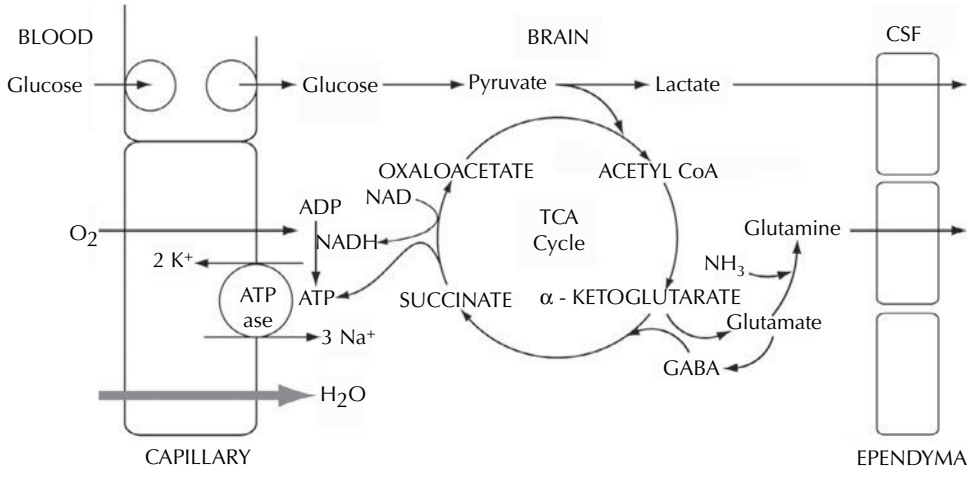

Figure 1–10. Chemiosmotic work that converts energy sources, such as glucose and oxygen, to ATP and other essential molecules. Glucose forms pyruvate and lactate (under anaerobic conditions). Pyruvate enters the TCA cycle to form ATP and amino acids, including glutamate, glutamine, and gamma-aminobutyric acid (GABA). The formation of ISF is accomplished by an ATPase pump that exchanges 3 Na+ for 2 K+, creating an osmotic gradient along which water passively flows.

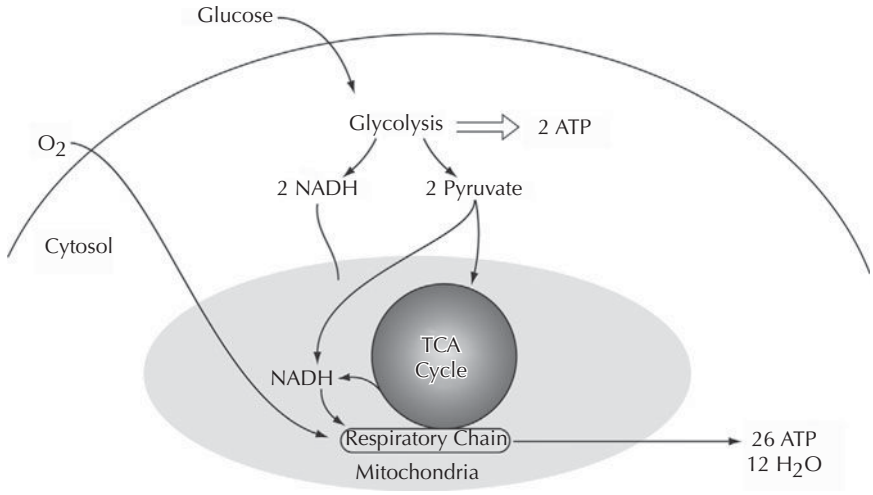

Figure 1–11. Conversion of oxygen and glucose to energy by glycolysis and the respiratory chain. Glycolysis yields only 2 ATP in the absence of oxygen. When oxygen is added, an additional 26 ATP are formed through the TCA. NADH is nicotinamide adenine dinucleotide, an electron donor essential for metabolism. ATP is adenosine triphosphate.

WHAT ARE THE SOURCES OF ENERGY?

The brain is the most metabolically active organ in the body. Accounting for only 2% of the weight of the body, the brain requires approximately 20% of the body's energy supply. To maintain this very large supply of energy, a mechanism of autoregulation of cerebral blood flow preserves flow through a wide range of blood pressures, breaking down only at the extremes of very high blood pressure, when disruption of the blood vessels leads to vasogenic edema, or very low pressure, when syncope occurs. This autoregulated system guarantees a steady supply of oxygen and glucose for all of the brain's metabolic needs under a wide variety of potentially damaging circumstances. Because of the great need for glucose by brain cells, specialized transport mechanisms at the endothelial cell level carry glucose into the brain across the cerebral blood vessels.

Glucose can be converted into the neurotransmitter glutamate, which is the most abundant amino acid in the brain Along with glucose, blood delivers oxygen; both substrates are needed for energy generation, which occurs during oxidative respiration. Glucose and oxygen are the major fuels for the metabolic pathways that form adenosine triphosphate (ATP) and reduced nicotinamide adenine dinucleotide (NADH), which, in turn, provide the energy to run the membrane pumps of the chemiosmotic machinery (Figure 1–10). Oliver H. Lowry developed the analytical methods to measure small amounts of energy metabolites and used these methods to describe the loss of ATP and other energy-generating molecules with acute ischemia.[28]

Glucose conversion to ATP is the source of the energy used for chemiosmotic work, such as membrane pumping, constriction of blood vessels, and secretion of CSF and ISF. Under aerobic conditions, glycolysis of glucose creates 2 molecules each of ATP, NADH, and pyruvate. Pyruvate enters the tricarboxylic acid (TCA) cycle (citric acid cycle or Krebs cycle) to form 26 molecules of ATP (Figure 1–11).

REFERENCES

1. Cushing H. The third circulation and its channels. *Lancet*. 1925;209:851.
2. Iadecola C, Nedergaard M. Glial regulation of the cerebral microvasculature. *Nat Neurosci*. 2007;10: 1369–1376.
3. Agre P. Homer W. Smith award lecture. Aquaporin water channels in kidney. *J Am Soc Nephrol*. 2000;11: 764–777.
4. Langman J, Guerrant RL, Freeman BG. Behavior of neuro-epithelial cells during closure of the neural tube. *J Comp Neurol*. 1966;127:399–411.
5. Kazanis I. The subependymal zone neurogenic niche: a beating heart in the centre of the brain: How plastic

is adult neurogenesis? Opportunities for therapy and questions to be addressed. *Brain*. 2009;132: 2909–2921.
6. Eriksson PS, Perfilieva E, Bjork-Eriksson T, et al. Neurogenesis in the adult human hippocampus. *Nat Med*. 1998;4:1313–1317.
7. Robel S, Berninger B, Gotz M. The stem cell potential of glia: lessons from reactive gliosis. *Nat Rev Neurosci*. 2011;12:88–104.
8. Lazarov O, Mattson MP, Peterson DA, et al. When neurogenesis encounters aging and disease. *Trends Neurosci*. 2010;33:569–579.
9. Spassky N, Merkle FT, Flames N, et al. Adult ependymal cells are postmitotic and are derived from radial glial cells during embryogenesis. *J Neurosci*. 2005;25: 10–18.
10. Sawamoto K, Wichterle H, Gonzalez-Perez O, et al. New neurons follow the flow of cerebrospinal fluid in the adult brain. *Science*. 2006;311:629–632.
11. Mirzadeh Z, Han Y-G, Soriano-Navarro M, et al. Cilia organize ependymal planar polarity. *J Neurosci*. 2010;30:2600–2610.
12. Knott GW, Dziegielewska KM, Habgood MD, et al. Albumin transfer across the choroid plexus of South American opossum (*Monodelphis domestica*). *J Physiol*. 1997;499(pt 1):179–194.
13. Stewart PA, Wiley MJ. Developing nervous tissue induces formation of blood-brain barrier characteristics in invading endothelial cells: a study using quail-chick transplantation chimeras. *Dev Biol*. 1981;84: 183–192.
14. Juranek J, Salman MS. Anomalous development of brain structure and function in spina bifida myelomeningocele. *Dev Disabil Res Rev*. 2010;16:23–30.
15. Bejjani GK. Definition of the adult chiari malformation: a brief historical overview. *Neurosurg Focus*. 2001;11:1–8.
16. Rall DP, Oppelt WW, Patlak CS. Extracellular space of brain as determined by diffusion of inulin from the ventricular system. *Life Sci*. 1962;1:43–48.
17. Margolis RU, Margolis RK. Nervous tissue proteoglycans. *Dev Neurosci*. 1989;11:276–288.
18. Afshari FT, Kwok JC, White L, et al. Schwann cell migration is integrin-dependent and inhibited by astrocyte-produced aggrecan. *Glia*. 2010;58: 857–869.
19. Yin J, Sakamoto K, Zhang H, et al. Transforming growth factor-beta1 upregulates keratan sulfate and chondroitin sulfate biosynthesis in microglias after brain injury. *Brain Res*. 2009;1263:10–22.
20. Scharrer E. A technique for the demonstration of the blood vessels in the developing central nervous system. *Anat Rec*. 1950;107:319–327.
21. Tennyson VM, Pappas GD. The fine structures of the choroid plexus adult and developmental stages. *Prog Brain Res*. 1968;29:63–85.
22. Broadwell RD, Oliver C, Brightman MW. Localization of neurophysin within organelles associated with protein synthesis and packaging in the hypothalamoneurohypophysial system: an immunocytochemical study. *Proc Natl Acad Sci USA*. 1979;76:5999–6003.
23. Nabeshima S, Reese TS, Landis DM, et al. Junctions in the meninges and marginal glia. *J Comp Neurol*. 1975;164:127–169.
24. Tripathi BJ, Tripathi RC. Vacuolar transcellular channels as a drainage pathway for cerebrospinal fluid. *J Physiol (Lond)*. 1974;239:195–206.
25. Welch K, Pollay M. Perfusion of particles through arachnoid villi of the monkey. *Am J Physiol*. 1961;201: 651–654.
26. Alcolado R, Weller RO, Parrish EP, et al. The cranial arachnoid and pia mater in man: anatomical and ultrastructural observations. *Neuropathol Appl Neurobiol*. 1988;14:1–17.
27. Schievink WI. Spontaneous spinal cerebrospinal fluid leaks and intracranial hypotension. *JAMA*. 2006;295: 2286–2296.
28. Goldberg ND, Passonneau JV, Lowry OH. Effects of changes in brain metabolism on the levels of citric acid cycle intermediates. *J Biol Chem*. 1966;241: 3997–4003.
29. Schade JP, Ford DH. *Basic Neurology*. Amsterdam: Elsevier; 1965.
30. Carpenter MB, Sutin J. *Human Neuroanatomy*. Baltimore: Williams & Wilkins; 1983.
31. Duvernoy HM, Delon S, Vannson JL. Cortical blood vessels of the human brain. *Brain Res Bull*. 1981;7: 519–579.
32. Peters A, Palay SL, deF Webster H. *The Fine Structure of the Nervous System: Neurons and Their Supporting Cells* (3rd Edition). Oxford University Press, New York, 1991. Pp. 349–351.

Chapter 2

Physiology of the Cerebrospinal and Interstitial Fluids

INTRODUCTION

Lumbar puncture for measurement of cerebrospinal fluid (CSF) pressure and analysis of the fluid is one of the most commonly employed diagnostic tests in neurology. Measurement of intracranial pressure and examination of the protein and cellular content of the fluids provide invaluable information for diagnosis of serious diseases, such as brain infection, increased intracranial pressure, multiple sclerosis (MS), Alzheimer's disease (AD), vascular dementia, and subarachnoid hemorrhage. When removal of CSF is done carefully without complications and the results are properly interpreted, lumbar puncture yields valuable information at a relatively low cost. Therefore, it is important to understand the dynamics and impact of disease on the CSF.

The method of removing fluid has changed little since it was first introduced into clinical care. Lumbar puncture is performed with a hollow needle containing a stylet, which is inserted into fluid space containing the spinal nerve roots below the termination of the spinal cord around L1. Generally, the needle is inserted in the L3-L4 space, which is the location of the pooled fluid. Ideally, the patient lies in the lateral recumbent position, and the test is done under sterile conditions at the bedside. Once the needle is determined to be in the lumbar sac, a manometer is placed on the needle and the CSF pressure is measured. After the sample is collected, it is sent for analysis of cells, protein, and other factors that may be useful in diagnosis.

Normal CSF is clear and colorless and resembles water. Three to four lymphocytes may be present, but generally there are no neutrophils.[1] The protein content is 40 to 60 mg%, in contrast to the 4 g of protein in the blood. The CSF pressure is between 80 and 180 mm H_2O in the

majority of patients. Low CSF pressure is associated with headaches and may be indicative of a CSF leak. It is important to obtain either a computed tomography (CT) or magnetic resonance imaging (MRI) scan to rule out a mass lesion or obstructive hydrocephalus prior to performing a lumbar puncture. Otherwise, there is a risk of herniation. Emergency lumbar puncture may be indicated when imaging is not available in patients with suspected bacterial meningitis.

PROTEINS IN THE CSF

Protein entry into the CSF is restricted by the tight junctions at the interfaces between blood, CSF, and brain tissue. In spite of the presence of a blood-brain barrier (BBB), small quantities of albumin and even smaller amounts of other proteins are found in the CSF. An elevated level of protein is a marker of an abnormal BBB. Albumin is produced by the liver and circulates in large quantities in the blood. While the level of albumin in the blood is around 4000 mg%, the normal amount in the CSF is 40 to 60 mg%. High levels of protein in the CSF are suggestive of disruption of the BBB, but alterations of the albumin content in the blood can influence the amount of albumin in the CSF. Therefore, it is more accurate to form the ratio of albumin in the CSF to that in the blood. This is called the *albumin index*, and it is a better indicator of the status of the BBB. Small amounts of other proteins are found in the CSF. These include immunoglobulins, particularly IgG, which is also at a much lower level in the CSF than in the serum. An increase in the intrathecal production of IgG suggests an immunological or infectious process in the CSF. The IgG index is elevated in autoimmune diseases such as MS. When infection or autoimmune reactions occur, there can be an increase in IgG. Abnormal permeability of the BBB allows IgG from the blood to enter the CSF. Separation of IgG formed within the central nervous system from the blood is critical in diagnostic testing. Therefore, it is common to calculate the IgG index, which is determined from the albumin in both compartments, using the formula

$$\text{IgG index} = (\text{IgG}_{csf}/\text{IgG}_{serum})/(\text{Alb}_{csf}/\text{Alb}_{serum})$$

An IgG index that is higher than 0.6 is abnormal. Any increase in the index is a reflection of IgG production in the CNS.

Measurement of other proteins in the CSF is an important diagnostic test in MS, and CSF analysis is indicated in the workup of patients with suspected MS. In addition to the IgG index, fragments of degraded myelin in the form of myelin basic protein can be measured. Detection of oligoclonal bands that differ from those present in the blood is highly suggestive of an immunological reaction in the central nervous system. Myelin basic protein can be elevated in other acute neurological disorders, and oligoclonal bands appear in other neuroinflammatory conditions, but they are extremely useful to support the diagnosis when clinical and imaging studies are also positive. The presence of myelin basic protein is only found during the acute attacks, while oligoclonal bands are more indicative of a chronic process and remain elevated. The pattern of expression of the IgG index, myelin basic protein, and oligoclonal bands is important to determine the stage of the MS attack. In the acute attack early in the illness, the IgG index and myelin basic protein are elevated without oligoclonal bands. In the chronic stage there may be an elevated IgG index and oligoclonal bands without myelin basic protein elevation.[2] Once the oligoclonal bands are increased in the CSF they remain elevated, in contrast to myelin basic protein, which falls after the acute process is over. Generally, in MS, there are fewer than 50 mononuclear cells; when the cell count is higher, other causes, such as vasculitis or infection, should be suspected.

Very high levels of CSF proteins can occur in meningitis, particularly due to fungal organisms, and in the Guillain-Barré syndrome. Brain and spinal cord tumors can sometimes increase CSF protein levels, but often these levels are normal. While CSF studies were once routinely done in patients with brain tumors, the use of multimodal imaging has replaced lumbar puncture. Generally, removal of CSF is not recommended in patients with brain tumors because of the threat of herniation. Rarely, markedly elevated CSF protein will obstruct the outflow of CSF, resulting in raised intracranial pressure with papilledema.

CSF PRESSURE REFLECTS VENOUS PRESSURE IN THE RIGHT HEART

The CSF is secreted by an energy-dependent process by choroid plexuses and capillaries. Measurements of CSF production indicate a rate of 0.3 mL/min. There is an estimated 120 mL of total CSF in the ventricles, the subarchnoid space, and the spinal region; 20 mL is found within the ventricles. Since about 500 mL of CSF is produced daily in humans, steady drainage is essential to avoid excess accumulation and increased pressure. Drainage of CSF occurs primarily across the arachnoid villi.

Cerebrospinal fluid, blood, and brain tissue contribute to the intracranial pressure. Expansion of any of these components creates a life-threatening situation because of the rigid skull encasing the brain. Alexander Monro noted in 1783 that since the brain was incompressible and the skull rigid, the amount of blood leaving by the veins had to be the same as that entering by the arteries. In 1824, George Kellie confirmed Monro's concept experimentally when he observed that animals killed by exsanguination had blood in the skull except where bone was removed with a trephin. George Burrows extended their observation in 1846 to include the CSF volume, and the limitation to expansion is referred to as the *Monro-Kellie doctrine* (Figure 2–1).

Measurement of CSF pressure with a manometer while the patient is in the lateral recumbent position reflects the sum of several compartments. Within the cranial vault the compartments are blood, CSF, and brain tissue. The smallest compartment is the blood, which represents about 2% of the total volume. When blood volume increases, there is a concomitant increase in CSF pressure. Any cause of vasodilatation will increase CSF pressure. For example, lung disease causes vasodilatation secondary to hypoxia, which often occurs during the night, resulting in headaches, and on rare occasions the increase in pressure is sufficient to produce papilledema. Brain tissue constitutes the largest compartment. Masses, such as hemorrhages and tumors, ischemic insults, and diffuse brain edema may lead to an increase in intracranial pressure.

Normal CSF pressure is between 80 and 180 mm H_2O and is dependent on the pressure in the superior sagittal sinus, which drains into the jugular veins. Since the pressure in the right side of the heart is generally low, pressure measured in the recumbent position at the time of lumbar puncture reflects the pressure in the venous system rather than arterial pressure, which is measured in millimeters of mercury[3] (Figure 2–2). Another factor involved in the venous control of CSF pressure is the transmission of pressure through the thin-walled veins, which occurs more readily than through the arterial system, the muscular wall of which exerts an opposing force. Thus, CSF pressure reflects the venous pressure and not the arterial pressure. When the patient takes a deep breath, the venous pressure in the chest is reduced. This pressure is transmitted to the CSF through the venous return from the brain and the manometer pressure falls, which is an excellent way to determine that the spinal needle is correctly positioned.

Elevated intracranial pressure is transmitted through the CSF along the optic nerve to

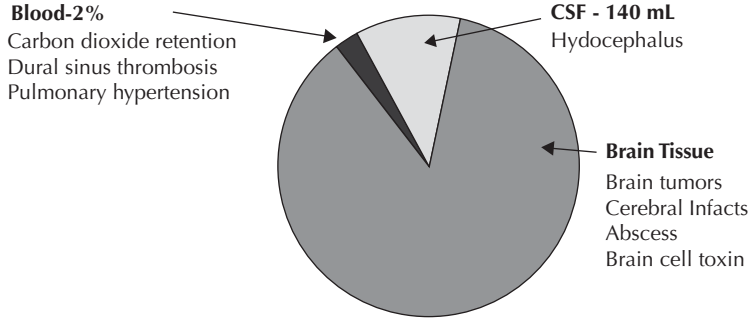

Figure 2–1. The Monroe-Kellie doctrine states that three compartments determine the pressure in the CSF: blood, CSF, and brain tissue.

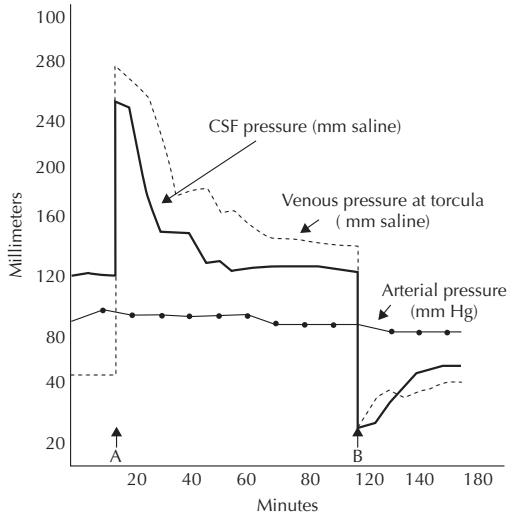

Figure 2–2. Cerebrospinal fluid pressure is determined by the pressure in the thin-walled veins rather than in the muscular arteries. This is shown by the compression of the jugular vein in the neck at time A. The rise in CSF pressure is seen in comparison to the venous pressure in the torcula. When the pressure is released, it returns to below the precompression value (B). Arterial pressure during the maneuver remains stable. Note that CSF pressure is measured in millimeters of water, while blood pressure is measured in millimeters of mercury. (Adapted from Ref. 3.)

the optic disc and can be seen as papilledema. Both eyes are generally involved in papilledema except in unusual circumstances where one of the optic nerves is compressed. Foster-Kennedy syndrome is a rare condition due to compression of one optic nerve by a mass, such as a meningioma, causing optic atrophy in the optic disc of the compressed nerve and papilledema in the other eye. Although there is no exact number, pressures over 200 mm H_2O are considered abnormal and often are associated with signs of acute or chronic bilateral papilledema. Papilledema is not always present when CSF pressure is increased. Large brain tumors may be present without signs of papilledema other than decreased venous pulsations in the eyes. One study using cisternography suggested that tumors that interfered with outflow of CSF were more likely to cause papilledema.[4]

The spinal cord has a unique system of venous drainage. There is an epidural space around the spinal cord that is more extensive than the epidural space of the brain. The veins around the spinal cord form a network of valveless veins that connect the deep pelvic veins and thoracic veins to the internal vertebral venous plexuses system, which is called *Batson's plexus*; because spinal veins lack valves, they are a route for the spread of cancer metastases and infection in the lung to the spinal cord and the brain.

FORMATION, CIRCULATION, AND ABSORPTION OF CSF

Formation of CSF by Choroid Plexuses

Choroid plexuses in the lateral, third, and fourth ventricles secrete 30% to 60% of the CSF. Formation of CSF by the choroid plexus epithelial cells involves active secretion of fluid by ion pumps and enzymes. Ames and his colleagues developed methods for collecting the freshly formed CSF in animals by filling the ventricles with oil and trapping the newly secreted CSF for measurements of ion content.[5] In a series of elegant experiments, they measured the CSF content of potassium and sodium, showing that it was regulated within a defined range different from that of the blood. Since the ionic content of CSF differed from that expected for an ultrafiltrate of plasma, they showed that CSF was formed by an active secretory process, which kept potassium levels in CSF within a very narrow range and allowed the sodium content to fluctuate more closely with serum levels.

Sodium-potassium adenosine triphosphatase (ATPase) and carbonic anhydrase are the major enzymes that control CSF secretion (Figure 2–3). Secretion of fluid is relatively independent of outside influences, which leads to clinical problems. Few drugs reduce the secretion of CSF, leading to increased intracranial pressure with or without hydrocephalus when the outflow pathways are obstructed. Inhibition of ATPase by ouabin reduces CSF formation, but it is highly toxic to the heart and can only be used in animal studies. Acetazolamide, a carbonic anhydrase inhibitor, also reduces CSF production and is used clinically to treat idiopathic increased intracranial pressure. The osmotic agent mannitol reduces CSF production and can be used for short periods to reduce intracranial pressure.

Histochemical studies show that the sodium-potassium-dependent ATPase is located on the microvilli of the apical (CSF-facing) surface of

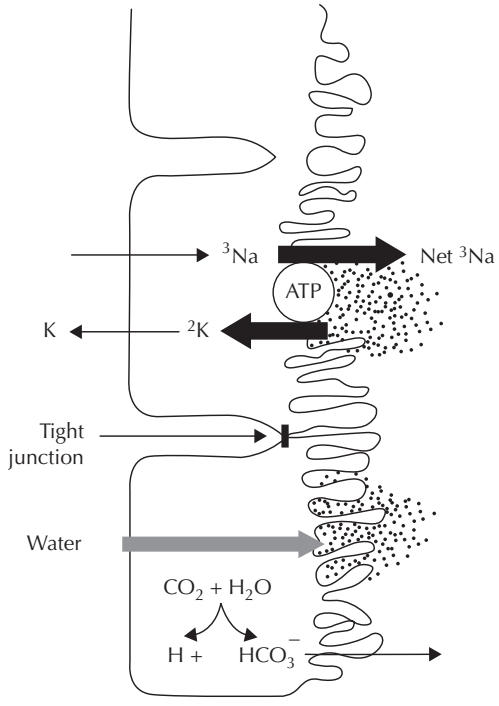

Figure 2–3. Mechanism of CSF formation at the choroid plexus. Ependymal cells are shown with tight junctions at the apical surface. An ATPase pump creates an osmotic gradient by importing more sodium ions into the CSF than potassium ions are removed. Another source of CSF is the conversion of CO_2 to HCO_3 by carbonic anhydrase.

the epithelial cells of the choroid plexus and that carbonic anhydrase is within the cells.[6] Cyclic nucleotides appear to be involved in CSF secretion; injection of cholera toxin into the ventricle, which stimulates adenylate cyclase, increases the CSF formation rate.[7] Adenylate cyclase is located along the basal plasmalemma of the choroid plexus.[6]

Although the choroid plexus and the ependymal cells lining the ventricles have a common epithelial cell origin, they differ in their secretory properties and enzymatic makeup. The ATPase located on the apical surface of the choroid plexuses appears on the basal (brain-facing) surface of the ventricular epithelium. Adenylate cyclase is found on the apical rather than the basal surface of the ependymal cells. Ependymal cells outside the choroid plexus have gap junctions and they restrict free water movement, which was shown when vasopressin infused into the CSF in cats caused an increase in water transport across the ependymal surface.[8]

Blood vessels in the stroma of the choroid plexus are similar to systemic vessels since they are fenestrated, permitting fluid, protein, and electrolytes to escape into the stroma underlying the ependymal cells of the choroid plexus. Tight junctions at the epithelial cell-like ependymal cells are located on the apical surface. Sodium enters the epithelial cell in exchange for hydrogen. Sodium is removed from the cell by an exchange at the apical surface of three intracellular sodium ions for two potassium ions in the CSF; the extra ion pumped by ATPase into the CSF increases the osmotic pressure on the surface, which results in the formation of CSF. Sodium ions accumulate on the apical surface as a result of the imbalance in their exchange with potassium. Excess sodium increases the osmolality at the CSF surface of the choroid cell. Water is removed from the cell by the osmotic pressure.

While the exact mechanism of CSF formation remains to be resolved, it is well accepted that an excess of ATPase molecules found on the apical end of the cleft creates an osmotic gradient with an excess of sodium ions on the apical surface. As part of CSF formation, HCO_3^- and Cl^- enter the CSF from plasma. Bicarbonate plays an important role in CSF formation by carbonic anhydrase. To balance the movement of HCO_3^-, there is a Cl-HCO_3 exchange that is driven by the need to maintain a steady-state intracellular HCO_3^- level.[9]

Although the primary driving force for CSF formation is Na^+/K^+ exchange at the apical surface, the HCO_3^- ion is linked to CSF secretion by cyclic adenosine monophosphate (cyclic AMP).[10] Few substances increase the rate of CSF formation. In underdeveloped countries with contaminated water supplies, cholera toxin, which is a potent stimulus of cyclic AMP, is a cause of an increase in CSF formation.[7]

The CSF formation rate varies for different species.[11] In humans, the rate of CSF production is 0.3 mL/min. However, formation of CSF as a function of choroid plexus weight is remarkably constant over a range of species (Table 2–1). Although several drugs can inhibit CSF production for a short period, they have proven to be of limited clinical use because of either their time frame of action or their toxicity. Acetazolamide, an inhibitor of carbonic anhydrase, reduces the CSF formation rate by up to 40%. Inhibitors of ATPase, such as digitalis, also reduce CSF formation; however, the

Table 2–1 **Rate of CSF Formation in Different Species**

Species	mL/min	mL/min/mg Choroid Plexus
Rabbit	10	0.43
Cat	20	0.5
Dog	50	0.63
Goat	154	0.36
Human	350	0.18

Source: From Ref. 11.

effect is too short-lived to be of clinical importance. Increased CSF pressure reduces CSF formation only slightly.[12]

Table 2.2 lists factors that influence the rate of CSF formation. Hyperosmolality produced by intravenous mannitol reduces CSF production by 50%,[13,14] and this drug is used clinically in patients with raised intracranial pressure to temporarily lower the pressure.[15] Mannitol is effective in doses of 0.25 mg/kg, which is below the amount needed to make a significant change in plasma osmolality, suggesting that it is working by other mechanisms. Hypothermia influences CSF production by reducing cerebral metabolism.

Choroid Plexus and Disease Biomarkers in CSF

The choroid plexus is involved in a variety of neurological disorders, including neurodegenerative, inflammatory, infectious, traumatic, neoplastic, and systemic diseases. Amyloid beta, Aβ, accumulates in the AD choroid plexus.[16] In MS, the choroid plexus could represent a site for lymphocyte entry in the CSF and brain and for presentation of antigens.[17] Measurement of biomarkers is important in the diagnosis not only of MS, but also of AD and vascular cognitive impairment (VCI). Measurement of CSF biomarkers, hyperphosphorylated tau (P-tau), total tau (T-tau), amyloid β_{1-42} (Aβ (42)) and neurofilament light polypeptide (NF-L) in patients with mild cognitive impairment (MCI), the early stage of AD, predicted VCI and AD at follow-up. Increased baseline concentrations of NF-L significantly separated MCI-VCI from stable MCI.[18] In another study of CSF biomarkers in advanced AD, T-tau, P-tau, and Aβ(42) could predict cognitive progression, the outcome of cholinesterase inhibitor treatment, and mortality in AD. A subgroup of patients with AD with extremely high levels of CSF biomarkers exhibits worse clinical outcomes over time, including faster progression of cognitive deficits, no response to cholinesterase inhibitor treatment, and higher mortality.[19]

Table 2–2 **Factors That Influence CSF Formation**

	Substance	Site of Action
Increased Production	Cholera toxin	Adenylate cyclase
	Adrenergic stimulation	Adenylate cyclase
Decreased Production	Ouabain/digitalis	Na^+/K^+-ATPase
	Acetazolamide	Carbonic anhydrase
	Hyperosmolality	Choroid plexus capillaries
	Hypothermia	Decreased metabolism

Absorption of CSF at the Arachnoid Villi

The absorption of CSF at the arachnoid villi is pressure sensitive (Figure 2–4); as the CSF pressure increases, so does the amount of CSF

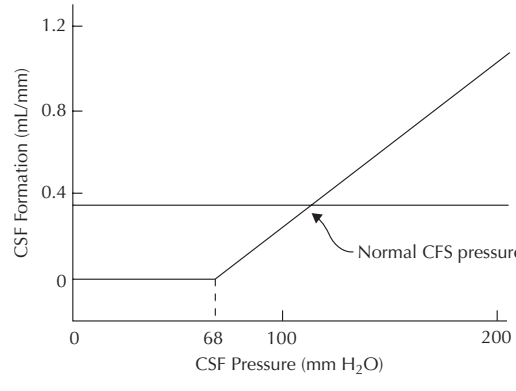

Figure 2–4. Absorption of CSF is dependent on its pressure. The formation rate is constant at 0.34 mL/min, and the rate of absorption increases above a threshold shown here at 68 mm H_20 as an example. The point where CSF formation and absorption cross determines the CSF pressure, measured by lumbar puncture with the patient lying on the side.

absorbed. Several explanations have been proposed to describe the absorption process. The arachnoid villi appear to act as one-way valves, which open with raised pressure and close as the pressure falls.[20] Larger particles are trapped by the arachnoid villi. Red blood cells from an intracranial bleed and white blood cells from an infection can be seen in the villi. Clogging of the absorption channels by cells or high protein levels impedes absorption of CSF, causing an increase in CSF pressure resulting in papilledema, and may lead under certain circumstances to communicating hydrocephalus.[21]

Circulation of CSF begins in the cerebral ventricles with the fluid exiting through the foramina of Luschka and Magendie into the cisterna magna. Flow of CSF within the subarachnoid space can follow two patterns (Figure 2–5). It can move up over the convexities to be absorbed into the blood across the arachnoid villi; alternatively, it can mix with the CSF in the spinal sac for subsequent removal into the vascular structures around the spinal cord or transport up over the hemispheres.

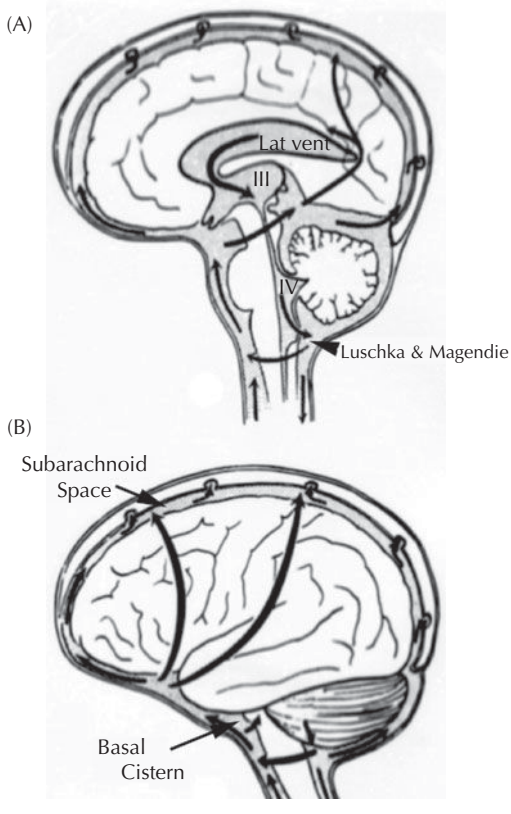

Figure 2–5. Pathways of CSF drainage from the cerebral ventricles to the arachnoid villi. (**A**) The CSF moves from the ventricles through the foramina of Luschka and Magendie into the subarachnoid space. (**B**) From the subarachnoid space it moves over the convexity to exit at the arachnoid villi.

Cisternography was developed at a time when normal pressure hydrocephalus (NPH) was initially described and predicted to be a cure for dementia.[22] This was prior to the realization that AD was a major cause of dementia, and enthusiasm for surgery to treat NPH waned. The CSF flow patterns can be determined clinically by the use of radioisotope cisternography, which involves the injection of radioactive substances into the lumbar spinal fluid.[23] Cisternography is done with the gamma emitter, technicium, labeled to diethylenetriaminepentaacetic acid, a large inert molecule. After injection of the isotope into the lumbar sac, nuclear brain scans are done at 2, 24, and 48 hours; the radioactive substances are transported slowly toward the head. If the molecular weight is large, the tracer ascends toward the head but remains in the subarachnoid space, where it exits through the sagittal sinus, which occurs within 24 hours under normal circumstances. Smaller molecular weight substances diffuse from the spinal canal through the vascular plexuses surrounding the cord.[24] When NPH is present, the tracer enters the ventricles and remains for up to 72 hours. If there is ventricular enlargement due to atrophy (hydrocephalus ex vacuo), the tracer can temporarily enter the ventricle; however, it does not remain as long as in NPH when there is transependymal absorption.[25]

Several other uses remain for cisternography, including determination of CSF leaks in patients with difficult-to-diagnose presentations of spontaneous intracranial hypotension. Patients with low CSF opening pressure often show contrast enhancement on MRI. Radioisotope cisternography is an additional diagnostic method to detect CSF leaks or pathological kinetics of radioisotope movement, particularly in cases with normal MRI findings.[26] Low-pressure headaches can occur after lumbar puncture but are usually transient. In an occasional patient, a persistent CSF leak requires a blood patch, which involves the injection of the patient's blood into the site of the lumbar puncture to speed the healing of the tear. Trauma to the nasal area can lead to CSF leaks. Basilar skull fractures are another cause.

Absorption of CSF is dependent on the state of the valve-like mechanism in the arachnoid villa. Several diseases lead to blockage of the absorption pathways with increased intracranial pressure and papilledema. Subarachnoid hemorrhage leads to the appearance of red blood cells in the CSF. These cells are large enough to clog the outflow passages. White blood cells are another potential blocker of the absorption mechanism. Rarely, CSF protein will be increased sufficiently to interfere with absorption.

Resistance of CSF outflow across the sagittal sinus can be measured by the infusion of artificial CSF into the lumbar sac. This is another test developed for use in the diagnosis of NPH that is rarely performed. To measure the outflow resistance, a spinal needle is inserted by lumbar puncture and connected to a manometer. While the patient is in a recumbent position, artificial CSF is infused slowly and the rise in pressure during the infusion is used to measure the outflow. Normal individuals can tolerate infusion of CSF at rates twice those of production without an increase in pressure.[27] When the CSF absorptive mechanism is impaired, there is a rise in pressure as the fluid is infused.

ELECTROLYTE BALANCE IN THE CSF

Sodium is the most abundant ion in the CSF, and it is important in transport and osmoregulation. Tracer studies with ^{24}Na have shown that the CSF and plasma levels are closely related.[28] Acetazolamide, an inhibitor of carbonic anhydrase, slows the entrance of radiolabeled sodium into the CSF.[29] Vasopressin enhances the movement of sodium from blood to brain.[30] The exchange time for ^{24}Na transport from blood to brain is about 2 hours and depends on the region sampled.

Cerebral capillaries have a membrane permeability to sodium of 1.4×10^{-7} cm/s, which is similar to their permeability to mannitol and in the same range as tight-junctioned epithelial membranes.[31] Both hypertonic saline and mannitol are used to temporarily control increased CSF pressure. The electrical resistance across a membrane is determined by the distribution of charged ions. In epithelial membranes the electrical resistance is regulated by the Na^+/K^+ ATPase pump. Epithelial sheets have a high electrical resistance due to the presence of tight junctions between the cells, and those with leaky junctions have a lower resistance.[32] Thus, measurement of the electrical resistance across the secreting epithelium gives an indication of the tightness of the junctions. The greater permeability of the choroid plexus epithelium is due in part to leaky intercellular junctions with an electrical resistance of 26 ohm/cm^2, which is similar to that of other leaky epithelium. For comparison, the electrical resistance of frog brain capillary is 1900 ohm/cm^2 and that of tight epithelium, such as toad bladder, is over 4000 ohm/cm^2.[33]

The potassium concentration is maintained within a very narrow range in the CSF.[5] The normal CSF potassium level is approximately 3 mEq/L. Changes in plasma potassium have little effect on CSF potassium.[34] Even at very high plasma levels, CSF potassium remains within the normal range.[35] Transport across the BBB is limited, and the half-time of exchange for potassium is 24 hours. When potassium levels in the CSF are increased, sodium is exchanged for potassium by an active transport mechanism. Potassium is critical for neuronal function and affects the release of neurotransmitters, making it important for it to be maintained at a constant level in the extracellular fluid.

Calcium in the CSF normally ranges between 2 and 3 mEq/L in CSF compared to plasma levels of 4 to 5.5 mEq/L.[36] Calcium is secreted from the choroid plexus and has a similar value in various CSF spaces. The rate of calcium entry from blood to CSF is relatively independent of the serum calcium level. The ratio of CSF to serum Ca^{2+} in humans is around 0.50.[37] The low CSF levels of calcium are maintained by transport mechanisms between blood and CSF.

Both acute and chronic changes in plasma calcium have little effect on brain calcium levels. Fluctuations of plasma calcium from 1 to 7 mmol/L in dogs change CSF calcium levels from 1 to 2 mmol/L; similarly, brain calcium remains constant during acute changes.[38] Young rats fed diets low or high in calcium showed a 40% fall or a 30% rise, respectively, in total plasma calcium; brain levels remained within 10% of those in controls.[39] Although calcium enters the brain at the various interfaces

comprising the BBB, transport across the choroid plexus is the dominant route for calcium entry from blood to brain.[40]

Regulation of calcium is essential for normal brain function. Marked increases in brain calcium produce impairment in thinking and can lead to coma, while very low levels of calcium cause seizures.[36] In order to maintain calcium homeostasis, active transport of calcium at the BBB barrier is necessary. Both the cerebrovascular endothelium and the choroid plexus participate in this process.[39]

Extracellular levels of unbound calcium are higher than intracellular ones. Calcium within the cell is sequestered in mitochondria and smooth endoplasmic reticulum. Entry of calcium into the cell occurs either by a change in the voltage across the membrane that accompanies depolarization or via agonist-operated channels activated by excitatory neurotransmitters. During pathological changes such as anoxia, the potassium concentration rises in the extracellular space and the calcium level falls.[41] The extracellular calcium enters the cell and leads to a cascade of molecular events that result in permanent cell damage.

Postsynaptic calcium channels are activated by glutamate and aspartate. Both amino acids are excitatory neurotransmitters ubiquitously distributed in brain tissue. Two of the glutamate receptors are transmembrane channels that are named according to the dominant molecule that excites them: *N*-methly-D-aspartate (NMDA) and α-amino-3-hydroxy-5-methyl-4-isoxazole propionic acid (AMPA) are ionotropic calcium channels. A metabotropic receptor coupled to a G-protein increases intracellular calcium. Glutamate excitatory receptors are mainly active in the synapses but have also been identified on axons. Found in high concentrations in the hippocampus and other regions sensitive to ischemic-anoxic injury, they are active in consolidation of memory through long-term potentiation. Glutamate ionotropic receptors open a sodium channel that allows sodium and chloride to enter the cell and another channel that permits calcium to pass. The calcium channel is strongly antagonized by magnesium, which may be important in the therapeutic action of magnesium.[42] Although calcium entry is a normal consequence of cell excitation by glutamate, excess calcium within the cell can lead to the activation of cellular processes that are detrimental to the cell, such as breakdown of cellular membranes and formation of products of inflammation.[43]

MENINGES AND SITES OF MASSES AND INFECTION

Three layers of meninges surround the brain and spinal cord. Dura mater is the tough fibrous layer beneath the skull that forms the inner layer of the cranial periosteum and tightly adheres to bone. Below the foramen magnum periosteum is separated from dura forming the epidural space, which is filled with fat. Arachnoid is the middle layer that is pressed against the dura. Cerebrospinal fluid fills the subarachnoid space and is contiguous with the glia limitans and pia mater covering the brain surface. Virchow-Robin spaces are lined with pia mater as they surround the blood vessels entering the brain from the surface.

Understanding the layers overlying the brain provides a rational explanation for the sites of infections and mass lesions. Arteries are present between the dura mater and the skull. When a fracture to the temporal bone tears the middle meningeal artery, a collection of blood accumulates rapidly under pressure in an epidural hematoma. If the injury results in tearing of the veins between the dura mater and the arachnoid, a subdural hematoma forms in the potential space.

Infections in the sinuses, particularly the ethmoid and the sphenoid, can spread into the subdural space to form a subdural empyema. Because the pus forms a layer of fluid beneath the dura mater, visualization by CT is not possible and MRI is the best diagnostic test. While subdural hematomas generally grow slowly and, if small, can be treated conservatively, subdural empyemas cause seizures and brain edema, and require high doses of antibiotics and urgent surgical treatment to drain the pus.

Below the arachnoid is the subarachnoid space that is crisscrossed with trabeculae and filled with CSF. Meningitis is a collection of cells in the subarachnoid space that can enter via blood or spread from the contiguous sinuses. Rupture of aneurysms on arteries in the subarachnoid space, commonly around the circle of Willis, results in severe headache with nuchal rigidity. Either blood or pus in the CSF can interfere with absorption of the CSF by

blocking the channels in the arachnoid granulations, resulting in an increase in CSF outflow resistance that raises the CSF pressure.

Infections can spread into the brain along the Virchow-Robin spaces that contain the arteries entering the brain from the surface. If the cells enter the Virchow-Robin spaces, meningoencephalitis results. Once infection has begun in the cerebral tissues, the cells form a cerebritis, which is localized. When the region of cellular accumulation forms a capsule, it is referred to as an *abscess*. Finally, when the cells are scattered more diffusely throughout the brain and accumulate around blood vessels, it is called an *encephalitis*. The sites of infection and masses in the meninges are shown in Figure 2–6.

The epidural space around the spinal cord is used as a site for injection of drugs for pain control. Infection can spread into the epidural space of the spinal cord from sites in the abdomen and lungs. Once an infection begins in the epidural space it can spread to multiple vertebral levels, but most dangerously it can compress the spinal cord, leading to paralysis. Suspected epidural abscesses can be seen on MRI and, if detected, require surgical removal and drainage to prevent paraplegia (Figure 2–7).

INTERSTITIAL FLUID

The composition of the interstitial spinal fluid (ISF) is thought to be similar to that of the CSF because of the continuity of the two fluids across the ependymal and pial surfaces. Formation of ISF occurs by active transport processes at the cerebral capillary, utilizing the high density of mitochondria that allows the capillary to act as a secretory epithelium. Estimates of the amount of CSF coming from ISF production, which is driven by Na^+/K^+ ATPase pumps on the abluminal side, range from 30% to 60%, depending on the species studied and the method of measurement.[44]

The extracellular matrix in brain contains complex carbohydrates and glycoproteins.

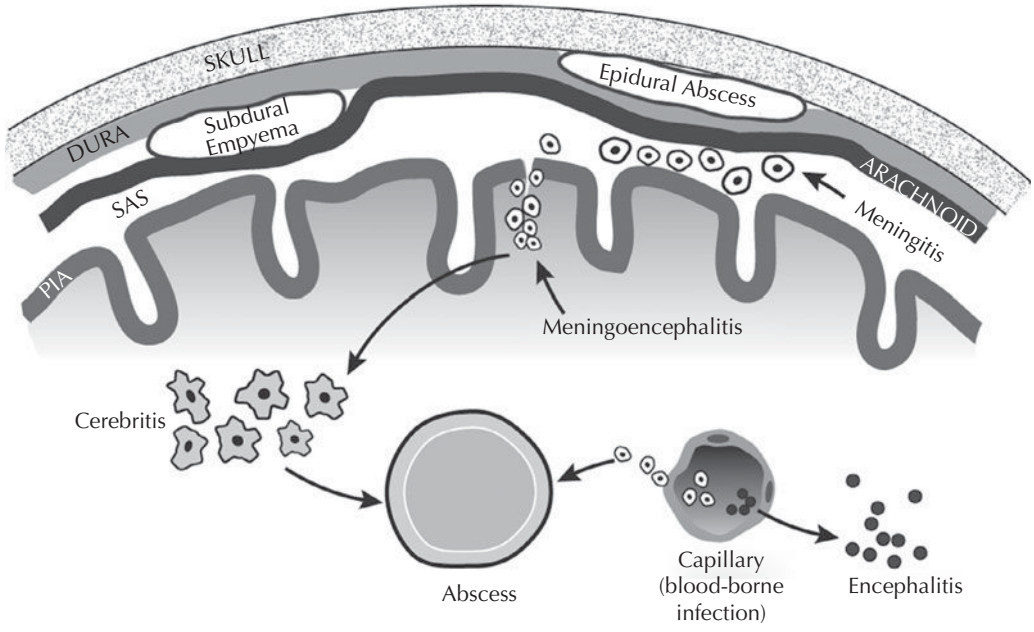

Figure 2–6. This drawing shows sites of potential brain infections and masses. Epidural hematomas occur beneath the skull and above the dura; these are ruptured blood vessels. Subdural empyemas are infections beneath the dura and over the surface of the brain. Meningitis indicates an infection limited to the subarachnoid space that contains the CSF. Meningoencephalitis indicates that the infection in the meninges has moved into the brain, often along the spaces formed as the blood vessels penetrate the surface (Virchow-Robin spaces). An infection within the brain begins as a cerebritis, and when it forms a wall, it is called an *abscess*. Encephalitis due to viral infections, such as herpes simplex, spreads within the brain.

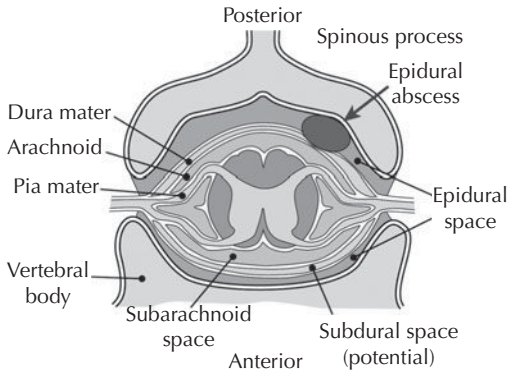

Figure 2–7. Transverse section of a vertebral body showing the locations of the epidural and subdural spaces. Epidural abscesses (arrow) arise from infections in the thoracic regions and lead to compression of the spinal cord. (Adapted from ref. 84)

The main extracellular molecules are the glycosaminoglycans: hyaluronic acid, heparin sulfate, dermatan sulfate, and chondroitin sulfate. Hyaluronic acid is highly hydroscopic and is found in larger amounts in the gray matter than in the white matter.[45]

LYMPHATIC DRAINAGE

Molecules injected into the caudate nucleus in several animal species drain into the ipsilateral cervical lymphatics.[46] In rabbits, dogs, and sheep, it is suggested that the substances move through the subarachnoid space and across the cribriform plate into the nasal mucosa. However, the significance of this route of ISF drainage in humans is unknown. Dogs normally drain CSF out of the brain into the nasal region.[24] Cats and sheep also have significant drainage by this route.

Lymphatic drainage into the cervical nodes is a potential route for antigenic fragments of brain tissue to reach the peripheral lymphatics where antibody formation could take place, which may be of importance in autoimmune diseases involving the brain.[47] Fragments of myelin released by traumatic injury or other pathological mechanisms could enter the lymph nodes by this route, but the role of lymphatic drainage in autoimmune diseases remains uncertain.

Direct injection of ^{131}I-labeled human albumin into the caudate nucleus resulted in greater drainage of the tracer into the ipsilateral lymphatics of the neck. When the radiolabeled albumin was injected into CSF, allowing it to move evenly throughout the subarachnoid space, the tracer appeared in both the ipsilateral and contralateral lymph.[46] This suggests that the drainage follows a route within brain tissue that is lateralized and unlikely to involve passage into the CSF in large amounts before it leaves the head.

Brain ISF flows via bulk flow along preferential pathways through the brain, contributing to the formation of CSF.[13,48,49] The evidence indicates an ISF bulk flow rate of 0.1–0.3 μL/min/g in rat brain along preferential pathways, especially perivascular spaces and axon tracts. Brain capillary endothelium is the main source of the fluid; capillaries have the necessary ion transporters, channels, and water permeability to generate fluid at a slow rate, which is much less than CSF secretion across choroid plexus epithelium. Some CSF may recycle from the subarachnoid space into arterial perivascular spaces on the ventral surface of the brain and join the circulating ISF, draining back via venous perivascular spaces and axon tracts into CSF compartments, and out of both through arachnoid granulations and along cranial nerves to the lymphatics of the neck. The bulk flow of ISF has implications for nonsynaptic cell-cell communication (volume transmission); for drug delivery, distribution, and clearance; for brain ionic homeostasis and its disturbance in brain edema; for the immune function of the brain; for the clearance of beta-amyloid deposits; and for the migration of cells (malignant cells, stem cells).[44]

WATER DIFFUSION, BULK FLOW OF ISF, AND DIFFUSION TENSOR IMAGING

Magnetic resonance imaging has the unique ability to show the diffusion of water. As MRI technology advanced, with faster scans and better computational programs, novel uses of MRI emerged. A particularly useful development was visualization of water movement in three dimensions. In 1990, Michael Moseley reported that water diffusion in white matter was anisotropic, which means that the effect of diffusion on proton relaxation varied,

depending on the orientation of fiber tracts relative to the orientation of the diffusion gradient applied by the imaging scanner. He also pointed out that this should best be described by a *tensor*, which is a vector that can be broken down into three directions of movement in Cartesian space.[50] Diffusion tensor imaging (DTI) is important when a tissue, such as the neural axons of white matter in the brain, has an internal fibrous structure analogous to the anisotropy of some crystals. Water will then diffuse more rapidly in the direction aligned with the internal structure, and more slowly as it moves perpendicular to the preferred direction. More extended DTI scans derive neural tract directional information from the data using three-dimensional or multidimensional vector algorithms based on six or more gradient directions, sufficient to compute the diffusion tensor. From the diffusion tensor, diffusion anisotropy measures such as fractional anisotropy can be computed. Moreover, the principal direction of the diffusion tensor can be used to infer the white matter connectivity of the brain (i.e., tractography, trying to see which part of the brain is connected to which other part).[51] Studies in complex neurological and psychiatric disorders, such as traumatic brain injury, stroke, MS, dementia, autism, and schizophrenia, have shown disordered patterns of white matter fiber tracts and have inferred that these changes in fiber tracts impact connectivity.

NEUROPEPTIDES AND FLUID HOMEOSTASIS

Neuropeptides, such as arginine vasopressin (AVP) and atrial natriuretic factor (ANF), influence water movement in the brain.[8,52–56] Vasopressin crosses the BBB very slowly, and AVP in the CSF is produced within the central nervous system. When injected into the CSF of rabbits, AVP lowered CSF pressure by increasing the transport of water across the arachnoid villi.[57] Increased intracranial pressure in humans results in an increase in the level of the hormone in the CSF, suggesting that it may be important in brain edema.[58] Further evidence for a role in brain edema comes from studying cold-injury edema, which is worsened after vasopressin injection into the CSF.[59]

There are numerous stimuli that lead to the release of AVP into the peripheral circulation. Hemorrhage, water deprivation, hypertonic sodium, and hypoxia cause an increase in plasma levels of vasopressin, while hemorrhage, hypoxia, and water deprivation lead to increased levels of the hormone in the CSF. There is a threshold effect with graded hypoxia, with release of hormones occurring only when the oxygen level is lowered to 10% of that of inspired air.[60] The stimuli that produce release into the periphery are not necessarily the same ones involved in release into brain tissue, which is reflected in the levels in the CSF. The CSF has been proposed as the conduit for transport of AVP from the site of release at the median eminence to other regions; however, the release into brain tissue with drainage into CSF is also possible.

Atrial natriuretic peptide (ANP) is released from cardiac atrial cells; it acts on the kidney and other peripheral organs to counteract the effect of AVP. Choroid plexus cells have receptors for atriopeptin, and infusion of ANP into the CSF reduced the rate of CSF production by 35%.[61] Atrial natriuretic peptide acts by stimulating the production of cyclic guanosine monophosphate, a second messenger. In isolated microvesse1s, ANP activated guanylate cyclase activity.

Increased intracranial pressure, such as in pseudotumor cerebri and subarachnoid hemorrhage, increases CSF vasopressin levels.[62] Hypoxia in animals increases vasopressin levels in both blood and CSF.[60] Two vasopressin receptors have been identified, namely, a V_1 and a V_2 receptor. In rat brain, a V_1-type receptor has been localized to the lateral septum and dorsal hippocampus. Isolated brain capillaries have a V_1-type receptor, and the pial arteries have vasopressin immunoreactive fibers.[63] The V_1 receptor is coupled to a phosphoinositol second messenger system, which in other organs is found near the alpha-adrenergic receptor. Activation of phosphoinositol results in inositol triphosphate phosphate (IP_3) and diacylglycerol (DAG) formation. These, in turn, activate protein kinase C and the phospholipases. Calcium plays a key role in this process since it is activated by DAG and augments phospholipase activation. Phospholipases C and A_2 can release membrane fatty acids, particularly arachidonic acid. Once arachidonic acid and other free fatty acids are formed, they have a series of

deleterious effects on cellular function. They inhibit Na^+/K^+-ATPase and lead to the formation of free radicals and leukotrienes, both of which are potent mediators of the inflammatory response. Edema occurs with intraventricular or intracerebral injection of AVP, suggesting that excessive stimulation of V_1 receptors on brain cells or blood vessels mediates volume regulation by AVP.[59,64]

Receptors for vasopressin are present in neurons, astrocytes, endothelial and smooth muscle cells of blood vessels, and choroid plexuses. A number of studies have shown increased release of vasopressin and expression of vasopressin receptors in the brain following ischemia, trauma, or subarachnoid hemorrhage, and antagonists of vasopressin V_1 receptors reduce brain edema. Vasopressin is also implicated in brain edema and in impairment of cerebral vasculature in hypo-osmotic states. Vasopressin V_1 receptor antagonists are being tested in experimental studies for treatment of cerebrovascular pathology.[65]

Hyponatremia is frequently associated with neurological disease, neurosurgical procedures, and the use of psychoactive drugs. Arginine vasopressin is the principal physiological regulator of water and electrolyte balance at the kidney, and disruption of the normal AVP response to osmotic stimuli by brain diseases is a common cause of dilutional hyponatremia in neurological disorders. Hyponatremia due to self-induced water intoxication, symptomatic hospital-acquired hyponatremia, and hyponatremia associated with intracranial pathology demand prompt intervention. The hyponatremia-induced shift in water from the extracellular to the intracellular compartment can lead to cerebral edema and serious neurological complications, especially if the decrease in serum sodium concentration is large or rapid. Overly rapid correction of the serum sodium level may lead to osmotic demyelination and irreversible brain injury.[66] Central pontine myelinolysis was initially described as a consequence of the damage to the white matter in the pons, but it is now recognized that more extensive damage to the white matter may occur. Fluid restriction is considered the first-line treatment; the pharmacological agents currently used in the treatment of hyponatremia are limited by inconsistent responses and adverse side effects. Arginine vasopressin receptor antagonists represent a new approach to the treatment of hyponatremia; they block tubular reabsorption of water by binding to V_2 receptors in the renal collecting ducts, resulting in aquaresis. Initial clinical experience with AVP receptor antagonists for hyponatremia has shown that these agents augment free water clearance, decrease urine osmolality, and correct serum sodium and serum osmolality. Controlled clinical trials now underway will help elucidate the role of AVP receptor antagonism in the treatment of hyponatremia.[67]

AQUAPORINS AND WATER TRANSPORT IN THE CENTRAL NERVOUS SYSTEM

Early experiments demonstrating that erythrocyte membranes are more permeable to water than expected from water diffusion through a lipid bilayer provided the first experimental evidence of the existence of water pores.[68] Many years passed before the discovery of pore-forming molecules, aquaporins (AQPs), for which Agre was awarded the Nobel Prize.[69] The aquaporins are a family of at least 13 members of small membrane-spanning proteins that assemble in cell membranes as homotetramers.[70–72] Each monomer is approximately 30 kDa, and six α-helical domains with cytosolically oriented amino and carboxy termini surround the water pore.[73] The AQPs transport water in both directions, depending on the pressure gradients from hydrostatic or osmotic forces.[74] The principal AQP in mammalian brain is AQP4; this molecule is heavily expressed at the borders between brain parenchyma and major fluid compartments, including astrocytic foot processes, glia limitans, ependymal cells, and subependymal astrocytes.[75–77] This distribution pattern indicates that AQP4 controls water flow into and out of the brain.[74] Aquaporin 1 is expressed in the apical membrane of the choroid plexus and plays an important role in CSF formation.[74,78,79] There was controversy about whether AQP9 is expressed in the brain.[78,80] However, one study using mice with targeted deletion of the AQP9 gene has provided conclusive evidence for expression of AQP9 in neurons.[81]

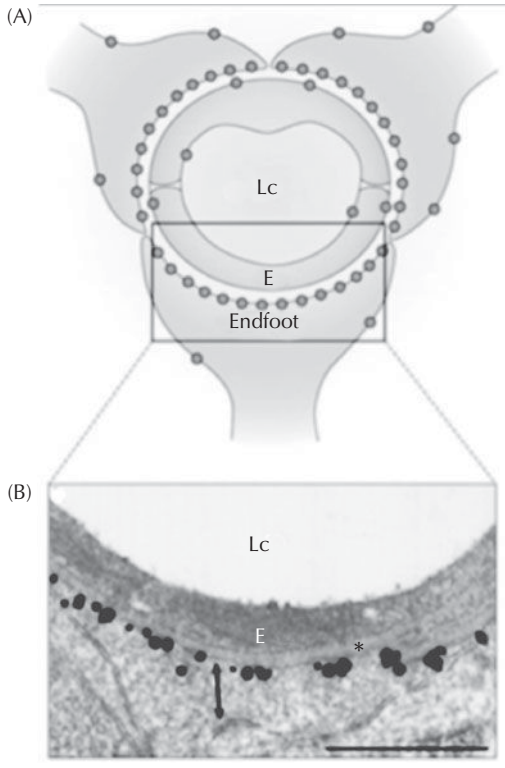

Figure 2–8. Drawing showing the expression pattern of AQP4 around brain microvessels. The concentration of AQP4 is high in the perivascular endfeet membrane domains that face the vessels and drops to low levels as soon as the membrane loses contact with the basal lamina. Endothelial cells express AQP4 at their adluminal as well as abluminal membranes but at much lower levels than the astrocytic endfeet. (**B**) An electron micrograph (corresponding to the box in (**A**) shows strong AQP4 immunogold labeling in the perivascular membrane of an astrocytic endfoot. (The endothelial AQP4 was not evident at this level of labeling sensitivity.) Asterisk, basal lamina; E, endothelium; Endfoot, astrocyte endfoot; Lc, capillary lumen. The arrow indicates the two membrane domains of the endfoot. Scale bar, 0.5 m. (From Ref. 83; See also the color insert.)

Water moving from the blood into the brain through an intact BBB has to cross three membranes: luminal and abluminal endothelial cell membranes and the membrane of the astrocyte foot processes.[74,82] A high density of AQP4 is present in the vascular-facing astrocytic membranes along with a lower density of AQP4 in endothelial cell membranes. Because of the close apposition of the astrocytic foot processes and their high density of AQP4, water that crosses the BBB will rapidly and preferentially end up in the perivascular astrocyte[82] (Figure 2–8).

REFERENCES

1. Fishman RA. *Cerebrospinal Fluid in Diseases of the Nervous System*. Philadelphia: W. B. Saunders; 1992.
2. Cohen SR, Herndon RM, McKhann GM. Radioimmunoassay of myelin basic protein in spinal fluid. An index of active demyelination. *N Engl J Med*. 1976;295: 1455–1457.
3. Davson H. *Physiology of the Cerebrospinal Fluid*. London: J. & A. Churchill; 1967.
4. van Crevel H. Rihsa cisternography in cerebral tumours. *Neuroradiology*. 1979;18:133–138.
5. Ames A III, Sakanoue M, Endo S. Na, K, Ca, Mg and Cl concentrations in choroid plexus fluid and cisternal fluid compared with plasma ultrfiltrate. *J Neurophysiol*. 1964;27:672–681.
6. Masuzawa T, Sato F. The enzyme histochemistry of the choroid plexus. *Brain*. 1983;106(1):P55-P99.
7. Epstein MH, Feldman AM, Brusilow SW. Cerebrospinal fluid production: stimulation by cholera toxin. *Science*. 1977;196:1012–1013.
8. Rosenberg GA, Kyner WT, Fenstermacher JD, et al. Effect of vasopressin on ependymal and capillary permeability to tritiated water in cat. *Am J Physiol*. 1986;251:F485–F489.
9. Johanson CE, Parandoosh Z, Smith QR. Cl-hco_3 exchange in choroid plexus: analysis by the dmo method for cell pH. *Am J Physiol*. 1985;249:F478–F484.
10. Saito Y, Wright EM. Bicarbonate transport across the frog choroid plexus and its control by cyclic nucleotides. *J Physiol*. 1983;336:635–648.
11. Cserr HF. Physiology of the choroid plexus. *Physiol Rev*. 1971;51:273–311.
12. Heisey SR, Held D, Pappenheimer JR. Bulk flow and diffusion in the cerebrospinal fluid system of the goat. *Am J Physiol*. 1962;203:775–781.
13. Rosenberg GA, Kyner WT, Estrada E. Bulk flow of brain interstitial fluid under normal and hyperosmolar conditions. *Am J Physiol*. 1980;238:42–49.
14. Sahar A, Tsipstein E. Effects of mannitol and furosemide on the rate of formation of cerebrospinal fluid. *Exp Neurol*. 1978;60:584–591.
15. Wise BL, Chater N. The value of hypertonic mannitol solution in decreasing brain mass and lowering cerebrospinal fluid pressure. *J Neurosurg*. 1962;19: 1038–1043.
16. Vargas T, Ugalde C, Spuch C, et al. Abeta accumulation in choroid plexus is associated with mitochondrial-induced apoptosis. *Neurobiol Aging*. 2010;31: 1569–1581.
17. Wolburg H, Paulus W. Choroid plexus: biology and pathology. *Acta Neuropathol*. 2010;119:75–88
18. Bjerke M, Andreasson U, Rolstad S, et al. Subcortical vascular dementia biomarker pattern in mild cognitive impairment. *Dement Geriatr Cogn Disord*. 2009;28: 348–356.
19. Wallin AK, Blennow K, Zetterberg H, et al. Csf biomarkers predict a more malignant outcome in Alzheimer disease. *Neurology*. 2010;74:1531–1537.
20. Welch K, Friedman V. The cerebrospinal fluid values. *Brain*. 1960;83:454–469.
21. Alksne JF, Lovings ET. The role of the arachnoid villus in the removal of red blood cells from the subarachnoid space: an electron microscopic study in the dogs. *J Neurosurg*. 1972;36:192–200.

22. Adams RD, Fisher CM, Hakim S. Symptomatic occult hydrocephalus with "normal" cerebrospinal fluid pressure: a treatable syndrome. *N Engl J Med*. 1965;273:117–126.
23. Di Chiro G, Reames PM, Matthews WB Jr. Risaventriculography and risa-cisternography. *Neurology*. 1964;14:185–191.
24. Di Chiro G, Stein SC, Harrington T. Spontaneous cerebrospinal fluid rhinorrhea in normal dogs: radioisotope studies of an alternate pathway of csf drainage. *J Neuropathol Exp Neurol*. 1972;31:447–453.
25. Benson DF, LeMay M, Patten DH, et al. Diagnosis of normal-pressure hydrocephalus. *N Engl J Med*. 1970;283:609–615.
26. Wiesemann E, Berding G, Goetz F, et al. Spontaneous intracranial hypotension: correlation of imaging findings with clinical features. *Eur Neurol*. 2006;56:204–210.
27. Hussey F, Schanzer B, Katzman R. A simple constant-infusion manometric test for measurement of csf absorption. II. Clinical studies. *Neurology*. 1970;20: 665–680.
28. Davson H, Pollay M. Influence of various drugs on the transport of 131-I and pah across the cerebrospinal fluid-blood barrier. *J Physiol* (*Lond*). 1963;167: 239–246.
29. Davson H, Luck CP. The effect of acetazolamide on the chemical composition of the aqueous humour and cerebrospinal fluid and the brain. *J Physiol* (*Lond*). 1957;137:279–293.
30. Fishman RA. Factors influencing the exchange of sodium between plasma and cerebrospinal fluid. *J Clin Invest*. 1959;38:1698–1708.
31. Rapoport SI. *Blood-Brain Barrier in Physiology and Medicine*. New York: Raven Press; 1976.
32. Crone C, Christensen O. Electrical resistance of a capillary endothelium. *J Gen Physiol*. 1981;77:349–371.
33. Olesen SP, Crone C. Substances that rapidly augment ionic conductance of endothelium in cerebral venules. *Acta Physiol Scand*. 1986;127:233–241.
34. Bradbury MWB, Stubbs J, Hughes IE, et al. The distribution of potassium, sodium, chloride and urea between lumbar cerebrospinal fluid and blood serum in human subjects. *Clin Sci*. 1963;25:97–105.
35. Katzman R, Graziani L, Ginsburg S. Cation exchange in blood, brain and csf. *Prog Brain Res*. 1968;29: 283–296.
36. Katzman R, Pappius HM. *Brain Electrolytes and Fluid Metabolism*. Baltimore: Williams & Wilkins; 1973.
37. Woodbury J, Lyons K, Carretta R, et al. Cerebrospinal fluid and serum levels of magnesium, zinc, and calcium in man. *Neurology*. 1968;18:700–705.
38. Wong RP, Bradbury MW. Permeability of the blood-brain barrier to calcium in adrenal insufficiency. *Brain Res*. 1975;84:361–364.
39. Murphy VA, Smith QR, Rapoport SI. Homeostasis of brain and cerebrospinal fluid calcium concentrations during chronic hypo- and hypercalcemia. *J Neurochem*. 1986;47:1735–1741.
40. Tai CY, Smith QR, Rapoport SI. Calcium influxes into brain and cerebrospinal fluid are linearly related to plasma ionized calcium concentration. *Brain Res*. 1986;385:227–236.
41. Nicholson C, Bruggencate GT, Steinberg R, et al. Calcium modulation in brain extracellular microenvironment demonstrated with ion-selective micropipette. *Proc Natl Acad Sci USA*. 1977;74:1287–1290.
42. Nowak L, Bregestovski P, Ascher P, et al. Magnesium gates glutamate-activated channels in mouse central neurones. *Nature*. 1984;307:462–465.
43. Rothman SM, Olney JW. Glutamate and the pathophysiology of hypoxic-ischemic brain damage. *Ann Neurol*. 1986;19:105–111.
44. Abbott NJ. Evidence for bulk flow of brain interstitial fluid: significance for physiology and pathology. *Neurochem Int*. 2004;45:545–552.
45. Margolis RU, Aquino DA, Klinger MM, et al. Structure and localization of nervous tissue proteoglycans. *Ann NY Acad Sci*. 1986;481:46–54.
46. Bradbury MW, Cserr HF, Westrop RJ. Drainage of cerebral interstitial fluid into deep cervical lymph of the rabbit. *Am J Physiol*. 1981;240:329–336.
47. Knopf PM, Cserr HF, Nolan SC, et al. Physiology and immunology of lymphatic drainage of interstitial and cerebrospinal fluid from the brain [review]. *Neuropathol Appl Neurobiol*. 1995;21:175–180.
48. Cserr HF, Ostrach LH. Bulk flow of interstitial fluid after intracranial injection of blue dextran 2000. *Exp Neurol*. 1974;45:50–60.
49. Rosenberg GA, Wolfson LI, Katzman R. Pressure-dependent bulk flow of cerebrospinal fluid into brain. *Exp Neurol*. 1978;60:267–276.
50. Moseley ME, Cohen Y, Kucharczyk J, et al. Diffusion-weighted mr imaging of anisotropic water diffusion in cat central nervous system. *Radiology*. 1990;176:439–445.
51. Le Bihan D, Mangin JF, Poupon C, et al. Diffusion tensor imaging: concepts and applications. *J Magn Reson Imaging*. 2001;13:534–546.
52. Raichle ME, Grubb RL Jr. Regulation of brain water permeability by centrally-released vasopressin. *Brain Res*. 1978;143:191–194.
53. Doczi T, Szerdahelyi P, Gulya K, et al. Brain water accumulation after the central administration of vasopressin. *Neurosurgery*. 1982;11:402–407.
54. Doczi T, Joo F, Szerdahelyi P, et al. Regulation of brain water and electrolyte contents: the opposite actions of central vasopressin and atrial natriuretic factor (anf). *Acta Neurochir Suppl* (*Wien*). 1988;43:186–188.
55. Rosenberg GA, Estrada E, Kyner WT. The effect of arginine vasopressin and v_1 receptor antagonist on brain water in cat. *Neurosci Lett*. 1988;95:241–245.
56. Rosenberg GA, Scremin O, Estrada E, et al. Arginine vasopressin v_1-antagonist and atrial natriuretic peptide reduce hemorrhagic brain edema in rats. *Stroke*. 1992;23:1767–1773; discussion 1773–1774.
57. Noto T, Nakajima T, Saji Y, et al. Effect of vasopressin on intracranial pressure of rabbit. *Endocrinol Jpn*. 1978;25:591–596.
58. Sorensen PS, Gjerris F, Hammer M. Cerebrospinal fluid vasopressin and increased intracranial pressure. *Ann Neurol*. 1984;15:435–440.
59. Reeder RF, Nattie EE, North WG. Effect of vasopressin on cold-induced brain edema in cats. *J Neurosurg*. 1986;64:941–950.
60. Wang BC, Sundet WD, Goetz KL. Vasopressin in plasma and cerebrospinal fluid of dogs during hypoxia or acidosis. *Am J Physiol*. 1984;247(1):E449-E455.
61. Steardo L, Nathanson JA. Brain barrier tissues: end organs for atriopeptins. *Science*. 1987;235:470–473.
62. Sorensen PS, Thomsen C, Gjerris F, et al. Increased brain water content in pseudotumour cerebri measured by magnetic resonance imaging of brain water self diffusion. *Neurol Res*. 1989;11:160–164.

63. Itakura T, Okuno T, Ueno M, et al. Immunohistochemical demonstration of vasopressin nerve fibers in the cerebral artery. *J Cereb Blood Flow Metab*. 1988;8:606–608.
64. Doczi T, Szerdahelyi P, Gulya K, et al. Brain water accumulation after the central administration of vasopressin. *Neurosurgery*. 1982;11:402–407.
65. Kozniewska E, Romaniuk K. Vasopressin in vascular regulation and water homeostasis in the brain. *J Physiol Pharmacol*. 2008;59(suppl 8):109–116.
66. Sterns RH, Nigwekar SU, Hix JK. The treatment of hyponatremia. *Semin Nephrol*. 2009;29:282–299.
67. Bhardwaj A. Neurological impact of vasopressin dysregulation and hyponatremia. *Ann Neurol*. 2006;59:229–236.
68. Sidel VW, Solomon AK. Entrance of water into human red cells under an osmotic pressure gradient. *J Gen Physiol*. 1957;41:243–257.
69. Gomes D, Agasse A, Thiebaud P, et al. Aquaporins are multifunctional water and solute transporters highly divergent in living organisms. *Biochim Biophys Acta*. 2009;1788:1213–1228.
70. Verkman AS. More than just water channels: unexpected cellular roles of aquaporins. *J Cell Sci*. 2005;118:3225–3232.
71. Agre P, King LS, Yasui M, et al. Aquaporin water channels—from atomic structure to clinical medicine. *J Physiol*. 2002;542:3–16.
72. Verkman AS. Physiological importance of aquaporins: lessons from knockout mice. *Curr Opin Nephrol Hypertens*. 2000;9:517–522.
73. Erkman AS, Yang B, Song Y, et al. Role of water channels in fluid transport studied by phenotype analysis of aquaporin knockout mice. *Exp Physiol*. 2000;85(spec no: 233S–241S).
74. Tait MJ, Saadoun S, Bell BA, et al. Water movements in the brain: role of aquaporins. *Trends Neurosci*. 2008;31:37–43.
75. Rash JE, Yasumura T, Hudson CS, et al. Direct immunogold labeling of aquaporin-4 in square arrays of astrocyte and ependymocyte plasma membranes in rat brain and spinal cord. *Proc Natl Acad Sci USA*. 1998;95:11981–11986.
76. Nielsen S, Nagelhus EA, Amiry-Moghaddam M, et al. Specialized membrane domains for water transport in glial cells: high-resolution immunogold cytochemistry of aquaporin-4 in rat brain. *J Neurosci*. 1997;17:171–180.
77. Badaut J, Lasbennes F, Magistretti PJ, et al. Aquaporins in brain: distribution, physiology, and pathophysiology. *J Cereb Blood Flow Metab*. 2002;22:367–378.
78. Zador Z, Bloch O, Yao X, et al. Aquaporins: role in cerebral edema and brain water balance. *Prog Brain Res*. 2007;161:185–194.
79. Boassa D, Stamer WD, Yool AJ. Ion channel function of aquaporin-1 natively expressed in choroid plexus. *J Neurosci*. 2006;26:7811–7819.
80. Saadoun S, Tait MJ, Reza A, et al. Aqp4 gene deletion in mice does not alter blood-brain barrier integrity or brain morphology. *Neuroscience*. 2009;161:764–772.
81. Mylonakou MN, Petersen PH, Rinvik E, et al. Analysis of mice with targeted deletion of aqp9 gene provides conclusive evidence for expression of aqp9 in neurons. *J Neurosci Res*. 2009;87:1310–1322.
82. Kimelberg HK. Water homeostasis in the brain: basic concepts. *Neuroscience*. 2004;129:851–860.
83. Amiry-Moghaddam M, Ottersen OP. The molecular basis of water transport in the brain. *Nat Rev Neurosci*. 2003;4:991–1001.
84. Baker AS, Ojemann RG. Spinal epidural abscess. NEJM. 1975;293:463–468.

Chapter 3

Neurovascular Unit

EARLY EXPERIMENTS ON THE BLOOD-BRAIN BARRIER

Endothelial cells provide a barrier that separates the systemic circulation from brain cells. Early anatomists, using Camillo Golgi's silver chromate stain showed that astrocyte foot processes attached to cerebral blood vessels. In the 1960s, Reese and Karnovsky found that the electron-dense particles ferritin and horseradish peroxidase were trapped in the clefts at the top of the luminal-facing junctions between endothelial cells, providing visual evidence of the blood-brain barrier (BBB).[1] The view that endothelial cells formed the BBB, ignoring the surrounding cells, was the dominant view until the mid-1990s, when the concept of the neurovascular unit emerged (Table 3–1).

THE NEUROVASCULAR UNIT AND TIGHT JUNCTION PROTEINS

Neuronal function is highly sensitive to the fluid and electrolyte composition of the extracellular fluid, which is maintained in balance with the intracellular fluids by a complex series of membrane pumps and ionic channels. The neurovascular unit is critical in preserving this delicate fluid and electrolyte balance through a series of interfaces that separate blood and brain cells. Endothelial cells, astrocytes, pericytes, and neurons comprise the neuro(glio) vascular unit[2,3] (Figure 3–1). Unlike the peripheral microvasculature, brain capillaries are not fenestrated and contain very few pinocytotic vesicles. Essential nonlipophilc molecules are actively transported across the BBB, while lipophilic molecules diffuse passively from the vascular space into the brain.

During central nervous system development, brain blood vessels acquire the unique characteristics that distinguish them from peripheral capillaries. Astrocytes and endothelial cells interact to form the proteins of the tight junctions and adherent junctions that connect brain endothelial cells (Figure 3–2). Although disruption of adherent junction proteins can lead to increased BBB permeability, it is primarily the tight junction proteins (TJPs) that confer the low paracellular permeability and high electrical resistance of the BBB.[4] By increasing the electrical resistance, TJPs convert the brain

Table 3–1 **Landmarks in the Concept of the Neurovascular Unit**

1885 Erhlich shows that intravenous dyes do not stain brain
1913 Goldmann shows that dyes injected into CSF stain brain
1873 Golgi applies his new silver staining method to brain, demonstrating the presence of neurons
1889 Ramŏn y Cajal shows that neurons are discrete and shares the Nobel Prize in 1906 with Golgi
1967 Reese and Karnovsky demonstrate the barrier at the endothelial cell

capillaries into epithelial sheets that block the transport of large molecules, charged substances, and nonlipid soluble substances.

The TJPs form an intricate complex of transmembrane (occludin, claudins, junctional adhesion molecule-1) and cytoplasmic (zona occludens-1 and -2, cingulin, AF-6, and 7H6) proteins linked to the cytoskeleton (Table 3–2). Occludin is a 60 to 65 kDa protein with four transmembrane domains and two extracellular loops that span the cleft between adjacent endothelial cells.[5] Occludins are highly expressed in cerebral endothelium and sparsely distributed in nonneural endothelia.[6] The phosphorylation state of occludins regulates its association with the cell membrane. In experimental autoimmune encephalomyelitis (EAE), a model of multiple sclerosis, occludin dephosphorylation precedes the neurological deterioration and increased leakage of plasma proteins across the BBB.[7] The C-terminal cytoplasmic domain of occludin is involved in its association with the cytoskeleton via accessory proteins, such as zona occludens-1 and -2. The other major intracleft TJPs are the claudins, a family of at least 24 members.[8] Claudins-5, -3, and -12 are localized at the BBB.[9] The extracellular tails of claudins from adjacent cells self-assemble to form the tight junctions, which are "zip-locked" together.[10] Junctional adhesion molecules mediate the early attachment of adjacent cell membranes via homophilic interactions.

Adherens junctions (or zonula adherens) are protein complexes that occur at cell-cell junctions in epithelial-like tissues, usually more basal than tight junctions. An adherens junction is defined as a cell junction whose cytoplasmic face is linked to the actin cytoskeleton. The adherens junctions are ubiquitously found in the cerebral vasculature, where they mediate several functions, including adhesion of endothelial cells to each other, contact inhibition during remodeling, and growth of the vasculature. VE-cadherin is an endothelial-specific Ca^{2+}-regulated protein that is linked to the cytoskeleton via catenins. Platelet endothelial

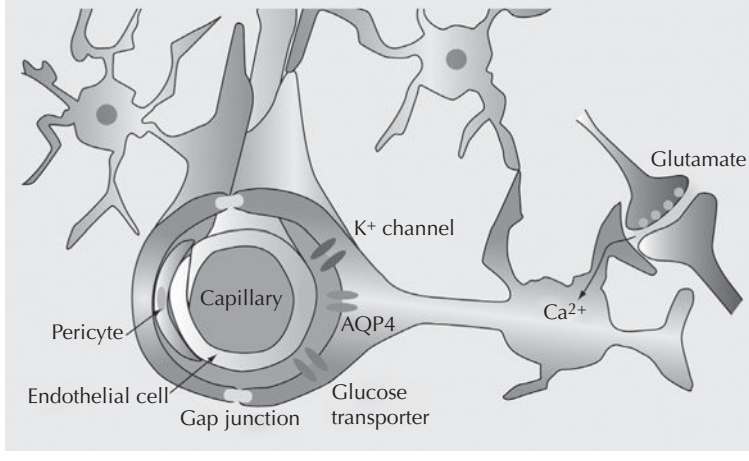

Figure 3–1. Drawing of the neurovascular unit. Penetrating arterioles are surrounded by astrocytic endfeet that express several specialized proteins. Astrocytes have fine processes in close proximity to synapses and occupy nonoverlapping spatial domains. Pericytes are in the basal lamina. A glutamate synapse is shown releasing calcium into the astrocyte, which will modulate the function of the blood vessel. AQP4, aquaporin 4. (Adapted from Ref. 3.)

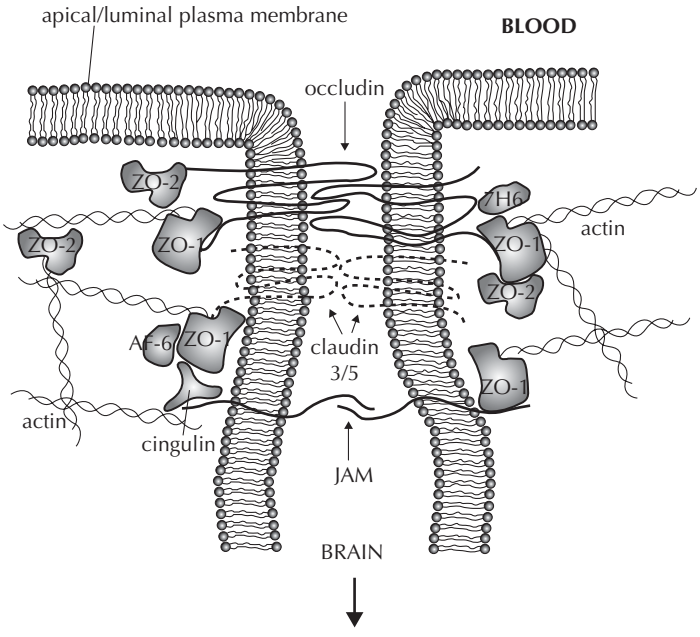

Figure 3–2. The TJPs form an intricate complex of proteins linked to the actin cytoskeleton. Claudins and occludin have four transmembrane domains with two extracellular loops, which are important in forming the "seal" between two adjacent endothelial cells. These proteins associate with the cytoskeleton via accessory proteins such as zona occludens (ZO)-1, ZO-2, AF6, and cingulin. The junctional adhesion molecule (JAM) family forms part of the TJPs and mediates attachment of cell membranes via homophilic interactions. The most important components of the adherent junctions are vascular endothelial (VE)-cadherin and platelet endothelial cell adhesion molecule-1 (PECAM-1). VE-cadherin is linked to the actin cytoskeleton via catenins. (From Ref. 4.)

cell adhesion molecule-1 (PECAM-1), also known as CD31, is a key participant in the migration of blood-borne cells across the BBB. Changes in the adherens junction proteins can lead to increased paracellular permeability and leukocyte trafficking.

On the abluminal surface of the endothelial cells is a thin layer of basal lamina composed mainly of type IV collagen, fibronectin, heparan sulfate, laminin, and entactin (Table 3–3).[11] Pericytes reside within the basal lamina. Mesenchymal in origin, pericytes form an incomplete envelopment around the endothelial cells and within the microvascular basement membrane of capillaries and postcapillary venules. Cell bodies and cytoplasmic processes of pericytes, as well as the endothelial cells, are enveloped by the same basal lamina, except for locations where they make direct contacts with each other. They are important in BBB stability as well as angiogenesis. Their expression of smooth muscle actin and desmin, two proteins found in smooth muscle cells, and their adherence to the endovascular cells make them very strong candidates for blood flow regulators in the microvasculature.[3] Pericytes are contractile and seem to serve as a smooth muscle equivalent in the brain capillaries. They also

Table 3–2 **Major Tight Junction Proteins**

Occludin
Claudin-5, -3, -12
Junctional adhesions molecule-1
Zona occludens-1, -2
Cingulin

Table 3–3 **Components of the Basal Lamina**

Collagen type IV
Fibronectin
Heparan sulfate
Laminin
Entactin

display several macrophage properties including phagocytosis and antigen presentation.[12] Interaction between pericytes and endothelial cells is important for the maturation, remodeling, and maintenance of the vascular system via secretion of growth factors or modulation of the extracellular matrix. There is also evidence that pericytes are involved in transport across the BBB and the regulation of vascular permeability.[13]

Astrocytes are generally thought to be essential cells for tight junction formation (Table 3–4). However, a study in embryos challenges this concept by showing that BBB qualities of the capillary form when the endothelial cells invade the central nervous system and pericytes are recruited to the developing vessels, which takes place over a week before astrocyte generation, showing that pericytes are critical for tight junction formation.[14] Another interesting study of pericytes showed that they decrease with age, which parallels an increase in BBB permeability.[15]

During development, leptomeningeal mesenchymal cells enter the brain and transform into microglia. Circulating monocytes provide another major source of brain microglia. Perivascular microglial cells, which are bone marrow derived, continuously turn over in the central nervous system and are immunoregulatory cells that connect the central nervous system with the peripheral immune system; they are recruited to the brain after stroke, which may be a mechanism involved in the recovery process.[16] Microglia are phagocytic cells with the capability of antigen presentation. They rapidly respond to a wide variety of stimuli including inflammation and hypoxia/ischemia. Activated microglia release several inflammatory factors, which modulate the permeability properties of the neurovascular unit.

Surrounding the endothelia and basal lamina are the astrocytic foot processes, which have multiple ion transporters and channels and heavily express aquaporin 4, suggesting that these processes facilitate ion and water transport across the BBB. Neurons and perivascular microglia are the other cellular components of the neurovascular unit. In the adult brain, neurons, which are not in direct contact with endothelial cells, probably exert an influence indirectly. However, astrocytes directly mediate the neurovascular connections by wrapping their foot processes around brain microvessels. By releasing vasoactive molecules, astrocytes mediate the neuron-astrocyte-endothelial signaling pathway and play a profound role in coupling blood flow to neuronal activity.

Interactions between the different cellular components of the neurovascular unit and the extracellular matrix determine permeability. In vivo studies, while more difficult to interpret, provide better information than cell culture systems, which generally include only one or two cell types. When endothelial cells are grown alone in culture, the electrical resistance across the vessels is much lower; adding astrocytes to the culture system can increase it, and adding pulsations further improves the system.[17]

Table 3-4 **Roles of Astrocytes**

Uptake of glutamate through glutamate uptake receptors
Cycling of glycolytic pathway molecules
Source of growth factors for surrounding cells
Aid in formation of tight junctions

INTEGRINS, SELECTINS, AND ENDOTHELIAL CELL ADHESION

Blood vessels are joined to the extracellular matrix by a series of integrins. Cells within cerebral microvessels express both the integrin and dystroglycan families of matrix adhesion receptors. Integrins and the dystroglycan complex are found on the matrix faces of both endothelial cells and astrocyte endfeet. Pericytes rest against the basal lamina. Matrix adhesion receptors are essential for the maintenance of the integrity of BBB permeability, and modulation of these receptors contributes to alterations in the barrier during brain injury.[18]

Integrins convey signals from the extracellular matrix outside a cell to the cytoskeleton inside the cell, coupling them to essential intracellular function through a series of protein kinases. Ligands of integrins include fibronectin, vitronectin, collagen, and laminin. Inflammatory cells migrate across the highly specialized endothelial cells and gain access to the central nervous system. Leukocyte recruitment across this vascular bed involves α4-integrins in the initial contact as well as adhesion with the endothelium (Figure 3–3).

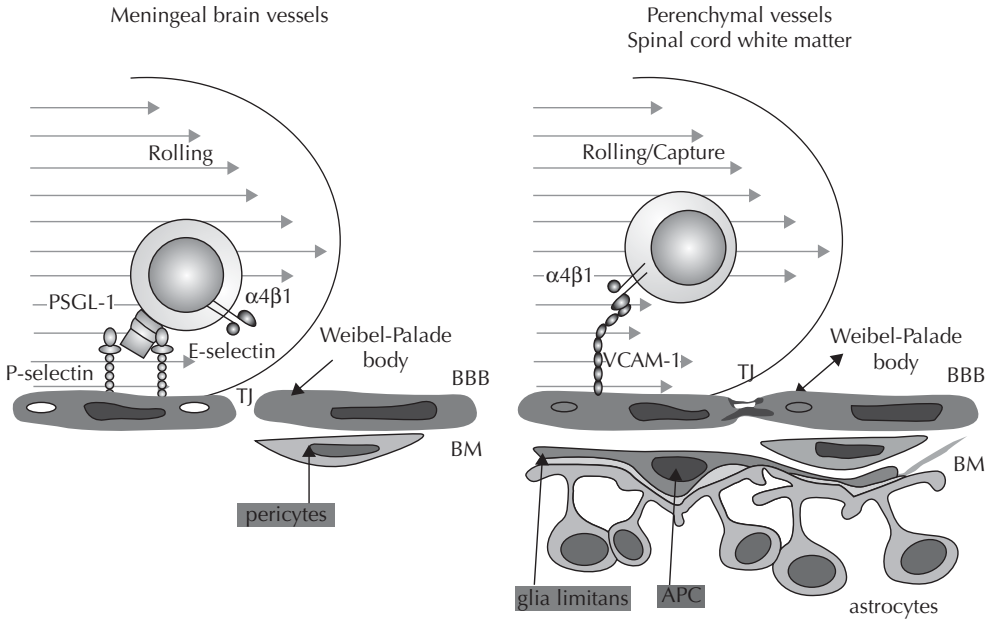

Figure 3–3. Differential contribution of selectins to immune cell interaction with the meningeal versus the parenchymal BBB. In meningeal microvessels endothelial E- and P-selectin and their leukocyte ligand (PSGL-1), as well as α4-integrin, contribute to leukocyte tethering and rolling. Meningeal microvascular endothelial cells store P-selectin in their Weibel-Palade bodies and can upregulate P-selectin expression during EAE. In contrast, parenchymal microvascular endothelial cells lack storage of P-selectin in their Weibel-Palade bodies. In deep cortical brain microvessels, which are inaccessible to intravital microscopy the molecular mechanisms of the initiation of lymphocyte recruitment across the BBB might differ, as antibodies directed against α4-integrin but not against E- and P-selectin or PSGL-1 inhibit inflammatory cell accumulation and EAE. The intravital microscopy of spinal cord microvessels supports a predominant role of α4-integrins in immune cell interaction with the BBB. BM, basal membrane; TJ, tight junction; APC, antigen presenting cells. (From Ref. 19.)

Intravital microscopic analysis of immune cell interaction with superficial brain vessels demonstrates a role for E- and P-selectin and their common ligand, P-selectin glycoprotein-1 (PSGL-1), in lymphocyte rolling.[19]

Adhesion and signaling molecules on leukocytes and endothelial cells mediate recruitment of leukocytes into brain tissue. Rolling white blood cells adhere to vessels through the action of selectins and vascular cell adhesion molecule-1 (VCAM-1). Experimental allergic encephalomyelitis is a T-cell-mediated autoimmune disease induced by injection of myelin basic protein in Freund's adjuvant, which is used to model for multiple sclerosis (MS).[20] An inflammatory process is induced around blood vessels with demyelination in the region of the inflammation. T cells adhere to the selectins by an α4β1-integrin on the leukocyte surface. Depending on the type of endothelial cell, either a selectin or VCAM-1 couples the cell to the endothelial surface, slowing the rolling and leading to the adhesion and diapedesis of the cells across vessels. Anti-inflammatory agents developed to block the adhesion of leukocytes are used to reduce inflammation in EAE and MS. One such agent is the humanized anti-α4-integrin antibody, natalizumab, which is an effective treatment for relapsing-remitting MS.[21] In the EAE model, natalizumab inhibits the firm adhesion but not the rolling or capture of human T cells on the inflamed BBB.[22] Although natalizumab is still used in selected MS patients with advanced disease who are poorly responsive to other agents, this treatment was severely curtailed when an increased incidence of progressive multifocal leukoencephalopathy, a fatal disease of the nervous system due to the JV virus, occurred in a number of patients.[23]

ASTROCYTES, PERICYTES, AND BASAL LAMINA

Immunostaining astrocytes with antibodies to aquaporin shows a dense pattern around

capillaries consistent with their important role in the neurovascular unit. Conventional staining of astrocytes with glial fibrillary acidic protein (GFAP) stains fewer astrocytes.[24] Densely packed astrocytes are arranged neatly around blood vessels (Figure 3–4). Astrocytes use calcium signaling to communicate, and calcium signaling spreads rapidly between astrocytes through gap junctions formed by Cx43 hemichannels.[25]

There are several types of astrocytes in brain tissue. In cortex, protoplasmic astrocytes are found mainly in layers 2–6, and are organized into domains associated with neurons and blood vessels. Fibrous astrocytes, which reside in white matter, are disorganized but are intercalated between oligodendrocytes and along blood vessels.

Astrocytes have diverse roles in brain function. One of the most important is uptake of glutamate, through glutamate uptake receptors, after it is released into the extracellular space during normal cell excitatory signaling. Glutamate also provides energy-generating substrates for the tricarboxylic cycle for use in the glycolytic pathways. Astrocytes supply surrounding cells with a variety of growth factors and are essential for the maintenance of the basal lamina. Because of their use of glycogen as a fuel source, astrocytes are thought

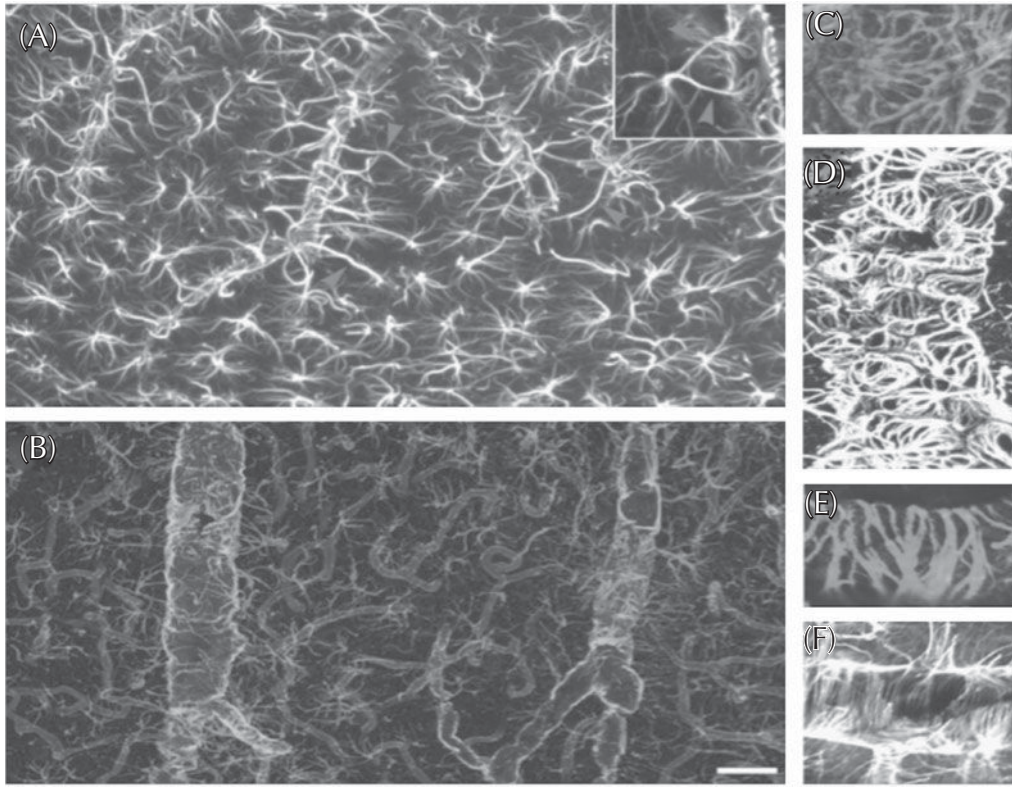

Figure 3–4. Not all vascular astrocytic endfoot processes are GFAP positive. (**A**) Glial fibrillary acidic protein immunolabeling of astrocytes in cortex. Individual astrocytes are star-shaped and distributed symmetrically, with minimal contact with neighboring astrocytes. Vascular processes differ from other processes by being straight, unbranched, and of wide diameter (arrowheads). The surfaces of large to medium-sized vessels were densely covered by GFAP-positive astrocytic endfeet. Inset: An astrocyte with two vascular processes. (**B**) Double immunolabeling of AQP-4 (red) and GFAP (green). Aquaporin-4 immunolabeling reveals that the entire network of vessels, including capillaries, is covered by astrocytic processes, albeit GFAP negative. Smaller vessels and capillaries are mostly GFAP negative but display intense labeling against the astrocyte-specific channel AQP-4. The AQP-4 labeling reveals continuous coverage by astrocytic endfeet. (**C–F**) Examples of the organization of GFAP in astrocytic endfeet around larger vessels. **C** and **D** display examples of wagon-wheel or rosette formation of GFAP filaments in the vascular endfeet, whereas **E** and **F** are examples on parallel arrays running perpendicular to the length of the vessel. C and E are double labeled against GFAP (green) and AQP-4 (red), whereas **D** and **F** are stained against GFAP only. Scale bar: inset, 40 μm; A, 10 μm; B, 60 μm; C, E, 5 μm; D, F, 30 μm. (From Ref. 51; See also the color insert for red and green colored images.)

to be better able to withstand hypoxia than neurons. Astrocytes are able to metabolize lactate, which makes them more resistant to hypoxia, and they provide substrates to neurons. Astrocytes secrete a number of vasoactive substances that vasodilate and vasoconstrict blood vessels. Synaptic activity releases glutamate, which stimulates an increase in astrocyte calcium. Neuronal activity increases intracellular Ca^{2+} in astrocytic perivascular endfeet, which can influence the diameter of cerebral arterioles.[3]

MOVEMENT OF SUBSTANCES INTO AND OUT OF BRAIN

Transport of essential nutrients into the brain is compromised by the extremely high electrical resistance in the cerebral capillaries, which reaches values of 1900 ohm/cm^2, equivalent to those in frog skin.[26] Tight junctions in brain capillaries create an intermediate electrical resistance compared to other tissues. By comparison, the tight junctions in urinary bladder epithelium create an electrical resistance of 3800 ohm/cm^2, while muscle capillaries have a resistance of 20 ohm/cm^2 and mesenteric capillaries have only 1–2 ohm/cm^2 resistance. In addition to the tight junctions, brain capillaries contain enzymatic barriers that effectively metabolize various substrates before they are allowed to enter the brain. These enzymes include alkaline phosphatase, pseudocholinesterase, aromatic-L-amino acid decarboxylase, and gamma-glutamyl transpeptidase.[27]

Transplantation studies have shown that the stimulus for capillaries to form tight junctions comes from brain. This was shown in transplantation studies using quail brains, which have specific markers for capillaries so that they can be identified and distinguished from other capillaries. Transplantation of systemic capillaries into quail brain induces capillaries with tight junctions.[28] Pericytes participate in the production of tight junctions in developing brain capillaries.[14] Astrocytes probably have an important role in maintaining the integrity of the tight junctions.

Cerebral capillaries are highly metabolic structures, which makes them vulnerable to traumatic and ischemic injuries that impair energy sources. Formation of interstitial fluid (ISF) occurs through the exchange of ions across membranes by Na/K adenosine triphosphatases (ATPases), which creates an osmotic gradient when three Na^+ molecules move out of the cell and two K^+ molecules move in. These high energy needs of cerebral capillaries are supplied by the large number of mitochondria that provide the adenosine triphosphate (ATP) for the Na^+/K^+ ATPase pumps.[29] Finally, cerebral capillaries contain proteins that act as transporters for glucose and amino acids, maintaining the levels of these essential substrates in brain tissues through a wide range of blood values (Figure 3–5). Understanding the mechanisms of transport of substances from blood to brain is of great clinical importance; it has influenced concepts of disease pathogenesis and been helpful in drug design.

Several factors impact the rate of transport of substances across the BBB (Table 3–5). These include molecular weight, molecular charge, lipid solubility, and carrier mechanisms. Lipid-soluble molecules pass most easily through the endothelial cell. This may occur either through lipoprotein pores in the membrane or by dissolving in the membrane matrix. For example, gases such as oxygen, carbon dioxide, and anesthetic agents are highly lipid-soluble and readily cross the membrane, while slow passage across the BBB of certain drugs limits their therapeutic usefulness. Modifying molecules to increase their lipid solubility has been used to design drugs with greater therapeutic effectiveness. The octanol/water ratio of a substance is a good index of the ease of movement across the BBB (Figure 3–6). Lipid-soluble compounds partition into the octanol layer, while nonlipids are dissolved mainly in the water. For example, aminopyrine is highly lipid- soluble and has a partition coefficient greater than 1, while sucrose is very insoluble in octanol and has a very low

Table 3–5 **Factors That Influence Transport Across the BBB**

Molecular weight
Extent of ionization
Lipid solubility
Presence of carrier molecules
Protein binding of drugs
P-glycoprotein transport out of brain

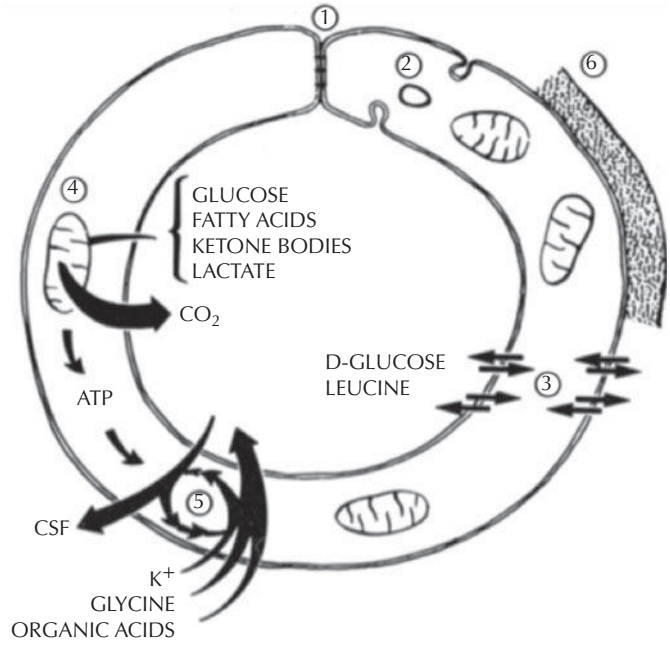

Figure 3–5. Cerebral capillary showing the major features that separate it from a systemic one. (1) Tight junctions. (2) Lack of pinocytosis and increased mitochondria. (3) Specialized transport molecules. (4) High metabolic activity is necessary to provide energy to ATPase pumps. (5) Formation of CSF/ISF. (6) Basal lamina.

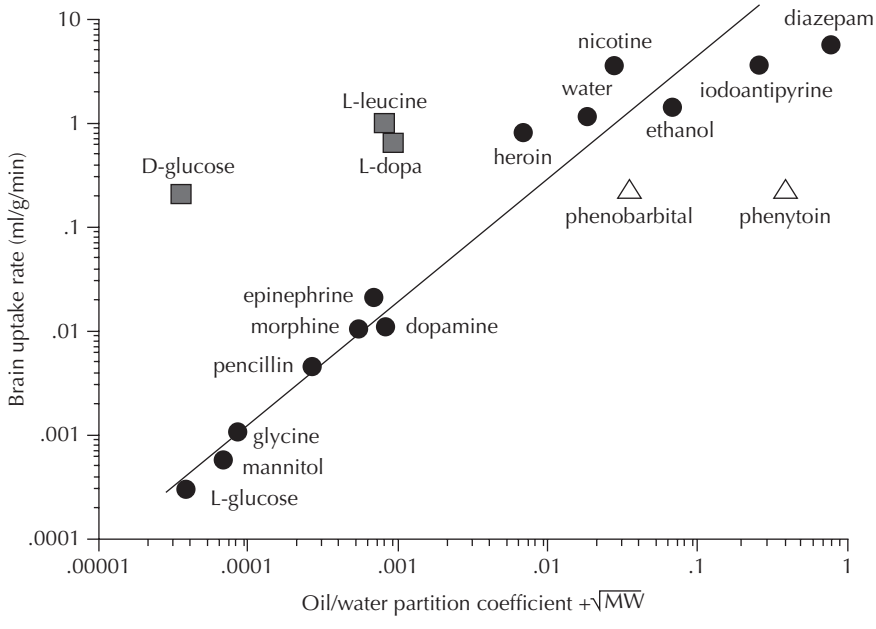

Figure 3–6. Graph showing that the increased brain uptake of various compounds is determined by the lipophilicity (higher oil/water partition coefficient). Drugs of abuse, such as ethanol, heroin, and nicotine, are rapidly taken into brain. (From Ref. 52.)

coefficient. Modification of morphine to create heroin increases its lipid solubility, allowing it to enter the brain more rapidly, which makes it more desirable as a substance of abuse. When a molecule has low permeability and remains in the blood, it can be used as a marker for the size of the vascular space. By contrast, a molecule that is highly permeable can be used to measure cerebral blood flow. Lipid solubility aids the transport of drugs across the BBB. The poor solubility of penicillin limits its access to the brain, making very high concentrations necessary for the treatment of brain diseases. Alternatives to penicillin, such as ampicillin, chloramphenicol, and the new-generation cephalosporins, penetrate into brain more readily than penicillin and are used to treat brain infections. Occasionally, an infection with a bacteria or fungus is sensitive only to a poorly permeable antibiotic, such as the treatment of coccidiomycoses with amphotericin; in that situation, it is necessary to bypass the BBB by the direct injection of the antibiotic intrathecally into the lumbar CSF, intracisternally or occasionally into the ventricles, depending on the site of the infection and the need to have the drug closer to the site. Chemotherapy for brain tumors is another example of the interference of the BBB in treatment. The anticancer drug, methotrexate, is used to treat brain tumors and childhood leukemia. However, because it is relatively impermeable and crosses the BBB slowly, intrathecal injection is often used.

Another unique aspect of the cerebral capillary is its high content of several enzymes. These enzymes metabolize neurotransmitters and limit the transport of these substances into brain. For example, L-dopa decarboxylase metabolizes L-dopa, reducing the amount of circulating L-dopa that can enter the brain. An inhibitor of dopa decarboxylase called *carbidopa* is added to L-dopa to form sinemet for the treatment of Parkinson's disease by dopamine replacement.

P-glycoprotein, an ATP-driven drug efflux transporter, is a critical element of the BBB. High level of expression, luminal membrane location, multispecificity, and high transport potency make P-glycoprotein a selective gatekeeper of the BBB and a primary obstacle to drug delivery into the brain. Expression of P-glycoprotein is modulated by a complex series of signaling pathways: several pathways share common signaling elements, including tumor necrosis factor receptor-1, endothelin B receptor, protein kinase C, and nitric oxide synthase (Figure 3–7). Signaling mechanisms could be blocked, providing potential therapeutic targets that could be used to modulate P-glycoprotein activity and increase drug delivery across the BBB.[30]

GLUCOSE AND AMINO ACID TRANSPORT

Glucose is carried into the brain by facilitated transport.[31] When the concentration of glucose in the blood is low, it is more avidly transported across the capillary by the carrier molecules. However, high concentrations of glucose saturate the carrier molecules. A smaller amount of glucose continues to enter the brain by diffusion. The transport process is described by equations derived from enzyme kinetics, with the carrier molecule acting as the enzyme that causes the reaction to occur but remains unchanged in the process. Carrier molecules specifically transport D-glucose rather than the L-form.

The analysis of glucose movement across the capillary is complicated because glucose is both transported and metabolized. To overcome this limitation, analogs of glucose have been used. One such analog, 3–0-methyl glucose, is transported by the D-glucose carrier but is not metabolized by the tricarboxylic acid cycle, making it a measure of glucose uptake.[32] Another analog of glucose, deoxyglucose, is transported and phosphorylated but not further metabolized, making it a useful tracer for autoradiographic and positron emission tomography (PET) studies of glucose metabolism.[33] An important advance in understanding brain metabolism occurred with the introduction of measurement of glucose metabolism in humans using PET, which is done with analogs of glucose labeled with positron-emitting isotopes.

Glucose transporters in the cerebral capillaries shuttle the glucose molecule from blood to brain. Carrier-mediated transport utilizes specialized proteins to shuttle glucose into the brain; the rate of transport is affected by the plasma glucose concentration. The transport constant term is called K^{T}_{m}. Once glucose is within the cell, its concentration, C_s, affects the formation of metabolic products, C_p, and the metabolic processes are described by $K_m{}^m$. As the plasma concentration of glucose increases, the rate of influx becomes saturated to reach

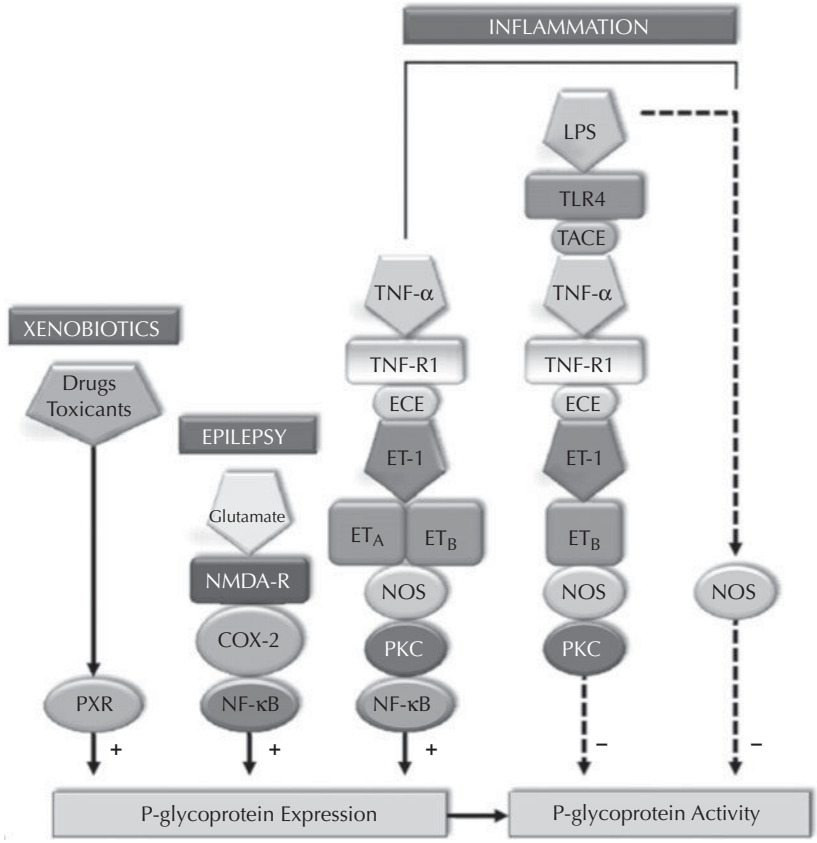

Figure 3–7. Network of signaling mechanisms that modulate P-glycoprotein activity in rodent brain capillaries. Shown is a compilation of signaling pathways disclosed over the past several years by studies on rat and mouse brain capillaries. Each step has been validated using pharmacological tools or knockout mice. At this time, two of these pathways, PXR and glutamate, have been validated in vivo. TLR4, Toll-like receptor 4; TACE, tumor necrosis factor-α converting enzyme; ECE, endothelin converting enzyme; NMDA-R, N-methyl-D-aspartate receptor; COX-2, cyclooxygenase-2; NF-kB, nuclear factor-kB; ET-1, endothelin-1; LPS, lipopolysaccharide; ECE, endothelin converting enzyme; NOS, nitric oxide. (From Ref. 30.)

a maximum; at this point, additional glucose enters by diffusion. Normal plasma levels are close to the estimated Michaelis-Menten constant (K_m) for half-maximum influx. After entering the cell, glucose is metabolized through glycolysis and the Krebs cycle.

The relationship of glucose transport (supply) to glycolysis (demand) is determined from the concentrations of the substrates and K_m. For glucose, the transport step involves molecular movement across the endothelial cell, through the extracellular space, and into the cell. The $K_m{}^T$ for transport is normally 6–10 μmol/mL, which is close to the normal value of glucose in the plasma (7–8 μmol/mL). Low blood glucose levels increase the transport, which is the rate-limiting step in glucose metabolism. Furthermore, high levels of glucose in plasma shift the rate-limiting step into the cell to the phosphorylation step. When the concentration of glucose in plasma is in the normal range, the transport system for brain is close to saturation and transport rather than phosphorylation through hexokinase is rate-limiting.

Amino acids are necessary for the formation of proteins and are abundant in the brain. The excitatory amino acids, glutamate and aspartate, are found in high concentrations. Important neurotransmitter amino acids found in lower concentrations are glycine and gamma-aminobutyric acid (GABA). Other brain amino acids are L-dopa, leucine, phenylalanine, tryptophan, methionine, histidine, and valine. The essential amino acids are required by the brain for protein synthesis and neurotransmission. To ensure the uptake of the essential amino acids into brain, carrier systems are found in the capillaries for their transport.

Carrier systems transport neutral amino acids, basic amino acids, and dicarboxylic amino acids.[34] Neutral amino acids are carried by the L-system (leucine-preferring). Competitive inhibition of the L-system carrier prevents the entry of essential amino acids in the presence of an excess of one of the transported molecules. In the hereditary disorder in which an excess of phenylalanine is present in the blood, competition for the L carrier blocks the entry of tryptophan; serotonin levels in the brain are reduced by the absence of its precursor tryptophan. Individuals with increased phenylalanine in the blood have mental retardation, which can be prevented with a diet low in phenylalanine or high in an amino acid that blocks the entry of phenylalanine.[35] The genetic disorder phenylketonuria is the inability to metabolize phenylalanine. Individuals with this disorder must regulate their intake of phenylalanine to prevent brain damage.

The A-system, which carries α-(methylamino) isobutyric acid into cells, appears to be absent from brain tissue. Glycine enters brain slowly, as does glutamate, *N*-acetylaspartate, and aspartate. Efflux from brain appears to occur actively for the acidic amino acids, glutamate and aspartate. Utilization of amino acids is determined by the rate of their transport across the capillary and the amount of enzyme available in the cell. The amino acids have a low transport rate into the brain and a high enzymatic utilization rate. Therefore, the rate-limiting step is the passage into the brain. Kinetic transport constants are in the range of the serum concentrations for the amino acids; inhibition of transport is thus possible. If the kinetic constants were high and enzyme utilization rates low, the amino acids could be transported easily into the brain and an excess of one amino acid in the serum would not competitively inhibit the entrance of another. Compared to glucose, the rate of entry of the amino acids into brain is slow.

The nonessential amino acids, glutamate and aspartate, are excitatory transmitters in the central nervous system. Glutamate is incorporated into proteins and peptides and is essential in ammonia regulation. The concentration of glutamate in brain is 13.6 μmol/g, compared with 4.4 μmol/g for glutamine, 2.3 μmol/g for GABA, and 0.4 μmol/g for lysine. Although its levels are high, glutamate is compartmentalized and only a very small portion is involved in neurotransmission. Glutamate is important in ammonia metabolism since when ammonia levels are increased, as in hepatic disease, ammonia is detoxified by conversion to glutamine, which is elevated in CSF and brain.

Essential amino acids are maintained in brain at levels close to those in plasma. Competitive inhibition interferes with transport of essential amino acids. Tyrosine, for example, moves into brain across cerebral capillaries by a carrier-mediated transport system. When amino acids using the same carrier are increased, the amount of tyrosine entering brain is reduced. Cells in the substantia nigra normally convert tyrosine into dopamine. In patients with Parkinson's disease, the dopamine-forming cells of the substantia nigra are damaged, and L-dopa is taken orally in order to replace brain dopamine. Large doses of L-dopa are needed to overcome the metabolic loss due to the enzymes dopa decarboxylase in the blood vessels. Carbidopa inhibits dopa decarboxylase so that smaller doses of L-dopa can be used. Tyrosine and L-dopa uptake can be competitively inhibited by the presence of other amino acids after ingestion of protein.

PROTEASES AND THE NEUROVASCULAR UNIT

Neutral proteases serve diverse roles in normal and pathological processes: they regulate molecular events at the cell surface, activate a number of growth factors to promote normal development, and control the death receptors involved in apoptosis. Normally, they remodel the extracellular matrix and participate in angiogenesis and neurogenesis. However, during an injury, they degrade the basal lamina around cerebral blood vessels, opening the BBB, and facilitate programmed cell death (apoptosis). Several classes of enzymes participate in a wide variety of cellular processes in the extracellular space, cytoplasm, and nucleus, including serine proteases, metalloproteinases, and caspases (Figure 3–8). Proteases are important in both normal and pathological processes, often playing dual roles; although self-digestion by proteases damages cells, without a process to clear cellular debris and recycle cellular molecular building blocks, the organisms would die. In many disease processes, enzymatic deficiencies result in so-called storage diseases. Of the neutral proteases, the best studied are the serine proteases and metalloproteinases.

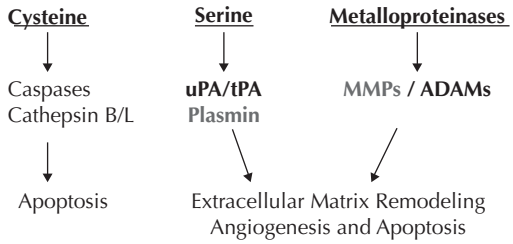

Figure 3–8 Classes of neutral proteases involved in tissue breakdown during injury.

Plasmin is an activator of other proteases and has taken on added importance because of its role in the action of tissue plasminogen activators. Metalloproteinases are the larger class that contains both matrix metalloproteinases (MMPs) and a disintegrin and metalloproteinases (ADAMs). The MMPs and ADAMs have dual natures: in the early stages of an injury they function to promote cell destruction, but later in the recovery phase they have a beneficial role. This duality complicates treatment strategies, which depend on the stage of the injury and its severity. However, when molecules signaling injury are released with infection, ischemia, or trauma, extracellular matrix proteases are induced and initially amplify the damage to the tissues; subsequently, they participate in removal of debris in the injured area.

Interacting with the metalloproteinases are two plasminogen activators, tissue plasminogen activator (tPA) and urokinase plasminogen activator (uPA), which are important in cancer, clotting mechanisms, and angiogenesis.[36,37] Another class of enzymes, the caspases, play a critical role in apoptosis of brain cells. The caspases are activated by intrinsic and extrinsic mechanisms that involve cell surface receptors in the tumor necrosis factor family and mitochondria. Caspases are important in programmed cell death or apoptosis, which is the mechanism the cell uses to break down DNA in the nucleus.

MATRIX METALLOPROTEINASES (MMPS)

The MMP family of proteins shares a common structure with four main domains: the pro-peptide, catalytic, hemopexin-like, and transmembrane domains (Figure 3–9). The pro-peptide domain contains a cysteine residue that bonds with zinc at the active site to form the so-called *cysteine switch*.[38] The binding of cysteine in the catalytic domain blocks the active zinc site, maintaining the latent or inactive state. Although there is continuous production of constitutively expressed MMPs and ADAMs, they remain latent until activated by free radicals or other enzymes through cleavage of the propeptide or breaking of the cysteine bond. The MMPs and ADAMs are primarily extracellular enzymes with a major role in controlling cell surface proteolysis. In addition, they regulate DNA in the cell nucleus.[39,40]

The MMPs are divided into four main subgroups based on domain structure: collagenases, gelatinases, stromelysins, and membrane-type MMPs (MT-MMPs). Collagenases degrade triple-helical fibrillar collagens, which are the major components of bone and cartilage. In the brain, 72 kD type IV collagenase, or gelatinase A (MMP-2), and 92 kDa type IV collagenase, or gelatinase B (MMP-9), have been most intensively studied because of the ease with which they can be identified by gelatin zymography and the prominent role they play in injury and repair (Table 3–6). Gelatinases degrade molecules in the basal lamina around capillaries, facilitate angiogenesis and neurogenesis, and participate in apoptosis. Stromelysins (MMP-3, MMP-10, and MMP-11) and matrilysin (MMP-7) are the smallest proteases in the family; they degrade most components of the extracellular matrix except the triple-helical fibrillar collagens. Membrane-type MMPs contain a furin cleavage site near the propeptide region; they are activated intracellularly by the proconvertase, furin, and the serine protease, plasmin. The MT-MMPs are membrane bound and act at the cell surface as sheddases with a number of important roles, including activation of other proteases, particularly MMP-2, and release and activation of growth factors.

Normally, proteases exist in a latent or inactive state, and proteolysis is tightly regulated to prevent unwanted tissue damage. An example is MMP-2, which is constitutively expressed in astrocytes and found in high concentrations in brain and CSF (Figure 3–10). Under normal conditions, MMP-2 remodels the extracellular matrix. During an injury, it is the first to react since it is already present in relatively large amounts and does not require induction through gene expression, which is a much slower process. The *mmp-2* gene has a promoter region that contains activator protein-2

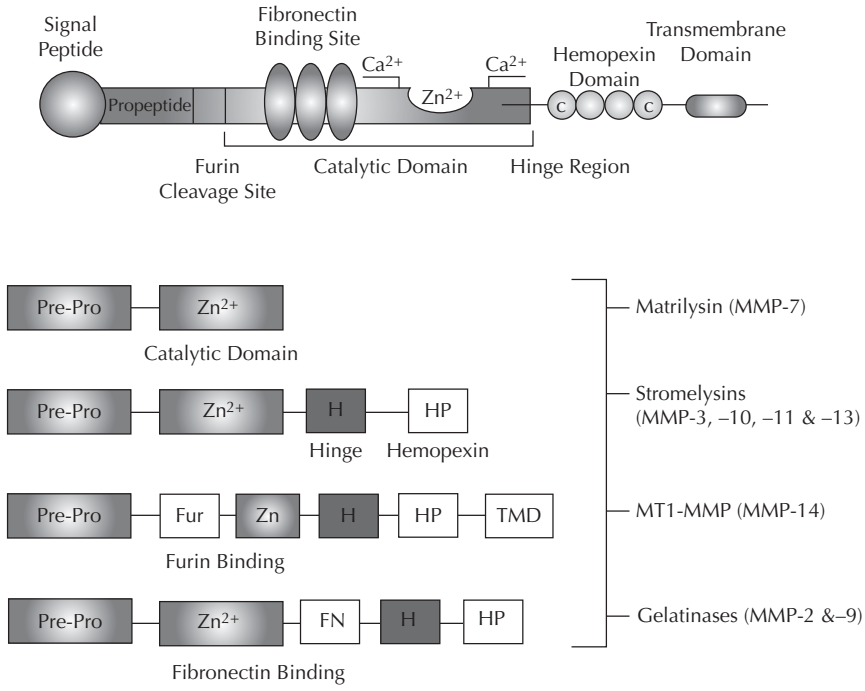

Figure 3–9. The components that make up the basic elements of the MMP molecule are shown in the top illustration. A signal peptide and the propeptide regions are part of the cysteine switch that folds over the zinc and maintains a latent state. A furin (Fur) cleavage site allows the proconvertase, furin, to activate the molecule by cleaving off the propeptide. A fibronectin (FN) binding site is present in the gelatinases (MMP-2 and MMP-9), connecting it with the basal lamina. The catalytic zinc site is present in all MMPs. A hemopexin (HP) domain is joined by a hinge (H) region to the catalytic site. Finally, some MMPs have a transmembrane domain (TMD). The illustration below shows the domains present in the major MMPs. (Adapted from Ref. 41.)

Table 3–6 Major Metalloproteinases in the Central Nervous System and their Endogenous Inhibitors

Name	Function	Inhibitor
Gelatinases (MMP-2 to -9)	Disruption of the BBB, angiogenesis, neurogenesis, remodeling of the basal lamina, regeneration of axons, remyelination, apoptosis	All TIMPs
Stromelysins (MMP-3 to -10) and matrilysin (MMP-7)	Proteolysis of proteins in the ECM, disruption of the BBB, angiogenesis, synaptic remodeling, glutamate receptor proteolysis, apoptosis	All TIMPs
Membrane-type MMP (MT1-MMP or MMP-14)	Forms a trimolecular complex with TIMP-2 and proMMP-2 for activation of MMP-2 at the cell surface	TIMP-3
ADAM10	α-Secretase in amyloid precursor protein proteolysis, degrades the NOTCH protein, acts as sheddase at the cell surface for growth factors, integrins, etc.	TIMP-1 TIMP-3
ADAM17 (TACE)	TACE forms 17 kDa TNF-α from the 28 kDa form, sheddase for TNFRs at the cell surface	TIMP-3

MMP, matrix metalloproteinases; ADAM, *ad*isintegrin *a*nd *m*etalloproteinase; BBB, blood-brain barrier; TIMP, tissue inhibitor of metalloproteinase; ECM, extracellular matrix; TNF, tumor necrosis factor; TACE, TNF-α converting enzyme; TNFRs, TNF receptors.

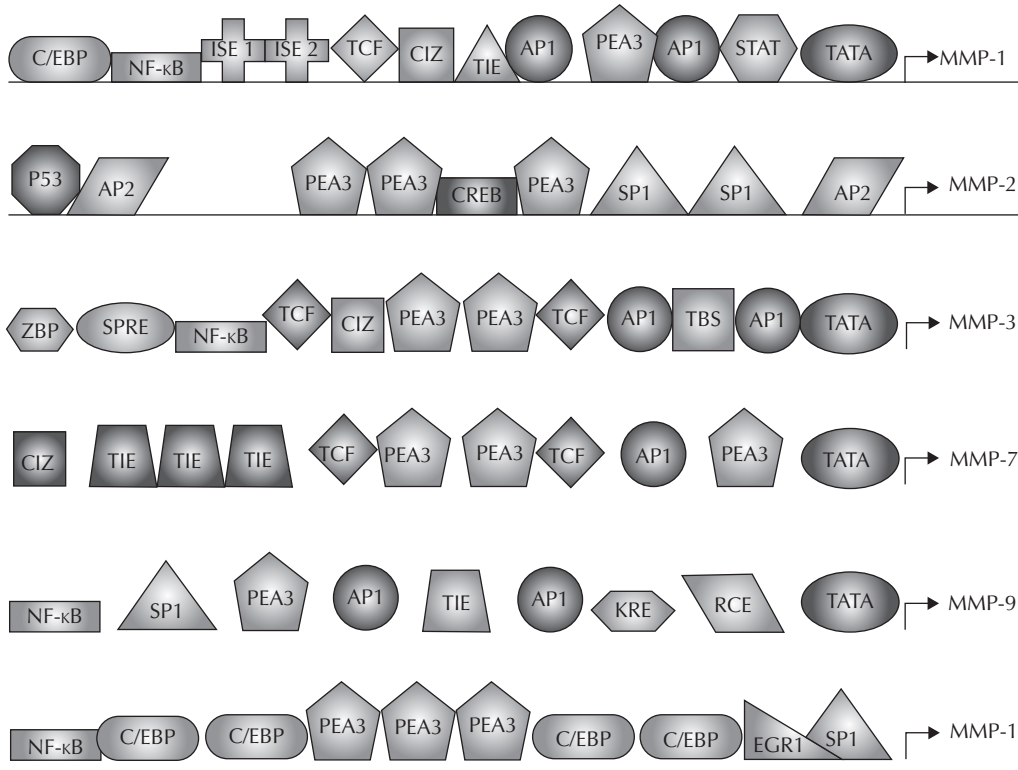

Figure 3–10. The promoter region in the MMP genes. The constitutive enzyme, MMP-2, has AP-2 and SP-1 sites and is present under normal conditions. MMP-1, MMP3, MMP-7, and MMP-9 have AP-1 sites, consistent with expression during inflammation. MMP-14 has an NF-κB site. Transcription-factor-binding sites include: the activator proteins (AP)-1 and -2 site, the core-binding factor 1 (CBFA1) site, the CCAAT/enhancer-binding protein (C/EBP) site, the CAS-interacting zinc-finger protein (CIZ) site, the early growth response-1 (EGR1) site, the immortalization-sensitive elements (ISE)-1, and -2, the keratinocyte differentiation-factor responsive element (KRE), the nuclear factor of B (NF-kB) site, the polyomavirus enhancer-A binding-protein-3 (PEA3) site, the retinoblastoma control element (RCE), the stromelysin-1 platelet-derived growth factor- responsive element (SPRE), the signal transducer and activator of transcription (STAT) site, the TATA-box (TATA), the T-cell factor (TCF) site, the transforming growth factor- inhibitory element (TIE) site, and the binding site for 89-kDa zinc-binding protein (ZBP-89). (Modified from Ref. 41.)

(AP-2), SP-1, and polyomavirus enhancer activation-3 (PEA3) binding sites, while other sites stimulated by cytokines are found in other MMPs[41] (Figure 3–11).

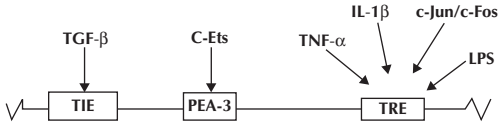

TIE ≡ TGF-β inhibitory element
PEA-3 ≡ Polyoma virus enhancer A-binding protein-3
TRE ≡ Phorbal ester responsive element

Figure 3–11. Transcription factors involved in the expression of various MMPs.

Matrix metalloproteinase-2 is a constitutive enzyme that can be seen by immunohistochemisty in the astrocytic processes, and along with the foot process it surrounds the endothelial cells next to the basal lamina (Figure 3–12). Being next to the basal lamina and the tight junctions is important in its action as a regulator of BBB permeability. Matrix metalloproteinase-2 is activated at the cell surface by membrane type-1 metalloproteinases (MT1-MMP or MMP-14). Activation of MMP-2 involves formation of a trimolecular complex composed of latent MMP-2, tissue inhibitor of metalloproteinases-2 (TIMP-2), and MMP-14. Membrane-bound MMP-14 constrains proteolysis to a small region close to the surface of the cell in the extracellular

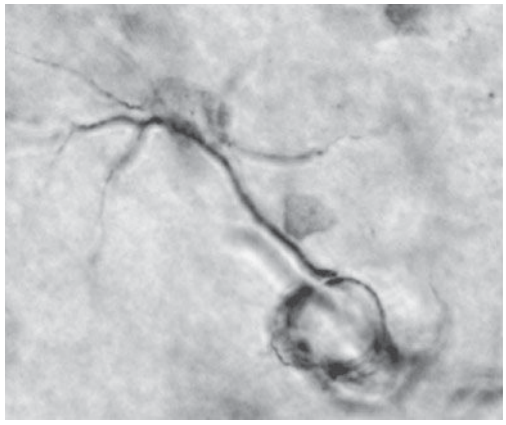

Figure 3–12. An astrocyte is shown that has been immunostained with MMP-2 (brown). The endfoot is seen encircling a small blood vessel. Relatively little immunostaining is seen in the cell body. (See also the color insert.)

space.[42] Inducible enzymes, such as MMP-3 and MMP-9, which are secreted and move about in the extracellular space, cause more extensive damage to the injury site. Both plasmin and furin can activate MMP-3, which is an activator of MMP-9 (Figure 3–13).

The promoter regions of the inducible MMPs, including *mmp-3, mmp-7*, and *mmp-9,* contain binding sites for transcription factors such as activator protein-1 (AP-1) and nuclear factor-κB (NF-κB), which are responsive to cytokines and play an important role in inflammatory responses in the brain. In addition, the *mt1-mmp* gene has an NF-κB binding site, suggesting that it can also be induced during inflammation. The AP-1 sites bind the transcription factors c-jun and c-fos. Cytokines such as tumor necrosis factor-α (TNFα) and interleukin-1β induce MMP-3 and MMP-9 at the transcription level, which

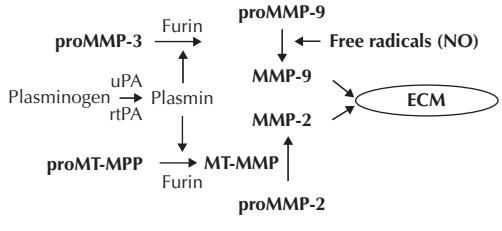

Figure 3–13. Interaction of MMPs and the plasminogen activators and plasmin. Activation of MMPs by plasmin leads to an excessive risk of hemorrhage in tPA treatment of stroke.

is important in the neuroinflammatory response under acute and chronic conditions (Figure 3–11). Since the inducible MMPs are produced in a latent form, similarly to the constitutive proMMP-2, they require activation. In the case of MMP-9, several activation mechanisms have been proposed, including other proteases, such as MMP-3 and free radicals including nitric oxide, which acts through *N*-nitrosylation.[43,44]

Hypoxia-inducible factor-1α (HIF-1α) contributes to the activity of MMP-2. Under conditions of low oxygen, HIF-1α accumulation leads to the expression of the *fur* gene and transcription of the protein Furin, which activates MMP-14, resulting in the activation of MMP-2. In acute ischemia, HIF-1α is elevated; it reverts to low levels after the acute insult. In more chronic situations, such as intermittent hypoxia, HIF-1α may remain elevated for longer periods. How this affects the activation of MMP-2 and other MMPs remains to be resolved.

A DISINTEGRIN AND METALLOPROTEINASE (ADAM)

The ADAMs are transmembrane proteins that bind to integrins and are important in intracellular signaling and cell adhesion.[45] While a number of ADAM members have been identified in this branch of the metalloproteinase family, the functions of only a few of them are known in brain (Table 3–6). The subunits of the ADAMs are comprised of a catalytic domain at the end of the extracellular extension, which is connected to three domains: a disintegrin, a cysteine-rich region, and epidermal growth factor (EGF) repeats. The cytoplasmic tail attached to an EGF domain protrudes through the membrane and signals cell surface events to the cytoplasm.[46] The disintegrin domain binds to integrins, while the cysteine-rich region interacts with proteoglycans. The catalytic region of the ADAMs molecules release bound proteins from the extracellular matrix and the cell surface through a process called *ectodomain shedding*. Several important examples of their role in the central nervous system include the processing of amyloid precursor protein (APP) and transforming growth factor-α (TGF-α). They are involved in proliferation, migration, differentiation, and

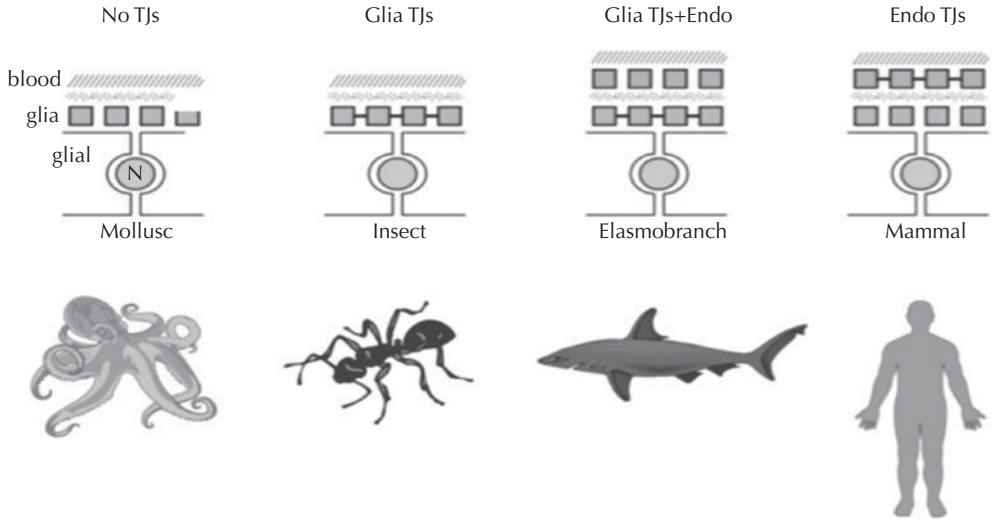

Figure 3–14. Modification of vascular barriers in several species. Molluscs have a glial barrier without tight junctions. Insects have a more restricted glial barrier. An endothelial cell without tight junctions has developed in the elasmobranch family that is situated above a restrictive glial layer of cells. In mammals, the restrictive barrier is in the endothelial cells rather than the glial cells. (Derived from Ref. 53.)

survival, as well as axonal growth and myelination.[47] ADAM10 is an α-secretase for APP.[48] Another example of the action of the ADAMs is the role of tumor necrosis factor-α converting enzyme (ADAM17) in the activation of TNF-α to form the active species.[49]

BARRIER SYSTEMS EVOLVED TO AN ENDOTHELIAL BARRIER

Understanding of the neurovascular unit in humans can be aided by placing it in an evolutionary perspective. Moving down the evolutionary tree, the importance of the cell layers beyond the capillaries can be more easily seen. The evolution of tight junctions at the endothelial cells is a late occurrence in evolutionary time. Earlier species had a variety of solutions to the problem of isolating the brain. They used cells beyond the endothelial layer to restrict transport between blood and brain. In the elasmobranch family, which includes the shark and skate, there is a glial rather than an endothelial barrier. Insects also have a glial barrier, while lower molluscs have no barrier (Figure 3–14). Insects have a structured extracellular matrix with acidic glycosaminoglycans and hyaluronic acid. The shifting of the barrier from cells beyond the endothelium to the endothelium itself provided a more protected environment for neural function. Moving away from the extracellular matrix, which was important in ion binding in crustaceans and cephalopods to the highly organized structure of the mammalian brain, involved shifting of the barrier sites from glial cells to endothelium.[50]

REFERENCES

1. Reese TS, Karnovsky MJ. Fine structural localization of a blood-brain barrier to exogenous peroxidase. *J Cell Biol*. 1967;34:207–217.
2. Ballabh P, Braun A, Nedergaard M. The blood-brain barrier: an overview: structure, regulation, and clinical implications. *Neurobiol Dis*. 2004;16:1–13.
3. Iadecola C, Nedergaard M. Glial regulation of the cerebral microvasculature. *Nat Neurosci*. 2007;10: 1369–1376.
4. Hawkins BT, Davis TP. The blood-brain barrier/neurovascular unit in health and disease. *Pharmacol Rev*. 2005;57:173–185.
5. Furuse M, Hirase T, Itoh M, et al. Occludin: a novel integral membrane protein localizing at tight junctions. *J Cell Biol*. 1993;123:1777–1788.
6. Hirase T, Staddon JM, Saitou M, et al. Occludin as a possible determinant of tight junction permeability in endothelial cells. *J Cell Sci*. 1997;110:1603–1613.
7. Morgan L, Shah B, Rivers LE, et al. Inflammation and dephosphorylation of the tight junction protein occludin in an experimental model of multiple sclerosis. *Neuroscience*. 2007;147:664–673.

8. Furuse M, Fujita K, Hiiragi T, et al. Claudin-1 and -2: novel integral membrane proteins localizing at tight junctions with no sequence similarity to occludin. *J Cell Biol*. 1998;141:1539–1550.
9. Wolburg H, Wolburg-Buchholz K, Kraus J, et al. Localization of claudin-3 in tight junctions of the blood-brain barrier is selectively lost during experimental autoimmune encephalomyelitis and human glioblastoma multiforme. *Acta Neuropathol* (*Berl*). 2003;105:586–592
10. Nitta T, Hata M, Gotoh S, et al. Size-selective loosening of the blood-brain barrier in claudin-5-deficient mice. *J Cell Biol*. 2003;161:653–660.
11. Zlokovic BV. The blood-brain barrier in health and chronic neurodegenerative disorders. *Neuron*. 2008; 57:178–201.
12. Perry VH, Gordon S. Macrophages and microglia in the nervous system [review]. *Trends Neurosci*. 1988;11: 273–277.
13. Dore-Duffy P, Katychev A, Wang X, et al. Cns microvascular pericytes exhibit multipotential stem cell activity. *J Cereb Blood Flow Metab*. 2006;26:613–624.
14. Daneman R, Zhou L, Kebede AA, et al. Pericytes are required for blood-brain barrier integrity during embryogenesis. *Nature*. 2010;468:562–566.
15. Bell RD, Winkler EA, Sagare AP, et al. Pericytes control key neurovascular functions and neuronal phenotype in the adult brain and during brain aging. *Neuron*. 2010;68:409–427.
16. Kokovay E, Li L, Cunningham LA. Angiogenic recruitment of pericytes from bone marrow after stroke. *J Cereb Blood Flow Metab*. 2006;26:545–555.
17. Krizanac-Bengez L, Hossain M, Fazio V, et al. Loss of flow induces leukocyte-mediated mmp/timp imbalance in dynamic in vitro blood-brain barrier model: role of pro-inflammatory cytokines. *Am J Physiol Cell Physiol*. 2006;291:C740-C.749
18. Del Zoppo GJ, Milner R, Mabuchi T, et al. Vascular matrix adhesion and the blood-brain barrier. *Biochem Soc Trans*. 2006;34:1261–1266.
19. Engelhardt B. Immune cell entry into the central nervous system: involvement of adhesion molecules and chemokines. *J Neurol Sci*. 2008;274:23–26.
20. Paterson PY. Experimental allergic encephalomyelitis: role of fibrin deposition in immunopathogenesis of inflammation in rats. *Fed Proc*. 1976;35:2428–2434.
21. Tubridy N, Behan PO, Capildeo R, et al. The effect of anti-alpha4 integrin antibody on brain lesion activity in ms. The uk antegren study group. *Neurology*. 1999;53:466–472.
22. Coisne C, Mao W, Engelhardt B. Cutting edge: natalizumab blocks adhesion but not initial contact of human t cells to the blood-brain barrier in vivo in an animal model of multiple sclerosis. *J Immunol*. 2009;182: 5909–5913.
23. Linda H, von Heijne A, Major EO, et al. Progressive multifocal leukoencephalopathy after natalizumab monotherapy. *N Engl J Med*. 2009;361:1081–1087.
24. Simard M, Arcuino G, Takano T, et al. Signaling at the gliovascular interface. *J Neurosci*. 2003;23:9254–9262.
25. Kang J, Kang N, Lovatt D, et al. Connexin 43 hemichannels are permeable to atp. *J Neurosci*. 2008;28: 4702–4711.
26. Crone C, Christensen O. Electrical resistance of a capillary endothelium. *J Gen Physiol*. 1981;77:349–371.
27. Bradbury MW. The structure and function of the blood-brain barrier [review; 56 refs]. *Fed Proc*. 1984;43:186–190.
28. Stewart PA, Wiley MJ. Developing nervous tissue induces formation of blood-brain barrier characteristics in invading endothelial cells: a study using quail-chick transplantation chimeras. *Dev Biol*. 1981;84: 183–192.
29. Oldendorf WH, Cornford ME, Brown WJ. The large apparent work capability of the blood-brain barrier: a study of the mitochondrial content of capillary endothelial cells in brain and other tissues of the rat. *Ann Neurol*. 1977;1:409–417.
30. Miller DS, Bauer B, Hartz AM. Modulation of P-glycoprotein at the blood-brain barrier: Opportunities to improve central nervous system pharmacotherapy. *Pharmacol Rev*. 2008;60:196–209.
31. Crone C. Facilitated transfer of glucose from blood into brain tissue. *J Physiol*. 1965;181:103–113.
32. Pardridge WM, Oldendorf WH. Kinetic analysis of blood-brain barrier transport of amino acids. *Biochim Biophys Acta*. 1975;401:128–136.
33. Sokoloff L. Relationships among local functional activity, energy metabolism, and blood flow in the central nervous system. *Fed Proc*. 1981;40:2311–2316.
34. Lajtha A, Wolstenholme GEW, Fitzsimons DW. Amino acid transport in the brain in vivo and in vitro. In: Wurtman RJ, ed. *Ciba Symposium on Aromatic Amino Acids in the Brain*. Amsterdam: Elsevier; 1974: 25–41.
35. Choi TB, Pardridge WM. Phenylalanine transport at the human blood-brain barrier. Studies with isolated human brain capillaries. *J Biol Chem*. 1986;261: 6536–6541.
36. Mignatti P, Rifkin DB. Plasminogen activators and matrix metalloproteinases in angiogenesis [review]. *Enzyme Protein*. 1996;49:117–137.
37. Hacke W, Furlan AJ, Al-Rawi Y, et al. Intravenous desmoteplase in patients with acute ischaemic stroke selected by mri perfusion-diffusion weighted imaging or perfusion ct (DIAS-2): a prospective, randomised, double-blind, placebo-controlled study. *Lancet Neurol*. 2009;8:141–150.
38. Van Wart HE, Birkedal Hansen H. The cysteine switch: a principle of regulation of metalloproteinase activity with potential applicability to the entire matrix metalloproteinase gene family. *Proc Natl Acad Sci USA*. 1990;87:5578–5582.
39. Kim YS, Kim SS, Cho JJ, et al. Matrix metalloproteinase-3: a novel signaling proteinase from apoptotic neuronal cells that activates microglia. *J Neurosci*. 2005;25:3701–3711.
40. Yang Y, Candelario-Jalil E, Thompson JF, et al. Increased intranuclear matrix metalloproteinase activity in neurons interferes with oxidative DNA repair in focal cerebral ischemia. *J Neurochem*. 2010;112: 134–149.
41. Overall CM, Lopez-Otin C. Strategies for mmp inhibition in cancer: innovations for the post-trial era. *Nat Rev Cancer*. 2002;2:657–672.
42. Strongin AY, Collier I, Bannikov G, et al. Mechanism of cell surface activation of 72-kda type iv collagenase. Isolation of the activated form of the membrane metalloprotease. *J Biol Chem*. 1995;270:5331–5338.
43. Nagase H. Activation mechanisms of matrix metalloproteinases [review]. *Biol Chem*. 1997;378:151–160.
44. Gu Z, Kaul M, Yan B, et al. S-nitrosylation of matrix metalloproteinases: signaling pathway to neuronal cell death. *Science*. 2002;297:1186–1190.

45. Blobel CP. Remarkable roles of proteolysis on and beyond the cell surface. *Curr Opin Cell Biol*. 2000;12: 606–612.
46. Yong VW. Metalloproteinases: mediators of pathology and regeneration in the cns. *Nat Rev Neurosci*. 2005;6:931–944.
47. Cauwe B, Van den Steen PE, Opdenakker G. The biochemical, biological, and pathological kaleidoscope of cell surface substrates processed by matrix metalloproteinases. *Crit Rev Biochem Mol Biol*. 2007;42:113–185.
48. Buxbaum JD, Liu KN, Luo Y, et al. Evidence that tumor necrosis factor alpha converting enzyme is involved in regulated alpha-secretase cleavage of the alzheimer amyloid protein precursor. *J Biol Chem*. 1998;273:27765–27767.
49. Gearing AJ, Beckett P, Christodoulou M, et al. Processing of tumour necrosis factor-alpha precursor by metalloproteinases. *Nature*. 1994;370:555–557.
50. Abbott NJ. Dynamics of cns barriers: evolution, differentiation, and modulation. *Cell Mol Neurobiol*. 2005;25:5–23.

This page intentionally left blank

PART 2

Metabolism, Disorders of Brain Fluids, and Mathematics of Transport

This page intentionally left blank

Chapter 4

Glucose, Amino Acid, and Lipid Metabolism

GLUCOSE METABOLISM

Brain glucose is metabolized to produce energy for cellular work or is converted into amino acids and lipids or other molecules for energy storage and protein synthesis. Because relatively little glucose is stored in brain tissue, it must be constantly replenished to maintain cellular function. Oxidative phosphorylation is the major pathway of energy production from glucose via the tricarboxylic acid (TCA) or Krebs cycle. Glucose is transported into the cell for glycolysis by specialized glucose transporters using a carrier-mediated mechanism. The glucose molecule is initially phosphorylated by hexokinase into glucose-6-phosphate before conversion by phosphofructokinase into fructose-1, 6-diphosphate. Then it is split into glyceraldehyde-3-phosphate and dihydroxyacetone phosphate. Phosphofructokinase is the rate-limiting enzyme: adenosine triphosphate (ATP), plasma creatinine (PCr), and citrate suppress its activity to reduce glycolysis, and adenosine diphosphate (ADP), inorganic phosphate (P_i), adenosine monophosphate (AMP), cyclic 3, 5-AMP, and NH^{4+} activate it when energy supplies need to be refurbished. The final products of glycolysis are pyruvate and lactate (Figure 4–1).

Pyruvate enters the Krebs cycle, which is crucial for production of the reduced nicotinamide adenine dinucleotide (NADH) needed to replenish ATP in the respiratory chain. Acetyl coenzyme A (CoA) is formed by fatty acid oxidation and amino acid breakdown. Acetyl CoA enters the cycle by forming citric acid after joining with oxaloacetate. Succeeding steps of metabolism convert citrate into α-ketoglutaric acid, succinic acid, fumaric acid, malic acid, and finally back to oxaloacetic acid, completing the cycle; α-ketoglutaric acid is metabolized to glutamate. One turn of the Krebs cycle makes 3 moles of reduced NADH; the NADH releases energy in the respiratory chain as electrons flow from it to oxygen:

$$NADH + {}^1/_2O_2 + H^+ \rightarrow NAD + H_2O$$

From glycolysis of glucose to pyruvate, 6 moles of ATP are formed:

$$\text{Glucose} + 2\ NAD + 2\ ADP + 2\ P_i \rightarrow 2\ \text{Pyruvate} + 2\ NADH + 2\ H_2O + 2\ ATP$$

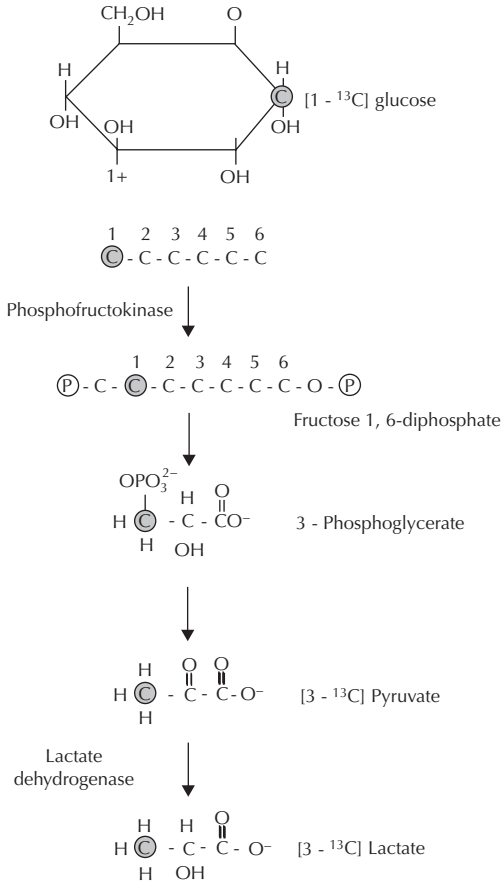

Figure 4–1. Glycolytic pathway to convert glucose into pyruvate and lactate. [1–^{13}C] glucose is converted into [3–^{13}C] lactate. The ability to follow ^{13}C-labeled compounds by nuclear magnetic resonance provides a means to determine metabolic pathways precisely.

Each NADH molecule that is formed outside the mitochondria and metabolized inside yields 2 ATP because of the loss of reducing potential during transport, accounting for the total of 6 ATP. Thus,

$$2\ \text{NADH} + 4\ \text{P}_\text{i} + 4\ \text{ADP} + \text{O}_2 \rightarrow 2\ \text{NAD} + 6\ \text{H}_2\text{O} + 4\ \text{ATP}$$

Formation of 2 acetyl CoA from 2 pyruvates inside the mitochondria yields 6 moles of ATP:

$$2\ \text{Pyruvate} + 2\ \text{NAD CoA} \rightarrow 2\ \text{Acetyl CoA} + 2\ \text{CO}_2 + 2\ \text{NADH}$$

$$2\ \text{NADH} + 6\ \text{P}_\text{i} + 6\ \text{ADP} + \text{O}_2 \rightarrow 2\ \text{NAD} + 8\ \text{H}_2\text{O} + 6\ \text{ATP}$$

Finally, as 2 molecules of acetate go through the Krebs cycle and the respiratory chain, additional ATP are formed:

$$2\ \text{Acetate} + 24\ \text{P}_\text{i} + 24\ \text{ADP} + 4\ \text{O}_2 \rightarrow 4\ \text{CO}_2 + 28\ \text{H}_2\text{O} + 24\ \text{ATP}$$

The energy yield from the complete metabolism of glucose is given by

$$\text{Glucose} + 36\ \text{P}_\text{i} + 36\ \text{ADP} + 6\ \text{O}_2 \rightarrow 6\ \text{CO}_2 + 42\ \text{H}_2\text{O} + 36\ \text{ATP}$$

Therefore, the transfer of energy from glucose to ATP is a highly efficient process that effectively allows the intact cell to burn glucose into calories for use and storage rather than for generation of heat. In the process of forming ATP, water is formed, which most likely is the "metabolic water" in the ISF.

Aerobic glycolysis provides both sources of energy in the form of ATP and NADH, but also forms the substrates that enter the TCA cycle to complete the metabolic process by the action of the respiratory chain. A substantial amount of the glucose is stored as amino acids, particularly glutamate, which has a high concentration in the brain, generally in the 10 mM range. Shuttling of amino acids into and out of the TCA cycle ensures sufficient neurotransmitters and energy substrates. In pathological conditions there is loss of oxygen, bringing the metabolic machinery to an abrupt halt and eventually depleting the neurotransmitter pools. Similarly, hypoglycemia with sufficient oxygen causes a more gradual onset of energy depletion, but the end result is cell death.

AMINO ACID NEUROTRANSMITTERS

Glutamate is the main excitatory neurotransmitter substance and gamma-aminobutyric acid (GABA) is the major inhibitory transmitter in brain. Only a small portion of the glutamate is used in neurotransmission, with the major portion sequestered in compartments for later use. High concentrations of glutamate are released into the synaptic clefts during a number of brain insults. Normally, flooding of the extracellular space with an excitatory neurotransmitter is prevented by the

compartmentalization of glutamate. In addition to the protection afforded by compartmentalization, there is conservation of the glutamate by a complex distribution of enzymes that control glutamate metabolism; some of these enzymes are present in glial cells, while others are present only in neurons.

The enzymes involved in glutamate/GABA metabolism are listed in Table 4–1. Gamma-aminobutyric acid is formed irreversibly from glutamate via the enzyme glutamic acid decarboxylase (GAD). Once formed, GABA may be released into the synaptic cleft, acting on GABA receptors to inhibit membrane firing. After glutamate is released, it can be taken up into neurons and astrocytes. Uptake mechanisms on the astrocytes control the concentration of glutamate in the synaptic cleft, keeping it at safe levels. Conversion of glutamate to glutamine occurs through the action of glutamine synthetase in glial cells. Glutamine can be transferred back into the neuron, while glutamate transport is restricted.

There are two routes for pyruvate metabolism that depend on the enzymes involved. The majority of pyruvate formed by glycolysis goes through pyruvate dehydrogenase (PDH) into acetylCoA and then into the TCA cycle. Glutamate dehydrogenase (GDH) converts α-ketoglutamate into glutamate, which can be further converted into GABA by GAD in the GABAergic neurons. An alternative route for pyruvate to enter the TCA cycle is through pyruvate carboxylase (PC), which is an anapleuritic reaction that restores carbon molecules that are depleted in the PDH pathway. Joining CO_2 to pyruvate, PC creates oxaloacetate, which enters the TCA cycle to form α-ketoglutarate, glutamine. and GABA (Figure 4–2).

Table 4–1 **Enzymes Involved in Glutamate and GABA Metabolism**

Enzyme	Action
Glutamate oxaloacetate aminotransferase (GOT)	Transmination between glutamate/α-ketoglutarate and aspartate/oxaloacetate
Glutamine synthetase (GLU-S)	Glutamine synthesis from glutamate and ammonia (ATP needed)
Glutamic acid decarboxylase (GAD)	GABA formation from glutamate
GABA transaminase (GABA-T)	GABA metabolism to succinate semialdehyde
Glutaminase (GLU-N)	Converts glutamine into glutamate

Once inside the cells, GABA-transaminase (GABA-T) and a dehydrogenase return it to the TCA cycle as succinate. The return of GABA to the TCA cycle is referred to as the *GABA shunt* (Figure 4–3). The enzymes GABA-T and succinic semialdehyde dehydrogenase (SSA) are located in the mitochondria. Nerve cell endings contain the enzyme GAD in the cytosol. Glial cells lack GAD; they can convert glutamate via glutamine synthetase into glutamine. α-Ketoglutarate available from the Krebs cycle, is converted into glutamate by GABA-T in the mitochondria.

Radioisotope studies have shown that there are two pools of glutamate: ^{14}C-glucose is mainly metabolized to glutamate, while ^{14}C-acetate is metabolized to glutamine. One pool is used for energy generation and the other for neurotransmitters.[1] Glucose and pyruvate enter both pools, while acetate, acetaldelyde, proprionate, butyrate, citrate, GABA, glutamate, aspartate, leucine, bicarbonate, ammonia, and succinate enter the small pool. A model has been proposed in which the GAD-containing neurons make GABA from glutamate for use in neurotransmission, while its catabolism occurs via the GABA shunt in the astrocytes, where it is converted by GABA-T into glutamate and by glutamine synthetase into glutamine. The glutamine is then transported to the neuron for reconversion into GABA (Figure 4–3).

Analysis of the TCA cycle has been done with ^{14}C-labeled substrates; radioactively labeled molecules show the total concentration of metabolic products, but they require chemical separations for full characterization of the metabolites. Nuclear magnetic resonance (NMR) spectroscopy uses differences in the energy levels of different protons attached to carbon atoms to map the location of an NMR-labeled compound in a molecule. Because ^{13}C has a magnetic moment, NMR can detect the location of the labeled carbon. This unique feature of NMR provides an accurate map of the metabolism of compounds enriched with ^{13}C. Use of ^{13}C labeling with NMR spectroscopy avoids the necessity for cumbersome chemical extractions and offers the possibility of in vivo studies. Thus, ^{13}C labeling and NMR provide a means to follow and completely characterize the passage of a labeled substrate through

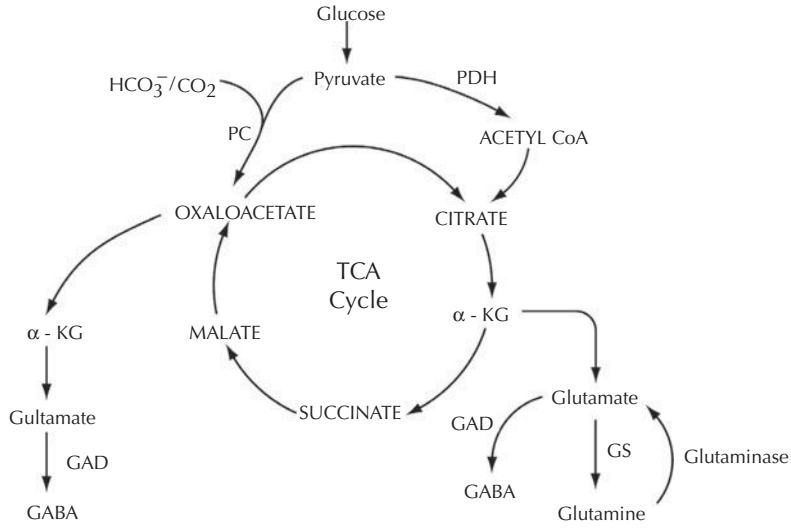

Figure 4–2. Glutamate and GABA synthesis in the TCA cycle starts with glucose. Pyruvate dehydrogenase (PDH) converts pyruvate to acetyl CoA. Glutamate dehydrogenase (GDH) forms glutamate. Conversion of glutamate to glutamine is done with glutamine synthetase (GS), and conversion back to glutamate uses glutaminase. Replenishment of carbon skeletons occurs through the pyruvate carboxylase (PC) pathway with glutamate and GABA formation. Glutamic acid decarboxylase (GAD) is necessary for conversion of glutamate to GABA. α-Ketoglutarate (α-KG) is an important intermediate in the production of glutamate.

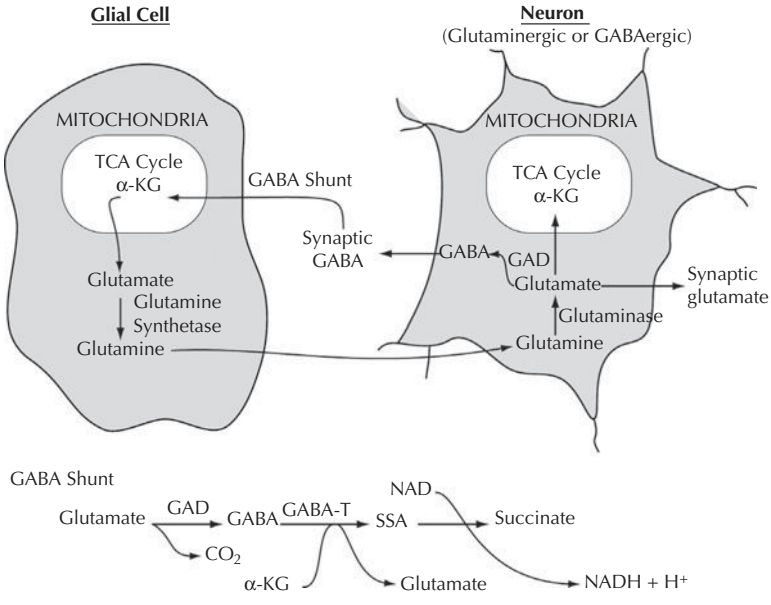

Figure 4–3. Exchange of glutamate between glial cells and neurons uses glutamine since glutamate cannot easily cross membranes. Glutamate formed in glial cells is converted to glutamine by glutamine synthetase, which is found only in glia. Glutamine transfers to the neuron, where glutaminase converts it back into glutamate for use in synaptic transmission, or it is stored for later metabolic energy. A neuron may be glutaminergic or GABAergic. Gamma-aminobutric acid does not penetrate the BBB and is therefore synthesized in vivo, using the enzyme L-glutamic acid decarboxylase (GAD) and pyridoxal phosphate (which is the active form of vitamin B_6) as a cofactor via a metabolic pathway called the *GABA shunt*. This process converts glutamate, the principal excitatory neurotransmitter, into the principal inhibitory neurotransmitter (GABA). α-KG, α-ketoglutarate; GABA-T, GABA-transaminase; SSA, succinic semialdehyde; NAD, nicotinic acid dehydrogenase; NADH, reduced nicotinamide adenine denucleotide.

glycolysis and the TCA cycle. An example of the use of ^{13}C labeling in metabolic studies is the metabolism of glucose labeled with ^{13}C in the 1 position, which becomes lactate labeled in the 3 position (see Figure 4–1). In the presence of oxygen, pyruvate is decarboxylated to acetyl CoA, which enters the Krebs cycle.

Following injection of [1–^{13}C]glucose into pentobarbital-anesthetized rats, it is converted mainly into [4–^{13}C]glutamate in the TCA cycle by the action of pyruvate decarboxylase. Ninety percent of the labeled glucose appears in [4–^{13}C] glutamate via PDH, while 10% is metabolized by pyruvate carboxylase to [2–^{13}C] glutamate.[2] The metabolism of [1–^{13}C]-glucose by pyruvate carboxylase occurs by the anaplerotic reaction in which oxaloacetate is formed; the ^{13}C label, therefore, is in the second carbon of glutamate and the fourth carbon of GABA. The location of the ^{13}C in GABA indicates the metabolic pathway followed. For example, [4–^{13}C]GABA is a product of pyruvate carboxylase, while [2–^{13}C]-GABA formed from [4–^{13}C]glutamate is a product of PDH (Figure 4–4).

The morphological basis of the current model of glutamate-glutamine interaction is

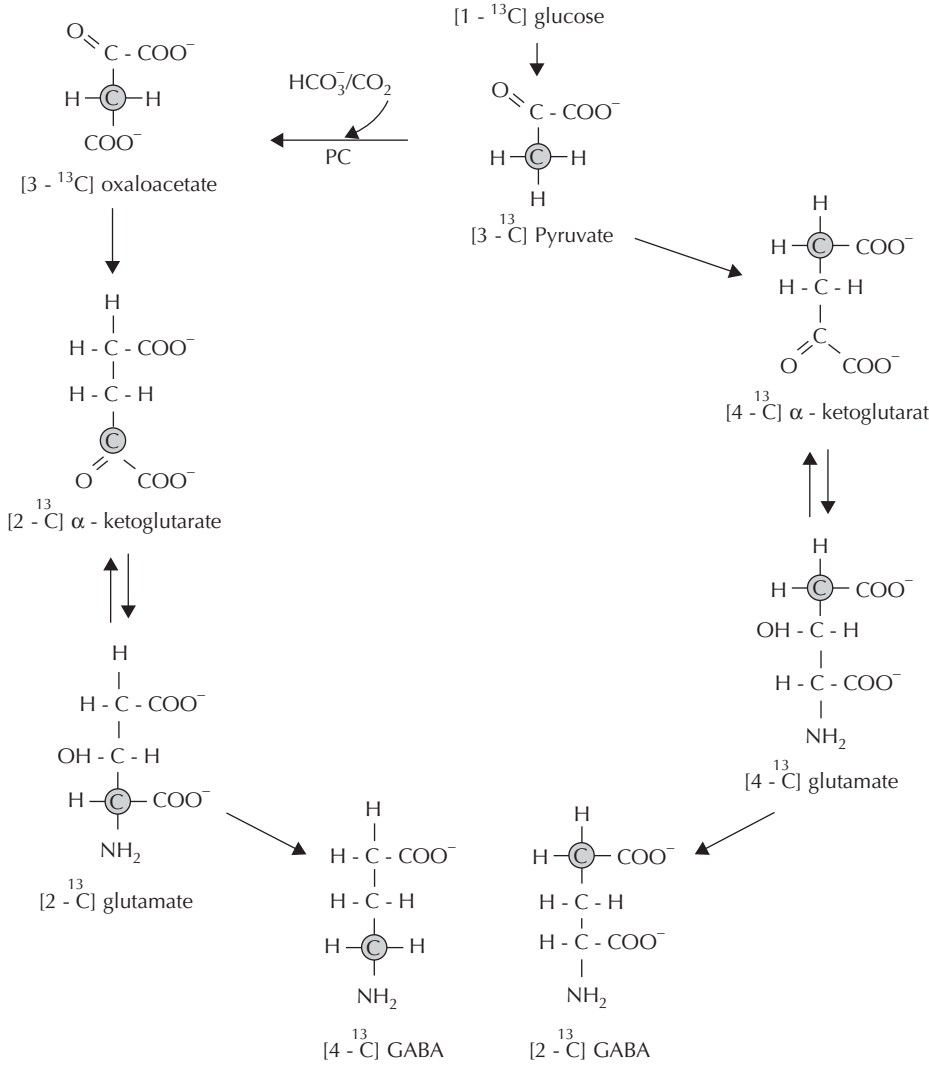

Figure 4–4. The metabolic pathway for GABA can be determined with [1–^{13}C] glucose. When the PC pathway is used, [4–^{13}C]GABA is the product, but PDH leads to [2–^{13}C] GABA.

controversial. Problems with isolation of pure fractions and possible differences between species have complicated the interpretation of data.[3] A major problem with the current model is the slow uptake of glutamine by neurons, which is important in the conversion of glutamine to glutamate in the neuron. Labeling of cortical glutamate and glutamine during a [2–^{13}C]glucose or [5–^{13}C]glucose infusion with a multicompartment model provides a way to assess the glutamate/glutamine cycle. About 75% of glucose oxidation in the neuronal pathway goes into the glutamate/glutamine cycle in the cerebral cortex of anesthetized rats. The glutamate/glutamine cycle is the predominant pathway of astrocyte/neuron glutamate substrate trafficking, accounting for at least 70% of the total flux. Anaplerosis accounts for 20%–25% of total glutamine synthesis under normoammonemic conditions. When the ammonia levels are increased, anaplerotic glutamine synthesis is directly coupled to nitrogen removal (ammonia detoxification).[4]

LIPID METABOLISM

Brain tissue has a high content of lipids. Cholesterol, sphingolipids, and glycerophospholipids comprise the three major categories of brain lipids.[5] Cholesterol is important in membrane structure for all cells, including those of brain tissue. Sphingolipids are important components of the myelin sheath. Glycerophospholipids are important in lipid metabolism since they play a role in normal metabolism and they release substances that lead to cellular disruption.

Glycerophospholipids are formed around the glycerol backbone. Two long chain fatty acids are present, along with a phosphate-linked substance from which the molecule derives its name (Figure 4–5). Fatty acids are named by the length of their chains, a, and the number of unsaturated double bonds, b (a:b). The commonly occurring ones are palmitic (16:0), stearic (18:0), and arachidonic (20:4) fatty acids; less commonly found in brain membranes are oleic (18:1) and linoleic (18:2) fatty acids. For example, phosphatidylinositol contains 45.5% arachidonic, 34.4% stearic, 9.5% palmitic, 6.4% oleic, and 2.3% docosahexaenoic acids.

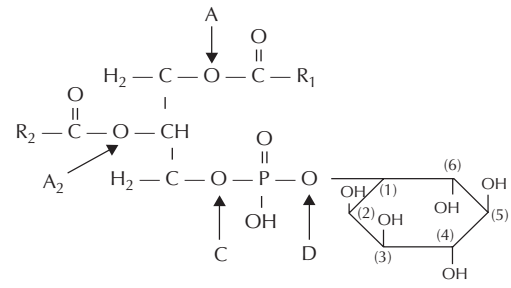

Figure 4–5. The basic structure of a phospholipid with molecules substituted at R_1, R_2, and A. Sites of cleavage of phosphatidylinositol by phosphospholipases (A, A_2, C, and D).

Phosphatidylethanolamine contains 12.5% arachidonic acid and 40.2% plasmalogen, while phosphatidylcholine has 46.9% palmitic acid and 6% arachidonic acid. This information is important in attempting to understand the mechanism of fatty acid release during brain injury. Phosphatidylinositol appears to play a central role in the release of arachidonic acid, which damages cells through its metabolic products.

Snake venom and pancreatic enzymes contain large amounts of phospholipase A_2 in a soluble, easily extractable form, making it convenient to study. In the pancreas, trypsin activates the enzyme. However, there are also phospholipases associated with membranes. A phospholipase A_2 has been purified from rat liver mitochondria, which is bound to membranes and present in low concentrations that are in continuous contact with an excess of substrate. When respiration of the mitochondria is reduced, the enzyme is activated and hydrolyzes membranes.

Phospholipase C, which releases inositol from phosphoinosital, has been identified in brain, muscle, platelets, and seminal fluid. The enzyme is important in the phosphatidylinositol cycle, where it hydrolyzes phosphatidylinositol to diacylglcerol and inositol 1, 4, 5-triphosphate. Both diacylglcerol and inositol triphosphate play important roles: diacylglcerol is the signaling molecule that acts at the membrane to activate protein kinase C, while inositol triphosphate works in the cytosol to mobilize Ca^{2+} from the endoplasmic reticulum. When Ca^{2+} is elevated, phospholipase A_2 is activated and forms arachidonic acid and docosahexanoic acid (DHA); both of these acids are important precursors of bioactive lipids that

act as dual messengers by modulating normal cellular function and mediating inflammatory responses to injury.

Arachidonic acid is a C20 fatty acid that is the precursor of a group of molecules collectively termed the *eicosanoids*. These include prostaglandins, thromboxanes, leukotrienes, and hydroxy-eicosanoic acids. The eicosanoids are formed by the action of cyclooxygenase and lipoxygenase in the presence of oxygen. Arachidonic acid is one of the essential fatty acids required by most mammals. Some mammals lack the ability to convert linoleic acid into arachidonic acid, making it an essential part of their diet. Since little or no arachidonic acid is found in common plants, such animals are obligate carnivores.

Arachidonic acid is one of the most abundant fatty acids in the brain, and is present in quantities similar to those of DHA. The two account for approximately 20% of its fatty acid content. As with DHA, neurological health is reliant upon sufficient levels of arachidonic acid.

Normally, the phosphatidylinositol cycle is activated as part of the second messenger system of membranes.[6] The arachidonic acid is also derived from the hydrolysis of phosphatidylcholine, where it is found in a small percentage of fatty acids, by the activation of phospholipase C. Molecules attach to receptors on the cell surface and activate the second messenger cascade. Phospholipase C is activated and initiates protein phosphorylation and calcium influx into the cytosol. This process is usually self-limiting and necessary in chemical signaling in the cell. However, at times it becomes excessive, and the by-products, such as arachidonic acid and calcium, damage cells.

EICOSANOID METABOLISM

Free fatty acids are released from cell membranes during hypoxia/ischemia and contribute to cell damage.[7] Increased levels of free fatty acids are found in severe hypoxia when oxygen levels are dramatically lowered.[8] Arachidonic acid produces a series of inflammatory mediators called the *eicosanoids*. In the presence of oxygen, prostaglandins, thromboxanes, and leukotrienes are formed (Figure 4–6). Normal prostaglandin metabolism to prostacyclin (PGI_2) is inhibited by ischemia; PGI_2 promotes vasodilatation and prevents platelet aggregation. In ischemia there is formation

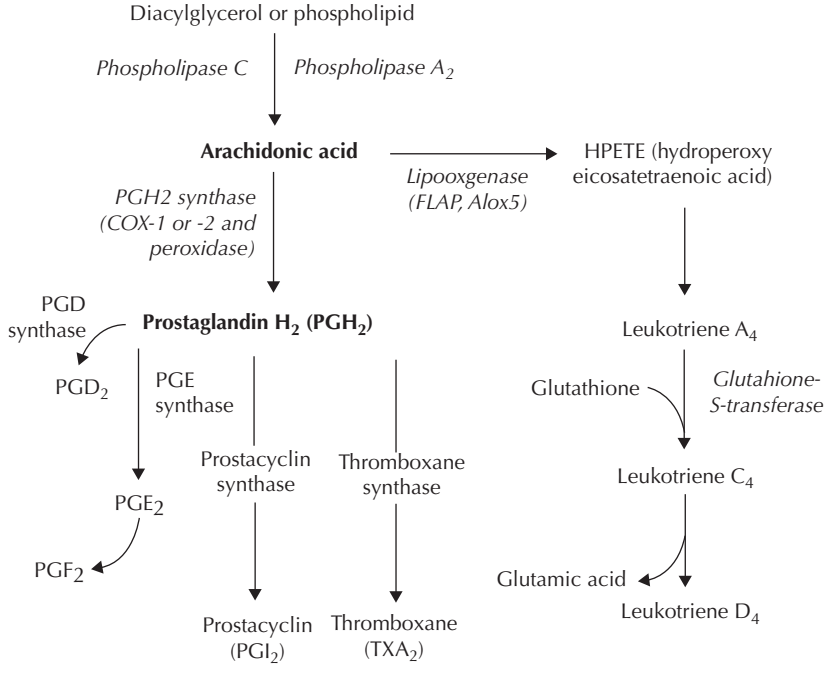

Figure 4–6. Pathways for metabolism of arachidonic acid into prostaglandins and leukotrienes.

of thromboxane A_2, which promotes platelet aggregation and vasoconstriction.

Normally, fatty acids are bound to membranes in phospholipids. The second messenger phosphatidylinositol uses a phospholipase in the activation of membrane receptors. As calcium enters the cell during depolarization, other lipases can be activated. Phospholipase A_2 acts on the phospholipid at the second position in the glycerol molecule to hydrolyze the fatty acids. The complex changes that occur in lipid membranes during hypoxia/ischemia are an important contributing factor in cell death. The sources of free fatty acids include phosphatidylcholine, phosphatidylethanolamine, phsophatidylserine, phosphatidylinositol, and triglycerides. Phospholipase C becomes active and removes inositol groups from the phosphotidylinositol-forming diacylglycerol and inositol triphosphate. With continued ischemia, activation of diacylglycerol lipase and monoacylglycerol lipase releases arachidonic acid (20:4) and stearic acid (18:0).

Metabolism of arachnoid acid takes place by two enzymes: a constitutively expressed cyclooxygenase-1 (COX-1) and an inducible COX-2. A series of inflammatory agents stimulate COX-2 mRNA, including cytokines, glutamate, platelet activating factor, and growth factors (Figure 4–7). During ischemia, calcium and glutamate stimulate the formation of arachidonic acid by phospholipase A_2, initiating the arachidonic acid cascade and prostaglandin, lipoxygenase, and thromboxane production. Glutamate acts through the *N*-methyl-D-aspartate receptor to release platelet-activating factor, starting protein kinase cascades that eventually lead to transcription of COX-2. In that cascade, the cytokines are powerful inducers of COX-2. Steroids inhibit the formation of COX-2. Free radical generation in the form of reactive oxygen species (ROS) is an important consequence of this pathway, and the excessive production of ROS causes oxidative damage.[9,10]

HEPATIC ENCEPHALOPATHY

Liver failure occurs in a variety of pathological conditions including alcoholic cirrhosis, infectious hepatitis, Reye's syndrome, and Wilson's disease, as well as with certain toxins.

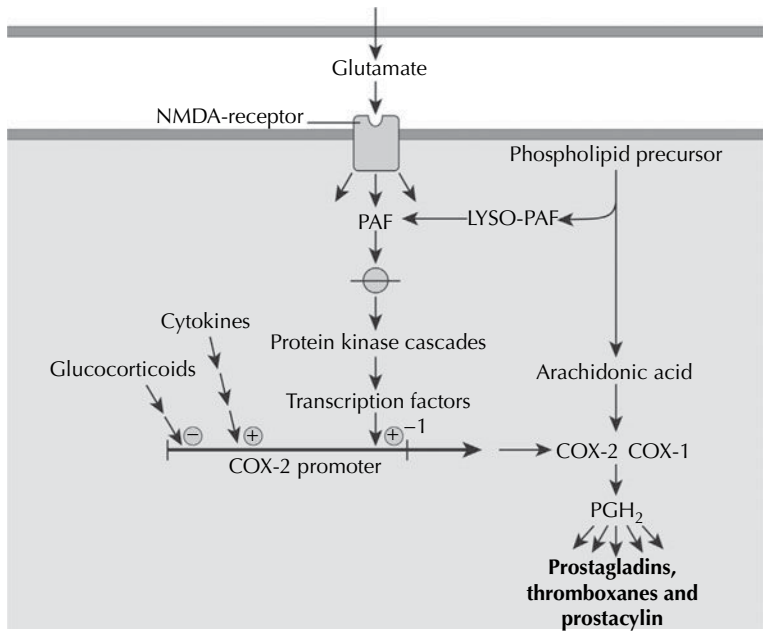

Figure 4–7. Glutamate stimulation of the NMDA receptor induces platelet activating factor (PAF). Protein kinase cascades lead to the transcription of COX-1 and COX-2, which are converted to prostaglandins, thromboxanes, and prostacyclin. (Adapted from Ref. 5.)

In hepatic encephalopathy, symptoms range from mild confusion with sleep disturbances to coma. In borderline liver failure, there may be intermittent symptoms produced by ingestion of meals high in protein content; these confusional episodes can be mistaken for seizures before the liver disease is discovered. In spite of many years of searching for the underlying etiology, hepatic encephalopathy remains enigmatic. The main theory centers on the role of gut-derived amino acids that are converted into ammonia. Astrocytes appear to be adversely affected. Characteristic pathological changes due to liver failure are seen in brain astrocytes, which have large, pale nuclei and prominent nucleoli.[11] Elevated levels of ammonia are found and are thought to contribute to the metabolic disturbance in brain tissue. Improvement in cerebral symptoms follows reduction of the high plasma ammonia level by either treating the liver disease or by reducing ammonia formation in the gut with antibiotics, lactulose, and a low-protein diet.

Elevated levels of ammonia may be the cause of the brain damage, but other possible toxins include short chain fatty acids and false neurotransmitters; it is possible that a combination of several factors is involved. Ammonia labeled with positron-emitting ^{13}N has been used to show that its uptake and metabolism is a linear function of arterial concentration.[12] Astrocytes are the primary cells involved in ammonia detoxification and show the greatest damage in hepatic encephalopathy. As astrocytes degenerate, their ability to perform essential cellular functions is impaired. Astrocytes in cell culture exposed to ammonia show hypertrophic changes followed by disturbances in membrane receptors and second messengers.[11]

Ammonia is removed from the brain by several mechanisms. It is incorporated into glutamate from the TCA cycle intermediate, α-ketoglutarate. Glutamate forms glutamine in the presence of ATP, NH_4^+, Mg^{+2}, and phosphate by the action of glutamine synthetase. Patients with hepatic encephalopathy have increased levels of glutamine in cerebrospinal fluid (CSF) and blood, while glutamate levels are unchanged. Glutamine formation uses energy in the form of ATP and depletes the TCA cycle intermediates needed to reduce NAD^+ to NADH for subsequent use in the respiratory chain.

Glutamine formation takes place in the cytoplasm of astrocytes. Ammonia interferes with energy reserves, possibly at the level of the malate-aspartate shunt that normally transfers reducing equivalents from cytoplasm to mitochondria for oxidation.[13] Accumulation of ammonia in brain could inhibit malate-aspartate exchange by combining with cytoplasmic glutamate to form glutamine and thus deplete the mitochondria of substrate (NADH) for oxidation phosphorylation.

Another theory is that GABA levels, which are elevated in serum, could enter brain through an altered blood-brain barrier (BBB), where they would inhibit normal neuronal function. Evidence for the GABA theory comes from the findings of elevated levels of GABA receptors in experimental animals. The GABA receptors are closely related to the benzodiazepine receptors, suggesting that these receptors, whose function in brain is unclear, may play a role in hepatic failure. Elevated intracellular ammonia levels result in altered neurotransmission mainly by acting as an agonist, increasing GABA inhibitory tone, as well as by causing cerebral energy failure.[14]

HYPOGLYCEMIA

When glucose levels in the blood fall below those needed for carrier-mediated transport, other sources of energy are mobilized within brain cells, including glutamate, glycogen, and ketone bodies derived from fatty acid metabolism in the liver. Glucose is stored at low levels in the brain; its depletion causes the brain to switch to alternative fuels such as amino acids and fatty acids, extending the time before cellular damage occurs. However, when all energy stores are depleted, hypoglycemia can cause extensive damage to brain tissues. A major cause of cerebral dysfunction in hypoglycemia is the loss of neurotransmitters, which are synthesized from glucose. Acetylcholine is derived from pyruvate, which is made from glucose by glycolysis. Amino acid pools, including glutamate and GABA, are depleted since glucose is the major source for their synthesis.

Prior to the introduction of insulin, hypoglycemia was rarely seen except in patients with insulin-secreting tumors, newborns with inborn errors of metabolism, and patients with liver disease. Once insulin became the standard therapy for diabetes, the number of cases

Table 4–2 **Causes of Hypoglycemia**

Excessive insulin in Type I diabetics
Drugs used to treat diabetes
Metformin
Glucosidase inhibitors
Glucagon-like peptide-1 receptor agonists
Other drugs
Sulfonylureas
Meglitinides
Alcohol
Critical illness with septic shock, renal insufficiency, etc.
Non islet cell tumors

of hypoglycemia increased. Attempts to tightly control blood glucose levels resulted in hypoglycemia; a more liberal approach to control has reduced hypoglycemic complications. There are other causes of hypoglycemia besides too much insulin, including diabetic drugs, other drugs, chronic liver disease secondary to alcoholism, non-islet cell tumors, Reye's syndrome, and, rarely, inherited metabolic diseases, such as maple syrup urine disease, which are found mainly in newborns and children (Table 4–2).

Excessive amounts of insulin from insulin-secreting tumors, self-injection of the drug, or iatrogenic causes result in hypoglycemia. Use of implantable devices to slowly release insulin resulted in improved control of blood glucose levels through a more natural pattern of insulin release. Occasional patients have hypoglycemia during the night, which goes unrecognized for long periods because of the release of epinephrine, stimulating glucose secretion. When the blood glucose levels are recorded in the morning, they are found to be normal. When there are multiple nocturnal episodes of unrecognized hypoglycemia, the patients can present with memory loss from damage to the large neurons in the hippocampus.[15]

Ketone bodies can be used for energy. Ketone bodies are transported from the liver to other tissues, where acetoacetate and β-hydroxybutyrate can be reconverted to acetyl-CoA to produce energy, via the citric acid cycle. The brain gets its energy from ketone bodies when glucose is unavailable (e.g., when fasting). In the event of low blood glucose, most other tissues have additional energy sources besides ketone bodies (such as fatty acids), but the brain does not. After the diet has been changed to lower blood glucose for 3 days, the brain gets 30% of its energy from ketone bodies.[16]

Starvation increases the level of ketones. The major ketone bodies formed by the liver when glucose is low are acetoacetate, D-3-hydroxybutyrate, and acetone. Carboxylation of pyruvate by pyruvate carboxylase forms oxaloacetate, which can restore carbon to the TCA cycle. Since fatty acids cannot be converted into glucose, the major source of gluconeogenesis, which is the reversal of glycolysis, is the liver. During starvation the liver forms glucose; fatty acids can be mobilized from adipose tissue and muscle. Insulin causes glucose to be stored in the liver, fat, and muscle, where it can be stimulated to be released by glucagon and epinephrine. Within 2 to 3 days after the start of a fast, glucose levels in the plasma fall from around 6 to 3 mM, where they remain; ketone body levels rise from zero to 4 to 5 mM. Acetoacetate is converted by CoA transferase into acetoactyl CoA and further converted by thiolase into acetyl CoA. This important reaction permits the ketone bodies to enter the TCA cycle directly without transfer into pyruvate. Use of ketone bodies as a fuel for the brain is highly efficient in terms of energy production, making the ketogenic diet possible. For many years, the benefit of the ketogenic diet in childhood epilepsy has been known. More recently, the ketogenic diet has been shown to reduce the effects of aging and to improve the outcome after stroke.[17,18]

Amino acid levels fall and ammonia levels rise in hypoglycemia. Glutamate combines with oxaloacetic acid to form aspartate and α-ketoglutarate (Table 4–3). The fall in pyruvate leads to excess oxaloacetate, resulting in the loss of glutamine, alanine, and GABA,

Table 4–3 **Metabolic Changes with Hypolglycemia**

Rise in ammonia levels as glutamate combines with NAD to form NADH
Increased aspartate and α-ketoglutamate and decreased pyruvate
Loss of glutamine, alanine, and GABA

which are needed for the formation of glutamate. Glutamate combines with NAD to form NADH and ammonia; large amounts of ammonia accumulate. In addition, lipids are metabolized as an energy source; membrane lipids are consumed when blood glucose levels fall below 20 mg/dL in rabbits.[19]

HYPONATREMIA, OSMOTIC DEMYELINATION, AND ACID BALANCE

Hyponatremia

Rapid correction of hyponatremia, which develops relatively acutely, causes the demyelinating syndrome of central pontine myelinolysis. Arieff and colleagues[20] showed that raising plasma sodium in hyponatremic individuals by more than 25 mEq/L within 48 hours to hypernatremic levels was associated with cerebral demyelinating lesions, whereas similar rapid elevations in plasma sodium to nonhypernatremic levels did not result in brain damage. This osmotic demyelination leads to altered states of consciousness, including confusion and inability to concentrate. A number of disease processes, including chronic renal failure with and without dialysis, chronic obstructive lung disease, and hepatic failure, are associated with rapid changes in extracellular acid base conditions. Hyponatremia often is found in these disorders, and altered brain pH regulation could induce central nervous system dysfunction in these patients.

Seizures may occur with hyponatremia if the plasma sodium concentration is less than 120 mEq/L. Once seizures complicate hyponatremia, treatment is urgent since correction of the low sodium level is necessary to stop the seizures, but rapid correction increases the risk of central pontine myelinolysis. In spite of many studies on osmotic demyelination, the cause remains uncertain. Magnetic resonance imaging shows the lesions in the white matter that were originally described in the pons, leading to the name *central pontine myelinolysis* (Figure 4–8). However, lesions may also be present in the white matter in the supratentorial regions.

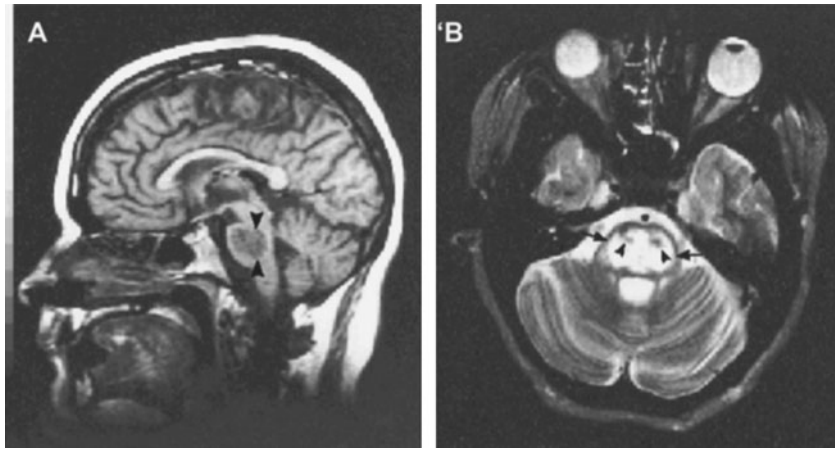

Figure 4–8. A 30-year-old alcoholic woman presented with confusion and disorientation after a grand mal seizure. Her serum sodium concentration on admission was 99 mmol/L. Treatment was initiated with a slow infusion of normal saline, resulting in serum sodium values of 102 mmol/L 4 hours after admission, 104 mmol/L at 8 hours, 115 mmol/L at 12 hours, 118 mmol/L at 18 hours, and 125 mmol/L at 24 hours. The patient initially had dysarthria, with slurred speech, and a slow finger-to-nose test on cerebellar examination, although there was no Babinski reflex. During days 2 to 6, with a normal serum sodium concentration, her condition gradually improved, although she interacted slowly with staff members and family and had difficulty following commands. On the seventh day she became unresponsive to commands and painful stimuli and had a Babinski reflex. Magnetic resonance imaging demonstrated central pontine myelinolysis as a region of prominent low signal intensity on a sagittal T_1-weighted image (panel **A**, arrowheads) and high signal intensity on an axial T_2-weighted image (panel **B**, arrows). The signal intensity on the periphery of the pons is normal on both images, and there is relative preservation of the corticospinal tracts (panel **B**, arrowheads). The patient remained in an unresponsive state for 7 weeks, but her sensorium gradually improved and she became fully responsive, alert, and oriented. (From Ref. 22.)

Hyperglycemia

Hyperglycemia is another cause of increased osmolality. Diabetes is the most common cause for a rise in blood glucose, and the increased blood osmolality causes an osmotic shift of water out of brain cells. Increases in blood osmolality lead to a compensatory increase in brain osmolality by the formation of *idiogenic osmoles*, which are most likely amino acids such as taurine. Osmoles created by amino acids or other molecules leave cells more slowly than water molecules. Because idiogenic molecules remain, keeping the osmolality of the brain cells high, it is dangerous to lower blood glucose rapidly. Even though the lowering of blood osmolality corrects the disturbance, it fails to reduce the osmotic gradient between the brain and the blood, and water moves from the blood into the brain along osmotic gradients, resulting in brain swelling. Before this paradoxical situation was understood, many patients with diabetic ketoacidosis and high plasma glucose levels died of cytotoxic brain edema in spite of what was thought to be proper treatment to restore blood osmolality to normal levels. Current treatment guidelines recommended for hyperglycemia and metabolic acidosis in patients with diabetic ketoacidosis are to slowly reverse the acidosis with bicarbonate and to gradually restore normal blood glucose.

Acidosis

Acidosis can be due to metabolic causes, such as bicarbonate loss with diarrhea, or respiratory causes including retention of CO_2. Gases exchange rapidly between the blood and brain, but charged molecules, such as bicarbonate, move very slowly between the two compartments. This creates a situation in which equilibration of CO_2 can occur rapidly, but levels of bicarbonate remain unbalanced for a much longer period of time. As a consequence of the differential rates of equilibration, metabolic acidosis leads to a compensatory respiratory alkalosis with a reduction in pH (Figure 4–9). Since the bicarbonate concentration is low in both the brain and blood, a respiratory alkalosis caused by hyperventilation raises the brain pH. A new steady state is reached with low brain bicarbonate compensated for by the reduced pCO_2. Treatment with bicarbonate, however, raises the blood pH and reduces the respiratory drive, leading to a buildup of pCO_2, which is rapidly transported into the brain. Since the bicarbonate concentration in the brain is low and there is limited transport from the blood, the brain pH falls due to the treatment, creating a life-threatening situation.[21] Patients' conditions deteriorate when there is a too rapid a replacement of bicarbonate.

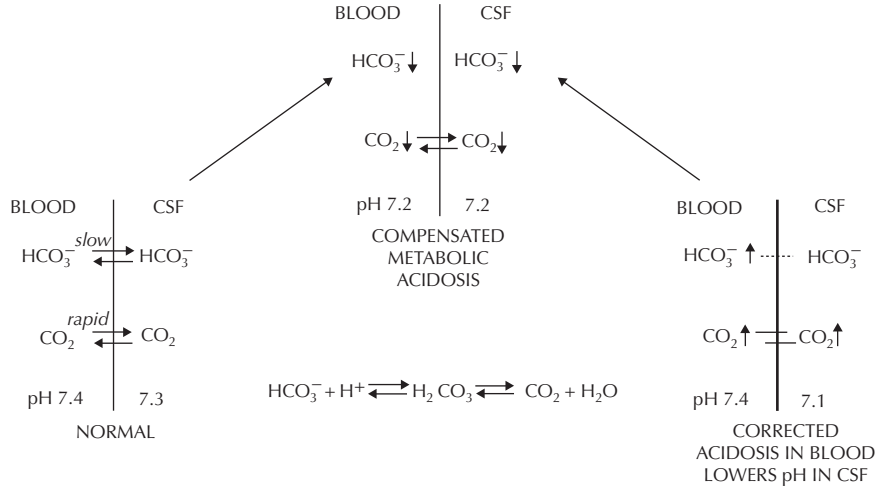

Figure 4–9. Correction of long-standing metabolic acidosis with infusion of bicarbonate can lead to worsening of the mental status and possibly coma. Because the bicarbonate in the blood and CSF is chronically reduced, there is compensatory hyperventilation with reduction of CO_2 in both the blood and CSF compartments. When the acidosis in the blood is corrected, hyperventilation ceases and CO_2 builds up. Since only the CO_2 crosses into the CSF and it does not encounter HCO_3, the pH of the CSF is driven down. A reduced mental state can occur in spite of optimal levels in the blood.

REFERENCES

1. van den Berg CJ, Garfinkel D. A stimulation study of brain compartments. Metabolism of glutamate and related substances in mouse brain. *Biochem J*. 1971;123: 211–218.
2. Brainard JR, Kyner E, Rosenberg GA. ^{13}C nuclear magnetic resonance evidence for gamma-aminobutyric acid formation via pyruvate carboxylase in rat brain: a metabolic basis for compartmentation. *J Neurochem*. 1989;53:1285–1292.
3. Hertz L. Functional interactions between neurons and astrocytes. Turnover and metabolism of putative amino acid transmitters. *Prog Neurobiol*. 1979;13:277–323.
4. Sibson NR, Mason GF, Shen J, et al. In vivo (13)C nmr measurement of neurotransmitter glutamate cycling, anaplerosis and tca cycle flux in rat brain during. *J Neurochem*. 2001;76:975–989.
5. Suzuki K, Siegel GJ, Albers RW, et al. Chemistry and metabolism of brain lipids. In: Siegel G, Albers RW, Brady S, Price D, eds. *Basic Neurochemistry*. Boston: Little, Brown; 1981:355–370.
6. Berridge MJ, Irvine RF. Inositol trisphosphate, a novel second messenger in cellular signal transduction. *Nature*. 1984;312:315–321.
7. Bazan NG Jr. Effects of ischemia and electroconvulsive shock on free fatty acid pool in the brain. *Biochim Biophys Acta*. 1970;218:1–10.
8. Gardiner M, Nilsson B, Rehncrona S, et al. Free fatty acids in the rat brain in moderate and severe hypoxia. *J Neurochem*. 1981;36:1500–1505.
9. Katsura K, Rodriguez de Turco EB, Folbergrova J, et al. Coupling among energy failure, loss of ion homeostasis, and phospholipase a2 and c activation during ischemia. *J Neurochem*. 1993;61:1677–1684.
10. Bazan NG. Lipid signaling in neural plasticity, brain repair, and neuroprotection. *Mol Neurobiol*. 2005;32: 89–103.
11. Norenberg MD, Rao KV, Jayakumar AR. Mechanisms of ammonia-induced astrocyte swelling. *Metab Brain Dis*. 2005;20:303–318.
12. Cooper AJ, Plum F. Biochemistry and physiology of brain ammonia. *Physiol Rev*. 1987;67:440–519.
13. Hindfelt B, Plum F, Duffy TE. Effect of acute ammonia intoxication on cerebral metabolism in rats with portacaval shunts. *J Clin Invest*. 1977;59: 386–396.
14. Cash WJ, McConville P, McDermott E, et al. Current concepts in the assessment and treatment of hepatic encephalopathy. *QJM*. 2010;103:9–16.
15. Suh SW, Gum ET, Hamby AM, et al. Hypoglycemic neuronal death is triggered by glucose reperfusion and activation of neuronal nadph oxidase. *J Clin Invest*. 2007;117:910–918.
16. Hasselbalch SG, Knudsen GM, Jakobsen J, et al. Brain metabolism during short-term starvation in humans. *J Cereb Blood Flow Metab*. 1994;14:125–131.
17. Puchowicz MA, Zechel JL, Valerio J, et al. Neuroprotection in diet-induced ketotic rat brain after focal ischemia. *J Cereb Blood Flow Metab*. 2008;28: 1907–1916.
18. LaManna JC, Salem N, Puchowicz M, et al. Ketones suppress brain glucose consumption. *Adv Exp Med Biol*. 2009;645:301–306.
19. Auer RN, Siesjo BK. Biological differences between ischemia, hypoglycemia, and epilepsy. *Ann Neurol*. 1988;24:699–707.
20. Ayus JC, Krothapalli RK, Arieff AI. Treatment of symptomatic hyponatremia and its relation to brain damage. A prospective study. *N Engl J Med*. 1987;317(19): 1190–1195.
21. Posner JB, Plum F. Spinal-fluid ph and neurologic symptoms in systemic acidosis. *N Engl J Med*. 1967;277:605–613.
22. Hart BL, Eaton RP. Osmotic myelinolysis. *N Engl J Med*. 1995;333:1259–1259.

Chapter 5

Disorders of Cerebrospinal Circulation: Idiopathic Intracranial Hypertension and Hydrocephalus

INTRODUCTION

Two important diseases that illustrate the importance of understanding the anatomy and physiology of brain fluids are idiopathic intracranial hypertension (IIH) and hydrocephalus. Both involve excessive amounts of fluid in the brain, raising intracranial pressure. Treatment involves either reducing fluid production with medications or enhancing drainage by shunting brain fluids to sites outside the brain. A major difference is the size of the ventricles; in IIH the ventricles are normal or small, while the opposite is the case in hydrocephalus. Diagnosis of hydrocephalus has been remarkably simplified by computed tomography (CT) and magnetic resonance imaging (MRI), which not only show the enlarged ventricles, but also indicates the sites of obstruction. The images are usually normal in IIH, but that in itself is important information.

Papilledema and markedly raised cerebrospinal fluid (CSF) pressure are hallmarks of IIH, and headache is a major symptom. Enlarged ventricles always accompany hydrocephalus, but the CSF pressure is variable. Depending on the site of CSF obstruction, intraventricular pressure may be evenly distributed in noncommunicating hydrocephalus, in which the ventricles are either internally blocked or obstruction is at the sites where fluid enters the cisterns around the brainstem. Communicating hydrocephalus occurs when the obstruction is beyond the exit foramina in the brainstem and is at the sites of CSF absorption.

Medical treatment is available for IIH, and surgery is used only when that fails. However, hydrocephalus generally requires surgical treatment. Normal pressure hydrocephalus is challenging to diagnose, since no single test is adequate, and a combination of clinical judgment and diagnostic tests is needed. Advances in imaging techniques are beginning to unravel the pathophysiology of both conditions.

CLINICAL FEATURES OF IIH

Many names are applied to the syndrome of raised intracranial pressure with papillema. In 1931, prior to the development of antibiotics,

Symonds referred to it as *otitic hydrocephalus*, recognizing the fact that it was often seen as an ear infection with papilledema; headaches and papilledema were assumed to be due to hydrocephalus because diagnostic imaging was not available.[1] When pneumoencephalography was introduced, and tumors and hydrocephalus could be seen by distortion of the ventricles on the x-ray films, some patients with papilledema suspected to have brain tumors were found to have normal studies. Davidoff used the term *pseudotumor cerebri* to describe the syndrome, which has remained in use by some investigators.[2] For some years, the term *benign intracranial hypertension* was the accepted diagnostic descriptor, but the syndrome could lead to blindness and was not always benign.[3] The best term at this time is *idiopathic intracranial hydrocephalus*, which shows the poor understanding of the pathophysiology and merely describes the findings.

Generally a benign condition that resolves spontaneously, IIH can have a malignant course and cause blindness due to encroachment of the swollen discs on the macular region of the retina. Headache is most often the presenting symptom in IIH patients. Typically, the headache occurs in the early morning, often awakening the patient from sleep. Transient obscuration of vision occurs when changing from a sitting to a standing position. Some patients complain of dizziness and tinnitus. Visual symptoms are common, ranging from obscuration and diplopia to loss of vision.

Because headache is a common complaint in general practice, unless time is taken to carefully examine the optic discs for the presence of blurring of the margins and loss of pulsations of the veins, diagnosis may be delayed for months. Visual fields show an enlarged blind spot due to the swollen optic nerve head. Prolonged papilledema may lead to sector scotomas and restriction of the visual fields. It is important to differentiate papillitis due to inflammation of the optic disc from papilledema due to increased CSF pressure; in papillitis vision is lost initially and the pupillary response is abnormal, while with papilledema vision is preserved until the late stages.

The majority of patients with IIH have a normal neurological examination except for papilledema. When the central nervous system is involved, IIH generally takes the form of cranial nerve involvement. Damage to one or both of the sixth cranial nerves may occur as an effect of shifts in cerebral tissue; because the sixth cranial nerve is remote from the site of the process producing intracranial hypertension, the cranial neuropathy is a false localizing sign. The sixth nerve has a long course as it travels to the orbit. After leaving the brainstem and before entering the orbit, it makes a 90-degree turn at the top of the clivus and goes through Dorello's canal at the tip of the temporal bone (Figure 5–1). It is possibly at this site that compression of the abducens nerve could occur because there are several rootlets that pass above and below the ligament that forms Dorello's canal.[4] Other causes of paralysis of the abducens nerve include direct injury in trauma of the skull with fracture of the petrous temporal bone; infections of the tip of the temporal bone in the region of Meckel's cave, which are referred to as *Gradenigo's syndrome*; diabetes; and vasculitis. The nerve is vulnerable as it passes over the sharp superior border of the apex of the petrous bone. In IIH, the mechanism of damage to the sixth nerve has been interpreted as a displacement of the encephalic mass toward the foramen magnum, thus putting more tension on the nerve where it straddles the petrous bone, but the exact mechanism of sixth nerve involvement remains unclear.

Diagnosis of IIH is essentially a process of ruling out other causes of increased intracranial pressure. All patients require a CT or MRI scan to look for hydrocephalus and mass lesions. After a mass lesion is ruled out, lumbar puncture is needed, with careful attention to accurate measurement of the CSF pressure, which must be elevated by definition. Positioning of the patient is important in order to obtain an accurate pressure. With the patient lying on one side, the lumbar puncture needle is placed in the lumbar sac and the manometer, with minimal loss of fluid, measures the pressure. Characteristically, CSF has normal or low protein, normal glucose, no cells, and elevated pressure. The upper limit of normal CSF pressure is 200 mm H_2O. Many IIH patients show CSF pressures above 300 mm H_2O, with occasional pressures exceeding 500 mm H_2O. Measurement of CSF pressure should be done with the legs extended and the neck straight. Performance of lumbar puncture with the patient in the sitting position should be avoided since the pressure cannot be measured. It is

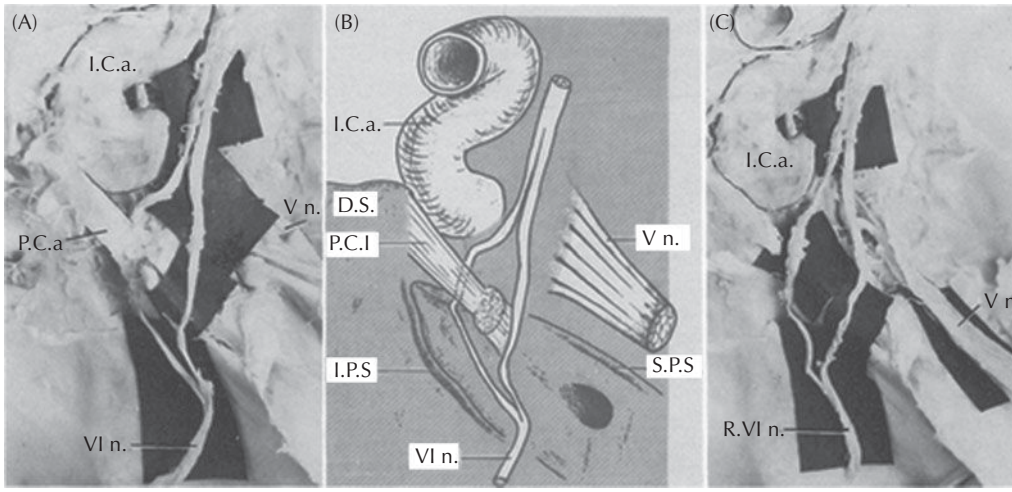

Figure 5–1. (**A**) Dissection showing one of the branches of a split sixth nerve passing above and the other below the petrosphenoidal ligament. Both branches fuse again into a single trunk in the cavernous sinus. (**B**) Schematic drawing of a dissection. (**C**) Dissection after removal of a ligament showing the branch below the petrosphenoidal ligament passing above the sharp edge of the petrous bone close to its tip. VI n. = abducens nerve; V n. = trigeminal nerve; I.C.A. = internal carotid artery; D.S. = dorsum sellae; P.C.l. = petroclinoid ligament (ligament of Gruber, or petrosphenoidal ligament); I.P.s. = inferior petrosal sinus; S.P.s. = superior petrosal sinus; D.M. = dura mater; S.T. = sella turcica; O.n. = optic nerve; S.O.f. = superior orbital fissure; L.R.m. = lateral rectus muscle; P.b. = petrous bone; C.s. = cavernous sinus. (From Ref. 4.)

important to obtain an accurate pressure reading at the time of the initial lumbar puncture, since measurements of pressure in subsequent lumbar punctures may be falsely reduced by damage to the dura with leakage of CSF.

Women develop IIH more frequently than men. Obesity and menstrual irregularities, with excessive premenstrual weight gain, are often present. Because many illnesses are associated with IIH, the search for an underlying cause is essential before the diagnosis is made by exclusion. Because obesity is often found in women with IIH, endocrine abnormalities are extensively investigated, but they are rarely discovered.

Drugs associated with the syndrome include tetracycline-type antibiotics, nalidixic acid, nitrofurantoin, sulfonamides, and trimethoprim-sulfamethoxazole. Paradoxically, the withdrawal of corticosteroids, which are used to treat increased intracranial pressure, can cause an increase in intracranial pressure. Large doses of vitamin A, which are used in the treatment of various skin conditions, may cause the syndrome. Hypercapnia leads to retention of carbon dioxide and an increase in blood volume. Sleep apnea and lung diseases may cause headaches and papilledema due to this mechanism. Less frequent causes include Guillain-Barré syndrome, in which the increase in intracranial pressure may be due to an increase in CSF protein or an inflammatory response with obstruction of the outflow of CSF at the level of arachnoid granulations. Uremic patients have an increased incidence of papilledema with IIH. Patients with renal failure have increased levels of vitamin A, use corticosteroids, and take cyclosporine, which have all been linked to IIH.

Idiopathic intracranial hypertension may be due to impaired venous flow in at least some patients. Venous pressure measurement has shown high pressure in the superior sagittal sinus and proximal transverse sinuses, with a drop in venous pressure distal in the transverse sinus.[5] Angiography does not show this well. In patients without a documented structural defect in the venous sinuses, increased right atrial filling pressure that was transmitted to the venous sinuses has been shown.[6] This procedure is not recommended since it is unproven in controlled trials and may have long-term consequences in patients who are generally young.

Magnetic resonance imaging has rekindled interest in conditions that cause occlusions of the venous sinuses because of the ability to visualize the venous drainage system with

MRI venography. When the sinuses draining blood from the brain are obstructed, absorption of CSF is reduced, causing CSF pressure to increase. Magnetic resonance venography is better for showing the thrombosis of the sinuses than conventional MRI (Figure 5–2). The importance of venous sinus obstruction in IIH, although it should be ruled out with venography, may be limited since there is no information on its incidence. Often the sinus occlusion is related to hypercoagulable states, which should be looked for in patients with venous sinus obstruction. Venous occlusions on MRI scans should be interpreted with caution because of the normal variability of the venous system in the general population.

Several studies have suggested the presence of brain edema in patients with IIH. A biopsy showed brain edema in one patient that was subjected to temporal decompression, a procedure that is no longer done.[7] Two recent MRI studies showed edema in the white matter in patients with IIH; there was an increase in the white matter water signal of a heavily T2-weighted imaging sequence obtained at 1.5T.[8] Another study compared diffusion maps of the apparent diffusion coefficient (ADC) in 12 patients fulfilling conventional diagnostic criteria for IIH and in 12 healthy volunteers. The authors reported a significantly larger ADC within subcortical white matter in the patient group than in the control group; there were no significant differences within cortical gray matter, the basal nuclei, the internal capsule, or the corpus callosum. In addition, four of seven patients with an increased ADC in subcortical white matter also had an increased ADC in gray matter.[9]Another group measured the mean diffusivity of water and the proton longitudinal relaxation time in 10 patients with idiopathic intracranial hypertension and 10 age-, sex-, and weight-matched controls. They failed to find significant differences in diffusion-weighted images and T1 values between the patient and control groups in any of the brain regions investigated, concluding that IIH is not associated with abnormalities of convective transependymal water flow leading to diffuse brain edema.[10] Thus, based on the results of MRI studies, there is no consensus as to the presence of brain edema.

In a small number of patients, the symptoms of IIH progress rapidly. Fulminant IIH can result in loss of vision from the progressive papilledema. Visual fields change over days to weeks. One series of 483 IIH patients included 16 obese young women with a fulminant course. All had headaches and visual loss. Half of them had transient visual obscurations. Five had diplopia, and all had severe papilledema with severely constricted visual fields. In spite of treatment with acetazolamide and intravenous methylprednisolone, all patients required surgical treatment, which included optic nerve sheath fenestration, lumboperitoneal shunt, or ventriculoperitoneal shunt.[11] Visual fields and fundus photographs from a patient with fulminant papilledema are shown in Figure 5–3.

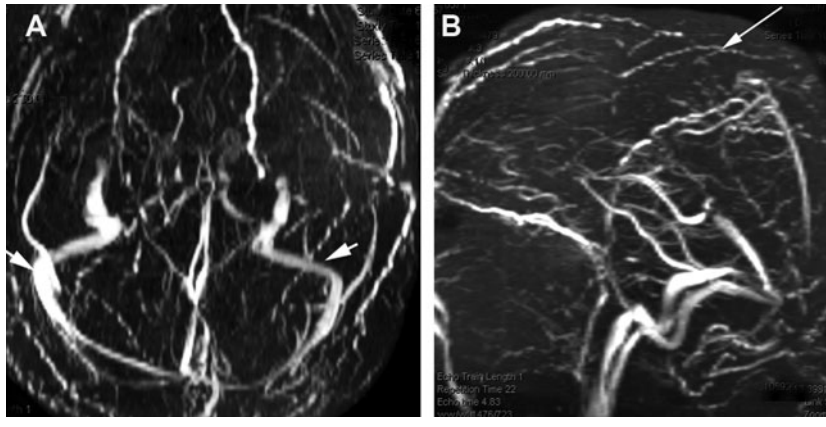

Figure 5–2. A 57-year old man with a 2-year history of blurred vision and dizziness. He had a remote history of idiopathic thrombocytopenic purpura. Papilledema was seen on examination. A magnetic resonance venogram showed sagittal sinus thrombosis. (**A**) Coronal view showing both transverse sinuses (arrows) with absence of the superior sagittal sinus. (**B**) Sagittal view showing the thrombosis of the superior sagittal sinus (arrow).

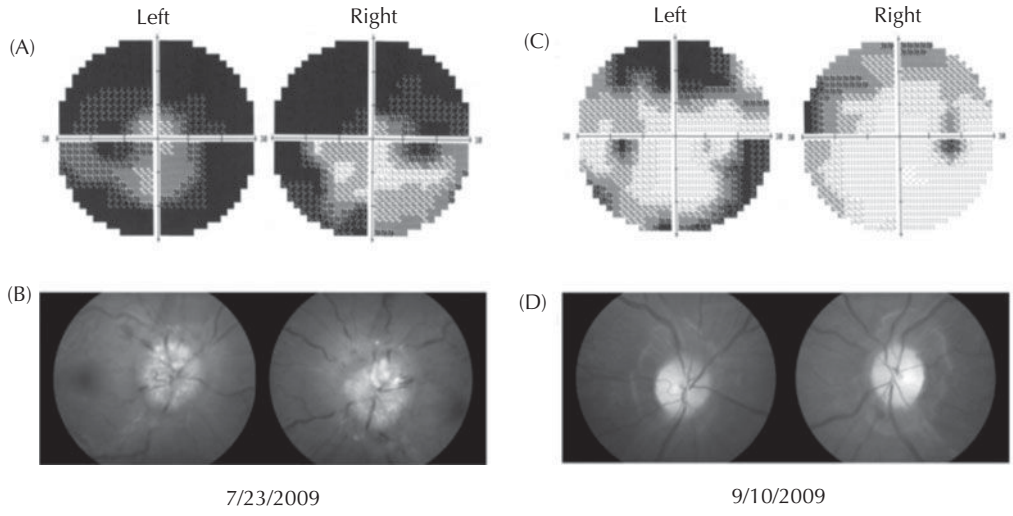

Figure 5–3. A 29-year-old overweight woman had headaches for 1 month and transient obscurations for 5 months. Lumbar puncture on admission showed a CSF pressure of 300 mm H_20. At that time, visual acuity was 20/20 in both eyes, with normal visual fields and color vision. She was treated with diet and diamox, but visual loss progressed rapidly. (**A**) Eight days later, the visual fields had changed markedly. (**B**) Papilledema was worse, and visual acuity had decreased to 20/60 on the right and 20/200 on the left. A lumboperitoneal shunt was placed stereotactically. (**C**) Two months lager, the visual fields were improved. (**D**) Papilledema had resolved. (Photographs of the fundi and visual fields courtesy of Thomas Carlow, M.D.)

TREATMENT OF IIH

Treatment involves reducing the intracranial pressure. Acetazolamide is an inhibitor of carbonic anhydrase that lowers CSF production and pressure. It is given in a dose of 250 mg twice daily, which may be increased to 1 g/day. Occasionally, even higher doses may be needed. Electrolytes must be monitored to look for metabolic acidosis. Distal paresthesias are reported to occur in up to 25% of patients. The hyperosmolar agent, glycerol (0.25–1.00 g/kg two or three times daily), was advocated at one time but is no longer used; the increased blood sugar caused weight gain.[12] Corticosteroids reduce increased intracranial pressure, but the pressure may increase when they are tapered. Drug effects are often transient, and when the syndrome does not resolve spontaneously, other treatments are needed. Although the relationship of obesity to IIH is uncertain, loss of weight can lead to resolution of the syndrome, and some patients have undergone surgical stomach size reduction to control the obesity.

Visual fields should be measured and the size of the blind spot plotted. The swelling of the optic disc causes the enlarged blind spot. When the papilledema spreads into the region of the macula, visual acuity falls and eyesight is threatened. Although most patients with IIH retain normal vision, a small percentage develop impairment of vision. When vision is threatened, and drugs and multiple lumbar punctures do not lower the CSF pressure, surgical intervention is necessary. Lumboperitoneal shunting has a reportedly high initial success rate. However, shunt malfunction is common in lumboperitoneal shunts. Fenestration of the optic nerve sheath to drain CSF into the orbital region reduces the intracranial pressure, and some consider it the treatment of choice in medically refractory patients. In obese patients with IIH, weight loss is an important adjunctive treatment, and some authors argue that it is as important as acetazolamide. Recently, the ability to perform stereotactic placement of the ventriculoperitoneal shunt has allowed this to be done in place of the lumboperitoneal shunt. At the present time, there is insufficient follow-up to evaluate the efficacy of the ventriculoperitoneal shunt in IIH.

HYDROCEPHALUS

Hydrocephalus is a general term used to describe an enlargement of the ventricular system.

The cause of hydrocephalus is obstruction of drainage of the CSF, which accumulates in the ventricles. The site of CSF obstruction defines the type of hydrocephalus: obstruction of CSF flow out of the ventricles is called *noncommunicating hydrocephalus*, and blockage outside the ventricles in the arachnoid granulations is referred to as *communicating hydrocephalus*. Although it is possible to detect enlarged ventricles by CT and MRI, the separation of ventricular enlargement due to hydrocephalus from that due to loss of brain tissue may be challenging. Patients with loss of brain tissue, as occurs in dementing illnesses, can have enlarged ventricles or hydrocephalus *ex vacuo*, which is generally accompanied by generalized atrophy, a finding absent in obstructive hydrocephalus.

In early life, obstruction of ventricular outflow most commonly occurs in the aqueduct, leading to noncommunicating hydrocephalus, while in the elderly, communicating hydrocephalus due to resistance to drainage of the CSF after its exit into the subarachnoid space is more common. Obstruction prior to the outflow of CSF at the foramina of Luschka and Magendie results in noncommunicating hydrocephalus, whereas in communicating hydrocephalus, enlargement of the ventricles takes place with preserved flow of CSF between the ventricle and the subarachnoid space. Enlargement of the cerebral ventricles in children less than 2 years of age produces enlargement of the head circumference because the skull sutures are still open. Children with head growth that is more rapid than expected for age are suspected of having hydrocephalus and undergo imaging. In the elderly, the onset of symptoms may be gradual, beginning with problems of gait and intellect, which can suggest many different diagnoses. Obstruction of CSF circulation may result in increased CSF pressure as the cerebral ventricles enlarge, but once that has occurred, compensatory drainage mechanisms may lower the CSF pressure, resulting in so-called *normal pressure hydrocephalus*.

Acute noncommunicating hydrocephalus develops rapidly, reaching 80% of maximal ventricular enlargement within 6 hours. A slower phase of enlargement follows the initial rapid expansion, and ventricular enlargement plus continual production of CSF causes fluid accumulation in the periventricular white matter interstitial space. When the hydrocephalus stabilizes and enters a chronic phase, the CSF pressure may decrease, resulting in normal pressure recordings on random measurements. Atrophy may occur in the chronically hydrocephalic white matter. When the rate of ventricular enlargement stabilizes in patients with incomplete ventricular obstruction, CSF production is balanced by absorption, which occurs across the ependyma, so-called *transependymal absorption*, which leads to fluid accumulation around the edges of the ventricles referred to as *interstitial edema*.[13] Absorption of CSF by this transependymal route appears to be an important compensatory mechanism in adults, but the manner in which the interstitial edema is resolved is unclear. Occasionally, patients assumed to have arrested hydrocephalus can undergo acute decompensation after many years of apparent stability.

Relatively little is known about the causes of hydrocephalus because of the limited information obtained from animal studies. One study of the cilia in the ventricles provided information about the potential for aberrant development of cilia in the pathophysiology of hydrocephalus. Disrupting ependymal ciliary beating results in an accumulation of CSF in the brain ventricles and is a pathogenic mechanism of hydrocephalus.[14] In addition to hydrocephalic mouse models in which the genetic defect disrupts ciliary motility or ciliogenesis, human patients with primary ciliary dyskinesia also develop hydrocephalus.[15] The planar polarized beating of ependymal cilia is therefore essential for normal brain function. However, very little is known about the mechanism of planar cell polarity in ependymal cells.

HYDROCEPHALUS IN CHILDREN

Hydrocephalus in children is often due to a structural abnormality, such as Chiari I or II malformation, congenital aqueductal stenosis, aqueductal stenosis due to intrauterine infection, or other congenital causes, such as anoxic injury, intraventricular hemorrhage, and obstruction of the CSF pathways after bacterial meningitis. Bulging of the anterior fontanelle may be seen, along with thinning of the skull and separation of the sutures. If the diagnosis is delayed, abnormal eye movements and optic atrophy may develop. Spasticity of the lower limbs may be observed at any stage. Acute enlargement of the ventricles is associated with nausea and vomiting.

During the neonatal and early childhood period, irritability is the most common symptom of hydrocephalus. The child eats poorly, appears fretful, and may be lethargic. In the older child, headache may be a complaint. Vomiting due to increased intracranial pressure may be present in the morning. Remote effects of the increased pressure may affect the sixth cranial nerves on one or both sides, leading to the complaint of diplopia. The enlarged ventricles affect gait. A wide-based ataxic gait may be present due to the stretching of the white matter tracts from the frontal leg regions around the ventricles.

Premature infants weighing less than 1500 g at birth have a high risk of intraventricular hemorrhage, and approximately 25% of these infants develop progressive ventricular enlargement, as shown by CT or ultrasound scans.[16] Ventricular size in the neonate may be followed at the bedside with B-mode ultrasound through the open fontanelle. Long-term follow-up studies of children with intraventricular hemorrhage due to prematurity show that 5% of these infants require shunting for hydrocephalus. The survivors of a large germinal plate hemorrhage often have multiple disabilities.

Once the sutures are closed, hydrocephalus causes signs of increased intracranial pressure rather than head enlargement. Meningitis, aqueductal stenosis, Chiari malformations, and mass lesions may be the cause of hydrocephalus in these young children. Tumors originating from the cerebellum and the brainstem produce acute symptomatology, including headaches with vomiting, diplopia, visual blurring, and ataxia. Symptoms are due to the acute hydrocephalus secondary to obstruction of the aqueduct of Sylvius and to pressure on brainstem structures.

Examination shows papilledema, possible sixth cranial nerve palsy, and spasticity of the lower limbs. When the hydrocephalus is more long-standing, endocrine dysfunction may occur, involving short stature, menstrual irregularities, and diabetes insipidus. Excessively rapid growth of the head is the hallmark of hydrocephalus in the child before closure of the sutures. Charts are available to plot head growth and to compare it with the standardized curves for normal children. Bulging of the anterior fontanelle is found even with the child relaxed and upright. After 1 year, the firmness of the fontanelle cannot be used because the sutures have closed. Other findings that are rarely seen because of the ease of obtaining imaging studies at the earliest suspicion of a problem include the "cracked-pot" sound on percussion of the skull (McEwen sign), engorged scalp veins, and abnormal eye movements. If the ventricular enlargement goes undetected and the frontal fibers around the ventricle are stretched, spasticity may be found with increased deep tendon reflexes.

Treatment involves shunting CSF from the ventricles to drain fluid into another body cavity. The shunt is generally placed in the peritoneal cavity, but the site varies depending on the age of the patient since the child's growth needs to be considered in choosing the final location. Complications of shunt placement include malfunction and shunt infection. Revisions of the shunt as the child grows are frequently necessary.

ADULT-ONSET HYDROCEPHALUS

In the adult, symptoms of acute hydrocephalus include headaches, papilledema, diplopia, and mental status changes. Sudden death may occur with severe increases in pressure. Although rare, hydrocephalus can cause an akinetic mutism due to pressure on the structures around the third ventricle. Other symptoms include temporal lobe seizures, CSF rhinorrhea, endocrine dysfunction (e.g., amenorrhea, polydipsia, and polyuria), and obesity, which suggest third ventricle dysfunction. Gait disturbances are reported in patients with aqueductal stenosis, but hyperreflexia with Babinski's sign is infrequent.

Adult-onset hydrocephalus has causes that are similar to those in children, but the frequencies differ. As in children, acute obstruction of the ventricles results in rapidly progressive hydrocephalus with symptoms of raised intracranial pressure. Adults are more likely than children to present with an acute blockage of CSF flow by intraventricular masses, such as a colloid cyst of the third ventricle or an ependymoma of the fourth ventricle. These tumors cause sudden headaches, ataxia, and loss of consciousness with symptoms that may be intermittent due to the ball-valve effect

of the masses. A CT or MRI scan reveals the colloid cyst in the ventricle.

Obstructive Hydrocephalus

Cerebellar hemorrhage and cerebellar infarction with edema cause an acute hydrocephalus by compression of the brainstem, occluding the aqueduct of Sylvius and the fourth ventricle outflow pathways and causing noncommunicating hydrocephalus, which can be seen on CT and MRI and results in acute elevation of intraventricular pressure. Patients with cerebellar hemorrhage usually have a history of hypertension. Increasing drowsiness and difficulty walking often follow the acute onset of headache. Hemiparesis and brainstem findings evolve after the ataxia, providing a clue that the origin of the problem is in the posterior fossa (Table 5–1). The expanding hemorrhagic mass in the posterior fossa, if it is encroaching on the brainstem, requires urgent neurosurgical attention, with placement of a ventricular catheter to decompress the lateral and third ventricles, followed by posterior fossa craniectomy to remove the mass effect and pressure on the brainstem.[17] In patients with cerebellar infarction, the progression is generally slower since the maximum swelling takes place in 24 to 48 hours, but the consequences of the enlarging posterior fossa mass are the same as with hemorrhage, and surgery may be necessary to remove the necrotic tissues and restore the normal flow of CSF.[18] Computed tomography is needed in the acute setting, particularly when MRI is not readily available, but visualization of the cerebellar infarction, which may be missed on CT, is clearly seen on the diffusion-weighted MRI.

Treatment of adult hydrocephalus involves an operation to insert a tube to shunt CSF from the ventricles to the peritoneal cavity. These devices have one-way valves that respond to pressure. In an emergency, hydrocephalic ventricles can be assessed readily due to the increase in their size. Shunt malfunction may cause abrupt decompensation. Symptoms of acute increased intracranial pressure from a shunt malfunction resemble those seen with onset of the hydrocephalic process.

Table 5–1 **Cerebellar Hemorrhage and Obstructive Hydrocephalus**

Abrupt onset of headache with ataxia
Hemiparesis develops later
Signs of brainstem compression including sixth and seventh nerve palsies
Acute enlargement of the ventricles due to CSF obstruction
May progress to death within 24 to 72 hours if not treated

Normal Pressure Hydrocephalus

Adult-onset hydrocephalus that is communicating may be due to a tumor in the basal cisterns, subarachnoid bleeding, or infection or inflammation of the meninges. In the preantibiotic era, syphilis, tuberculosis, and fungal infections were common causes of hydrocephalus due to the chronic obstruction of the subarachnoid pathways.[19] Cultures of the CSF are indicated in the elderly patient with enlarged ventricles, and a search for other sources of infection in lungs and other organs may be helpful in establishing the type of infection. In the majority of patients with adult-onset hydrocephalus, the etiology remains obscure and the term *idiopathic adult-onset hydrocephalus* is used. In 1965, Adams and colleagues described the syndrome of normal pressure hydrocephalus (NPH) as a cause of dementia with gait problems.[20] This has remained an important cause of mental impairment in the elderly, but the cause of the syndrome in most patients continues to be obscure.[21]

Chronic hydrocephalus in the adult can produce symptoms of gait disturbance, incontinence, and memory loss, with or without symptoms and signs of raised intracranial pressure, including headache, papilledema, and false localizing signs (Table 5–2).[22] Causes of chronic hydrocephalus include subarachnoid hemorrhage, chronic meningeal infections, and slow-growing tumors blocking the CSF pathways.

Table 5–2 **Normal Pressure Hydrocephalus**

Gait impairment (ataxia of gait)
Incontinence
Dementia
Communicating hydrocephalus with transependymal flow

Typically, patients with NPH have the triad of mental impairment, gait disturbance, and incontinence. Normal pressure hydrocephalus can develop secondary to trauma, infection, or subarachnoid hemorrhage, but in about one-third of patients no etiology is found. Enlarged ventricles are seen on CT or MRI (Figure 5–4). By definition, lumbar puncture generally reveals a normal or minimally elevated CSF pressure. *Normal pressure* is an unfortunate term because patients who have undergone long-term monitoring with this syndrome have intermittently elevated pressures, often during the night.

The presenting symptoms may be related to gait or to mental function. When gait disturbance is the presenting symptom, the prognosis for treatment is better. Normal pressure hydrocephalus causes an apraxic gait, which is an inability to lift the legs as if they were stuck to the floor. Motor strength is intact, reflexes are usually normal, and the Babinski sign is absent. In some patients, attempts to elicit a Babinski sign will result in a grasp response of the toes suggestive of a frontal lobe abnormality. Patients may be misdiagnosed as having Parkinson's disease because the gait disorder is similar in the two syndromes, suggesting that the etiology of the problem in the hydrocephalic patient lies in the basal ganglia. Because many of these patients also have hypertension, and some have had small or large strokes, there may be other neurological findings, including spasticity and hyperreflexia with a Babinski sign. The combination of cerebrovascular disease and hydrocephalus is a poor prognostic indicator for treatment with shunts.

Normal pressure hydrocephalus leads to a reduction in intellect, which at times may be subtle. The dementia is of the subcortical type, and involves slowing of verbal and motor responses with preservation of cortical functions, such as language and spatial resolution. Neuropsychological testing quantifies the decline in intellect and the degree of dementia. Patients are apathetic and appear depressed. Incontinence of urine may occur early in the course, particularly in patients with prominent gait disturbance. In the early stages of the illness, presumably as the ventricles are undergoing enlargement, patients can experience drop attacks or brief loss of consciousness. Headache and papilledema are generally not part of the syndrome.

Diagnosis of adult-onset hydrocephalus and selection of patients for placement of a ventriculoperitoneal shunt are difficult.[22] Many of these patients have hypertensive vascular disease with lacunar infarcts.[23,24] Features of Parkinson's disease were noted in earlier reports of the syndrome, and it is now recommended that all patients with Parkinson's disease have scans to rule out hydrocephalus. Computed tomography and MRI have aided in

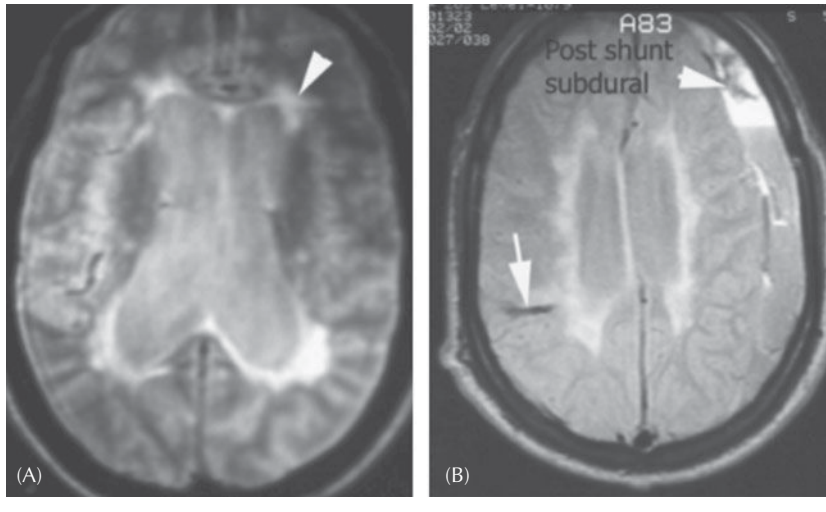

Figure 5–4. Normal pressure hydrocephalus. (**A**) Fluid attenuated inversion recovery (FLAIR) MRI showing the enlarged ventricles and the transependymal flow of interstitial fluid (arrowhead). (**B**) Postventriculoperitoneal shunt (arrow). A subdural hematoma developed after the ventricles collapsed (arrowhead).

differentiating Parkinson's disease, the lacunar state, and NPH, although NPH may occasionally coexist with these diseases. Patients diagnosed with vascular diseases, such as lacunar state or subcortical arteriosclerotic encephalopathy (Binswanger's disease), along with the hydrocephalus respond poorly to shunting, and if there is a positive response, it may be transient as the underlying disease progresses.[25] Selection of patients for shunting requires a combination of clinical findings and diagnostic test results, because no single test can predict with certainty whether a patient will benefit from an operation.

There may be a correlation between improvement in gait after removal of CSF and improvement after shunting. Cisternography has been used in diagnosis; it involves the injection of a radiolabeled tracer into the CSF with monitoring of its absorption for 3 days. Normally, the radiolabeled material fails to enter the ventricles, moving over the convexity of the brain and leaving the CSF space within 12 to 24 hours. In patients with large ventricles due to atrophy, there may be a delay in circulation time, with some isotope being seen in the ventricles during the first 24 hours. Communicating hydrocephalus with abnormal CSF circulation shows persistent ventricular filling for more than 48 hours. In patients with NPH, there is reflux of the tracer into the cerebral ventricles by 24 hours and retention in the ventricles for 48 to 72 hours. This suggests that transependymal absorption is occurring and that periventricular white matter has become an alternate route of CSF absorption. A positive cisternogram is seen in some patients with hypertensive cerebrovascular disease and Binswanger's encephalopathy because of the overlap in the three syndromes.

Neuroimaging in patients with NPH has shown enlargement of the temporal horns of the lateral ventricle with less cortical atrophy than anticipated for the age of the patient. This is in contrast to the findings in patients with hydrocephalus *ex vacuo* due to a degenerative disease, such as Alzheimer's disease, in which there is atrophy of the cerebral gyri and enlargement of the ventricles. Another useful finding on proton density MRI is the presence of presumed transependymal fluid in the frontal and occipital periventricular regions. Quantitative cisternography using single-photon emission CT has been successfully used to predict the results of a shunt. Other proposed diagnostic methods, including measuring the rate of CSF absorption by infusion of saline or artificial CSF into the thecal sac, clinical improvement after CSF removal, or the prolonged monitoring of intracranial pressure, have been used with some success to select patients for surgery. Decreased cerebral blood flow has been reported in NPH; regional cerebral blood flow is reduced in both cortical and subcortical regions.[26] Patients who show clinical improvement with shunting have a concomitant increase in cerebral blood flow. Removal of CSF may result in an increase in cerebral blood flow in patients in whom NPH is likely to respond to shunt therapy.

The number of patients undergoing shunt operations at most centers has fallen as the initial enthusiasm for this procedure, which resulted in many shunts and a low success rate, has waned. None of the currently available tests by themselves identifies the patients who will benefit from shunting. Most helpful is a combination of clinical signs and judiciously chosen laboratory tests.

Various success rates for shunt placement have been reported; some reports describe improvement in approximately 80% of treated patients, while others report lower rates. In the early days of treatment of NPH patients with shunts, a high rate of shunt failure occurred, with complications of shunting being a major problem. Serious complications occurred in as many as one-fourth of the patients, including infection and subdural hematomas. More recently, the rates of correct diagnosis and complication-free treatments have improved, but the definitive diagnostic test and complication-free treatment remain elusive goals. Clearly, more information is needed to aid in the diagnosis and management of patients with this potentially treatable syndrome

REFERENCES

1. Symonds CP. Otitic hydrocephalus. *Brain*. 1931;54: 55–71.
2. Davidoff LM. Pseudotumor cerebri; benign intracranial hypertension. *Neurology*. 1956;6:605–615.
3. Greer M. Management of benign intracranial hypertension (pseudotumor cerebri). *Clin Neurosurg*. 1968; 15:161–174.
4. Nathan H, Ouaknine G, Kosary IZ. The abducens nerve. Anatomical variations in its course. *J Neurosurg*. 1974;41:561–566.

5. King JO, Mitchell PJ, Thomson KR, et al. Cerebral venography and manometry in idiopathic intracranial hypertension. *Neurology*. 1995;45:2224–2228.
6. Donnet A, Metellus O, Le Vrier O, et al. Endovasclar treatment of idiopathic intracranial hypertension: Clinical and radiological outcome of 10 consecutive patients. *Neurology*. 2008;641–647.
7. Sahs AL, Joynt RJ. Brain swelling of unknown cause. *Neurology (Minneapolis)*. 1956;6:791–803.
8. Gideon P, Sorensen PS, Thomsen C, et al. Increased brain water self-diffusion in patients with idiopathic intracranial hypertension. *AJNR Am J Neuroradiol*. 1995;16:381–387.
9. Moser FG, Hilal SK, Abrams G, et al. MR imaging of pseudotumor cerebri. *AJR Am J Roentgenol*. 1988;150:903–909.
10. Bastin ME, Sinha S, Farrall AJ, et al. Diffuse brain oedema in idiopathic intracranial hypertension: a quantitative magnetic resonance imaging study. *J Neurol Neurosurg Psychiatry*. 2003;74:1693–1696.
11. Thambisetty M, Lavin PJ, Newman NJ, et al. Fulminant idiopathic intracranial hypertension. *Neurology*. 2007;68:229–232.
12. Katzman R, Clasen R, Klatzo I, et al. Report of Joint Committee for Stroke Resources. IV. Brain Edema in Stroke. *Stroke*. 1977;8:512–540
13. Rosenberg GA, Saland L, Kyner WT. Pathophysiology of periventricular tissue changes with raised csf pressure in cats. *J Neurosurg*. 1983;59:606–611.
14. Ibanez-Tallon I, Gorokhova S, Heintz N. Loss of function of axonemal dynein mdnah5 causes primary ciliary dyskinesia and hydrocephalus. *Hum Mol Genet*. 2002;11:715–721.
15. Afzelius B. Cilia-related diseases. *J Pathol*. 2004;204: 470–477.
16. Papile LA, Burstein J, Burstein R. Incidence and evolution of subependymal intraventricular hemorrhage: a study of infants with birth weight less than 1500 grams. *J Pediatr*. 1978;92:529–534.
17. Fisher CM, Picard EH, Polak A, et al. Acute hypertensive cerebellar hemorrhage: diagnosis and surgical treatment. *J Nerv Ment Disord*. 1965;140:38–57.
18. Jensen MB, St Louis EK. Management of acute cerebellar stroke. *Arch Neurol*. 2005;62:537–544.
19. McHugh PR. Occult hydrocephalus. *Q J Med*. 1964;33: 297–308.
20. Adams RD, Fisher CM, Hakim S. Symptomatic occult hydrocephalus with "normal" cerebrospinal fluid pressure: a treatable syndrome. *N Engl J Med*. 1965;273:117–126.
21. Marmarou A, Young HF, Aygok GA, et al. Diagnosis and management of idiopathic normal-pressure hydrocephalus: a prospective study in 151 patients. *J Neurosurg*. 2005;102:987–997.
22. Boon AJ, Tans JT, Delwel EJ, et al. The Dutch normal-pressure hydrocephalus study. How to select patients for shunting? An analysis of four diagnostic criteria. *Surg Neurol*. 2000;53:201–207.
23. Earnest MP, Fahn S, Karp JH, et al. Normal pressure hydrocephalus and hypertensive cerebrovascular disease. *Arch Neurol*. 1974;31:262–266.
24. Koto A, Rosenberg G, Zingesser LH, et al. Syndrome of normal pressure hydrocephalus: possible relation to hypertensive and arteriosclerotic vasculopathy. *J Neurol Neurosurg Psychiatry*. 1977;40:73–79.
25. Tullberg M, Hultin L, Ekholm S, et al. White matter changes in normal pressure hydrocephalus and Binswanger disease: specificity, predictive value and correlations to axonal degeneration and demyelination. *Acta Neurol Scand*. 2002;105:417–426.
26. Tanaka A, Kimura M, Nakayama Y, et al. Cerebral blood flow and autoregulation in normal pressure hydrocephalus. *Neurosurgery*. 1997;40:1161–1165; discussion 1165–1167.

Chapter 6

Quantification of Cerebral Blood Flow and Blood-Brain Barrier Transport by Nuclear Magnetic Resonance and Positron Emission Tomography

INTRODUCTION

The discovery of the mathematical equations for tomographic imaging by Godfrey Hounsfield in the mid-1970s led to the proliferation of studies on brain structure and function that have revolutionized the neurosciences and improved clinical practice. Brain images are now routinely available during life that were previously accessible only at autopsy. Initially, these images were made with x-rays by computed tomography (CT), but the same mathematical approach was applied to magnetic fields with magnetic resonance imaging (MRI) and gamma rays with positron emission tomography (PET). All of these complex technologies require cooperation between teams of physicians, physicists, chemists, engineers, and computer scientists. While it is not necessary to understand the underlying mathematical principles to utilize the new technology, a basic understanding of each method aids in the selection of the appropriate clinical test or research tool. The basic equations that are now used to analyze hundreds of thousands of pixels to construct an image of a brain function are the same ones that were initially developed for single regions. Besides structural information, which was the primary value of early CT scanners, it is now possible to obtain images of brain chemistry with magnetic resonance spectroscopy (MRS) and neural activity with functional MRI (fMRI) (Table 6–1).

Table 6–1 **Imaging Modalities in Brain Studies**

Computed tomography (CT)	x-rays
Positron emission tomography (PET)	Positrons
Magnetic resonance imaging (MRI)	Protons in water
Magnetic resonance spectroscopy (MRS)	Multinuclear (^{13}C, ^{31}P, ^{1}H)
Functional MRI (fMRI)	Oxygenation of blood (BOLD)

Blood oxygen level dependent (BOLD).

The basic equations for measurements of cerebral blood flow (CBF) are based on the Frick principle, which in the early days of CBF measurements required extensive canalization of arteries and veins and measured flow to the whole brain rather than to specific regions. These measurements can now be done without injections with MRI or with only intravenous injections, and flow in small regions of the brain can be measured. Each of the new modalities, PET, MRI, and CT, can be used to measure CBF.

MATHEMATICAL APPROACH TO CBF AND TRANSPORT

CBF: The Schmidt-Kety Approach

Kety was the first to measure CBF, basing his approach on Fick's law,[1] which states that the change in the amount of a substance, Q, within a given volume, v, is equal to the amount entering that volume of tissue, Q_{in}[mmoL/g], minus the amount leaving, Q_{out} [mmoL/g] over a short time interval Δt:

$$Q/\Delta t = Q_{in}/\Delta t - Q_{out}/\Delta t \qquad (6\text{–}1)$$

Using this equation enables determination of the cerebral metabolic rates of oxygen, glucose and lactate. Q is the product of the flow to organ F [mL/min/g] and the concentration of substance C [mmoL/g]:

$$dQ/dt = F \times C \qquad (6\text{–}2)$$

For oxygen, the amount entering a given volume dQ/dt is equal to the blood flow F [mL/min/g] multiplied by the difference between the arterial and venous concentrations of oxygen $C_a(t)_i$ and $C_v(t)$ [mmoL/ml] respectively. Then

$$dQ/dt = F(C_a(t)—C_v(t)) \qquad (6\text{–}3)$$

By using a measurable tracer, it is possible to calculate blood flow F from the above equation by knowing the concentration of the tracer in arterial $C_a(t)$, and venous blood $C_v(t)$ at time t; the tissue concentration could be obtaind from

$$C_T(t) = \lambda_T C_v(t) \qquad (6\text{–}4)$$

where λ_T, the constant partition coefficient, relates to the cerebral parenchyma–blood partition coefficient of the indicator. By solving equation (6–3) and considering equation (6–4), we can find the concentration of oxygen in tissue at time t_1 from the following equation:

$$C_T(t) = \lambda_T K \int_t^{t_1} C_a(t) e^{-K(t_1-t)} dt \qquad (6\text{–}5)$$

with $K = F/\lambda$. When blood flow to an organ is known from a separate determination, the oxygen consumption of that organ can be determined. On the other hand, when the substance is not metabolized, it can be used to measure blood flow. The anesthetic agent, nitrous oxide (N_2O), is an inert gas that can be inhaled in amounts lower than those used to produce the anesthetic effect and that equilibrates with brain tissue in 10 to 15 minutes. The arterial concentration can be sampled, and the venous concentration coming from the brain can be obtained from the jugular bulb.

The mass conservation equation for a substance that is metabolized is given by

$$Q_a = Q_v + Q_m + Q_i \qquad (6\text{–}6)$$

where Q_a is the amount in the artery, Q_v is the amount in the vein, Q_m is the metabolized portion, and Q_i is the amount of gas taken up by the organ.

For oxygen, which is practically all metabolized $Q_i = 0$, while for N_2O, which is inert, $Q_m = 0$ and Q_i can be calculated from equation (6–2).

At equilibrium, part of the gas is in the brain and part is in the blood. In a given amount of brain tissue, there is a quantity of gas equal to

$Q_i(T)$ at time T. The amount in the brain can be estimated from the venous concentration by the so-called blood-gas partition coefficient λ defined by equation (6–4). This is necessary because the actual amount of N_2O in brain tissue cannot be measured. Nitrous oxide is a marker of blood flow because it has a partition coefficient of 1 after equilibrium time. For convenience, equation (6–4) can be expressed for N_2O in the following form:

$$\lambda_{N_2O} = [Q_i(T)/\rho]/C_v(T) \qquad (6–7)$$

In equation (6–7), ρ is the tissue density. This equation represents the fact that the CBF for a given weight is the flow divided by the weight, *F/W*. Using equation (6–7) in equation (6–5), it is straightforward to calculate the partial extraction of N_2O by organ. For the measurement of CBF, the subject inhales 15% N_2O and its concentration in the arterial blood and the jugular bulb is sampled at multiple time points over 10 minutes. The integral of the arteriovenous difference and the CBF are calculated.

Regional Blood Flow

Methods to measure regional cerebral flow were developed based on the Kety-Schmidt approach, but using tracers rapidly transported into brain. A xenon radioisotopic method was developed for use with external radiation detectors and an autoradiographic method for use in experimental animals.[2] The essential feature of the regional method is the ability to measure a substance both in the brain region of interest and in the blood. The equations are similar to those for the N_2O method except that the concentration of the substance in the vein (C_v) is estimated from the partition coefficient, λ_i, and the brain concentration (C_i):

$$Cv(t) = \lambda_T C_i(t)/\lambda \qquad (6–8)$$

so that the basic equation (6–3) becomes

$$dC_i/\rho dt = F_i(C_a(t)—C_i(t)/\lambda_i) \qquad (6–9)$$

and if a flow rate constant is defined by

$$K_i = \rho F_i/\lambda_I \qquad (6–10)$$

then

$$dCi/\rho dt = K_{i\lambda}\lambda_i C_a(t)—K_i C_i(t) \qquad (6–11)$$

and a solution to this differential equation at time t_1 gives the concentration at tissue T:

$$C_i(t) = \lambda_i K_i \int_t^{t_1} C_a(t) e^{-Ki(t_1-t)} dt \qquad (6–12)$$

Inputs to this equation are the flow rate constant K_i, the partition coefficient λ_i, the concentration in the arterial blood $C_a(t)$, and the time-dependent tissue concentration $C_t(t)$. Several substances have been used to measure blood flow by autoradiography. The one that has proven most useful is ^{14}C-iodoantipyrine, which has a partition coefficient of 0.8.[3] The tracer is injected intravenously and sampled arterially multiple times for several minutes, at which time the brain is rapidly removed and sectioned on a cryostat for autoradiography. From the time curve of the amount of tracer in the blood and the amount in the various brain regions at the end of the experiment, the CBF is determined. Xenon is a stable gas that acts like N_2O. It alters the tissue characteristics on CT, which makes it useful to study CBF. Stable xenon provides regional maps of CBF and has been used in studying a number of neurological conditions.

Transport Between Blood and Brain

A number of techniques can be used to measure the transport of substances across the blood-brain barrier (BBB). While most of them are useful only for animal studies, several are available for studies in humans, using CT and MRI with contrast. Computed tomography provides a rapid method of obtaining regions of contrast leakage with iodine-based contrast agents. Multichannel CT scanners can obtain images in rapid succession, collecting changes in contrast concentration over time, which allows for extraction of permeability coefficients.[4] Magnetic resonance imaging is another modality to study the BBB. There are several reasons that MRI replaced CT: there is no radiation, the contrast agent has almost no allergic reactions, and high-resolution anatomical images can be superimposed. In favor of CT permeability measurements is that they can be obtained in a shorter time than MRI.

Compared to studies of the physiology of the BBB in humans, animal studies offer a much greater choice of methods. Selection of the appropriate method depends on the type of information desired, the technical difficulty, the species of animal used, and the characteristics of the tracer substance studied. Methods that use a carotid injection and measure a single passage through the brain are excellent for rapidly transported substances but are too insensitive to detect those that are more slowly transported (Figure 6–1). For the more slowly transported molecules, intravenous infusion of a bolus or an amount to maintain a steady blood level can be used. Some methods utilize blood entering and leaving the brain, so they are limited to those regions sampled to obtain data or to whole brain measurements, while others can be done with autoradiograms or tomography and yield regional information. Finally, when the substance being measured is rapidly transported out of the blood into the brain, it can serve as a marker of CBF.

Permeability of a membrane to a given substance is the rate with which that substance crosses the membrane. Although permeability is a complex function of the membrane structure and the reaction of the membrane to the substance, a functional definition relates the rate of movement across the membrane to the concentration of the substance on the either side. The blood dilutes both impermeable and permeable substances when they are injected into the carotid. However, permeable molecules diffuse across the endothelial cell membrane to enter the brain and CSF. Therefore, after injection into the carotid artery, if both the arterial concentration and the venous concentration as sampled at the sagittal sinus are known, the amount extracted during passage through the brain can be calculated. In other words, injecting into the carotid and sampling at the sagittal sinus gives the arteriovenous (AV) difference.

The amount of a substance extracted by the brain (E) as the blood flows through the region is defined as the concentration in the artery, C_a, minus that in the vein, C_v, with the difference divided by the arterial concentration:

$$E = (C_a — C_v)/C_a \qquad (6–13)$$

or

$$E = 1 — (C_v/C_a) \qquad (6–14)$$

After injection, dilution occurs and the arterial concentration is unknown. Since both test and reference substances are equally diluted, the ratio of the concentration of the permeable test substance to that of the impermeable reference substance in the injection fluid is known and remains constant. However, the removal of the permeable test substance by the brain changes the ratio of test and reference substances in the venous blood. Thus, ratios rather than absolute amounts reflect the amount of test substance lost to the brain. Knowing the concentrations of the test and indicator substances in both the injectate and in the venous outflow provides sufficient information to calculate the amount extracted.

Flux relates the extraction value to permeability of the membrane; it is the product of flow through a surface area, A, and the change in concentration, dC, using the relationship:

$$P = \text{Flux}/(A \times dC) \qquad (6–15)$$

Another way of expressing the flux is by blood flow. The flux equals the blood flow (F) through the vessel and the arteriovenous difference,

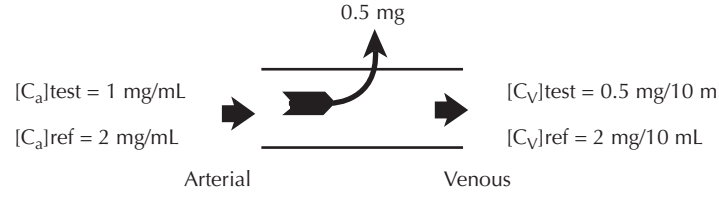

Figure 6–1. Illustrative example of the calculation of the extraction fraction (E) using the indicator dilution method with a partially permeable, extracted test substance of concentration $[C_a]_{test}$ in the artery and an impermeable reference substance $[C_a]_{ref.}$.

that is, the arterial concentration, C_a, and the venous concentration, C_v:

$$\text{Flux} = \text{F}\ (C_a - C_v) \qquad (6\text{–}16)$$

Leading to the relationship,

$$\text{PA} = (\text{F}\ [C_a - C_{v]})/dC \qquad (6\text{–}17)$$

The change in concentration is not known, and it can be estimated empirically with the relationship:

$$dC = (C_a — C_v) / [1\text{n}(C_a/C_v)] \qquad (6\text{–}18)$$

Substituting this into the earlier equation gives:

$$\text{PA} = -\text{F}\ 1\text{n}(1\text{-E}) \qquad (6\text{–}19)$$

The flow and the extraction rate can be estimated or experimentally determined so that the permeability of the surface area can be calculated. Estimating the surface area allows calculation of the permeability itself. The indicator-dilution method is best suited for repeated measurements of moderately permeable molecules, such as glucose. Limitations of the method include extracerebral contamination of sinus blood, changes in blood flow by the injection, and lack of regional specificity.

Oldendorf measured brain uptake of a rapidly diffusible ^{3}H-labeled reference substance and a less diffusible test substance labeled with ^{14}C; both substances were injected into the carotid, and brain tissue was rapidly sampled to obtain a ratio of the two substances to calculate the brain uptake coefficient[5] (Figure 6–2). Fifteen seconds after injection of the tracers into the carotid, the brain is removed and the amount of both the test and reference substances in brain is measured. Ratios of the test substance to the reference substance in both the brain and the blood can be measured. A brain uptake index (BUI) can be calculated by the expression

$$\text{BUI} = (C_t/C_r)_{\text{brain}}/(C_t/C_r)_{\text{injectate}} \times 100 \qquad (6\text{–}20)$$

where C_t is the concentration of the test substance and C_r is that of the reference compound either in the brain or in the injectate. Generally, the reference molecule is ^{3}H-labeled water and the test substance is a ^{14}C-labeled compound. Ideally, the reference substance would be completely extracted in a single passage through the brain in order to be able to calculate an accurate value for extraction of the test substance; a less permeable reference substance would lower its concentration in the brain and falsely elevate the BUI.[6] Although

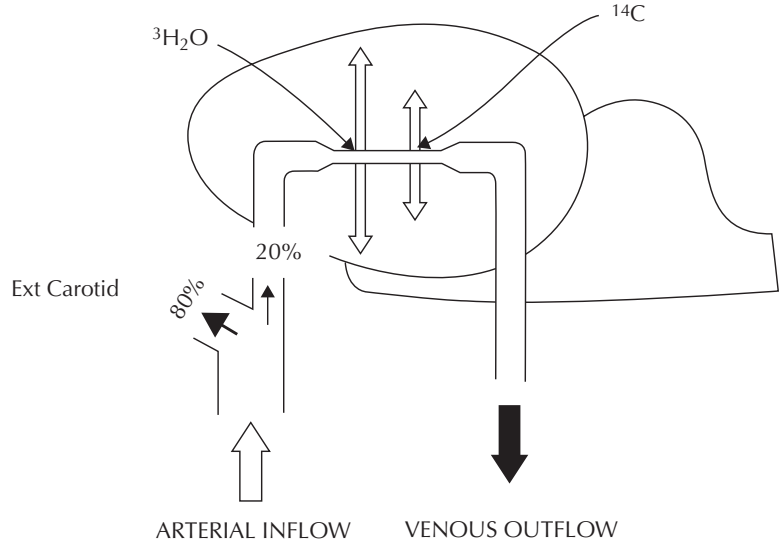

Figure 6–2. Diagram of the brain uptake index method. A buffered solution containing a ^{14}C-labeled test solute and ^3H_2O is injected into the common carotid artery of a rat, and the animal is decapitated 15 seconds later. (From Ref. 5.)

water moves across the endothelial cell, its uptake into brain is slightly limited by its diffusion across the capillary.[7] The slower than expected diffusion rate makes the amount of water extracted dependent on the rate of CBF. This can present a problem since intracarotid injection may alter the blood flow. In fact, the carotid injection of a 200 μL bolus in less than 1 second alters blood flow. To overcome the problem caused by the diffusion limitation of water, ^{14}C-butanol has been used as the reference tracer because it is more rapidly transported. In spite of the flow limitation, very useful information has been obtained using the BUI method; for most molecules the effect of water limitation is minimal, and for those where it is a problem, corrections can be made for the lower extraction rate. Therefore, the BUI method has been used to study moderately permeable molecules such as the narcotics, the peptides, and the amino acids.

Another approach utilized the steady-state intravenous infusion of a radiolabeled test substance with an infusion apparatus that maintained a constant blood level.[8] This method can be used to study less permeable substances, such as sodium, that require a longer time to enter the brain. A modification of the intravenous method that utilizes a bolus intravenous injection has also been used to measure the transport of substances with low permeability and negligible back flux.[9]

Another way to express BUI is by use of the extraction fraction, E, which includes other factors. Conversion of BUI to *E,* can be done, assuming that there is negligible back flux of test tracer, by the formula

$$E = (c\text{BUI})/100 \qquad (6\text{–}21)$$

where c is a constant that depends on blood flow, the reference tracer, the decapitation time, and the brain region sampled. An estimate of PA is then obtainable with equation (6–19). The BUI method has been used extensively because it is relatively simple to perform. However, translation of BUI to PA has been hampered by the need to determine the constants.

Although it is appealing to express the movement of a test substance from the blood to the brain in terms of permeability, the inability to directly measure the surface area introduces considerable uncertainty into the measurement. The capillary surface area has been estimated for different brain regions. The capillary is a dynamic structure that undergoes changes in its surface area in response to changes in its environment. Therefore, the combined expression for permeability and surface area should be used unless the surface area can be unambiguously determined.

POSITRON EMISSION TOMOGRAPHY

Positrons are positively charged particles emitted from an unstable nucleus. When a positron and an electron collide they are annihilated, and two gamma rays are formed that are 180° to each other.[10] The PET scanner has an array of detectors arranged in a circle. An event is recorded when detectors at 180° to each other are simultaneously activated. A large array of opposing radiation detectors allows localization of the point source of positron emission. The detection of two simultaneous events is recorded for multiple lines of coincidence, and the data are reconstructed analogously to the mathematical process used in CT scanning. The principles used for data analysis and image reconstruction are similar for CT, MRI, and PET. The major benefits of PET scanning are that it allows location of the point source in three dimensions and very small amounts of tracer can be detected.

The positron-emitting atoms commonly used for labeling with PET studies are ^{15}O, ^{13}N, ^{11}C, and ^{18}F, with half-lives of 2, 10, 20, and 110 minutes, respectively (Table 6–2). These

Table 6–2 **Uses for Various Positron Emitters**

Isotope	Half-Life (min)	Function
^{15}O	2	rCBF, rOER
^{11}C	20	Amyloid plaques (^{11}C-P1B)
^{18}F	110	Amyloid plaques

rCBF, regional cerebral blood flow; rOER, regional extraction oxygen ratio; ^{11}C-P1B (Pittsburgh compound B).

compounds are given in 5 to 100 mCi doses, depending on the compound labeled and the organ to be studied. The total radiation dose to the patient is 1 to 2 rads, with a maximum permissible dose of 5 rads. Repeated studies with certain compounds can therefore lead to appreciable radiation exposure.[11]

Positron emission tomography, like autoradiography, shows regional substrate utilization. Glucose metabolism is measured with 2-deoxy-2-[^{18}F]fluoro-D-glucose (FDG), which is phosphorylated upon entry into brain cells and trapped as the phosphorylated compound. Since little of the tracer is metabolized in the first few minutes, transport into brain cells can be measured. Some of the originally injected tracer remains in blood and extracellular fluid during this short time period, making corrections for regional blood volume necessary. Generally, a 30 to 40 minute delay after injection is necessary for complete phosphorylation of the tracer, and during this time some metabolism by phosphatase may have occurred. The problems with the use of an analog are the long measurement time, the large radiation dose, particularly with ^{18}F, and the potential toxicity from compounds that interfere with glucose metabolism.

Several methods have been used to measure CBF and oxygen metabolism with PET. The ^{15}O steady-state inhalation model provides measurements of regional CBF, oxygen extraction ratio (rOER), and oxygen utilization (rCMRO$_2$).[12] The technique involves continuous inhalation of tracer amounts of C^{15}O$_2$. In the lungs, CO_2 is converted to ^{15}O-water. After 10 minutes a steady state is reached, with the rate of delivery to the brain balanced by the washout of the tracer into the venous circulation. Regional CBF is related to the arterial (C_a) and tissue (C_i) concentrations of ^{15}O-water by the relationship

$$\text{rCBF} = \tau/[(C_a/C_i)—1] \qquad (6–22)$$

where τ is a correction factor to account for loss from decay. The rOER is measured by the inhalation of $^{15}O_2$ with corrections for recirculation of labeled water. From the blood flow and oxygen extraction the rCMRO$_2$ can be determined:

$$\text{CMRO}_2 = \text{CBF} \times [\text{O}_2]\text{arterial} \times \text{OER} \qquad (6–23)$$

Errors in the use of these equations occur because the extraction of H_2O is less than 100% and due to the variability of cerebral blood volume, which needs to be calculated. Current models of rCBF and rOER measurement incorporate terms to correct for these factors. Measurements of rCBF and rOER with the steady-state continuous inhalation method require 1.5 to 2 hours; patient cooperation is essential for these long studies.

Another method used to measure CBF by PET besides inhalation of ^{15}O-labeled CO_2 is the injection of ^{15}O-water. ^{15}O is well suited to blood flow measurements because it has a short half-life and can, therefore, be used for repeated measurements without producing too great a radiation exposure. Measurement of CBF with ^{15}O-water is based on the Kety approach to describing the exchange of an inert gas between blood and tissue. ^{15}O-water is injected intravenously, and arterial samples are collected over several minutes while the ^{15}O is detected in the brain. The main problem with the use of ^{15}O-water is that it is not freely diffusible across the capillary. The diffusion rate for water is slower than that for a freely diffusible substance.[7] Blood flow measurements made with water are underestimated.[13] The advantage of ^{15}O-water is that it has a short half-life with low radiation exposure from a single study, making multiple studies possible in a single subject.

The extent of the diffusion limitation with water has been studied with a more readily diffusible substance, [^{11}C]butanol. Butanol is an alcohol that readily crosses the BBB.[14] Compared to water, it is more completely extracted. The amount of butanol and water extracted by the brain differs; the difference in the amount of each isotope extracted by the brain provides a means to calculate the permeability of the capillary to water.

Although [^{11}C]butanol is a better compound for measuring CBF, it has several disadvantages that limit its usefulness. The longer half-life of ^{11}C results in slow decay of the radioactivity, which interferes with subsequent isotopic studies and limits the number of times blood flow can be measured. For this reason, the ^{15}O-labeled compounds have been more frequently used to measure CBF.

Imaging of brain neurotransmitter receptors with positron-labeled receptor-binding molecules has been used to study patients with

parkinsonism, schizophrenia, and epilepsy. The dopamine D2 receptor has been imaged in humans with the receptor ligand, ^{11}C-*N*-methylspiperone. Normally, the ligand binds specifically to the dopamine receptors in the caudate.

Pittsburgh Compound-B (PIB) is an amyloid-binding compound labeled with a positron emitter that shows the presence of amyloid plaques in the brains of patients with Alzheimer's disease (AD). Compared with controls, AD patients typically showed marked retention of PIB in areas of association cortex known to contain large amounts of amyloid deposits in AD. In the AD patient group, PIB retention was increased most prominently in frontal cortex but was also seen in parietal, temporal, and occipital cortex and striatum[15] (Figure 6–3). These early results suggested that PET imaging with the novel tracer PIB can provide quantitative information on amyloid deposits in living subjects with AD. With further studies, however, the nonspecific nature of amyloid binding in brains of normal individual reduces the clinical utility of amyloid-binding compounds. A community-based sample of 43 volunteers, aged 65 to 88 years, who did not meet diagnostic criteria for AD or mild cognitive impairment were studied with PIB. Nine (21%) showed evidence of early amyloid deposition, demonstrating that amyloid deposition can be identified among cognitively normal elderly persons during life, and the prevalence of asymptomatic amyloid deposition may be similar to that of symptomatic amyloid deposition.[16]

Single-Injection External Registration

Positron emission tomography studies can be done with a method that utilizes intracarotid

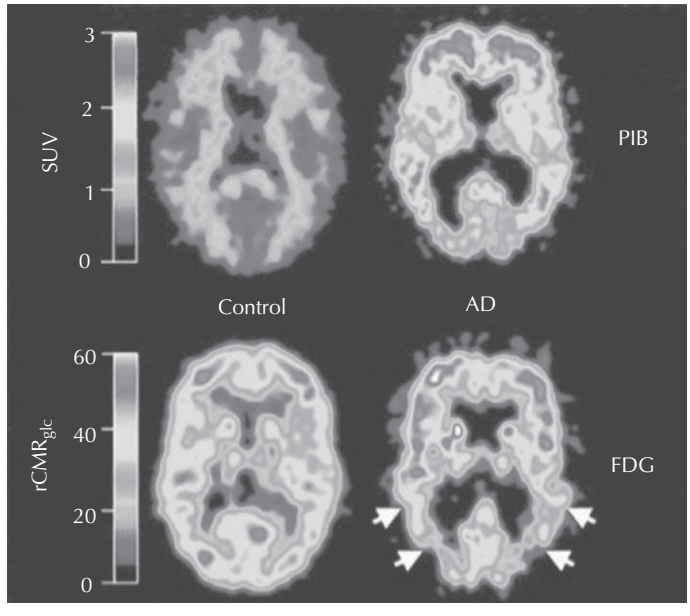

Figure 6–3. Pittsburgh Compound-B standardized uptake value (SUV) images demonstrate a marked difference between PIB retention in Alzheimer's disease (AD) patients and healthy control (HC) subjects. Positron emission tomography images of a 67-year-old HC subject (left) and a 79-year-old AD patient (AD6; mini-mental status examination (MMSE) = 21; right). Top: SUV PIB images summed over 40 to 60 minutes. Bottom: ^{18}Fluorodeoxyglucose regional cerebral metabolic rate for glucose(^{18}FDG rCMRglc) images (mol/min/100 mL). The left column shows lack of PIB retention throughout the gray matter of the HC subject (top left) and normal ^{18}FDG uptake (bottom left). Nonspecific PIB retention is seen in the white matter (top left). The right column shows high PIB retention in the frontal and temporoparietal cortices of the AD patient (top right) and a typical pattern of ^{18}FDG hypometabolism present in the temporoparietal cortex (arrows; bottom right) along with a preserved metabolic rate in the frontal cortex. The PIB and ^{18}FDG scans were obtained within 3 days of each other. (From Ref. 15; See also the color insert.)

or intravenous injection of a short-lived radioisotope that is rapidly taken up by the brain.[14] A positron-labeled substance such as ^{15}O-labeled water or ^{11}C-labeled carbon monoxide is injected into the carotid or intravenously. External detectors register the appearance of the tracer in the head and its clearance. Since water is rapidly transported, it provides a useful estimate of the rate of blood flow (its slight diffusion limitation results in an underestimation in high-flow states). This method has been used to show changes in water permeability induced by various agents including vasopressin and osmotic agents. Use of PET to measure permeability is cumbersome compared to CT and MR methods. The short half-life of positron-labeled compounds requires that they be made by a cyclotron close to the PET scanner, and they must be attached to the study molecule and injected intravenously. A large team of physicists, chemists, and radiologists is necessary to carry out these costly experiments. The development of autoradiography provided a theoretical basis for the use of CT and MRI in studies of the BBB in humans.

Patlak Graphical BBB Method for Autoradiography and MRI

Autoradiography was used in animals to map the distribution of the labeled isotope in specific brain regions. Equations to measure the permeability constants were developed by Patlak and colleagues based on a graphical method. The advantage of the graphical method is that it provides regional measurements of BBB transport, which are of interest in the study of pathological processes such as stroke, brain tumors, traumatic brain injury, cavernous malformations, and multiple sclerosis.

In the autoradiographic method, aminoisobutyric (AIB) acid is an amino acid that is passively transported into brain; normally, its transport is slow; however, in pathological conditions, the rate is increased.[17,18] The amino acid concentration in blood is recorded at multiple points after its intravenous injection; at a given time, the brain is removed and cryosections are prepared for autoradiography. The AIB method is excellent for analysis of pathological states since, under normal conditions, AIB is very slowly taken up by brain. Transfer constants are obtained from the information in the blood curve and the brain autoradiogram using Patlak's equations.

Adaptation of the graphical method to CT and MRI has facilitated measurements of BBB permeability in humans. Contrast-enhanced MRI scans provide useful qualitative information for highly permeable regions of the brain. Quantification of regional permeability requires the use of multiple measurements over time. Originally developed in animals and proven accurate by comparison with autoradiograms, the graphical method can be used not only to visualize the regions of increased uptake but also to quantify the effects of treatments.

Gadolinium-diethylenetriaminepentaacetic acid (Gd-DTPA)-enhanced MRI scans are performed with a series of rapid T1-weighted measurements and are made after injection of the contrast agent. This method has been referred to as *dynamic contrast-enhanced MRI* (DCEMRI); comparison of ^{14}C-sucrose autoradiographic measurements of BBB permeability with Gd-DTPA MRI measurements was done in the same rat brains, demonstrating excellent correlation of the two methods.[19] The ability of Gd-DTPA-enhanced MRI to localize and quantitate BBB opening was evaluated against quantitative autoradiographic imaging of the ^{14}C-AIB distribution in animals with stroke. The blood-to-brain transfer constant (K_i) for Gd-DTPA was determined by MRI in rats with focal cerebral ischemia and compared with that of AIB as determined by quantitative autoradiography done soon afterward. Estimates of K_i came from Patlak plots constructed from the time course of Gd-induced blood and tissue T1 changes. Mean K_i values of AIB were highly correlated with those of Gd-DTPA across multiple brain regions. In most instances, Gd-DTPA MRI accurately localized areas of BBB opening.[20]

The benefit of using an MRI method for estimation of BBB permeability is that it can show pixel-by-pixel changes in permeability and can be used in human studies in a clinically relevant time frame. In addition, in animal studies, the ability of MRI to study multiple parameters in an ischemic region including CBF, diffusion-weighted imaging, and infarct size, makes it the method of choice for studies of stroke in both animals and humans.

MRI IN CBF AND TRANSPORT MEASUREMENT

Magnetic resonance imaging provides noninvasive approaches for quantitative assessment of CBF and transport. Most successful approaches in CBF measurements by MRI are based either on tracking a bolus of paramagnetic contrast agent (an exogenous MRI-visible tracer) or on arterial spin labeling (an endogenous MRI-visible tracer). This method, which is called *arterial spin labeling* (ASL), uses magnetically labeled arterial blood as an endogenous flow tracer. Radiofrequency inversion is used to tag the blood. In order to acquire the ASL image, an image is acquired from the tagged inflowing arterial blood by magnetic inversion. The acquisition is repeated without tagging to be used as the control image**.** The control image is subtracted from the tagged image to compute the arterial inflow.

MRI AND SPECTROSCOPY

Nuclear magnetic resonance (NMR) spectroscopy (magnetic resonance spectroscopy [MRS]) provides a unique method for the in vivo study of the chemistry of metabolism. Molecules containing ^{13}C, ^{19}F, ^{23}Na, and ^{1}H have magnetic moments that can be detected[21] (Table 6–3). Because of the innocuous nature of MRS, in vivo noninvasive measurements of brain metabolism can be easily repeated and a pathological process followed over time. Although a true understanding of the concepts behind the biological use of NMR are complex and require quantum mechanics for a full appreciation, basic concepts can be grasped without resorting to mathematical formulations. Therefore, what follows is a simplified discussion focused on those aspects necessary for an understanding of MRI and MRS.

Nuclei with magnetic moments align themselves parallel to a magnetic field. Certain atoms possess magnetic properties that make them detectable by NMR. Atoms have nuclear spins whose value depends on the mass number and the atomic number of the nucleus. Those nuclei with spins of 1/2, 3/2, 5/2, and so on will resonate when placed in an applied magnetic field. The resonant frequency will depend on the magnetogyric ratio, γ, which is a proportionality constant specific for each particular atom. The fundamental resonance condition for all NMR experiments is given by the Larmor equation:

$$\nu_0 = \gamma B_0/2\pi \qquad (6\text{–}24)$$

where ν_0 is the frequency (Hz) at which a nucleus of a given magnetogyric ratio resonates when a magnetic field, B_0, is applied. The field or the frequency may be varied in order to obtain spectra. The strength of a magnetic field is described in Tesla or kilogauss (1 T = 10 kG). When nuclei with magnetic moments are exposed to radio waves of a specific frequency, they emit a signal of the same frequency as that applied. Atoms with magnetic moments can assume one of several discrete energy states when placed in a magnetic field. When another magnetic field is applied, the atom undergoes a transition from one energy state to another.

Energy levels in NMR are in the radio frequency range of 107 Hz. Visible light is at a frequency of 1015 Hz, while that of x-rays is 1017 Hz (Figure 6–4). Therefore, the amount of radiation needed for NMR studies is very

Table 6–3 **NMR Properties of Other Nuclei Compared to Hydrogen**

Nucleus	Resonance Frequency at 5T (mHz)	Spin Number	Natural Abundance (%)	Relative Sensitivity Compared to Protons
^{1}H	213.0	1/2	99.98	100
^{13}C	53.5	1/2	1.1	1.6×10^{-2}
^{15}N	21.6	1/2	0.36	3.7×10^{-4}
^{19}F	200.0	1/2	100.0	83.0
^{31}P	86.2	1/2	100.0	6.6
^{23}Na	56.3	3/2	100.0	9.3

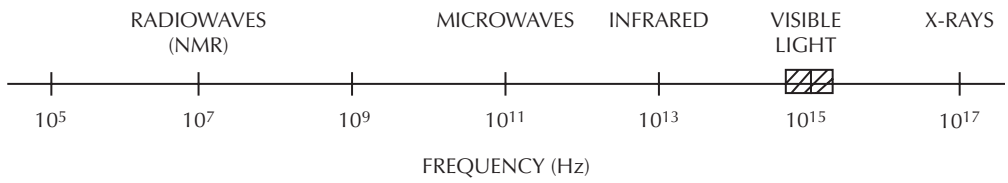

Figure 6–4. Regions of the electromagnetic spectrum. The visible light region occupies a small band around 10^{15} Hz. Nuclear magnetic resonance is at the radiowave energy level.

low. Spectroscopy involves raising the energy level of a substance and recording its return to the unexcited state. Energy is absorbed and emitted in discrete packets. Increasing the energy state causes a transition to the higher level. Because the magnetic forces of atoms are small, the amount of energy needed to raise the energy state is in the 10^5 to 10^7 Hz range. X-rays, in comparison, excite electrons at 10^{17} Hz, while microwaves, at l0^{11} Hz, induce molecular rotation and heating. The NMR signal depends on the weak attraction of one nucleus for another; for example, ^{1}H near a carbon atom has a slightly different response to the applied field, depending on the position of the carbon in the molecule.

The strength of the magnetic field can vary over a wide range, from very low fields of 0.05 T to high fields of 11 T. In order to detect magnetic atoms in molecules of lower concentrations and separate signals with close resonances, it is necessary to go to higher fields. Superconducting helium-cooled magnets are needed to produce the higher field strength for in vivo spectroscopy: the higher the fields, the better the ability to detect substances present in lower concentration and for nuclei of lower sensitivity, such as ^{31}P and ^{13}C. An added advantage of high-field magnets is that as the field strength increases the signal-to-noise ratio improves, so that sharper peaks with better spectral definition are possible.

Multinuclear NMR

In addition to protons, other atoms, such as ^{31}P, ^{23}Na, ^{13}C, and ^{15}N, can be detected by NMR, but with weaker signals than those seen with water because of their much lower abundance. Electrons in orbits around the atoms modify the magnetic signal from the atom. Since hydrogen has only one orbital electron, it has the greatest response to the applied magnetic field. That is, the proton experiences a greater effect than an atom with more electrons and, therefore, more atomic shielding. The electrons, as they spin around the atom, set up electromagnetic fields that modify the magnetic field they experience. Atoms are compared to protons to describe their sensitivity. The sensitivity of certain atoms compared to water is given in Table 6–3.

Nuclear magnetic resonance is possible because certain nuclei behave as tiny bar magnets, aligning themselves along magnetic lines (Figure 6–5). When a magnetic field, B_o, is applied, the spinning nuclei orient themselves either in the direction of or opposite to the applied field. If a second magnetic field is induced electronically at right angles to the originally applied field, and if the new magnetic field is oscillating at the resonant frequency, ν_o, for that atom then they move up to a higher energy level:

$$\Delta E = h\nu_0 \qquad (6\text{–}25)$$

where ΔE is the increase in energy and h is the Plank constant. The resonant frequency needed to excite different nuclei is determined from the magnetogyric ratio and is related to the magnetic field. Each nucleus has a different magnetogyric ratio and resonates at a different frequency. Since the magnetogyric ratio varies from atom to atom, for a given field there is a characteristic resonance frequency for each atom.

In a strong magnetic field, only a portion of the atoms are aligned to the field at a given time. Since millions of atoms are involved, the number actually aligned in the field direction may be only a few parts per million (ppm). Homogeneous magnetic fields are needed to produce sufficient signal for spectra formation; inhomogeneous fields degrade the signal. This can be due to magnet design problems or to characteristics of the sample being studied that lead to inhomogeneities.

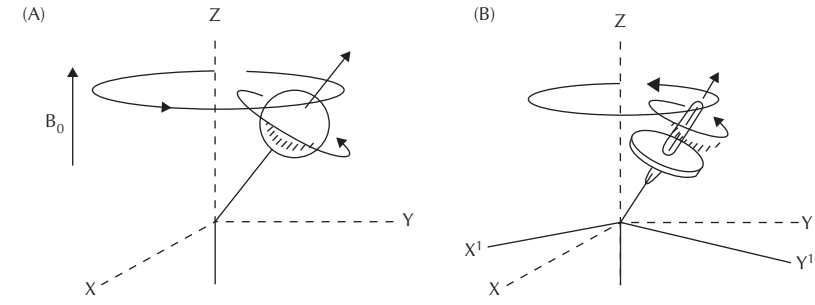

Figure 6–5. (**A**) Atoms with magnetic moments line up along the magnetic field lines when placed in a magnetic field ($\mathbf{B}_0$). The atoms spin about their own axis and rotate (precess) about the main axis of the field.

Magnet homogeneity is important in biological NMR. Because the forces between atoms that are detected by NMR are very small, the magnets capable of detecting them require homogeneities that exceed a few parts per million. Spectrometers used for high-resolution NMR are capable of distinguishing spectra separated by less than 1 ppm. The basic notion of electron shielding underlies all of the current uses of NMR spectroscopy. Therefore, an understanding of the concept of chemical shift is critical for the following discussion.

Each nucleus within a molecule may experience a slightly different magnetic field because the electrons within the molecule shield the nuclei from the full force of the applied field. This so-called nuclear shielding, δ, is proportional to the applied field. In effect, the other nuclei have shifted the resonant frequency, and a new term is introduced to relate the amount of shift to a reference compound. The Larmor equation (6–24) is now written as

$$\nu_A = \gamma B_0 (1 - \sigma_A)/2\pi \qquad (6–26)$$

where σ_A is the screening constant for nucleus A.[22] An example of the effect of nuclear shielding on proton NMR spectra is given in Figure 6–6. Methanol has the chemical formula CH_3OH and contains four protons. In a magnetic field with homogeneity greater than 10^7, the protons near the carbon can be distinguished from those near the oxygen. The methyl protons ($-CH_3$) are shielded more than the hydroxyl protons (–OH). This causes the methyl protons to resonate at a lower frequency.

The chemical shift is defined as the nuclear shielding divided by the applied field. A reference compound either external to the measured material or within it is needed. The chemical shift of the nucleus A is given as

$$\delta_A = [(\nu_A — \nu_{ref}/\nu_{ref})/\nu_{ref}] \times 10^6 \text{ ppm} \qquad (6–27)$$

where ν_{ref} is the effective field experienced by a reference compound and ν_A is that of the sample. The shielding effect produces a shift that is dimensionless and expressed in parts per million; the higher the applied or reference magnetic field, the greater the separation

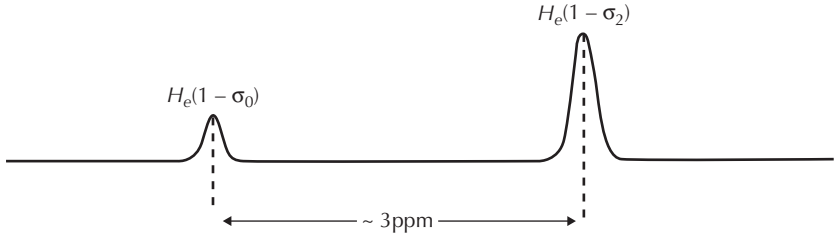

Figure 6–6. Proton NMR spectrum of methanol (CH_3OH) in a magnetic field with uniformity greater than 10^7. Two chemically shifted lines are resolved arising from the methyl and hydroxyl protons. The three methyl protons are three times higher than the one hydroxyl proton. (From Ref. 22.)

in Hertz. Two peaks with a separation of 60 Hz in a 60 MHz field (1 ppm) will be 100 Hz apart in a 100 MHz spectrometer. This is the reason that higher field magnets are better for spectroscopic studies, while imaging is not necessarily better at higher fields where other effects may interfere with the water signal.

Nuclear magnetism is extremely small compared to, for example, paramagnetism, which is found in materials in which magnetic fields can be induced. Hydrogen nuclei act as tiny bar magnets in a strong magnetic field. Normally, the nuclei are aligned randomly, with some pointing up and others down. The net effect is no magnetic moment. Protons of hydrogen have a spin of 1/2 and two possible energy states. As they line up in the field, they experience a force that causes them to gyrate about their axis. The angular velocity at which they gyrate or precess depends on the field strength and the characteristics of the nuclei. For example, hydrogen with a spin of 1/2 has two possible positions $(2j+1)$, where j is the spin number.

An NMR spectrometer works by inducing an oscillating field around the sample at a frequency that causes nuclei in the sample to resonate. When the resonating frequency induced equals the characteristic frequency for that substance, there is a transition from the lower to the higher energy state and energy is absorbed. Normally, there is a small preponderance of nuclei that are in the lower energy state. This amounts to less than 1 part in 10^6. The slight energy absorption can be detected with a sensitive electronic amplifier. The resonance frequency causes the nuclear magnets to precess synchronously. The spectrometer detects the signals, which begin to decay with time. Older spectrometers changed the magnetic field to find the resonant frequency and produce the signal. This form of NMR, called *continuous NMR*, was very time-consuming. A major advance occurred with the use of Fourier transforms. This allowed the simultaneous recording of multiple frequencies at the same magnetic field.

Fourier transformation converts the signal from the time domain to the frequency domain (Figure 6–7). By turning the signal on and off rapidly at a time interval of t seconds, a range of frequencies centered about the original frequency, F, occurs. This form of NMR, which is referred to as *pulsed Fourier transform NMR*, has become the NMR method of choice. When the pulse is applied, a single decaying curve is obtained in the time domain, which converts to a single peak in the frequency domain. A pulse of time, t, produces a frequency response that has an inherent uncertainty of $1/t$. In other words, the shorter the pulse, the greater the frequency spread. Relaxation of molecules when the pulse is stopped leads to the return to the unexcited state, that is, the alignment of the nuclei in the field is lost. Relaxation to the unexcited state is referred to as *T1 relaxation*. Interactions between nuclei also occur, and relaxation of the interacting nuclei is referred to as *T2 relaxation*.

T1 and T2 are used extensively in image formation. A T1-weighted MRI scan has a shorter

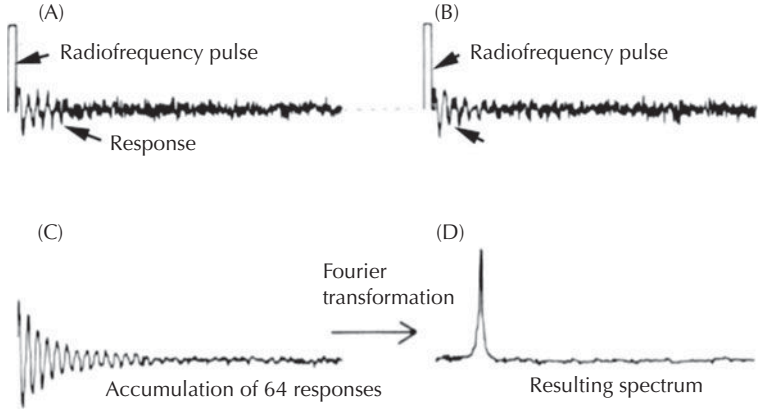

Figure 6–7. Spectra from a single resonance are accumulated. (**A,B**) Two consecutive responses to radiofrequency pulses of 20 milliseconds' duration and at intervals of about 1 second. (**C**) Accumulation of 64 responses or scans. (**D**) The spectrum obtained on Fourier transformation of the accumulation. (From Ref. 23.)

relaxation time and shows signals in protons attached to molecules in membranes, while the longer-relaxing molecules that remain spinning are not observed. Thus, in the T1-weighted image, water appears as a dark region and the tissue is lighter, which can be readily visualized by the very dark regions inside the water-filled cerebral ventricles. By contrast, T2-weighted images are formed at longer relaxation times, when the water molecules are still spinning, resulting in detection of the molecules with long resonances. The technique of allowing the spinning atoms to return to the original state is referred to as *spin-echo* because it refocuses the water molecules during the longer recording times. Water molecules on the inelastic membranes lose resonance while those in the water continue to spin, allowing them to be detected.

An important addition to the imaging sequences was the use of FLAIR (fluid attenuated inversion recovery), which uses shorter imaging times to show water that is relaxing at an intermediate speed. This allows the water in the tissues to be seen, revealing edema fluid clearly, but reduces the signal from the water in the ventricles, which is still spinning. The FLAIR sequence is an important improvement that shows water in tissue while suppressing the water proton signal in CSF. This is an excellent sequence to detect the transependymal flow of water in hydrocephalus and early edema formation in the ischemic brain.

The Relaxation Phenomenon and the Rotating Frame

A convenient way of thinking about the relaxation phenomenon is to use the concept of the rotating frame. Earlier in the chapter, the fundamental equation (6–24) related the frequency of precession of the nuclei of a given atom to the magnetic field strength and the characteristic magnetogyric ratio. In a magnetic field, B_0, a sample of nuclei with nuclear spin 1/2 will precess around the direction of the field with a frequency of ν_o, which is called the *Larmor frequency*. The nuclei will align either with or against the field (up or down). A slight excess of nuclei align themselves in the direction of the field, with a resulting net magnetization in that direction. The magnetization vector is referred to as M_o. If the *xy*-plane were set to rotate in the same direction as the precessing nuclei, they would appear stationary and could be simply described by a bulk magnetization vector. This construct is useful in imagining the effects of pulse sequences. The concepts of the rotating frame, pulse sequences, and relaxation are central to understanding biological NMR; they are discussed in greater detail in NMR textbooks.[23]

Radiating the sample with another pulse of the same frequency as the Larmor frequency but along the *y*-axis results in tipping of the magnetization vector into the *xy*-plane. When the appropriate radiofrequency pulse in a magnetic field excites nuclei, they have a net magnetic moment in the direction of the excitation. If we assume that the original moment is in the *z* direction of the *xyz* reference frame, then relaxation back to the unexcited state takes a certain amount of time. Relaxation back to the original *z*-plane is referred to as *spin-lattice relaxation*. Spin-lattice or T1 recovery can be measured by the inversion-recovery method (Figure 6–8). The original alignment in the field along the B_o field lines results in alignment of the nuclei in the *z* direction. A pulse of radiofrequency energy of sufficient length to invert the magnetic moment 180° is applied. After a waiting period of length τ, the signal begins to recover. Another pulse of 90° is given, and the amount of signal that has recovered is recorded during the collection time, t_D. Signal collection occurs in the *y*-plane; the 90° pulse is needed after the 180° inversion pulse to position the signal in the correct plane. An inversion-recovery pulse sequence is given as

$$(180°-\pi\text{—}90°-AT\text{—}D)_n \qquad (6\text{–}28)$$

where *AT* is the acquisition time for the signal to be collected and *D* is the delay between collections, which is at least four times the T_1 value. T_1 measurements are made by collecting spectra at different *t* values and plotting the value of $1n(M_{inf}—M_t)$ against *T*. A straight line results with a slope of $1/T_1$.

The interaction between molecules is measured by the T_2 or spin-spin relaxation methods. Spin-spin measurements are more difficult to do and more subject to error than T1. The reason for this is that inhomogeneities in the magnetic field contribute to the apparent spin-

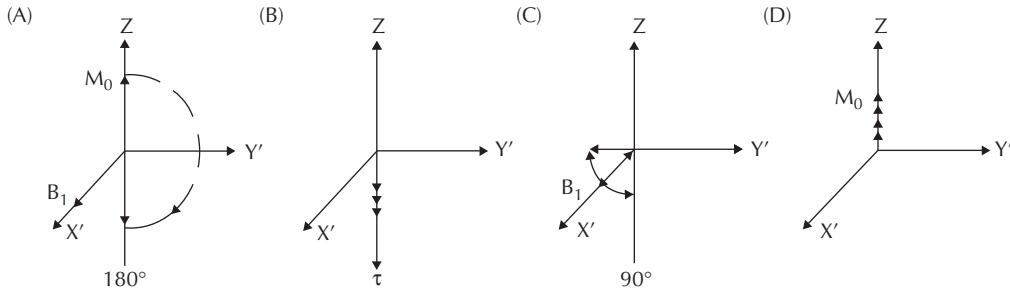

Figure 6–8. Inversion-recovery Fourier transform method for T1 determination. (**A**) Net magnetization in the *z* direction equals M_0. A 180° pulse inverts the magnetizations vector. (**B**) M_z then recovers toward its initial value, M_0, during time τ. (**C**) A 90° pulse tilts this magnetization into the recording *xy*-plane. The size of the resulting signal is determined by the magnetization at the time of recording. (**D**) After a delay of time $D > 4$ T1, the magnetization, M_z, has relaxed to its initial value of M_0 and the cycle can then be repeated (From Ref. 23).

spin relaxation time. Measurements of T2 relaxation are done by the spin-echo method (Figure 6–9). The magnetization is tilted 90° into the *xy*-plane. The phase coherence is gradually lost because of slight inhomogeneities in the field. This results in the faster-moving molecule dephasing ahead of the slower-moving one. When the field is flipped 180°, the slower-moving nuclei are placed inside the faster-moving ones so that they refocus at the same time, partially correcting the effect of the inhomogeneity. After a time delay, the signal has dephased around the *z*-axis. Another pulse of 180° reverses the dephasing signal, and continued fanning brings the signal to a focus along the *y*-axis, forming a mirror image or echo of the original signal. The echo can be repeated a number of times at every 2*t* seconds. As with the T1 measurements, over time the signal intensity at each echo is slightly less and T2 can be calculated from a plot of 1n(*My—Moy*) against time.

Relaxation measurements are made after pulse sequences have been applied to help identify the origin of the signals. Bound molecules, such as those in crystals or membranes, have

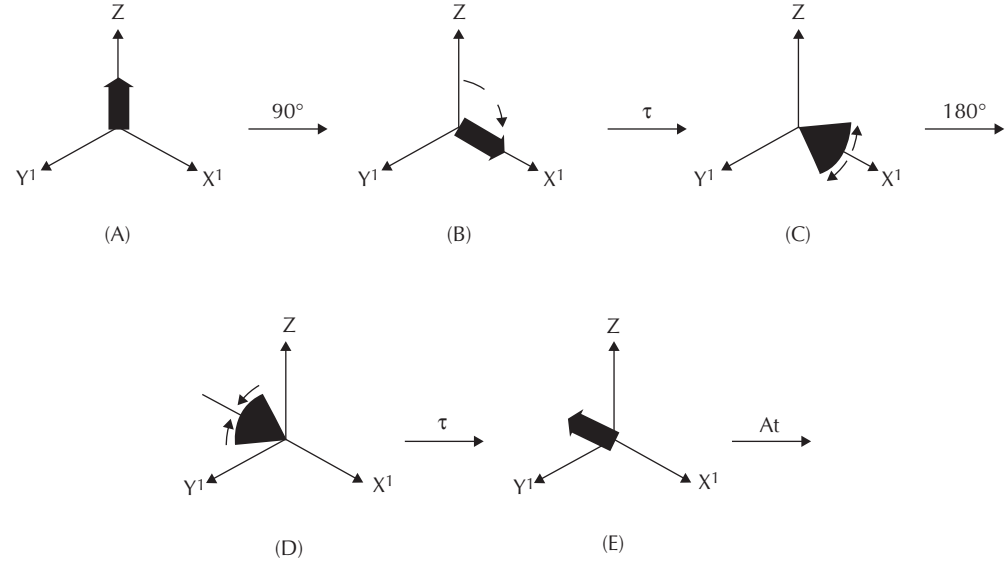

Figure 6–9. Spin-echo T2 measurement. (**A**) Magnetization in the *z*-direction. (**B**) A 90° pulse tilts the magnetization onto the *x′*-axis. (**C**) The field in homogeneity causes the vector to diphase or fan out over time. (**D**) A 180° pulse about the *x′*-axis reverses the magnetization. (**E**) The precessing atoms come together or refocus into an echo during time τ (From Ref. 23).

shorter relaxation times because they are less mobile than unbound ones. Therefore, altering the delay time before signal acquisition after the final pulse in the sequence determines the components included in the signal. For example, a long delay time removes the broad signals from bound membrane compounds since they have relaxed early and allows the selective acquisition of the smaller, more mobile metabolites that take longer to fully relax. This is very important in proton spectroscopy of biological systems because the more abundant protons in membrane lipids overwhelm the protons from more mobile metabolites that are present in smaller amounts. Appropriate choice of delay times gives better definition of the spectra and allows more accurate peak identification.

A particular advantage of NMR is that the intensity of the NMR signal indicates the concentration of the observed nuclei. Quantities can be measured from areas under the spectral curves as determined by the integral. For example, signals from three protons will produce an integral three times as large as the signal from one proton. Areas under the curve determined by the integrals are an accurate measure of quantity, although the complexity of the spectra often makes calculations of area from integral difficult; instead, an approximation is determined with the use of peak heights. There are numerous problems with precise measurement of peak areas, and none of the various ways of estimating areas in chemical samples has been optimal for in vivo studies. When the signals are indexed to water rather than calculated as ratios, there is an increase in accuracy.[24]

^{31}P-MRS

Nuclei with wider part per million separation are more easily identified by NMR. Figure 6–10 shows the part per million spread for the three atoms of biological importance, ^{1}H, ^{31}P, and ^{13}C. For example, the C3 carbon of lactate resonates at 21 ppm at 300 Hz, while the C1 carbon of glucose resonates at 96 ppm. This wide spread allows for unequivocal identification. Phosphorus-31 has a 30 ppm spread from adenosine triphosphate (ATP) to phosphomonoesters. Protons, on the other hand, are more difficult to identify, particularly at low field strength or with inhomogeneous fields, because the part per million spread is from 1 to 10, with many compounds of interest in the 1 to 4 regions.

Phosphorus and proton spectroscopy have been of the greatest interest in in vivo spectroscopy because of their relatively short acquisition times, particularly with higher field strength magnets. Phosphorus spectra show the four phosphorus atoms in ATP— inorganic phosphate, phosphocreatine, phosphodiesters, and phosphomonoesters. Each phosphorus atom can be identified from its chemical shift in the high-resolution ^{31}P spectra. Phosphocreatinine (PCr) is set at 0.00 ppm as the reference standard. The polyphosphate region contains the γ-, α-, and β-ATP phosphates along with the nucleotide diphosphate. The β-ATP is the only ATP resonance that has no contribution from the dinucleotides.

Phosphorus can be used to follow high-energy phosphate metabolism and to measure pH shifts. Phosphocreatinine is used as the standard to measure the chemical shifts of inorganic phosphate and to calculate pH. As the pH falls, the chemical shift difference between inorganic phosphate and PCr narrows. Measurement of pH with ^{31}P-NMR has provided interesting information on pH regulation since it is an accurate method for in vivo studies. In one study, brain pH was shown to change with the level of blood glucose.[25] A diabetic patient with a stroke had several ^{31}P-NMR recordings over a week while the blood glucose

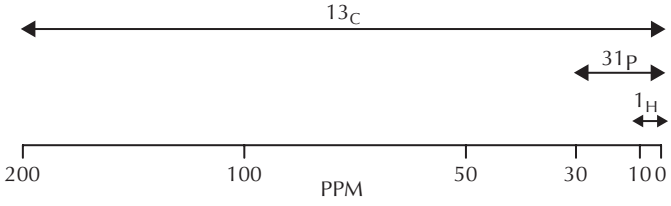

Figure 6–10. The part per million spread of ^{1}H, ^{31}P, and ^{13}C is shown. ^{13}C has the greatest spread and the more readily resolved spectrum, whereas ^{1}H, with the smallest spread, is most difficult to resolve.

remained elevated. Normal brain pH, which has a lower value than the value of 7.4 in the blood, has been recorded at 7.1 in humans with in vivo ^{31}P-NMR. Hypoxia/ischemia leads to a fall in brain pH to as low as 6.5.[26] Although elevated glucose can drive the brain pH down, there are factors other than lactate that cause brain acidosis.

^{13}C-MRS

Of the nuclei used for in vivo spectroscopy, ^{1}H, ^{19}F, and ^{31}P are 100% abundant, while ^{13}C, which has a spin of 1/2, has a natural abundance of only 1.1%, making it difficult to detect by NMR. The sensitivity is much less than that of protons: 1.6×10^{-2} at natural abundance concentrations. Enrichment of the ^{13}C is required to obtain spectra.[27] Enrichment is possible by synthesizing compounds labeled with ^{13}C. By injecting labeled substances into animals, it is possible to follow metabolic processes without extensive biochemical analyses that require extraction of the molecules from the removed tissue samples.[28]

A major advantage of ^{13}C in NMR studies is the wide part per million range for ^{13}C-NMR, which provides a method to identify the position of ^{13}C atoms within a molecule. This is helpful in natural abundance studies where the chemical structure can be determined. More important for biological studies, however, is the ability to use enriched molecules as tracers. In this respect, the low natural abundance of ^{13}C is an asset. A ^{13}C spectrum from glutamate and gamma-aminobutyric acid (GABA) is shown in Figure 6–11. Each atom has a unique part per million signal so that full identification is possible.

Injection of glucose with a ^{13}C molecule in the 1 position, [^{13}C]-1-glucose, into an animal results in the incorporation of the ^{13}C into brain glycolytic and nonglycolytic metabolites. The ^{13}C labeled in the 1 position appears in the lactate labeled in the C3 position. After entering the Krebs cycle, it is incorporated into the C4 position of glutamate, and with subsequent turns it is seen in the C2 and C3 positions.

Following injection of [1–^{13}C]glucose intravenously into rat, the tracer is seen in several compounds after 30 minutes. Although long collection times are necessary for ^{13}C analysis of a single rat brain, it is possible to shorten the collection time considerably by combining several brains for analysis. These studies can be done in chemically extracted brain tissue, which improves the resolution because of the long collection times possible.

The sensitivity of ^{13}C detection is enhanced by the use of heteronuclear decoupling. The protons coupled to ^{13}C molecules produce a signal that differs from the signal of protons coupled to ^{12}C. This method enables the measurement of ^{1}H after irradiation of ^{13}C. If the protons on ^{13}C are decoupled, they can be detected with those on ^{12}C, and by subtracting the results of the coupled and decoupled spectra, the protons on ^{13}C can be determined. The ^{1}H observe/^{13}C decouple method has been

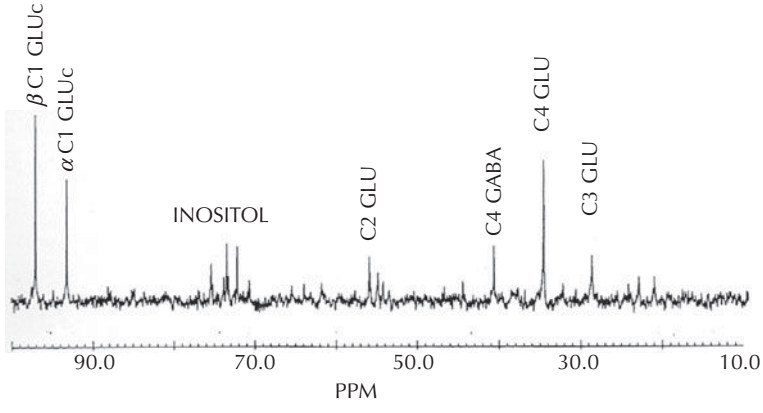

Figure 6–11. The ^{13}C NMR spectrum of brain extract obtained 30 minutes after [1–^{13}C]-glucose injection. The major metabolic products are C4 glutamate (glut) from one turn through the TCA cycle and C2 glut and C3 glut from a second turn. Two forms of glucose (gluc) are seen. (Courtesy of Dr. J. Brainard, Los Alamos national Laboratory.)

used to follow glutamate labeling with ^{13}C in vivo in rat brain.[29] Use of high-field magnets allows detection of low-abundance ^{13}C metabolites. This method has been used to follow the metabolism of glucose into glutamate and related compounds.[28]

^{1}H-MRS

Protons are the most abundant atoms in the brain. Most of the protons are on water molecules, which are the most abundant, and the NMR resonances from protons on water swamp other proton signals. To overcome the signals from the large amount of water, which obscure signals from protons on other molecules, novel pulse sequences that suppress the water protons reveal a rich variety of protons on other molecules. Techniques to suppress the water and other solvent signals while leaving the signals from other protons intact involve pulses that null the water signal. One early pulse sequence to accomplish this used a 180° pulse to suppress the water signal in the *z*-axis. Protons on water relax in the *z*-axis after a 180° pulse, moving toward the zero point in the *xy* plane. Another, more slowly relaxing substance will be below the *xy*-plane when the water is in the zero position, the molecule of interest will be tilted into the *xy*-plane, and its relaxation will be recorded. Thus, a (180°—π—90°) pulse sequence can be used to suppress water.

^{1}H-MRS spectra contain numerous compounds of importance in brain metabolism, which can be separated by magnets operating above 1.5T (Figure 6–12). Glutamate, for example, produces peaks at 2.0 and 2.3 ppm. *N*-acetyl groups resonate at 2.0 ppm, while the methyl protons on lactate are seen at 1.3 ppm. Concentrations of these substances can reach millimolar amounts so that in vivo detection is possible.

Lipids form a high percentage of brain tissue. The membrane-bound lipids produce a broad signal in vivo. Since this is undesirable for some studies, pulse sequences are used with longer delay times that allow the bound molecules to relax. Bound lipids remain undetected, while signals from more mobile lipids are still seen. These lipids have been poorly characterized but may represent those that are part of the membrane cytoskeleton or suspended in the cytosol or extracellular space. With short-echo

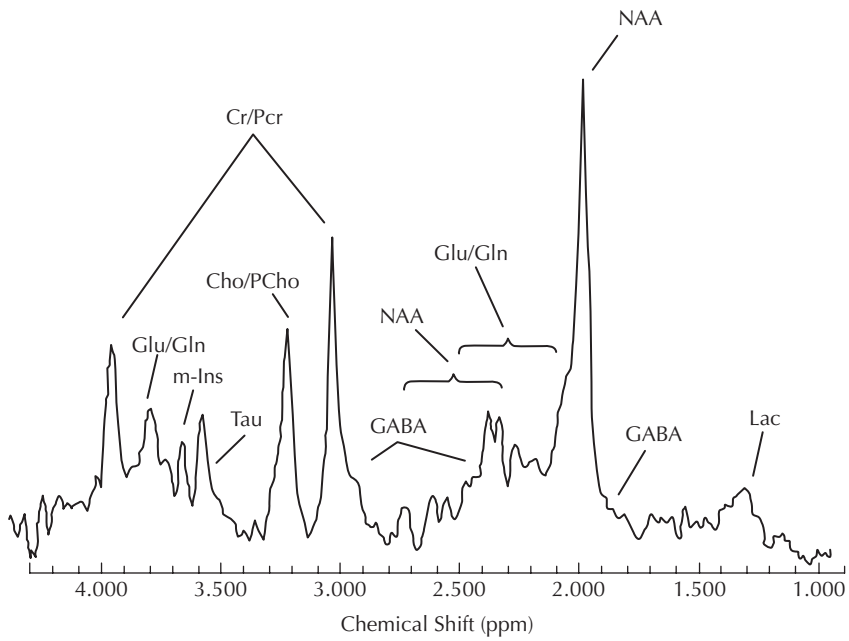

Figure 6–12. In vivo ^{1}H-MRS from a human brain at 4T. The major peaks are *N*-acetylaspartate (NAA), creatine/phosphocreatine (Cr/PCr), choline/phosphocholine (Cho/PCho), glutamate/glutamine (Glu/Gln), gamma-aminobutyric acid (GABA), lactate (Lac), myo-inositol (m-Ins), and taurine (Tau). (From Ref. 33.)

times, it is possible to detect lipid molecules that are released after an ischemic injury.

Spectroscopic imaging with fast pulse sequences provides spectra from multiple sites using small volumes of tissue. The dominant signal in brain is from *N*-acetylaspartate (NAA), which is present in high concentration in brain. Brain injuries from a number of sources cause a fall in the level of NAA, making it a biomarker for injury. The NAA is thought to arise from the axons and neurons, but other cells may also be involved since the exact origin of these signals is not well understood. Other injury markers in the proton spectra are choline and creatine/phosphocreatine. At 3T and above, it is possible to resolve signals from glutamate and GABA. With special pulse sequences, lactate signals can be detected. Certain pathological processes have patterns that are unique, such as the genetic abnormality called *Canavan's syndrome*, where a deficiency of aspartoacylase causes elevation of NAA in the brain, which can be detected by ^{1}H-MRS. More common is a loss of NAA, which is seen in stroke, brain injury, multiple sclerosis, and other pathological processes.

A unique use of ^{1}H-MRS is in the detection of ischemic/hypoxic injury in patients with vascular cognitive impairment (VCI). One form of VCI due to small vessel disease with arteriolosclerosis produces extensive damage to the deep white matter, which is at the end of the cerebral circulation (*watershed*); when blood flow is reduced for any reason, this is one of the most vulnerable areas. Injury to the axons in the white matter leads to astrocytosis with glial scar formation. However, in some elderly individuals, the white matter appears to be ischemic in that it has white matter hyperintensities (WMHs) on MRI, but these individuals are symptom-free and scarring is not seen at autopsy. Quantitative ^{1}H-MRS of the white matter shows a fall in NAA in persons with ischemic injury, but it is normal when the WMHs are due to aging.[30,31] Patients with AD have reductions in NAA in the white matter, which may indicate that they have both AD and VCI (mixed dementia).[32]

REFERENCES

1. Kety SS, Schmidt CF. The nitrous oxide method for the quantitative determination of cerebral blood flow in man: theory, procedure and normal values. *J Clin Invest*. 1948;27:476–483.
2. Gur D, Yonas H, Wolfson SK Jr, et al. Xenon and iodine enhanced cerebral ct: a closer look. *Stroke*. 1981;12:573–578.
3. Sakurada O, Kennedy C, Jehle J, et al. Measurement of local cerebral blood flow with iodo[^{14}C]antipyrine. *Am J Physiol*. 1978;234:59–66.
4. Hom J, Dankbaar JW, Soares BP, et al. Blood-brain barrier permeability assessed by perfusion ct predicts symptomatic hemorrhagic transformation and malignant edema in acute ischemic stroke. *AJNR Am J Neuroradiol*. 2011;32:41–48.
5. Oldendorf WH. Measurement of brain uptake of radiolabeled substances using a tritiated water internal standard. *Brain Res*. 1970;24:372–376.
6. Bradbury MW, Patlak CS, Oldendorf WH. Analysis of brain uptake and loss of radiotracers after intracarotid injection. *Am J Physiol*. 1975;229:1110–1115.
7. Raichle ME, Eichling JO, Grubb RL Jr. Brain permeability of water. *Arch Neurol*. 1974;30:319–321.
8. Davson H, Welch K. The permeation of several materials into the fluids of the rabbit's brain. *J Physiol* (*Lond*). 1971;218:337–351.
9. Ohno K, Pettigrew KD, Rapoport SI. Lower limits of cerebrovascular permeability to nonelectrolytes in the conscious rat. *Am J Physiol*. 1978;235:299–307.
10. Phelps ME, Hoffman EJ, Mullani NA, et al. Application of annihilation coincidence detection to transaxial reconstruction tomography. *J Nucl Med*. 1975;16:210–224.
11. Raichle ME. Positron emission tomography. *Annu Rev Neurosci*. 1983;6:249–267.
12. Frackowiak RS. Pet scanning: can it help resolve management issues in cerebral ischemic disease? *Stroke*. 1986;17:803–807.
13. Eckman WW, Phair RD, Fenstermacher JD, et al. Permeability limitation in estimation of local brain blood flow with [^{14}c]antipyrine. *Am J Physiol*. 1975;229:215–221.
14. Raichle ME, Eichling JO, Straatmann MG, et al. Blood-brain barrier permeability of ^{11}c-labeled alcohols and ^{15}o-labeled water. *Am J Physiol*. 1976;230:543–552.
15. Klunk WE, Engler H, Nordberg A, et al. Imaging brain amyloid in Alzheimer's disease with Pittsburgh Compound-B. *Ann Neurol*. 2004;55:306–319.
16. Aizenstein HJ, Nebes RD, Saxton JA, et al. Frequent amyloid deposition without significant cognitive impairment among the elderly. *Arch Neurol*. 2008;65:1509–1517.
17. Patlak CS, Blasberg RG, Fenstermacher JD. Graphical evaluation of blood-to-brain transfer constants from multiple-time uptake data. *J Cereb Blood Flow Metab*. 1983;3:1–7.
18. Blasberg RG, Fenstermacher JD, Patlak CS. Transport of alpha-aminoisobutyric acid across brain capillary and cellular membranes. *J Cereb Blood Flow Metab*. 1983;3:8–32.
19. Ewing JR, Knight RA, Nagaraja TN, et al. Patlak plots of gd-dtpa mri data yield blood-brain transfer constants concordant with those of ^{14}c-sucrose in areas of blood-brain opening. *Magn Reson Med*. 2003;50:283–292.
20. Knight RA, Nagaraja TN, Ewing JR, et al. Quantitation and localization of blood-to-brain influx by magnetic resonance imaging and quantitative autoradiography in a model of transient focal ischemia. *Magn Reson Med*. 2005;54:813–821.

21. Budinger TF, Lauterbur PC. Nuclear magnetic resonance technology for medical studies. *Science*. 1984; 226:288–298.
22. Shaw D, Kaufman L, Crooks LE, et al. In vivo chemistry with nmr. In: Kaufman L, Crooks LE, Margulis AR, eds. *Nuclear Magnetic Resonance Imaging in Medicine*. New York: Igaku-Shoin; 1981:147–183.
23. Gadian DG. *Nuclear Magnetic Resonance and Its Application to Living Systems*. Oxford: Oxford University Press; 1982.
24. Gasparovic C, Song T, Devier D, et al. Use of tissue water as a concentration reference for proton spectroscopic imaging. *Magn Reson Med*. 2006;55:1219–1226.
25. Chopp M, Frinak S, Walton DR, et al. Intracellular acidosis during and after cerebral ischemia: in vivo nuclear magnetic resonance study of hyperglycemia in cats. *Stroke*. 1987;18:919–923.
26. Levine SR, Welch KM, Helpern JA, et al. Prolonged deterioration of ischemic brain energy metabolism and acidosis associated with hyperglycemia: human cerebral infarction studied by serial ^{31}P nmr spectroscopy. *Ann Neurol*. 1988;23:416–418.
27. Prichard JW, Shulman RG. Nmr spectroscopy of brain metabolism in vivo. *Annu Rev Neurosci*. 1986;9: 61–85.
28. Sibson NR, Mason GF, Shen J, et al. In vivo (13)C nmr measurement of neurotransmitter glutamate cycling, anaplerosis and tca cycle flux in rat brain during. *J Neurochem*. 2001;76:975–989.
29. Rothman DL, Behar KL, Hetherington HP, et al. ^{1}H-observe/^{13}C-decouple spectroscopic measurements of lactate and glutamate in the rat brain in vivo. *Proc Natl Acad Sci USA*. 1985;82:1633–1637.
30. Sappey Marinier D, Calabrese G, Hetherington HP, et al. Proton magnetic resonance spectroscopy of human brain: applications to normal white matter, chronic infarction, and mri white matter signal hyperintensities. *Magn Reson Med*. 1992;26:313–327.
31. Brooks WM, Wesley MH, Kodituwakku PW, et al. ^{1}H-mrs differentiates white matter hyperintensities in subcortical arteriosclerotic encephalopathy from those in normal elderly. *Stroke*. 1997;28:1940–1943.
32. Meyerhoff DJ, MacKay S, Constans JM, et al. Axonal injury and membrane alterations in Alzheimer's disease suggested by in vivo proton magnetic resonance spectroscopic imaging. *Ann Neurol*. 1994;36:40–47.
33. Jensen JE, Renshaw PF, Wong DF, et al. Neuroimaging. In Siegel GJ, Albers RW, Brady ST, et al. Eds. Basic Neurochemistry, Elsevier, Amsterdam 2006.

PART 3

Ischemia, Edema, and Inflammation

This page intentionally left blank

Chapter 7

Mechanisms of Ischemic/Hypoxic Brain Injury

EPIDEMIOLOGY, RISK FACTORS, AND PREVENTION OF STROKE

Stroke is the third leading cause of death and the major cause of disability, and with the projected increase in the number of elderly individuals, the number of people suffering from stroke will increase. In spite of extensive research only one drug, recombinant tissue plasminogen activator (rtPA), has received approval from the U.S. Food and Drug Administration for stroke treatment.[1] Currently, prevention remains the best option for reducing the incidence of stroke. Recognized risk factors include smoking, hypertension, diabetes mellitus, hypercoagualability, blood dyscrasias, and hereditary disorders of the blood vessels (Table 7–1). The majority of strokes are due to thrombi and emboli, which accounts for about 85% of all strokes. Primary intracerebral hemorrhage (ICH) comprises the remainder. In Asia the incidence of ICH is higher, approaching 50% of strokes. Emboli from the heart and carotids are important potentially treatable causes of stroke. The incidence of stroke has declined over the past several decades due to improved treatment of hypertension, hyperlipidemia, carotid disease, and programs to stop smoking. However, the total number of patients with stroke remains high because of the increase in the age of the population, offsetting the gain.

Epidemiological data from 1994 to 2004 obtained from the Canadian Mortality Database showed a striking decrease of 30% in the overall age- and sex-standardized

Table 7–1 **Risk Factors in Stroke**

Hypertension
Diabetes mellitus
Hyperlipidemia
Smoking
Coagulopathy
Older age

rate of death from cardiovascular disease.[2] Similar results were reported in the long-term Framingham Study: over three consecutive periods (1950–1977, 1978–1989, and 1990–2004), the investigators studied 9152 men and women free of stroke who underwent follow-up for up to 50 years. They found a decrease in the incidence of stroke over 50 years without a decline in lifetime risk, which they attributed to improved life expectancy.[3] Certain regions of the United States have a higher incidence of stroke and heart disease than others; the Deep South is referred to as the *stroke belt* because of the high incidence of stroke in that region.[4]

Poorly controlled hypertension is the single most important factor in determining the risk of stroke. Large cohort studies confirm that moderate reductions in blood pressure significantly reduce the incidence of heart attacks and stroke. A meta-analysis showed that in older patients with isolated systolic hypertension, lowering the systolic blood pressure by 10 mm Hg and the diastolic pressure by 4 mm Hg reduced the risk of stroke and myocardial infarction by 30% and 23%, respectively. In patients with predominantly diastolic hypertension, the corresponding benefits produced by a 5–6 mm Hg decline in diastolic pressure were 38% and 16%, respectively.[5] Another meta-analysis of 20 randomized clinical trials revealed that angiotensin receptor blockers provide benefit in preventing stroke when compared with placebo. However, there was no evidence of the benefit when angiotensin receptor blockers were compared with angiotensin converting enzyme inhibitors and with calcium antagonists.[6] Vascular complications are prominent in diabetes mellitus, which is a major risk factor for stroke. Finally, hyperlipidemia and smoking both increase the stroke risk, and treatment of hyperlipidemia with statins and cessation of smoking both reduce the risk of stroke.

MOLECULAR CASCADE IN ISCHEMIC TISSUE RESULTS FROM ENERGY FAILURE

When efforts to reduce risk factors fail and ischemia develops, there is a dramatic drop in the supply to vital brain structures of glucose and oxygen, which are the main sources of energy in the brain. Loss of energy causes release of the excitatory neurotransmitter, glutamate, into the synaptic clefts, stimulating glutamate receptors and triggering increases in intracellular calcium. Rising intracellular calcium activates transcription of genes involved in cytokine formation, which, in turn, leads to expression of enzymes that participate in the breakdown of cellular membranes. While oxygen and glucose are the primary energy substrates, brain cells can use ketones from fatty acids as a source of fuel in energy metabolism. However, if cerebral blood flow is maintained, other sources of energy can be delivered to the brain in the form of lipids that will temporarily sustain energy needs for hours and prevent the loss of membrane ion pumps. When cerebral blood flow is abruptly lost, as occurs during a cardiopulmonary arrest, energy supplies are rapidly lost and processes that will lead to cell death begin after several minutes. Thus, even brief interruption of the blood flow to brain tissue initiates a series of events that lead to cell death.

Loss of oxygen is referred to as *hypoxemia*, while loss of blood flow is called *ischemia*; since they occur together when blood flow stops, the term *hypoxia/ischemia* is often used to describe a stroke or cerebral infarction. When cerebral blood flow is maintained and oxygen content falls, as when nitrogen is substituted for oxygen, which occasionally happens in an anesthetic accident or with carbon monoxide poisoning, hypoxia alone damages the cells after the oxygen remaining in the circulating blood is absorbed. Consciousness is lost after an average of 7 seconds of ischemia, but cells can survive if the flow of blood is restored.

Molecular events initiated by the loss of oxygen lead through a series of stages to cell death within several days. With prolonged oxygen loss, the center of the infarct, called the *core*, undergoes necrosis and is irreversibly damaged. Around the core, however, the penumbra remains potentially salvageable. Peri-infarct

depolarization causes spreading depression from excessive potassium release. Early in the injury, there is activation of the genes that will promote the inflammation that leads to cell apoptosis (Figure 7–1). With oxygen loss, the membrane pumps that depend on adenosine triphosphate (ATP) fail. Failure to pump sodium out of the cell in exchange for potassium leads to the buildup of sodium inside the cell, causing cytotoxic edema. Initially, the cell membrane remains intact, averting cell death, and function can be restored once the energy supply is resumed. Aquatic mammals can survive for long periods without oxygen by using lactate as fuel for the production of ATP.[7] However, once the cell membranes are damaged, cells die by necrosis, which is a rapid form of cell death that leads to release of intracellular contents and the initiation of an inflammatory response. Apoptosis, or programmed cell death, is a slower process of cellular involution without inflammation. Apoptosis is initiated at an early stage after the ischemic injury but manifests over several days. Prolonged ischemia/hypoxia initiates a chain of molecular events that culminate in autodigestion by proteolytic enzymes involved in taking apart the cell's membranes by the process of necrosis with rapid death and inflammation or apoptosis without inflammation (Figure 7–2).

In an important series of early experiments, Lowry and colleagues, who pioneered analytical methods of measuring energy substrates in rats, studied the chemistry of the anoxic brain.[8,9] Because the energy molecules are lost quickly after the onset of an ischemic injury, they rapidly froze the brain by pouring liquid nitrogen through a funnel onto the exposed skull. With multiple animals sacrificed at multiple time points, they unraveled the time course of energy failure in the brain. In rat models of cerebral ischemia the initial changes occur in the ATP molecule. The lactate level rises more slowly and contributes to the fall in pH; the initial level of glucose determines the amount of increase in lactate.[10] Proteolysis of membranes leads to an increase in free fatty acids.[11,12]

The extent of injury depends on multiple factors. From a clinical viewpoint, the most important of these are hyperglycemia, hyponatremia, and fever, each of which increases the size of the infarcted tissue (Table 7–2). When glucose is high, lactate increases and pH falls; acidosis increases cell death through the action of acid hydrolysis. Hyponatremia interferes with the removal of potassium, calcium, and protons from the cells, all of which depend on a sodium exchanger. When hyponatremia is present, the removal of protons from the cell is impeded; proton buildup reduces the pH. Hyperthermia worsens stroke outcome by increasing metabolism, and hypothermia improves the outcome by slowing it, making temperature a major factor in stroke.[13] In fact, hypothermia is used in patients with cardiac arrest: controlled trials show that it is effective.[14] Maintaining a low body temperature is a challenge for many reasons. Patients need to be sedated due to the discomfort. Methods to reduce body temperature range from cooling in ice to pumping cooled blood through the patient's arteries. Although animal data on the

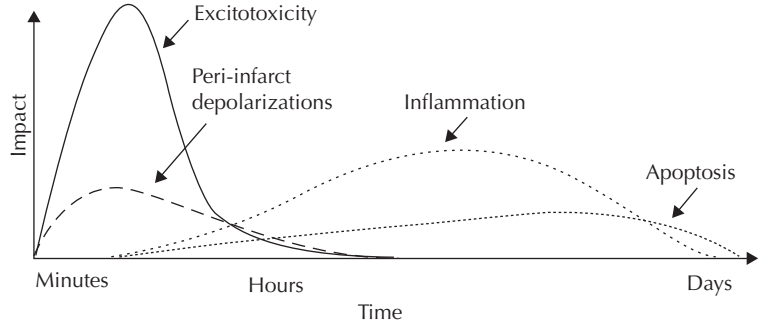

Figure 7–1. Putative cascade of damaging events in focal cerebral ischemia showing the time course of an ischemic injury. Within minutes the loss of energy results in depolarization, which causes the release of glutamate and triggers neuroinflammation. Peri-infarct depolarizations contribute to the inflammatory phase. Apoptosis begins gradually, reaching a maximum after several days. Because of the slower nature of the inflammation and apoptosis, these patients are targeted for treatment. (From Ref. 94.)

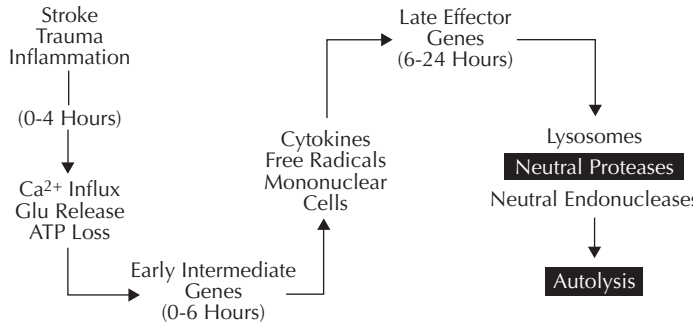

Figure 7–2. Molecular cascade of events in an ischemic injury. Shortly after the injury occurs, loss of ATP leads to energy failure with release of glutamate. Stimulation of glutamate receptors increases calcium within the cell. Early immediate genes are activated and cytokines, free radicals, and chemokines are formed that recruit leukocytes. After several hours, another set of genes are activated by the cytokines and free radicals that lead to late effector gene expression. Finally, the production of proteases causes cell death by self-digestion.

use of hypothermia in stroke are promising, its use in stroke patients remains to be proven in controlled clinical trials.[15]

Glucose is transported into the brain by carrier-mediated, facilitated transport**.** In the blood-brain barrier (BBB), glucose transporter-1 (GLUT1) is the main carrier molecule for glucose. Once across the BBB, glucose is phosphorylated by hexokinase to glucose-6-phosphate in the process of glycolysis, which takes place in the cytosol; the rate-limiting enzyme, phosphofructokinase, converts it to fructose-1,6-diphosphate (Figure 7–3). The pivotal molecule, pyruvate, can be converted to lactate, yielding 2 ATP molecules; alternatively, when oxygen is present, it can be taken into the mitochondria, where the Krebs cycle stores it as glutamate and the electron transport chain converts it to energy, creating 36 molecules of ATP. When the process is working smoothly, about 70% of the ATP goes into maintaining ionic adenosine triphosphatase (ATPase) pumps on various membranes.

Table 7–2 **Factors to Control to Prevent Worsening of Acute Stroke**

High glucose: increases lactate and lowers pH
Low sodium: impedes sodium exchange with potassium and protons and lowers pH
Fever: increases the metabolic rate and tissue damage
Low blood pressure from hypertensive medications: reduces cerebral blood flow
Hypoxia: from pneumonia or sleep apnea

EXCITATORY AND INHIBITORY NEUROTRANSMITTERS

In the 1960s, Olney discovered that glutamate, which was thought at that time to be benign, caused excitotoxic damage to neurons, but it took many years before this finding was generally accepted since glutamate is a normal neurotransmitter present in high concentrations in brain.[16] Peri-infarct depolarization (spreading depression) with energy failure in an ischemic insult causes glutamate to be released into the extracellular space. Normally, glutamate inside cells is sequestered in a large energy storage compartment, which exchanges with a small neurotransmitter pool available for synaptic function. Glutamate is found in high concentration in the brain, most of which is formed from glucose and stored in a compartment for use in metabolism. Several routes are available to glucose through the glycolytic pathway to form glutamate. Conversion of pyruvate to acetyl coenzyme A (CoA) by the enzyme pyruvate dehydrogenase (PDH) leads to α-ketoglutarate, which is a major intermediate in glutamate formation. Glutamate can be converted to the inhibitory neurotransmitter, gamma-aminobutyric acid (GABA), by glutamic acid decarboxylase (GAD) or to glutamine by the enzyme, glutamine synthetase. This is an important function of the tricarboxylic acid (TCA) cycle. As carbon molecules are consumed by metabolism of protein formation, new sources of carbon are needed to maintain the TCA cycle. An important mechanism for this is the use of an alternate route of

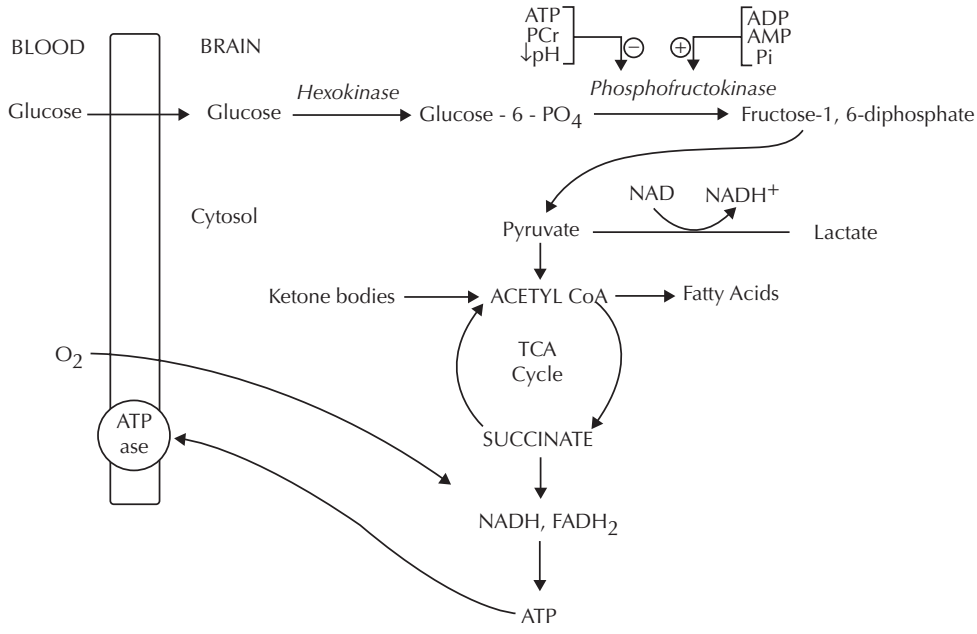

Figure 7–3. Schematic drawing of the metabolic pathways that are important in preserving cellular function. The major fuel sources are glucose and ketone bodies. Oxygen is essential. Several factors influence glycolysis through phosphofructokinase. Sufficient supplies of ATP and phosphocreatinine (PCr) reduce the activity of the enzyme, while adenosine diphosphate (ADP), adenosine monophosphate (AMP), and (Pi) enhance it. Ketone bodies can directly enter the TCA cycle for the production of energy in the form of nicotinamide adenine dinucleotide (NADH), flavin adenine dinucleotide ($FADH_2$) and ATP. Membrane function is maintained by ATP through the ATPase exchange pumps. Pi is inorganic phosphate.

entry of carbon skeletons into the TCA cycle by the conversion of pyruvate to oxaloacetate by incorporation of carbon molecules by the aid of the enzyme, pyruvate carboxylase (PC; Figure 7–4). Studies using ^{13}C-glucose indicate that this anapleritic route is important for the formation of GABA.[17] Thus, anaplerosis, which literally means "filling up," restores TCA intermediates that are consumed in biosynthetic reactions.

Glutamate is the major excitatory amino acid, and release of small amounts of glutamate into the synaptic clefts is essential for brain function. Hypoxia causes an excess of glutamate to flood the synaptic cleft; activation of glutamate receptors leads to an influx of calcium into the cell. The rapid increase in intracellular calcium signals that the cell is under stress and in danger of dying. Calcium is the major mediator of glutamate-initiated excitotoxicity: both the release of glutamate and the influx of calcium occur very soon after the onset of ischemia/hypoxia, making them very difficult to inhibit. In fact, clinical trials of calcium inhibitors in the treatment of stroke have generally failed. Likewise, inhibitors of glutamate receptors, which were originally heralded as major advances in stroke treatment based on numerous animal studies, have proven unsuccessful in clinical trials because of the side effects produced by the inhibitors that were available at the time.[18,19]

Glutamate in excessive amounts leads to prolonged depolarization and synaptic activity with excessive sodium and calcium influx. In hippocampal slice preparations subjected to hypoxic conditions, glutamate produced prolonged depolarization with ion and water influx from the extracellular space. Cell damage from glutamate appears to occur in two phases: a rapid phase mediated by sodium and chloride influx with osmotic changes and a delayed phase related to the cellular events triggered by calcium influx. Excitatory amino acid neurotransmitters are decreased in ischemia in whole brain preparations, but their extracellular levels are increased in ischemia: the extracellular level of the excitatory amino acids is related to cellular excitation.

To avoid excitotoxicity, glutamate uptake transporters maintain extracellular glutamate at

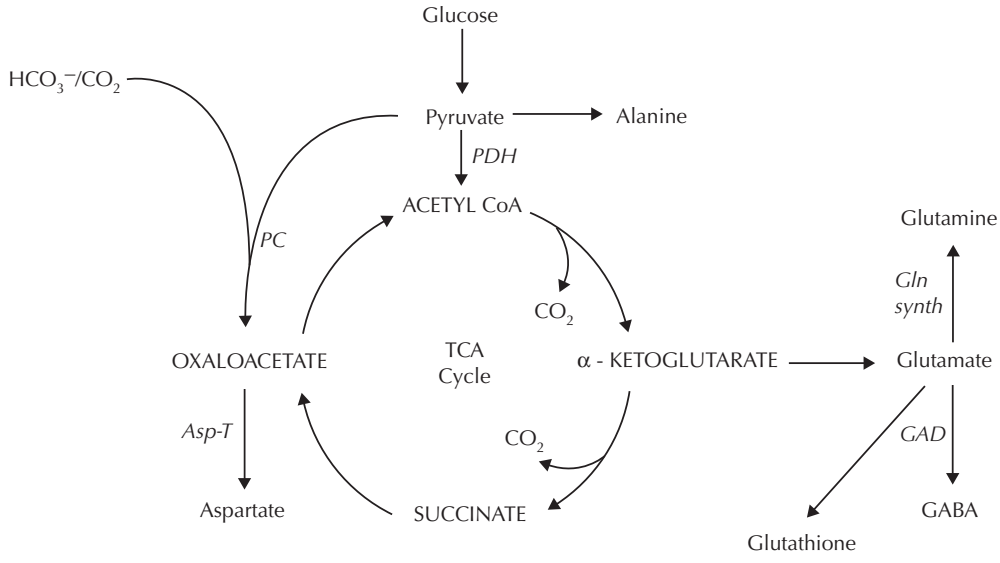

Figure 7–4. In the early stages of injury, the TCA cycle can have carbon replenished through the action of the anapleurotic pathway. Fixation of carbon can occur through pyruvate carboxylase (PC), and Krebs cycle intermediates can be maintained in the absence of glucose. Normal production of glutamate, glutamine, and GABA can continue by conversion of α-ketoglutarate. GAD, glutamic acid decarboxylase; Gln synth, glutamine synthase; Asp-T, aspartate transaminase.

a low concentration. The level of glutamate in hippocampal brain slices has been shown to be as low as 25 nM, which would have negligible actions on most glutamate receptors, indicating that small increases in extracellular glutamate could have an effect at the synapse.[20] The small pool of glutamate used in neurotransmission is highly concentrated in the synaptic vesicles of the nerve terminals. Conservation of the glutamate is achieved by glutamate uptake into astrocytes, where it is converted into glutamine by the enzyme, glutamine synthetase. The glutamine is transferred to the neuron and converted back into glutamate, which can be combined with α-ketoglutarate for entry into the TCA cycle (Figure 7–4).

The postsynaptic membrane contains the glutamate receptors (Table 7–3). Three of the receptors form ion channels, and the fourth is a metabotropic receptor. There is also a voltage-gated calcium channel that opens when the cell membrane is depolarized. The major glutamate receptor is *N*-methyl-D-aspartate (NMDA), which is mainly a calcium channel. Another channel-forming receptor is α-amino-3-hydroxy-5-methyl-4-ioxazole propionic acid (AMPA), mainly a sodium channel. The third glutamate receptor responds to kainic acid (KA). The metabotropic receptor is coupled with a G-protein (Figure 7–5). The glutamate receptors are densely located in the CA1 zone of the rat hippocampus, an area selectively vulnerable to ischemia. Low concentrations of Mg^{2+} block the glutamate receptors, as do several compounds that are structurally similar to glutamate.

During hypoxia and ischemia the neurotransmitter amino acids undergo complex changes. Synthesis of GABA by GAD continues, while its degradation by GABA-transaminase (GABA-T) is reduced. Glutamic acid decarboxylase has a pH optimum below 7. Glutamate and ATP, both of which fall in ischemia, inhibit it, favoring the formation of GABA. In addition, the degradation of GABA by GABA-T is reduced in hypoxia, since it is dependent on availability of the TCA cycle intermediate α-ketoglutarate. Thus, GABA will increase in hypoxia/ischemia.

Table 7–3 Glutamate Receptors

N-methyl-D-aspartate (NMDA)
α-Amino-3-hydroxy-5-methyl-4-ioxazole, propionic acid (AMPA)
Kainic acid (KA)
G-protein-coupled receptors (metabotropic)

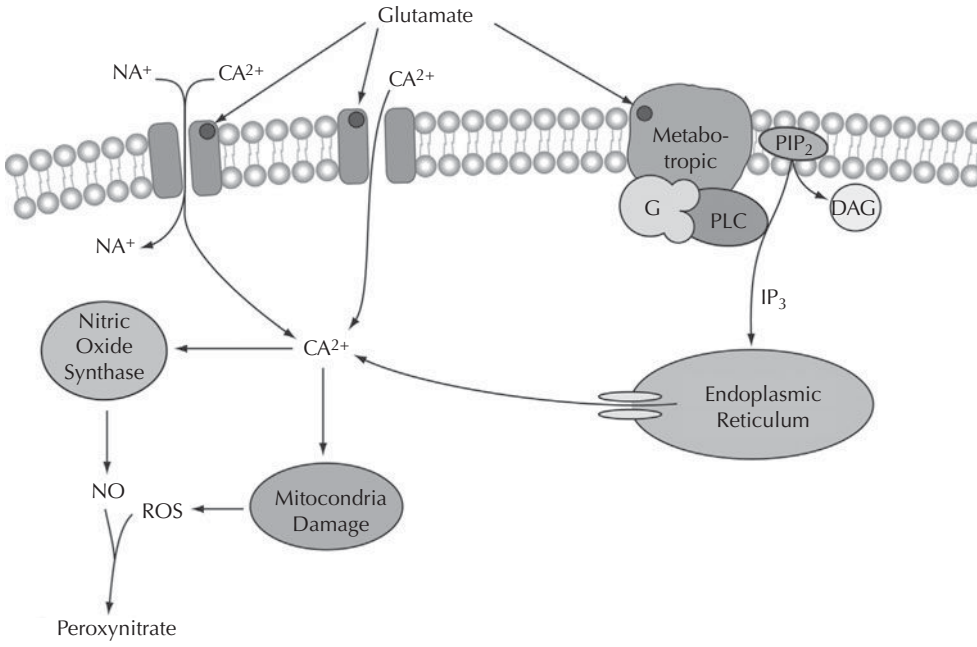

Figure 7–5. Glutamate receptors are shown schematically. The *N*-methyl D-aspartate (NMDA) allows sodium and calcium to enter (left), and the α-amino-3-hydroxy-5-methyl-4-isoxazolepropionic acid receptor (AMPA) receptors are channels for the entry of extracellular calcium (middle). A metabotropic channel acts through a G-protein and phospholipase (right). Activation of the metabotropic receptor leads to metabolism of inosital phosphate (PIP_4) to inositol triphosphate (IP_3), and diacylglyerol (DAG), which goes to the endoplasmic reticulum and causes the release of calcium. High levels of calcium inside the cell turn on free radical production and produce mitochondrial damage through the formation of peroxynitrate.

NEUROINFLAMMATION IN STROKE

Inflammation (Latin *inflammare*, "to set on fire") in the body is initiated as a response of vascular tissues to harmful stimuli. Although generally thought of in a negative sense related to the amplification of tissue injury, inflammation may also protect the body by facilitating removal of the offending organisms and initiating the healing process. Originally, inflammation referred mainly to the reaction triggered by an infectious agent. The current definition encompasses a wider range of reactions, including those of the body to internal noxious stimuli, as occur in stroke, trauma, and immunological reactions. When infectious agents are involved, such as in meningitis, the influx of neutrophils dominates the inflammatory response,with less impact from endogenous cells, including microglia and macrophages. The opposite situation arises in an ischemic injury; the initial response to the tissue hypoxia is activation of the intrinsic cells and later recruitment of the systemic white blood cells. In both the exogenously and endogenously driven reactions, a characteristic chain of molecular events leads to induction of cytokines, chemokines, and proteases.

The hallmark of any inflammatory response is disruption of the blood vessels, which are the primary sites of inflammation (Table 7–4). During a systemic response, vasodilation and its resulting increased blood flow cause redness (*rubor*) and increased heat (*calor*). Increased permeability of the blood vessels results in infiltration of white blood cells and leakage of plasma proteins with entrained fluid that results in tissue swelling (*tumor*). Neutrophils

Table 7–4 **Inflammatory Mechanism in Brain**

Energy failure causes Ca^{2+} influx
Nuclear transcription factors activated and form cytokines and chemokines
Disruption of the BBB with influx of neutrophils
Activation of astrocytes and microglia

migrate along a chemotactic gradient created by chemokines, released by local cells in response to the injury stimulus, to reach the injury site. Pain due to the tissue swelling causes a loss of function (*functio laesa*) in the injury area.

While inflammation in the brain has similarities to that occurring in the rest of the body, the differences in the responses in brain tissue have led to a new term, *neuroinflammation*, which is used to broadly describe the amplification of the molecular injury response that occurs through the action of cytokines and chemokines and involves free radicals and proteases that are specific to brain tissue. Inflammation in the brain follows the classic pattern of dolor, calor, rubor, and tumor. Although the redness and heat produced by the damage to the blood vessels cannot be observed in brain, disruption of the BBB causes vasogenic edema. As is the case with inflammation elsewhere in the body, the destructive phase is followed by a repair phase characterized by macrophage-mediated removal of dead and damaged tissues followed by a period of angiogenesis and neurogenesis. One of the major goals of stroke researchers is to find agents that provide neuroprotection from ischemic injury by reducing secondary inflammation. Treating the early injury is difficult because it occurs within hours, but the delayed inflammation offers a longer therapeutic window. Attempts to treat inflammation have another, more important complication. Blocking the detrimental aspects of inflammation interferes with the subsequent beneficial aspects. Finding the proper balance between the two extremes is necessary for any agent that will be used for neuroprotection. This has proven to be an elusive goal because of the large number of molecular events uncovered and the positive benefits of aspects of the inflammatory response.

PROTEASES IN HYPOXIA/ISCHEMIA

Proteases are essential in many normal processes, but when produced as part of the neuroinflammatory cascade, they are highly toxic to brain tissues. Proteases contribute to secondary damage as the final common pathway in the ischemic injury cascade. Activation of the protease genes is mainly controlled by the inflammatory cytokines, such as tumor necrosis factor-α (TNF-α) and nuclear factor-kappa B (NF-κB). A complex pattern of matrix metalloproteinase (MMP) expression in hypoxic/ischemic injury is emerging from many laboratories.[21–24] In the reperfusion model, there is an early increase in MMP-2, which is transient but results in the early reversible opening of the BBB. An elevation in MMP-2 in the early stages of the injury has been observed in rodents and nonhuman primates.[25,26] Tight junction proteins are degraded by MMP-2 but remain within the vessels after 3 hour of reperfusion. However, by 24 hours, the tight junction proteins are no longer seen in the vessels.[26] Following the initial opening of the BBB, there is a second opening between 24 and 48 hours, depending on the time of occlusion. During this phase there is a marked increase in MMP-9, which leads to more extensive damage to the blood vessels (Figure 7–6).

A number of other factors are involved in the later disruption of the blood vessels since cytokines, proteases, and free radicals are released at this stage of the injury. Another major difference between the first wave of MMP-induced injury and the second is that MMP-2 is tethered to the cell surface by membrane-type MMP (MT-MMP) and requires the presence of tissue inhibitor of metalloproteinase-2 (TIMP-2) in order to undergo activation. This restricts the proteolytic action of MMP-2 to the immediate vicinity of the protease. On the other hand, MMP-9 is released into the extracellular space where it is not constrained, and degrades multiple proteins in the extracellular matrix, including those in the matrix around neurons.

Free radicals are involved in BBB opening and cell death, and cyclooxygenase (COX) inhibition limits BBB disruption following ischemic stroke and bacterial meningitis. Indomethacin, an inhibitor of COX-1 and COX-2, reduced BBB damage at 24 hours and significantly attenuated MMP-9 and MMP-3 expression and activation, preventing the loss of endogenous radical scavenging capacity and indicating that MMP-mediated BBB disruption during neuroinflammation can be significantly reduced by administration of COX inhibitors.[27]

Arachidonic acid is a polyunsaturated fatty acid that is released from membrane phospholipids by the action of phospholipase A_2 (Figure 7–7). Large amounts of arachidonic acid are released following brain ischemia and

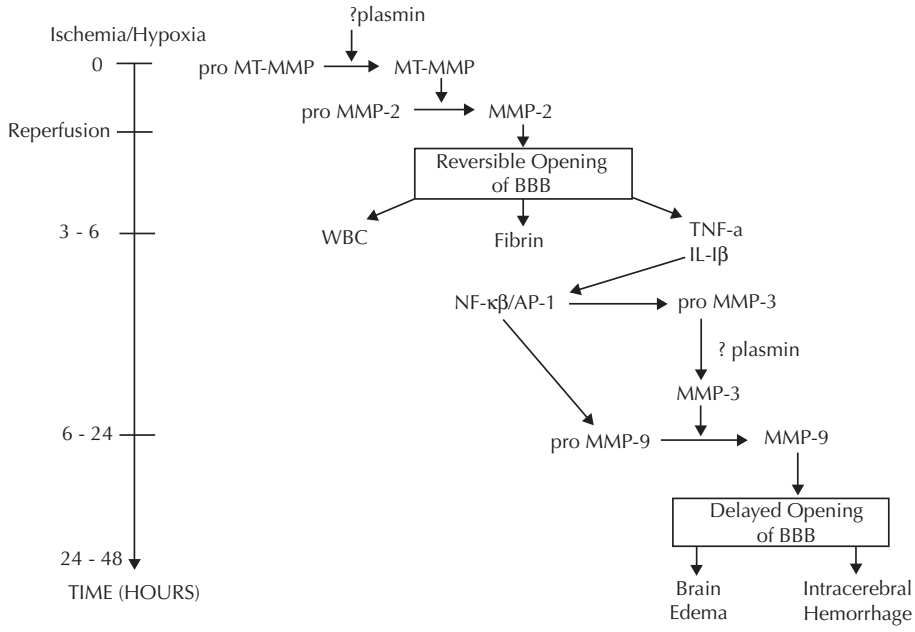

Figure 7–6. Summary of the potential reactions in the ischemic brain. The scenario depicted involves transient occlusion of the blood vessel with reperfusion. The time course is depicted on the *y*-axis with the time of occlusion at the top and onset of reperfusion shown at a later time. There is a biphasic opening of the BBB, with the initial injury related to activation of the constitutively expressed matrix metalloproteinase-2 (MMP-2) by MT-MMP, which is activated by plasmin. If the ischemic injury is prolonged, a secondary reaction begins through the white blood cells (WBCs), fibrin deposition, and cytokines. Stimulation of the AP-1/NF-κB sites in the promoter regions of the proinflammatory MMP genes leads to MMP-3 and -9 production, and the opening of the BBB with edema and hemorrhage. (From Ref. 95.)

trauma. Arachidonic acid has been implicated in vasogenic cerebral edema.[28] The deleterious effects of arachidonic acid, which may contribute to cerebral edema, include enhanced production of prostanoids and free radicals via its metabolism by cyclooxygenase (COX) and lipoxygenase (LOX) enzymes.

Reactive oxygen species (ROS) and nitric oxide (NO) are the major free radicals identified in ischemic brain (Table 7–5). Arginine

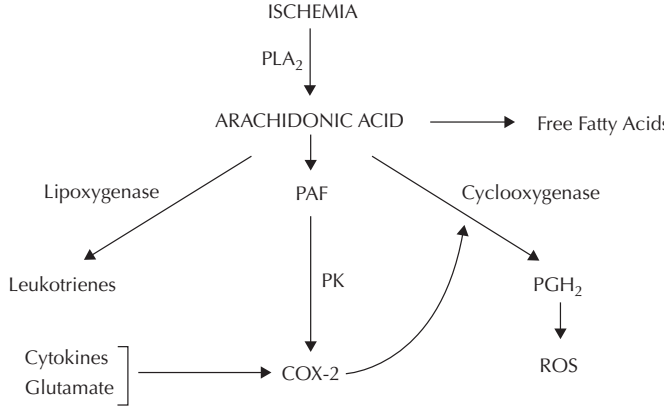

Figure 7–7. Arachidonic acid metabolism is central to the damage done by ischemic injury. Phospholipase A2 (PLA_2) produces arachidonic acid and free fatty acids. Cyclooxygenase converts arachidonic acid to prostaglandin H_2 (PGH_2). Platelet activating factor (PAF) acts through protein kinases (PK) to induce formation of COX-2. Other factors, such as the cytokines and glutamate, contribute to free radical production through the COX-2 enzyme.

Table 7–5 **Nitrous Oxide Synthetases (NOS)**

Endothelial NOS (eNOS)	Protects during ischemia
Neuronal NOS (nNOS)	Increases cell damage
Inflammatory NOS (iNOS)	Increases cell death

combines with oxygen through the action of nitric oxide synthetase (NOS) to form cituline, NO, and oxygen; NO is a potent vasodilator. Free radicals of oxygen are formed in the electron transport chain. If the reactive oxygen joins with NO, peroxynitrate is formed (Figure 7–8).

Many studies have shown that pharmacological blockade of ion channels, including nonselective cation channels, reduces cytotoxic edema and ischemic brain injury in animal models of focal ischemia. The following cation channels have been shown to participate in the development of cytotoxic edema following brain injury: the NMDA receptor channel, acid-sensing ion channels (ASICs), sulfonylurea receptor 1 (SUR1)-regulated Ca^{2+}-activated, $[ATP]_i$-sensitive nonspecific cation ($NC_{Ca\text{-}ATP}$) channels ($NC_{Ca\text{-}ATP}$) channels, transient receptor potential (TRP) channels and the electroneutral cotransporter (NKCC) channel.

The SUR1-regulated $NC_{Ca\text{-}ATP}$ channel has recently received much attention due to growing evidence from preclinical and clinical studies demonstrating the therapeutic potential of blocking SUR1 by sulfonylureas, such as glibenclamide (glyburide), in conditions associated with cytotoxic edema, such as ischemic stroke and spinal cord injury.[29] The SUR1-regulated $NC_{Ca\text{-}ATP}$ channel is not constitutively expressed in the central nervous system, but it is strongly upregulated under conditions of hypoxia or injury in all members of the neurovascular unit. The SUR1-regulated $NC_{Ca\text{-}ATP}$ channel conducts all inorganic monovalent cations, and opening of this channel induces a strong inward current that depolarizes the cell completely and leads to oncotic cell swelling. In a rodent model of massive ischemic stroke with malignant cerebral edema, pharmacological blockade of the SUR1-regulated $NC_{Ca\text{-}ATP}$ channel with glibenclamide dramatically reduced mortality and cerebral edema.

CASPASES AND CELL DEATH

Caspases are serine proteases that are implicated in programmed cell death. Inflammation occurs with release of cellular contents during necrosis, with extensive irreversible damage to the cell that occurs as the cell membrane ruptures and the contents of the cell are released into the extracellular space, causing recruitment of macrophages and microglial cells to the injury site, where they participate in removal of the damaged cells. Astrocytes form a glial scar to wall off the necrotic cells and other debris from normal brain tissue. If the cells avoid the initial necrotic destruction, they may still die by apoptosis.[30] Fragmentation of nuclear DNA by the caspases produces apoptotic bodies seen in involuting cells. Because apoptosis takes

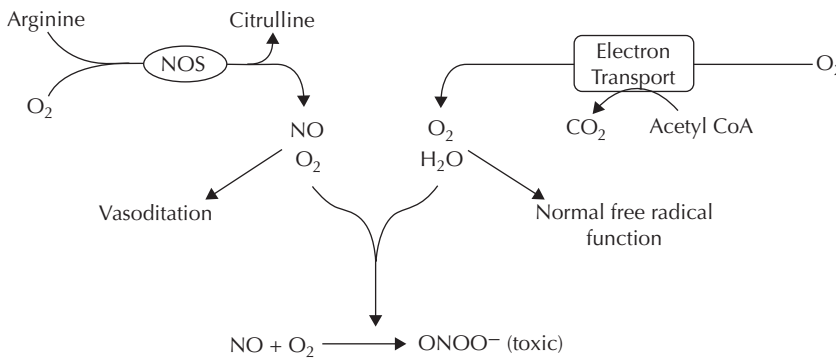

Figure 7–8. Nitric oxide synthetase (NOS) forms nitric oxide (NO) from arginine and oxygen. NO joins with oxygen to form peroxynitrate ($ONOO^-$).

place over several days and is a late effect of the ischemic cascade, drugs that block apoptosis provide protection and have therapeutic potential.[31]

Apoptosis is the process of programmed cell death, with biochemical events leading to characteristic cell changes in morphology and death. These changes include blebbing, loss of cell membrane asymmetry and attachment, cell shrinkage, nuclear fragmentation, chromatin condensation, and chromosomal DNA fragmentation. In contrast to necrosis, which is a form of traumatic cell death that results from acute cellular injury, apoptosis, in general, confers advantages during an organism's life cycle.

A normal amount of apoptosis prevents undesirable cell growth, as occurs in cancer cells. In that situation, as opposed to an ischemic injury, apoptosis is beneficial in containing the excessive growth.

Death receptors on the cell surface of the tumor necrosis factor (TNF) gene family include the Fas receptor (also known as *Apo-1* or *CD95*), which binds the Fas ligand (FasL), a transmembrane protein part of the TNF family. The interaction between Fas and FasL results in the formation of the *death-inducing signaling complex* (DISC), which contains the FADD, caspase-8 and caspase-10. The Fas ligand and TNF-α bind to their respective receptors and initiate a cascade that includes activation of caspase-8, which activates caspase-3, the major caspase mediator of cell death. Because the cell surface death receptors are involved, this is called the *extrinsic pathway*. Another pathway, the *intrinsic pathway*, is initiated by caspase-8 through a cytoplasmic factor, the Bcl-2 interacting domain (BID), which goes to the mitochondria, where it leads to release of cytochrome c, activating caspase-3. Caspase inhibitors block apoptosis in animal models of stroke, but none have been tested in clinical trials.[32,33] The MMPs and caspases are central to a series of mechanisms that damage cells through multiple mechanisms (Figure 7–9).

TISSUE INHIBITORS OF METALLOPROTEINASES AND APOPTOSIS

Metalloproteinases are inhibited by several molecules, including four tissue inhibitors of metalloproteinases (TIMPs),[34] which are relatively small proteins with molecular weights between 21 and 28 kDa with highly conserved regions in the genes and overlapping functions (Table 7.6). Although all of them have some inhibitory actions against most MMPs, they have predilections: TIMP-1 inhibits mainly MMP-9, while TIMP-2 inhibits MMP-2 and, paradoxically, contributes to the activation of proMMP-2. TIMP-3 is unique in that it is

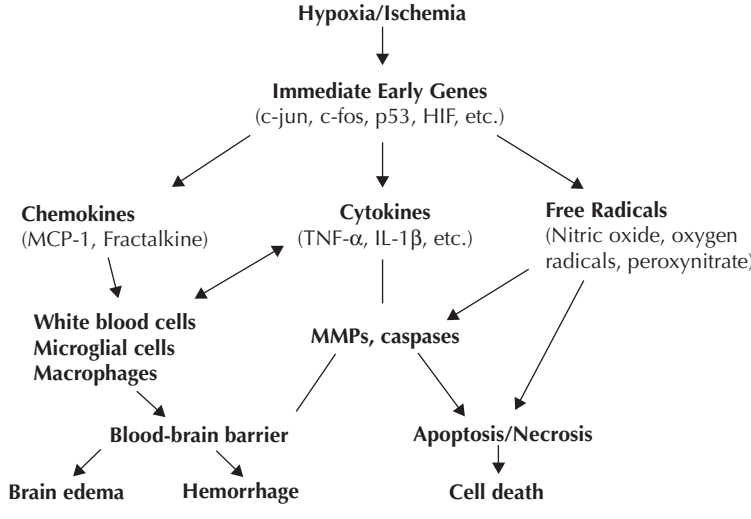

Figure 7–9 Schematic drawing showing the multiple factors involved in edema, hemorrhage, and death. HIF = hypoxia inducibe factor; MCP-1 = monocyte chemotactic protein-1.

Table 7–6 **Nomenclature, Molecular Weights, Functions, and Location of Tissue Inhibitors of Metalloproteinases**

Name	Mol. Wt. (kDa)	MMPs Inhibited	Other Functions	Location
TIMP-1	28	All ADAM10	Strong inhibitor of MMP-9	Secreted
TIMP-2	21	All	Forms trimolecular complex with pro-MMP-2 and MT1-MMP to activate MMP-2	Secreted
TIMP-3	24/27	All MMPs ADAM10 ADAM17	Apoptosis Inhibits angiogenesis	Bound to extracellular matrix
TIMP-4	22	All	Inhibits angiogenesis	Secreted

Source: Modified from Ref. 93.

bound to the extracellular matrix.[35] TIMP-3 inhibits several membrane-constrained molecules with sheddase functions. These include MMP-14, MMP-3, and tumor necrosis factor-α converting enzyme (TACE), indicating that TIMP-3 plays a central role in several important reactions in brain involving growth, cell death, and tissue repair.[36] TIMP-3 is expressed early in ischemia and contributes to apoptosis of neurons in the middle cerebral artery suture occlusion model.[37,38] TIMP-3 mRNA was found to be overexpressed in developing brain and after injury in rats.[39] Lipopolysaccharide (LPS) stimulation of cultured astrocytes leads to formation of TIMP-3, while TIMP-3 inhibits activation of MMP-2 in neurons.[40] Although a forth TIMP has been identified, its function in brain is obscure.

TIMP-3 plays a prominent role in controlling activities at the cell surface. It prevents the release of death receptors of the TNF superfamily from being shed from the surface of the cell; by blocking shedding of the death receptors, TIMP-3 facilitates apoptosis of cancer cells.[41,42]

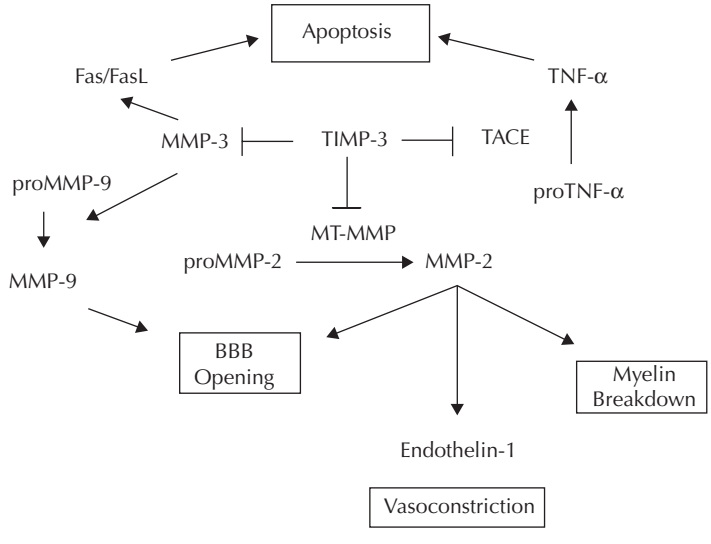

Figure 7–10. Central role of TIMP-3 in MMPs and ADAMs. TIMP-3 inhibits MT-MMP, MMP-3, and TACE. MT-MMP contributes to the trimolecular complex that activates MMP-2, which opens the BBB, converts big endothelin to endothelin-1 (a vasoconstrictor), and degrades myelin. MMP-3 activates MMP-9, contributing to BBB opening, and releases Fas from the membrane. TACE converts proTNF to TNF and sheds TNF receptor.

Several key MMPs interact with TIMP-3 and regulate cell death (Figure 7–10). TIMP-3 blocks MT-MMP, TACE, and MMP-3; this combination of actions controls both cell survival and cell death, making interpretation of the role of TIMP-3 complex.

MMP-3 has a neuroprotective action through regulation of (Fas-FasL) at the cell surface. Two mechanisms appear to be involved: (1) MMP-3 may be protective by neutralizing FasL and (2) MMP-3 increases the bioavailability of insulin growth factor-1 (IGF-1), nerve growth factor-1 (NGF-1), and binding protein-3, which frees biologically active IGF-1 at the cell surface.[43] Additionally, proNGF can be released and cleaved to its mature form by MMP-3 at the cell surface.[44] When proNGF binds to the p75 neurotrophin receptor, it triggers cell death; but when mature NGF binds to the tyrosine kinase receptor (TrkA) high-affinity NGF receptor, it promotes neuronal survival.[45] Thus, MMP-3 and its inhibitor, TIMP-3, can influence whether the cell undergoes cell death or survives.

Multiple mechanisms likely contribute to the cell death observed in neuroinflammatory pathologies. TACE releases TNF-α and TNF receptor (TNFR) from the cell membranes, while MMP-3 acts on Fas at the cell surface. When TIMP-3 blocks the action of MMP-3 and TACE, the death-promoting functions of Fas and TNF-α are facilitated.[38] Apoptosis of hippocampal neurons occurs after transient bilateral carotid occlusion, and mice lacking the *timp*-3 gene are protected from hippocampal cell apoptosis.[46] Because TIMP-3 blocks both release of TNF receptors from the cell surface and cleavage of TNF-α into an active form, the role of TIMP-3 in regard to TNF action is difficult to predict. However, the release of Fas by MMP-3 is more readily understandable since TIMP-3 blocking of MMP-3-mediated release of Fas from the cell surface would promote apoptosis.

TIGHT JUNCTION PROTEINS AND MMPS

Brain capillaries are acted on by MMPs, which are found in all the elements of the neurovascular unit. Endothelial cells have mainly MMP-9, pericytes express MMP-3 and MMP-9, and astrocytes have MMP-2, MMP-9, and MMP-14 in the endfeet that surround the endothelial cells. Resting astrocytes mainly express MMP-2, but once activated, other MMPs are induced. White blood cells secrete MMPs, which facilitates their ability to cross the BBB. Neutrophils contain an activated form of MMP-9 that is released during inflammation.

Astrocytes with MMP-2 are found around blood vessels; also found in the cells are the activator of MMP-2, MT-MMP, as well as its activator, furin (Figure 7–11A–C). The MMPs disrupt proteins in the basal lamina and tight junctions. Since the MMPs are secreted by the endothelial cells, the astrocytes, and the pericytes, it is unclear where the unraveling of the basal lamina and tight junctions begins. It is possible that disassembly starts with the outer layers of the basal lamina and proceeds to the tight junctions once they are exposed, but endothelial cells may be able to directly attack the tight junction proteins in their clefts (Figure 7–11D). Ischemia induces cytokines, which, in turn, induce MMP-9 and MMP-3. Pericytes around the cells are a major source of MMP-3, which is an activator of MMP-9. Another source of MMP-9 is the neutrophils recruited into the injury site. However, these are produced late in the injury, and the contribution of the endogenous and exogenous MMPs is uncertain.

MMPS AND TPA-INDUCED BLEEDING

When tissue plasminogen activator (tPA) is given for the treatment of acute stroke, it activates plasminogen to plasmin and initiates the activation of the MMPs. In the situation where the BBB is disrupted early after onset of the ischemic injury, the tPA/plasmin may enter the brain and initiate proteolysis by MMPs, enhancing the hemorrhagic conversion of the tissues. Proteases are activators of MMPs, and this becomes important in the proteolytic disruption of the BBB, where the combination of the release of MMP-3 by pericytes and the release of MMP-9 by microglia and endothelial cells results in the activation of MMP-9 by MMP-3, with amplification of the damage to the BBB.

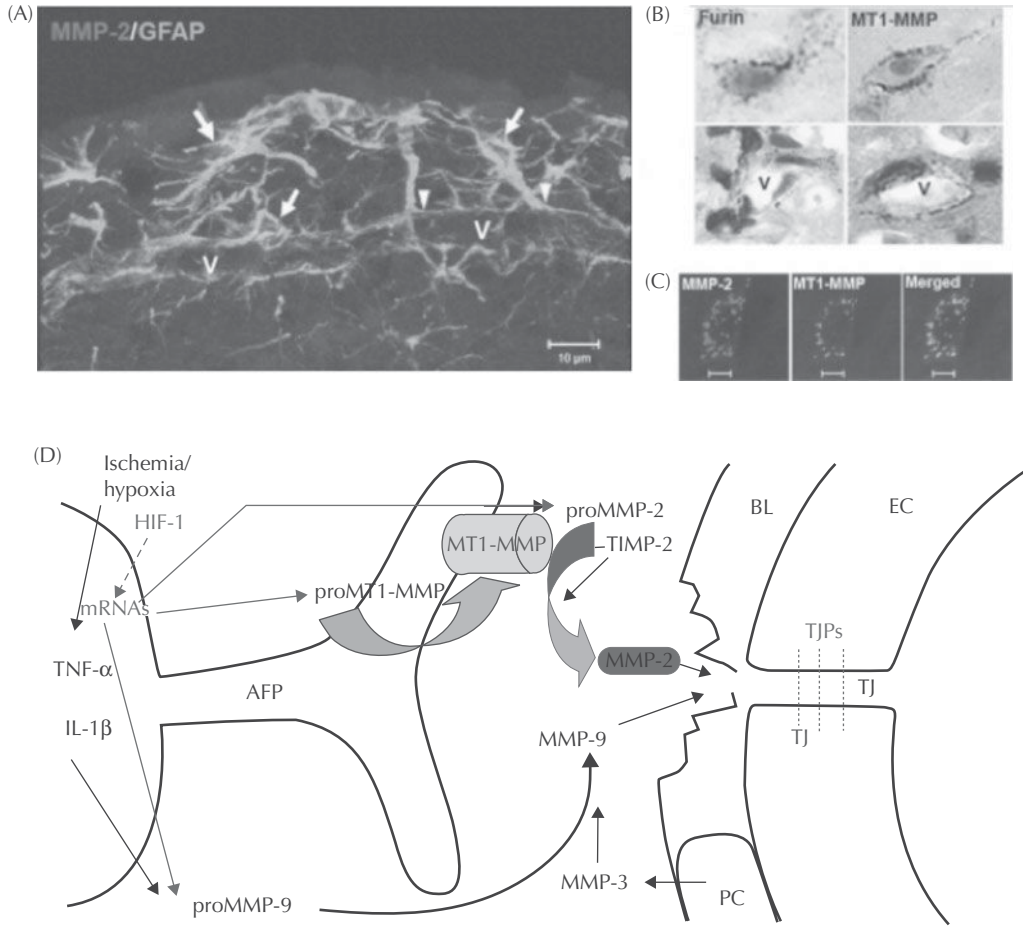

Figure 7–11. (**A**) Confocal immunohistochemistry shows GFAP-positive astrocytes around a vessel (V) that express MMP-2 (arrows) in intact rat brain tissue. The arrowheads indicate the astrocyte endfeet around the vessel. (**B**) Expression of furin and MT1-MMP in brain cells and around vessels (V). (**C**) Confocal images show the colocalization of MMP-2 and MT1-MMP immunohistochemistry in brain cells. (**D**) Schematic drawing showing that the activation of MMP-2 occurs through the action of the trimolecular complex during the early opening of the BBB in 3 hours of reperfusion after 90 minutes of MCAO. In the astrocytic foot processes (AFP), MT1-MMP joins with TIMP-2 to activate proMMP-2 in a spatially constrained manner close to the basal lamina (BL). In the BL are the pericytes (PC). The endothelial cells (ECs) have tight junctions (TJ). The activated MMP-2 has direct access to the portion of the BL beneath the AFP, and components of the BL are degraded. The manner in which this disruption of the BL leads to increased permeability is unclear since the role of the BL in maintaining the integrity of the blood vessel is uncertain. (From Ref. 96; See also the color insert.)

Proteolytic disruption of the BBB by MMPs occurs normally in stroke. Magnetic resonance imaging in human cardioembolic stroke showed hemorrhagic transformation in 68% of infarcts, suggesting that hemorrhagic transformation is a regular finding in medium-sized and large cardioembolic infarcts.[47] Plasma levels of MMP-9 correlate with hemorrhagic transformation and intracerebral hemorrhage.[48] Tissue plasminogen activator, which is given for acute strokes within 3 hours of onset, increases the risk of hemorrhage approximately 10-fold.[1] Treatment of rats with tPA increases mortality and increases the opening of the BBB and hemorrhage; treatment with the broad-spectrum MMP inhibitor, BB-94, blocks the opening of the BBB and hemorrhage and dramatically reduces hemorrhage.[49,50] Opening of the BBB after administration of tPA leads to increased mortality; when the BBB is closed with an MMP inhibitor, the death rate is dramatically reduced (Figure 7–12). Tissue plasminogen activator increased the expression and activation of MMP-9; at 12 hours, tPA-treated

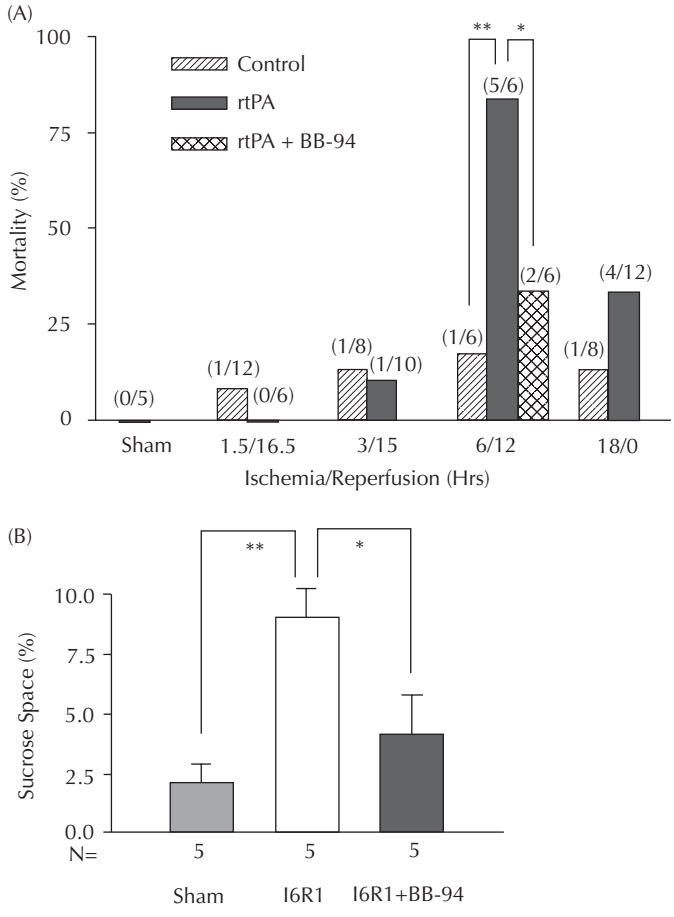

Figure 7–12. (**A**) Effect of rtPA on mortality in animals with different intervals of ischemia and reperfusion. Mortality is shown in percentages, with the number of animals dying and the number of animals studied shown in parentheses above the bars. When reperfusion was delayed to 6 hours, mortality was increased markedly in rtPA-treated animals (**$P < .01$). Treatment with BB94 reduced rtPA-associated mortality significantly (*$P < .05$). Control animals had MCAO without rtPA treatment. (**B**) Opening of the BBB, as measured by the sucrose space in rats with 6 hours of ischemia and 1 hour of reperfusion (I6R1). Compared with sham-operated animals, BBB permeability was markedly increased in untreated rats (**$P < .01$). BB94 given 2 and 5 hours after MCAO markedly decreased BBB opening (*$P < 0.01$). (Adapted from Ref. 50.)

rats showed significantly higher levels of pro-MMP-9 and cleaved MMP-9 than untreated controls, and by 24 hours, all rats showed evidence of hemorrhagic transformation in the ischemic territory. Rats treated with BB-94 and tPA showed significantly reduced hemorrhage volumes compared with those that received tPA alone.[51] When the BBB remains intact, the fibrinolytic agent acts on fibrin within the blood vessels; however, if the BBB is compromised, the tPA escapes into the brain and acts on the MMPs. Agents that maintain the integrity of the BBB may therefore extend the therapeutic window for treatment.

The MMPs contribute to DNA damage, indicating that they are important inside the nucleus as well as in the extracellular space.[52] Nuclear proteins, poly-ADP-ribose polymerase-1 (PARP-1), and X-ray cross-complementary factor 1 (XRCC1), as well as DNA repair enzymes, are important in DNA fragmentation and cell apoptosis. Rats exposed to a 90-minute middle cerebral artery occlusion (MCAO) had increased MMP-2 and MMP-9 activity in neuronal nuclei by 3 hours, which was associated with DNA fragmentation at 24 and 48 hours of reperfusion. Nuclear extracts showed cleaved fragments of PARP-1 and XRCC1, indicating

proteolytic digestion. Treatment with a broad-spectrum MMP inhibitor, BB1101, blocked the ischemia-induced degradation of both PARP-1 and XRCC1. Free radicals may contribute to intranuclear MMP activity, as shown by the elevation of oxidized DNA, apurinic/apyrimidinic sites, and 8-hydroxy-2′-deoxyguanosine, in ischemic brain cells at 3 hours of reperfusion. Again, BB1101 markedly attenuated the early increase of oxidized DNA. Finally, tissue from stroke patients showed intranuclear MMP expression. Taken together, these observations expand the role of MMPs to damage inside the nucleus in ischemic injury.

Multiple sclerosis (MS) is an autoimmune central nervous system demyelinating disease that affects young adults; it has a significant inflammatory component that is related to MMP action on the BBB and myelin.[53,54] The CSF of MS patients in an acute exacerbation contains elevated levels of MMP-9.[55] The MMPs attack myelin and break myelin into myelin basic protein (MBP) fragments.[56] High-dose steroids, which are used to treat acute MS exacerbations, dramatically reduce MMP-9 in the CSF.[57] Steroids block the activator protein-1 (AP-1) site in the MMP-9 gene promoter region. The MMP-9 comes from the brain compartment. This was convincingly demonstrated in studies that measured MMP-9 levels in the blood and CSF, indexing the MMP-9 to albumin in both compartments by analogy with the IgG index used in the diagnosis of MS.[58]

Treatment of animals with experimental allergic encephalomyelitis (EAE) with MMP inhibitors reduces the severity of the illness.[59] Direct inhibitors of MMPs have not been tested in the treatment of MS. However, a tetracycline derivative, minocycline, which has anti-inflammatory actions, including inhibition of MMPs, improved patients with MS in an uncontrolled clinical trial involving a small number of subjects.[60,61] Minocycline suppresses production of MMP-9 but has other effects on the inflammatory response, including inhibition of the reduction in the microglia response, making it difficult to determine its mechanism of action.

In the test tube, myelin can be degraded into immunogenic fragments of MBP by the addition of MMPs.[62,63] Furthermore, MMP-7 knockout mice displayed reduced inflammation and white blood cell entry into the brain as well as across an in vitro cell culture system, suggesting that MMP-7 may contribute to the inflammatory response.[64] Several broad-spectrum MMP inhibitors, such as BB-1101 and GM6001, improve function and reduce weight loss in EAE.[65] BB-1101 is also an inhibitor of TACE, which may contribute to its effect.[66]

Acute inflammation of the meninges causes opening of the BBB associated with release of MMPs into the CSF. Elevated levels of MMPs are found in viral, bacterial, and fungal meningitis.[67] Matrix metalloproteinases and TACE contribute synergistically to the pathophysiology of bacterial meningitis; TACE proteolytically releases several cell-surface proteins, including the proinflammatory cytokine, TNF-α, and its receptors, which in turn stimulate cells to produce active MMPs, facilitating leukocyte extravasation into brain with degradation of extracellular matrix components and vasogenic edema.[68] Treatment with BB-1101, a hydroxamic acid-based inhibitor of MMP and TACE, downregulated the CSF concentration of TNF-α and decreased the incidence of seizures and mortality. Several types of organisms that cause meningitis increase MMP expression, which can be detected by zymography in the CSF. Organisms other than bacteria induce MMPs, including those causing Lyme disease, viral infections, and tuberculosis.[67] A water-soluble MMP inhibitor, TNF484, with actions against both MMPs and TACE, was shown to be effective in an experimental model of bacterial meningitis.[69]

ANIMAL MODELS IN STROKE

Several animal models have been used to analyze brain hypoxic/ischemic damage. Graded hypoxia is produced by the substitution of nitrogen for oxygen. Hypoxia results from agents that poison oxidative metabolism or reduce the oxygen-carrying capacity of hemoglobin. Cyanide injection produces anoxia by reacting with cytochrome oxidase and binding to hemoglobin. Carbon monoxide (CO) combines with hemoglobin to form carboxyhemoglobin, which is unable to carry oxygen. The toxicity of CO is due mainly to the hypoxia resulting from its effect on hemoglobin, but CO also reacts with cytochrome oxidase and interferes with oxidation.[12]

Brain ischemia produced by occlusion of vessels in the neck is difficult to induce reproducibly in animals because of the collateral circulation from external to internal carotid and a rete mirabile around the circle of Willis. Methods to overcome this limitation include the addition of hypoxia to carotid occlusion,[70] prior cauterization of the vertebrals with later occlusion of the carotids producing a four-vessel occlusion,[71] and occlusion of the middle cerebral artery through the orbit.[72] A major problem with each of these models that limits their application is the variability from animal to animal, so large numbers of experiments are often needed. Gerbils have an incomplete circle of Willis, so unilateral carotid occlusion results in strokes on the ipsilateral side to the obstruction in approximately 40% of the animals, and unilateral or bilateral carotid occlusion in the gerbil has been used as a model to study the time course in the evolution of the ischemic lesion.[73] Seizures occur in some of the animals with stroke; this complicates the interpretation of the data. The small size of the gerbil brain and the lack of reagents for immunohistochemisty and Western blot analysis have limited their use in stroke research.

A suture model of MCAO is used extensively in stroke research.[74] Transgenic mice can be studied with an analogous suture method of MCAO. The variability in infarct development seen in the suture model was reduced by coating the suture with poly-L-lysine, which caused a marked improvement in consistency in infarct size.[75] Although used extensively, the suture model mimics only the reperfusion injury. Permanent occlusion of an artery is probably more common as a cause of stroke in humans.

None of the current models is adequate to study the spectrum of cerebral infarction in humans. Because of the use of one model for a short time period, a number of studies of drugs developed for stroke treatment failed, greatly reducing the enthusiasm of the pharmaceutical industry to test new drugs for stroke. To overcome this difficulty, use of several models with multiple time points and the inclusion of long-term recovery data is now advocated.[76] The consequence of initiating the molecular cascades involved in cell death is the activation of a number of pathways (Figure 7–9). The number and complexity of these multiple pathways that simultaneously come into play make the use of a single agent for the treatment of ischemic/hypoxic injury unlikely and most likely explains the failure of most studies of single agents in the treatment of stroke.[77] These cascades occur in a sequence that makes it possible to consider treatments at different stages

ARTERIOVENOUS MALFORMATIONS AND CAVERNOUS HEMANGIOMAS

Aberrant development of blood vessels takes several forms. Large tangles of blood vessels with shunting of blood from the arteries to the veins are referred to as *arteriovenous malformations* (AVMs). These are high-flow structures with a tendency to bleed, making them potentially life-threatening. These abnormal vessels can grow over long periods of time. There is evidence that they use growth factors such as vascular endothelial growth factor and MMPs to grow.[78,79]

Another type of vascular malformation that can only be visualized on MRI is the cavernous malformation. These malformations are small tangles of blood vessels that are not visible on CT or cerebral angiograms. They are hereditary and occur in families; they are often multiple and can be found in all regions of the brain. Generally, they present as seizures or headaches. On MRI there may be several cavernous angiomas, and studies have shown that they grow in number over time. Rings of hemosiderin around the cavernous malformations indicate occult episodes of bleeding. Large bleeds are rare and seldom need to be surgically excised.

At one institution between 1986 and 1993, the histories and imaging studies of 29 patients whose lesions were suggestive of cavernous angiomas were identified in 5000 cranial MRI reports. Patients ranged from 3 to 66 years of age, and 27 were of Hispanic origin. The number of malformations per patient ranged from 1 to 30, and 24 patients had more than 1 lesion. The number of lesions per patient increased at a rate of one lesion per decade of age, but the mean size of the lesions was smaller with advancing decade ($p < .05$).[80]

It is estimated that cerebral cavernous malformations (CCMs) are present in some 20 million people worldwide. They are responsible for

seizures, migraine, hemorrhage, and other neurological problems. Familial CCM can be inherited as an autosomal dominant disorder with variable expression. A gene for CCM (*CCM1*) has been mapped to the 4 cM interval of chromosome 7q in a large Hispanic family.[81,82]

MAGNETIC RESONANCE IMAGING, POSITRON EMISSION TOMOGRAPHY, AND ELECTRON PAPAMAGNETIC RESONANCE IN HYPOXIA/ISCHEMIA

Magnetic Resonance Imaging and Magnetic Resonance Spectroscopy

^{1}H-Nuclear magnetic resonance (^{1}H-NMR) has been used experimentally, either alone or in combination with ^{31}P-NMR, to follow metabolic changes. In a study with both ^{31}P-NMR and ^{1}H-NMR used to study bicucculline-induced seizures, lactate was shown to be elevated longer than the duration of the seizure; the signal attributed to lactate persisted in spite of a return of pH to normal.[83] Lactate and pH measurements have been made in traumatic brain injury.[84] During brain injury, there was a transient fall of brain pH along with a transient rise in the lactate level; the increase in lactate correlated with the fall in pH. However, the NMR changes were similar in moderately and severely injured animals, and functional recovery was worse in the severely injured ones. Dissociation of lactate and pH was found in intracerebral hemorrhage induced in rats with bacterial collagenase injection into the caudate; although the lactate was increased, the pH, as measured with ^{31}P-magnetic resonance spectroscopy (^{31}P-MRS), remained normal.[85] There was vasogenic edema, which caused the lactate to rise, but tissue ischemia was not present and the pH remained normal. Few clinical uses have been identified for spectroscopic measurements of lactate. One exception is mitochondrial encephalopathy, lactic acidosis, stroke-like episodes (MELAS), a syndrome of children and young adults with dysfunction of the mitochondria that causes stroke-like episodes and white matter damage; ^{1}H-MRS shows an increase in lactate in the brain.[86]

Stroke patients have cytotoxic edema that causes cell swelling with reduced extracellular space that slows water diffusion; this causes a reduction in the apparent diffusion coefficient (ADC), which is seen as a dark area on MRI. At the same time, there is an increase in the diffusion-weighted image (DWI) that appears white on MRI. Another technique is to perform a perfusion study with the use of a contrast agent, gadolinium-diethylenetriaminepentaacetic acid (DTPA). Transit of the gadolinium-DTPA through the circulation is slowed when the tissue is ischemic. Combining the ADC, which indicates the ischemic core, with the perfusion image, which presumably shows the vulnerable tissue that has not infarcted, provides information about the penumbra where the tissue is potentially salvageable. Finding this "mismatch" suggests that this is the penumbra, indicating that more aggressive treatment may be undertaken. Although the concept has a strong theoretical basis, attempts to confirm it by the use of other methods including positron emission tomography reveal some discrepancies. This use of magnetic resonance diffusion and perfusion imaging to identify an ischemic penumbra has been augmented with ^{1}H-MRS. Comparison of *N*-acetylaspartate (NAA), which is found in intact neurons, and lactate, an indicator of anaerobic metabolism, with diffusion/perfusion parameters in stroke patients showed that NAA differentiated abnormal from normal tissues, but it failed to separate areas with mismatch of DWI and perfusion-weighted images (PWIs). Regions that were thought to be definitely abnormal had the highest levels of lactate. However, there was no correlation between NAA and ADC or PWI values, but high lactate correlated with low ADC and prolonged mean transit times. Thus, ADC and mean transit time indicate the presence of ischemia, as shown by elevated lactate, but not neuronal damage, as indicated by reduced NAA in acute ischemic stroke, suggesting that caution is required if ADC and PWI parameters are used to differentiate salvageable from nonsalvageable tissue.[87]

Positron Emission Tomography

Positron emission tomography (PET) provides dynamic measurements of cerebral blood flow (CBF), cerebral metabolic rate of oxygen

($CMRO_2$), oxygen extraction fraction (OEF), cerebral blood volume (CBV), and cerebral metabolic rate of glucose (CMRGlu).[88] Shortly after a fall in cerebral perfusion, there is vasodilatation producing a compensatory increase in CBV; the OEF and $CMRO_2$ remain normal. With further decreases in perfusion pressure, the fall in oxygen delivery results in an increase in OEF, while $CMRO_2$ remains normal. At this preinfarction stage, the CBF is variable, and there is reduced oxygen extraction. As the damage progresses, there is a reduction in CBF, $CMRO_2$, and OEF.

After an infarct is established the $CMRO_2$ can be decreased, as is the OEF, while the CBF is elevated. This elevation of CBF above metabolic demands is termed *luxury perfusion* and can be seen in strokes. Positron emission tomography studies have shown that CBF is an unreliable indicator of recovery. A better predictor appears to be $CMRO_2$.

Occlusion of the internal carotid artery may lead to an increase in CBV in the ipsilateral hemisphere.[89] The increase in CBV means that resistance is lower and CBF is maintained in spite of the occlusion. A more advanced stage is seen in some patients with maximally dilated vasculature ipsilateral to the carotid occlusion and reduced CBF with an exhausted hemodynamic reserve.

The loss of tissue viability occurs in infarction. The ischemia preceding infarction shows a maximal rise in the OEF that is due to an attempt to remove as much oxygen as possible by the damaged tissue. Infarcted tissue has a lower metabolic rate. The reduced $CMRO_2$ remains low in spite of increased CBF, and the tissue changes are generally irreversible[90] (Figure 7–13). Therefore, PET has shown the interplay of homeostatic mechanisms in ischemic tissue that lead to infarction. Firstly, the cerebral vessels dilate to reduce peripheral resistance and maintain flow. When the hemodynamic reserve is exhausted and vasodilation is maximal, the oxygen-carrying reserve and rate of oxygen extraction increase. Finally,

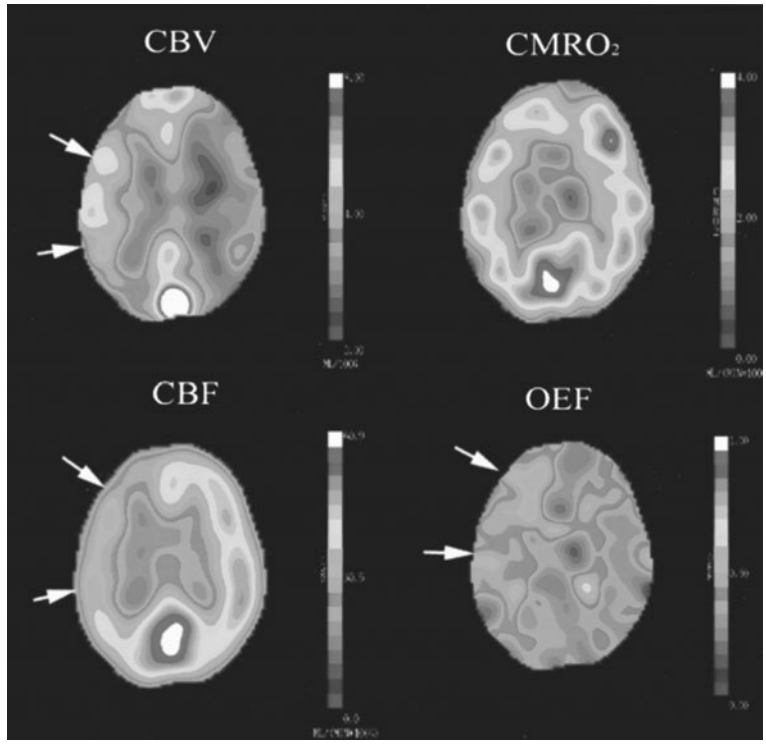

Figure 7–13. Stage 2 haemodynamic failure. Increased CBV indicates autoregulatory vasodilation (CBV, arrows). This is insufficient to maintain flow, however, and flow falls (CBF, arrows). In this situation, the brain can increase the fraction of oxygen extracted from the blood (OEF, arrows) in order to maintain normal oxygen metabolism ($CMRO_2$) and brain function. (From Ref. 90; See also the color insert.)

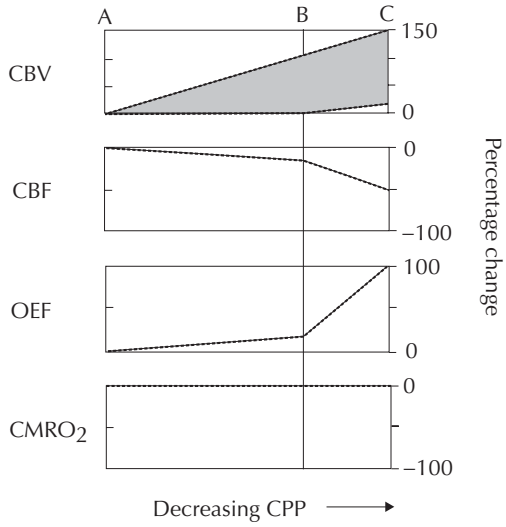

Figure 7–14. Modified model of hemodynamic and metabolic responses to reductions in cerebral perfusion pressure (CPP). Point A represents the baseline. The distance between points A and B represents the autoregulatory range. The distance between points B and C represents exceeded autoregulatory capacity where CBF falls passively as a function of pressure. Point C represents the inability of compensatory mechanisms to maintain normal oxygen metabolism and the onset of true ischemia. Cerebral blood flow may not change or may increase within the autoregulatory range (between A and B). Once the autoregulatory capacity is exceeded (between B and C), CBV may increase slightly (10%–20%), remain elevated, or continue to increase (up to 150%). Cerebral blood flow falls slightly, to 18%, through the autoregulatory range (between A and B). Once the autoregulatory capacity is exceeded, CBF falls passively as a function of pressure to 50% of baseline values (between B and C). The OEF increases slightly, to 18%, with the reductions in CBF through the autoregulatory range (between A and B). After autoregulatory capacity is exceeded and flow falls by up to 50% of baseline, OEF may increase by up to 100% from baseline. The $CMRO_2$ remains unchanged throughout this range of CPP reduction (between A and C) due to both autoregulatory vasodilation and increased OEF. (From Ref. 90.)

loss of both blood flow and oxygen extraction reserves leads to tissue infarction as the energy demands can no longer be met (Figure 7–14).

Electron Paramagnetic Resonance

Oxygen measurements in ischemic tissue can be made by NMR and by electron paramagnetic resonance (EPR), a novel method of studying oxygen and free radicals in vivo. In vivo EPR is a magnetic resonance technique that provides physiological information by using paramagnetic probes to assess tissue pO_2, pH, and identification of free radical species, with EPR measurements performed noninvasively. The measurement of cerebral pO_2 with EPR oximetry is facilitated by the use of the oxygen-sensitive paramagnetic probe, lithium phthalocyanine. Electron paramagnetic resonance was used to measure oxygenation in the penumbral region after an MCAO with reperfusion. Treatment with normobaric hyperoxia reduced the damage to tissue after an infarction; 95% oxygen after a stroke in rats restored oxygen to the penumbra, resulting in reduced expression of MMP-9 and the disruption of the BBB in the penumbral region.[91]

Electron paramagnetic resonance-sensitive compounds can be injected intravenously and used to form images of tissue oxygenation. One such class of compounds is nitroxides that cross the BBB and enter brain cells, becoming trapped and acting within the cells as paramagnetic probes. These nitroxides accurately report local O_2 concentrations using low-frequency EPR spectroscopy as an imaging modality. Using these compounds, it was possible to map the O_2 in an ischemic mouse brain in real time. The change of O_2 concentration in this experimental paradigm of brain ischemia was clearly visualized by EPR spectral-spatial imaging of the nitroxide line width. The hypoxic zone in the EPR images matched well with the infarction area in the brain, as revealed by diffusion-weighted MRI. Electron paramagnetic resonance imaging indicated that the hypoxic region with $pO_2 < 5$ mm Hg was relatively small, even though the MR diffusion image showed a relatively large infarction area after 30 minutes of focal cerebral ischemia, suggesting that not all tissues in the infarcted area, as defined by DWI or TTC staining, are highly hypoxic**.** Treatment with normobaric hyperoxia treatment significantly increased overall tissue pO_2 and reduced the hypoxic region in the ischemic mouse brain.[92]

REFERENCES

1. Anonymous. Tissue plasminogen activator for acute ischemic stroke. The National Institute of Neurological Disorders and Stroke rt-pa Stroke Study Group [see comments]. *N Engl J Med*. 1995;333:1581–1587.
2. Tu JV, Nardi L, Fang J, et al. National trends in rates of death and hospital admissions related to

acute myocardial infarction, heart failure and stroke, 1994–2004. *CMAJ*. 2009;180:E118-E125.
3. Carandang R, Seshadri S, Beiser A, et al. Trends in incidence, lifetime risk, severity, and 30-day mortality of stroke over the past 50 years. *JAMA*. 2006;296: 2939–2946.
4. Liao Y, Greenlund KJ, Croft JB, et al. Factors explaining excess stroke prevalence in the u.s. stroke belt. *Stroke*. 2009;40:3336–3341.
5. Staessen JA, Wang JG, Thijs L. Cardiovascular protection and blood pressure reduction: a meta-analysis. *Lancet*. 2001;358:1305–1315.
6. Lu GC, Cheng JW, Zhu KM, et al. A systematic review of angiotensin receptor blockers in preventing stroke. *Stroke*. 2009;40:3876–3878.
7. Hochachka PW, Guppy M. *Metabolic Arrest and the Control of Biological Time*. Cambridge, MA Harvard University Press; 1987.
8. Lowry OH, Roberts NR, Wu ML, et al. The quantitative histochemistry of brain. II Enzyme measurements. *J Biol Chem*. 1954;207:19–37.
9. Lowry OH, Passonneau JV, Hasselberger FX, et al. Effect of ischemia on known substrates and cofactors of the glycolytic pathway in brain. *J Biol Chem*. 1964;239:18–30.
10. Duffy TE, Nelson SR, Lowry OH. Cerebral carbohydrate metabolism during acute hypoxia and recovery. *J Neurochem*. 1972;19:959–977.
11. Bazan NG Jr. Effects of ischemia and electroconvulsive shock on free fatty acid pool in the brain. *Biochim Biophys Acta*. 1970;218:1–10.
12. Siesjo BK. *Brain Energy Metabolism*. Chichester, UK: Wiley; 1978.
13. Maier CM, Ahern K, Cheng ML, et al. Optimal depth and duration of mild hypothermia in a focal model of transient cerebral ischemia: effects on neurologic outcome, infarct size, apoptosis, and inflammation. *Stroke*. 1998;29:2171–2180.
14. Bernard SA, Gray TW, Buist MD, et al. Treatment of comatose survivors of out-of-hospital cardiac arrest with induced hypothermia. *N Engl J Med*. 2002;346: 557–563.
15. Den Hertog HM, van der Worp HB, Tseng MC, et al. Cooling therapy for acute stroke. *Cochrane Database Syst Rev*. 2009:CD001247.
16. Olney JW, Sharpe LG. Brain lesions in an infant rhesus monkey treated with monsodium glutamate. *Science*. 1969;166:386–388.
17. Brainard JR, Kyner E, Rosenberg GA. ^{13}C nuclear magnetic resonance evidence for gamma-aminobutyric acid formation via pyruvate carboxylase in rat brain: a metabolic basis for compartmentation. *J Neurochem*. 1989;53:1285–1292.
18. Rothman SM, Olney JW. Glutamate and the pathophysiology of hypoxic-ischemic brain damage. *Ann Neurol*. 1986;19:105–111.
19. Tekkok SB, Ye Z, Ransom BR. Excitotoxic mechanisms of ischemic injury in myelinated white matter. *J Cereb Blood Flow Metab*. 2007;27:1540–1552.
20. Herman MA, Jahr CE. Extracellular glutamate concentration in hippocampal slice. *J Neurosci*. 2007;27: 9736–9741.
21. Rosenberg GA, Navratil M, Barone F, et al. Proteolytic cascade enzymes increase in focal cerebral ischemia in rat. *J Cereb Blood Flow Metab*. 1996;16: 360–366.
22. Heo JH, Lucero J, Abumiya T, et al. Matrix metalloproteinases increase very early during experimental focal cerebral ischemia. *J Cereb Blood Flow Metab*. 1999;19:624–633.
23. Gasche Y, Fujimura M, Morita-Fujimura Y, et al. Early appearance of activated matrix metalloproteinase-9 after focal cerebral ischemia in mice: a possible role in blood-brain barrier dysfunction. *J Cereb Blood Flow Metab*. 1999;19:1020–1028.
24. Wang X, Jung J, Asahi M, et al. Effects of matrix metalloproteinase-9 gene knock-out on morphological and motor outcomes after traumatic brain injury. *J Neurosci*. 2000;20:7037–7042.
25. Chang DI, Hosomi N, Lucero J, et al. Activation systems for latent matrix metalloproteinase-2 are upregulated immediately after focal cerebral ischemia. *J Cereb Blood Flow Metab*. 2003;23:1408–1419.
26. Yang Y, Estrada EY, Thompson JF, et al. Matrix metalloproteinase-mediated disruption of tight junction proteins in cerebral vessels is reversed by synthetic matrix metalloproteinase inhibitor in focal ischemia in rat. *J Cereb Blood Flow Metab*. 2007;27: 697–709.
27. Aid S, Silva AC, Candelario-Jalil E, et al. Cyclooxygenase-1 and -2 differentially modulate lipopolysaccharide-induced blood-brain barrier disruption through matrix metalloproteinase activity. *J Cereb Blood Flow Metab*. 2010;30:370–380.
28. Chan PH, Fishman RA. The role of arachidonic acid in vasogenic brain edema. *Fed Proc*. 1984;43:210–213.
29. Simard JM, Kahle KT, Gerzanich V. Molecular mechanisms of microvascular failure in central nervous system injury—synergistic roles of nkcc1 and sur1/trpm4. *J Neurosurg*. 2010;113:622–629.
30. Kerr JF, Wyllie AH, Currie AR. Apoptosis: a basic biological phenomenon with wide-ranging implications in tissue kinetics. *Br J Cancer*. 1972;26:239–257.
31. Fink K, Zhu J, Namura S, et al. Prolonged therapeutic window for ischemic brain damage caused by delayed caspase activation. *J.Cereb.Blood Flow Metab*. 1998;18:1071–1076.
32. Endres M, Namura S, Shimizu-Sasamata M, et al. Attenuation of delayed neuronal death after mild focal ischemia in mice by inhibition of the caspase family. *J.Cereb Blood Flow Metab*. 1998;18:238–247.
33. Broughton BR, Reutens DC, Sobey CG. Apoptotic mechanisms after cerebral ischemia. *Stroke*. 2009;40: e331–e339.
34. Brew K, Nagase H. The tissue inhibitors of metalloproteinases (timps): an ancient family with structural and functional diversity. *Biochim Biophys Acta*. 2010;1803:55–71
35. Leco KJ, Khokha R, Pavloff N, et al. Tissue inhibitor of metalloproteinases-3 (timp-3) is an extracellular matrix-associated protein with a distinctive pattern of expression in mouse cells and tissues. *J Biol Chem*. 1994;269:9352–9360.
36. Cunningham LA, Wetzel M, Rosenberg GA. Multiple roles for MMPs and timps in cerebral ischemia. *Glia*. 2005;50:329–339.
37. Wallace JA, Alexander S, Estrada EY, et al. Tissue inhibitor of metalloproteinase-3 is associated with neuronal death in reperfusion injury. *J Cereb Blood Flow Metab*. 2002;22:1303–1310.
38. Wetzel M, Li L, Harms KM, et al. Tissue inhibitor of metalloproteinases-3 facilitates Fas-mediated neuronal

cell death following mild ischemia. *Cell Death Differ*. 2008;15:143–151.
39. Jaworski DM. Differential regulation of tissue inhibitor of metalloproteinase mrna expression in response to intracranial injury. *Glia*. 2000;30:199–208.
40. Liu W, Furuichi T, Miyake M, et al. Differential expression of tissue inhibitor of metalloproteinases-3 in cultured astrocytes and neurons regulates the activation of matrix metalloproteinase-2. *J Neurosci Res*. 2007;85:829–836.
41. Smith MR, Kung H, Durum SK, et al. Timp-3 induces cell death by stabilizing tnf-alpha receptors on the surface of human colon carcinoma cells. *Cytokine*. 1997;9:770–780.
42. Bond M, Murphy G, Bennett MR, et al. Tissue inhibitor of metalloproteinase-3 induces a Fas-associated death domain-dependent type II apoptotic pathway. *J Biol Chem*. 2002;277:13787–13795.
43. Fowlkes JL, Serra DM, Bunn RC, et al. Regulation of insulin-like growth factor (igf)-1 action by matrix metalloproteinase-3 involves selective disruption of igf-1/igf-binding protein-3 complexes. *Endocrinology*. 2004;145:620–626.
44. Lee R, Kermani P, Teng KK, et al. Regulation of cell survival by secreted proneurotrophins. *Science*. 2001;294:1945–1948.
45. Harrington AW, Leiner B, Blechschmitt C, et al. Secreted proNGF is a pathophysiological death-inducing ligand after adult cns injury. *Proc Natl Acad Sci USA*. 2004;101:6226–6230.
46. Walker EJ, Rosenberg GA. Timp-3 and mmp-3 contribute to delayed inflammation and hippocampal neuronal death following global ischemia. *Exp Neurol*. 2009;216:122–131.
47. Hornig CR, Bauer T, Simon C, et al. Hemorrhagic transformation in cardioembolic cerebral infarction. *Stroke*. 1993;24:465–468.
48. Rosell A, Ortega-Aznar A, Varez-Sabin J, et al. Increased brain expression of matrix metalloproteinase-9 after ischemic and hemorrhagic human stroke. *Stroke*. 2006;37:1399–1406.
49. Lapchak PA, Chapman DF, Zivin JA. Metalloproteinase inhibition reduces thrombolytic (tissue plasminogen activator)-induced hemorrhage after thromboembolic stroke. *Stroke*. 2000;31:3034–3040.
50. Pfefferkorn T, Rosenberg GA. Closure of the blood-brain barrier by matrix metalloproteinase inhibition reduces rtpa-mediated mortality in cerebral ischemia with delayed reperfusion. *Stroke*. 2003;34:2025–2030.
51. Sumii T, Lo EH. Involvement of matrix metalloproteinase in thrombolysis-associated hemorrhagic transformation after embolic focal ischemia in rats. *Stroke*. 2002;33:831–836.
52. Yang Y, Candelario-Jalil E, Thompson JF, et al. Increased intranuclear matrix metalloproteinase activity in neurons interferes with oxidative DNA repair in focal cerebral ischemia. *J Neurochem*. 2010;112:134–149.
53. Noseworthy JH, Lucchinetti C, Rodriguez M, et al. Multiple sclerosis. *N Engl J Med*. 2000;343:938–952.
54. Yong VW, Zabad RK, Agrawal S, et al. Elevation of matrix metalloproteinases (mmps) in multiple sclerosis and impact of immunomodulators. *J Neurol Sci*. 2007;259:79–84.
55. Gijbels K, Masure S, Carton H, et al. Gelatinase in the cerebrospinal fluid of patients with multiple sclerosis and other inflammatory neurological disorders. *J Neuroimmunol*. 1992;41:29–34.
56. Chandler S, Cossins J, Lury J, et al. Macrophage metalloelastase degrades matrix and myelin proteins and processes a tumour necrosis factor-alpha fusion protein. *Biochem Biophys Res Commun*. 1996;228:421–429.
57. Rosenberg GA, Dencoff JE, Correa N Jr, et al. Effect of steroids on csf matrix metalloproteinases in multiple sclerosis: relation to blood-brain barrier injury. *Neurology*. 1996;46:1626–1632.
58. Liuzzi GM, Trojano M, Fanelli M, et al. Intrathecal synthesis of matrix metalloproteinase-9 in patients with multiple sclerosis: implication for pathogenesis. *Mult Scler*. 2002;8:222–228.
59. Hewson AK, Smith T, Leonard JP, et al. Suppression of experimental allergic encephalomyelitis in the Lewis rat by the matrix metalloproteinase inhibitor ro31–9790. *Inflammation Res*. 1995;44:345–349.
60. Metz LM, Zhang Y, Yeung M, et al. Minocycline reduces gadolinium-enhancing magnetic resonance imaging lesions in multiple sclerosis. *Ann Neurol*. 2004;55:756.
61. Yong VW, Giuliani F, Xue M, et al. Experimental models of neuroprotection relevant to multiple sclerosis. *Neurology*. 2007;68:S32-S37; discussion S43-S54.
62. Chandler S, Coates R, Gearing A, et al. Matrix metalloproteinases degrade myelin basic protein. *Neurosci Lett*. 1995;201:223–226.
63. Opdenakker G, Van den Steen PE, Van Damme J. Gelatinase b: a tuner and amplifier of immune functions. *Trends Immunol*. 2001;22:571–579.
64. Buhler LA, Samara R, Guzman E, et al. Matrix metalloproteinase-7 facilitates immune access to the cns in experimental autoimmune encephalomyelitis. *BMC Neurosci*. 2009;10:17.
65. Clements JM, Cossins JA, Wells GM, et al. Matrix metalloproteinase expression during experimental autoimmune encephalomyelitis and effects of a combined matrix metalloproteinase and tumour necrosis factor-alpha inhibitor. *J Neuroimmunol*. 1997;74: 85–94.
66. Gearing AJ, Beckett P, Christodoulou M, et al. Processing of tumour necrosis factor-alpha precursor by metalloproteinases. *Nature*. 1994;370:555–557.
67. Leppert D, Lindberg RL, Kappos L, et al. Matrix metalloproteinases: multifunctional effectors of inflammation in multiple sclerosis and bacterial meningitis. *Brain Res Brain Res Rev*. 2001;36:249–257.
68. Leib SL, Clements JM, Lindberg RL, et al. Inhibition of matrix metalloproteinases and tumour necrosis factor alpha converting enzyme as adjuvant therapy in pneumococcal meningitis. *Brain*. 2001;124:1734–1742.
69. Echchannaoui H, Leib SL, Neumann U, et al. Adjuvant tace inhibitor treatment improves the outcome of TLR2-/- mice with experimental pneumococcal meningitis. *BMC Infect Dis*. 2007;7:25.
70. Levine S. Anoxic-ischemic encephalopathy in rats. *Am J Pathol*. 1960;36:1–17.
71. Pulsinelli WA, Brierley JB. A new model of bilateral hemispheric ischemia in the unanesthetized rat. *Stroke*. 1979;10:267–272.
72. O'Brien MD, Jordan MM, Waltz AG. Ischemic cerebral edema and the blood-brain barrier. Distributions of pertechnetate, albumin, sodium, and antipyrine in brains of cats after occlusion of the middle cerebral artery ischemic cerebral edema. Distribution of water

in brains of cats after occlusion of the middle cerebral artery. *Arch Neurol*. 1974;30:456–460.
73. Levine S, Payan H. Effects of ischemia and other procedures on the brain and retina of the gerbil (*Meriones unguiculatus*). *Exp Neurol*. 1966;16:255–262.
74. Longa EZ, Weinstein PR, Carlson S, et al. Reversible middle cerebral artery occlusion without craniectomy in rats. *Stroke*. 1989;20:84–91.
75. Belayev L, Alonso OF, Busto R, et al. Middle cerebral artery occlusion in the rat by intraluminal suture. Neurological and pathological evaluation of an improved model. *Stroke*. 1996;27:1616–1622; discussion 1623.
76. Saver JL, Albers GW, Dunn B, et al. Stroke Therapy Academic Industry Roundtable (stair) recommendations for extended window acute stroke therapy trials. *Stroke*. 2009;40:2594–2600.
77. Savitz SI, Fisher M. Future of neuroprotection for acute stroke: in the aftermath of the saint trials. *Ann Neurol*. 2007;61:396–402.
78. Hashimoto T, Matsumoto MM, Li JF, et al. Suppression of mmp-9 by doxycycline in brain arteriovenous malformations. *BMC Neurol*. 2005;5:1.
79. Chen Y, Zhu W, Bollen AW, et al. Evidence of inflammatory cell involvement in brain arteriovenous malformations. *Neurosurgery*. 2008;62:1340–1349; discussion 1349–1350.
80. Kattapong VJ, Hart BL, Davis LE. Familial cerebral cavernous angiomas: clinical and radiologic studies. *Neurology*. 1995;45:492–497.
81. Marchuk DA, Gallione CJ, Morrison LA, et al. A locus for cerebral cavernous malformations maps to chromosome 7q in two families. *Genomics*. 1995;28: 311–314.
82. Johnson EW, Iyer LM, Rich SS, et al. Refined localization of the cerebral cavernous malformation gene (CCM1) to a 4-cm interval of chromosome 7q contained in a well-defined yac contig. *Genome Res*. 1995;5:368–380.
83. Petroff OAC, Prichard JW, Ogino T, et al. Combined ^{1}H and ^{31}P nuclear magnetic resonance spectroscopic studies of bicuculline-induced seizures in vivo. *Ann Neurol*. 1986;20:185–193.
84. McIntosh TK, Faden AI, Bendall MR, et al. Traumatic brain injury in the rat: alterations in brain lactate and ph as characterized by ^{1}H and ^{31}P nuclear magnetic resonance. *J Neurochem*. 1987;49:1530–1540.
85. Mun-Bryce S, Kroh FO, White J, et al. Brain lactate and pH dissociation in edema: ^{1}H- and ^{31}p-nmr in collagenase-induced hemorrhage in rats. *Am J Physiol*. 1993;265:R697-R702.
86. Melberg A, Akerlund P, Raininko R, et al. Monozygotic twins with melas-like syndrome lacking ragged red fibers and lactacidaemia. *Acta Neurol Scand*. 1996;94:233–241.
87. Cvoro V, Marshall I, Armitage PA, et al. MR diffusion and perfusion parameters: relationship to metabolites in acute ischaemic stroke. *J Neurol Neurosurg Psychiatry*.81:185–191.
88. Phelps ME, Mazziotta JC, Huang SC. Study of cerebral function with positron computed tomography. *J Cereb Blood Flow Metab*. 1982;2:113–162.
89. Frackowiak RS. Pet scanning: can it help resolve management issues in cerebral ischemic disease? *Stroke*. 1986;17:803–807.
90. Derdeyn CP, Videen TO, Yundt KD, et al. Variability of cerebral blood volume and oxygen extraction: stages of cerebral haemodynamic impairment revisited. *Brain*. 2002;125:595–607.
91. Liu S, Liu W, Ding W, et al. Electron paramagnetic resonance-guided normobaric hyperoxia treatment protects the brain by maintaining penumbral oxygenation in a rat model of transient focal cerebral ischemia. *J Cereb Blood Flow Metab*. 2006;26:1274–1284.
92. Shen J, Sood R, Weaver J, et al. Direct visualization of mouse brain oxygen distribution by electron paramagnetic resonance imaging: application to focal cerebral ischemia. *J Cereb Blood Flow Metab*. 2009;29:1695–1703.
93. Baker AH, Edwards DR, Murphy G. Metalloproteinase inhibitors: biological actions and therapeutic opportunities. *J Cell Sci*. 2002;115:3719–3727.
94. Dirnagl U, Iadecola C, Moskowitz MA. Pathobiology of ischaemic stroke: an integrated view. *Trends Neurosci*. 1999;22:391–397.
95. Rosenberg GA, Cunningham LA, Wallace J, et al. Immunohistochemistry of matrix metalloproteinases in reperfusion injury to rat brain: activation of mmp-9 linked to stromelysin-1 and microglia in cell cultures. *Brain Res*. 2001;893:104–112.
96. Candelario-Jalil E, Yang Y, Rosenberg GA. Diverse roles of matrix metalloproteinases and tissue inhibitors of metalloproteinases in neuroinflammation and cerebral ischemia. *Neuroscience*. 2009;158:983–994.

Chapter 8

Vascular Cognitive Impairment and Alzheimer's Disease

REGULATION OF CEREBRAL BLOOD FLOW

Blood vessels deliver 20% of the total cardiac output to the brain, which consumes 25% of the oxygen used by the body. To meet this extraordinary need for an uninterrupted supply of blood, the heart has complex regulatory mechanisms that function under both normal and adverse conditions. When the heart fails to supply adequate blood to the brain, there is a loss of consciousness that can be transient and have little impact on the survival of the cells or prolonged, with extensive damage to multiple brain regions. In order to meet this large demand for blood and maintain it at an uninterrupted level, cerebral blood flow to brain is tightly autoregulated (Table 8–1). Several factors determine the amount of blood delivered, including the pumping potential and the rate and rhythm of the heart, and the vascular resistance of the cerebral blood vessels. Cardiac arrest is the event most damaging to the brain, while long-standing hypertension causes serious damage but over a longer time course. Blood vessels are extremely sensitive to the levels of carbon dioxide and oxygen in the blood. Increased carbon dioxide and decreased oxygen are powerful vasodilators, while reduced carbon dioxide is a potent vasoconstrictor. A number of molecules, such as nitric oxide, regulate cerebral blood flow.

Autoregulation of cerebral blood flow occurs over a wide range of blood pressures. When mean arterial blood pressure falls below a threshold value, there is a fall in cerebral blood flow (CBF), which results in syncope. At the opposite extreme, when blood pressure increases, vessels dilate, causing vasodilation and breakdown of the blood-brain barrier (BBB). The autoregulatory curve, plotting mean arterial blood pressure against CBF, has a characteristic shape, which is dependent on the health of the blood vessels (Figure 8–1). When considering the impact of drastic changes in blood pressure on blood flow, it is important to take into account the age of the individual and the presence of hypertension or

Table 8–1 **Extreme Metabolic Needs of the Brain**

25% of oxygen is used by the brain
20% of cardiac output goes to the brain
Autoregulation of CBF occurs over a wide mean arterial blood pressure range
Even short periods of loss of CBF lead to loss of consciousness

other disease-modifying effects on the blood vessels, such as diabetes and arteriolosclerosis, which cause stiffer and less elastic blood vessels. Young individuals with low blood pressure and compliant vessels tolerate a drop in blood pressure better than older individuals with less compliant, chronically hypertensive vessels. The clinical implication is that overaggressive treatment of blood pressure in the elderly can lead to frequent episodes of dizziness and occasional fainting at levels of blood pressure that are easily tolerated in younger people. By contrast, elderly persons can better tolerate markedly elevated blood pressure because of their stiffer blood vessels. Thus, the level of blood pressure needed to induce a hypertensive crisis is much lower in the younger individual.

An example of this is seen in patients with eclampsia, who are young women with blood pressure that is normally low; they can develop a hypertensive crisis with moderate increases in blood pressure. Hypertensive crises cause vasogenic edema due to damage to the BBB with a characteristic appearance on magnetic resonance imaging (MRI): fluid attenuated inversion recovery (FLAIR) and T2 images show excess fluid in white matter that is particularly evident in the parieto-occipital regions of the brain. Since this is mainly vasogenic edema without ischemic injury to brain cells, the diffusion-weighted image (DWI) is dark rather than white, as is seen in ischemia, and the apparent diffusion coefficient (ADC) is white rather than dark. The vasogenic edema releases fluid from the blood into the brain, where it moves through the white matter; as a result, the diffusion rate is increased, which is the opposite of ischemic edema. When this pattern of vasogenic edema is present, the prognosis is good unless the edema in the white matter has produced cell death due to the increased pressure. Once the blood pressure is controlled, the edema subsides (Figure 8–2).

Patients other than those with eclampsia can have a similar MRI appearance. In one series of 15 patients with vasogenic edema in the posterior regions of the brain, 7 were receiving immunosuppressive therapy after transplantation or as treatment for aplastic anemia, 1 was receiving interferon for melanoma, 3 had eclampsia, and 4 had acute hypertensive encephalopathy associated with renal disease (2 with lupus nephritis, 1 with acute glomerulonephritis, and 1 with acetaminophen-induced hepatorenal failure). Twelve patients had abrupt increases in

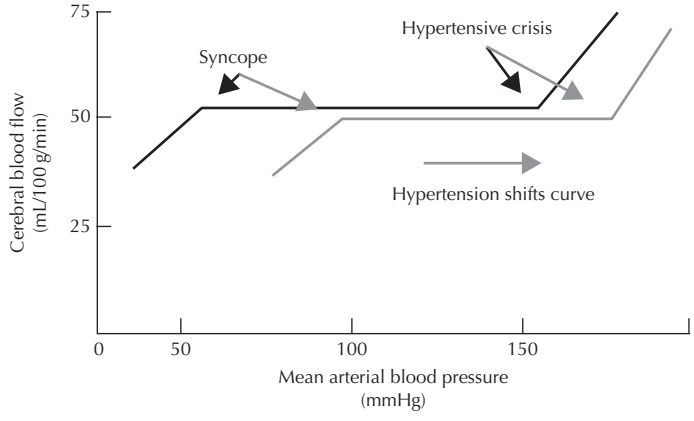

Figure 8–1. Autoregulation of CBF. The average CBF is 50 mL/100 g/min, which is an average between the higher cortical CBF in gray matter and the lower CBF in white matter. The level when the CBF falls and syncope occurs depends on the state of the blood vessels. In a normal blood vessel, the level is lower than in a fibrotic blood vessel secondary to long-standing hypertension. At the upper level, the breakthrough point occurs at a higher level in the hypertensive blood vessel than in the normal one.

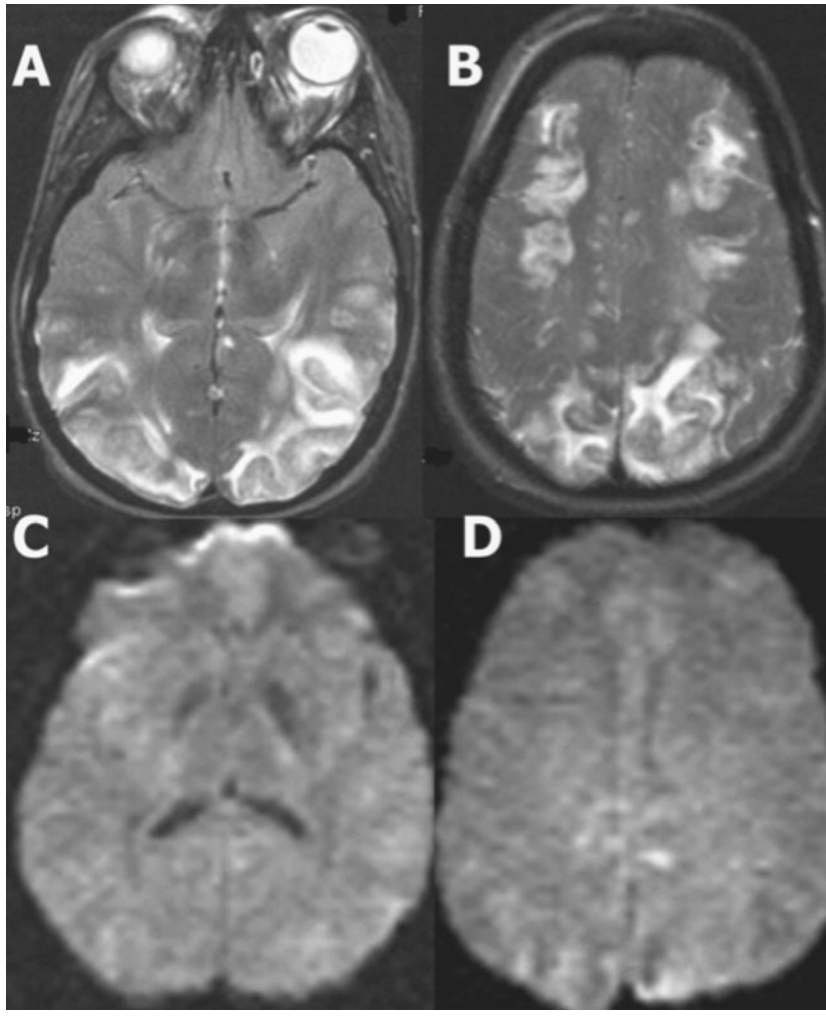

Figure 8–2. A patient with hypertensive encephalopathy secondary to eclampsia with the HELLP (hemolysis, elevated liver enzymes, and low platelets) syndrome. (**A** and **B**) Two T2-weighted MRI scans from a lower (**A**) and higher (**B**) region, showing extensive cerebral edema in the posterior white matter regions with less involvement of the gray matter. (**C** and **B**) Diffusion-weighted images from axial images in the same plane as **A** and **B**. The lack of DWI changes except for one small area of involvement suggests this is not an ischemic injury, but more compatible with a vasogenic type of edema. Consistent with lack of ischemia is the fact that the patient had a good recovery without residual effects.

blood pressure, and eight had some impairment of renal function. Clinical findings included headaches, vomiting, confusion, seizures, cortical blindness, and other visual abnormalities, along with motor signs. Computed tomography (CT) and MRI studies showed extensive bilateral white matter abnormalities suggestive of edema in the posterior regions of the cerebral hemispheres. Treatment with antihypertensive medications or withdrawal of immunosuppressive therapy caused the clinical conditions to resolve within 2 weeks.[1]

Compared to the young patient, in the elderly patient with long-standing hypertension with or without diabetes, blood vessels have undergone extensive remodeling, becoming stiffer and less responsive. Hypertension leads to fibrosis of the cerebral blood vessels and loss of compliance. Therefore, hypertension shifts the autoregulatory curve to the right, which means that syncope can occur at a higher blood pressure, but there is a greater capacity to withstand marked increases in blood pressure before a hypertensive crisis occurs. Thus,

the low point at which syncope occurs and the high point at which breakdown of the BBB takes place are highly dependent on the state of the cerebral blood vessels: reduced cerebral blood flow when high blood pressure is treated occurs earlier in fibrotic vessels than in normal ones. The clinical implication of this important curve is that aggressive treatment of hypertension in the elderly should be carefully monitored to avoid episodic hypotension. However, aggressive treatment of hypertension is warranted in younger patients, who are at risk of BBB disruption with vasogenic edema.

HYPOXIA/ISCHEMIA IN CARDIAC ARREST

Cardiac arrest suddenly reduces blood flow to the entire brain. The first consequence of the sudden loss of blood flow is anoxia with loss of consciousness. A study done on navy recruits in the Second World War showed that a cuff placed around the neck and inflated to greater than blood pressure resulted in loss of consciousness within 7 to 12 seconds; several of the subjects had seizures before the cuff pressure was released.[2] Short periods of anoxia such as occur during a fainting spell lasting for seconds are well tolerated, assuming that no injury occurs from falling. Longer periods of oxygen loss are needed to produce brain cell damage. If anaerobic conditions persist for more than several minutes, there can be an increase in lactate and a fall in pH. With persistent failure to restore blood circulation, brain cells undergo energy failure and begin to show signs of cytotoxic edema. With prolonged hypoxia, brain cells undergo necrosis and apoptosis, resulting in autodigestion by neutral and acid proteases that causes irreversible brain damage with cell death due to loss of membrane function. At any point in the process, there may be sufficient anoxia to begin the process of gene activation that can result in delayed injury even after CBF is restored.

Loss of oxygen leads to the activation of hypoxia-inducible factor-1α (HIF-1α), which is a major regulator of a cassette of genes related to hypoxia and angiogenesis. These genes transcribe many proteins that signal to the brain that a switch from aerobic to anaerobic metabolism is needed: there is induction of glycolytic pathways, production of red blood cells by erythropoietin, and eventually angiogenesis and neurogenesis (Figure 8–3).

Hypoxia and acidosis lead to changes in vascular tone with dilatation and an increase in blood volume. Biochemical changes in the

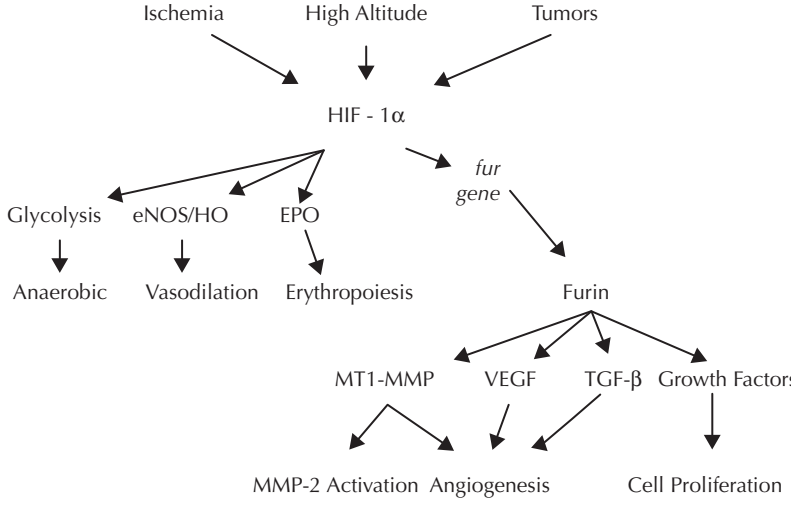

Figure 8–3. Hypoxia inducible factor-1α is induced when oxygen is low and turns on a cassette of genes involved in aiding the brain in withstanding the hypoxic conditions. Glycolysis is increased. Endothelial nitric oxide synthase (eNOS) causes vasodilation, and erythropoiesis (EPO) increases the red blood cell mass. Furin is a convertase activated by the *fur* gene. Furin induces the activator of MMP-2, MT1-MMP, vascular endothelial growth factor (VEGF), transforming growth factor-β (TGF-β), and other growth factors. HO is heme oxygenase.

blood are more severe during prolonged arrest and lead to a greater degree of brain damage. Resuscitation is used to maintain some flow of blood to the brain during the time of the arrest before cardiac function is restored. If cardiopulmonary resuscitation is done very early after the arrest and circulation can be effectively restored to the brain, the extent of brain damage can be limited, which is possible mainly when the cardiac arrest occurs in a hospital. However, often the interval between arrest and restoration of blood flow is too long to permit a return of normal brain function.

Prognosis for Recovery After Cardiac Arrest

Longstreth and colleagues evaluated 459 patients who had an out-of-hospital cardiac arrest; 39% of those examined never regained consciousness, and of the 61% (279) who awoke, 30% (91) had persistent neurological deficits.[3] A large multicenter study determined the factors affecting recovery in a group of patients with nontraumatic or drug-induced comas.[4] The majority of these patients had hypoxia/ischemia due to cardiac arrest. As would be expected, those who awoke soon after the arrest had the best prognosis for full recovery, while those showing loss of brainstem function had the worst prognosis. Only 1 of the 120 patients with absent pupillary or corneal responses regained function. Surviving comatose patients remained in a coma with their eyes closed for about 1 week before they evolved into the vegetative state in which their eyes were open, as if they were awake, but there was no evidence of awareness or comprehension. Except for younger patients with a head injury or drug overdose, recovery is rare; only in very rare circumstances does an adult with a hypoxic/ischemic insult regain limited function.[5]

In the patients who fall between those who awaken shortly after the onset of coma and those who become vegetative, prediction of recovery is difficult. Levy and colleagues used positron emission tomography (PET) scanning to study the regional CBF and the glucose metabolic rate in a group of patients who were either in a persistent vegetative state or who were locked in due to brainstem infarcts that left them awake but totally paralyzed. The glucose metabolic rate was reduced 50% to 60% of normal in those in a vegetative state: the depression of metabolism was seen in all regions measured.[6] Patients with metabolic causes of coma have the best chance of regaining function, while those with stroke have the worst prognosis; patients with hypoxia/ischemia due to cardiac arrest have only a 12% chance of recovery.[4]

When the hypoxic/ischemic insult is severe and the patient survives, often the patient remains comatose with the eyes open and has preservation of some primitive functions; this condition was originally referred to as the *persistent* vegetative state.[7] These patients are unaware of their surroundings, but their primitive functions are preserved and they appear to be awake. Since some of these patients have recovered, the term *persistent* is no longer used. Functional magnetic resonance imaging (fMRI) has added a novel dimension to the study of these altered states of consciousness. Data emerging from the use of fMRI in patients in the vegetative state reveal that a small number of them can answer questions by changing their brain activity.[8] Such patients are considered to be in a minimally conscious state. The long-term implications of finding such patients remains to be established.[9]

Cardiac Surgery and Memory Loss

Less severe episodes of hypoxia/ischemia can also cause cerebral damage. Patients undergoing cardiac surgery are at risk for subtle changes secondary to hypoxia/ischemia during surgery.[10] This is particularly true of elderly individuals who may experience long hypotensive periods during surgery.[11] These patients are frequently confused upon awakening from anesthesia, and an occasional patient is left with permanent amnesia or dementia. In patients with anoxic damage after cardiac surgery, the cerebral deficit is related to the type of surgery.[12] Replacement of damaged and infected heart valves results in a high incidence of strokes. Coronary bypass surgery leads to more diffuse symptoms such as confusion and memory loss. Postsurgical disorientation, which was originally attributed to psychosis from sensory deprivation in the intensive care environment, was probably due to cerebral anoxia and small emboli from the heart lung machine.

Up to 80% of patients undergoing coronary artery bypass surgery show diffuse cerebral impairment in the immediate postoperative period, which has been suggested to be related to an initial hypocapnia with onset of the operation and a subsequent hypercapnia.[13] The degree of transient neuropsychometric deficit was reduced in a group of patients in whom the partial pressure of carbon dioxide (pCO_2) was more carefully controlled. Although the majority will eventually recover without cognitive problems, one-third of these patients continue to show deficits at 1 year postoperatively.

Self-reported cognitive and memory complaints after coronary artery bypass graft (CABG) operations are common. Measures of subjective memory complaints were compared in two groups: 220 CABG patients and 92 nonsurgical cardiac patients at 3 months and at 1, 3, and 6 years. At early (3-month or 1-year) follow-up, the CABG patients reported subjective memory complaints more often than the nonsurgical controls. However, by 6 years, the frequency of complaints was similar (52%) in both groups. The authors speculated that the increase in subjective complaints over time might be related to progression of underlying cerebrovascular disease.[14] Although cognitive decline may be a late effect of coronary artery bypass surgery, the degree of this decline is similar to that observed in patients of similar age with CABG surgery who have not undergone cardiopulmonary bypass, suggesting that cognitive decline that occurs late in life is not related to the type of operation.[15]

Delayed Postanoxic Leukoencephalopathy

Some patients who awaken from a hypoxic episode may remain awake for 1 to 2 weeks before again lapsing into coma. When this occurs, the condition is referred to as *delayed postanoxic leukoencephalopathy*. These patients have extensive damage to the white matter.[16] In delayed postanoxic leukoencephalopathy, there is a period of confusion following the anoxia, but then the patient regains consciousness for a short time before lapsing back into coma. Some patients who survive are left with a permanent impairment in global intellectual function. These patients are demented but the dementia does not progress, as occurs with degenerative diseases such as Alzheimer's disease (AD). An MRI scan from a patient who developed postanoxic leukoencephalopathy after taking one tablet of "diverted" methadone obtained from a friend for abdominal pain shows the extensive damage to the white matter that occurred as a result of the respiratory and cardiac arrest (Figure 8–4) This patient gradually improved over 6 months and by 1 year had returned to work.

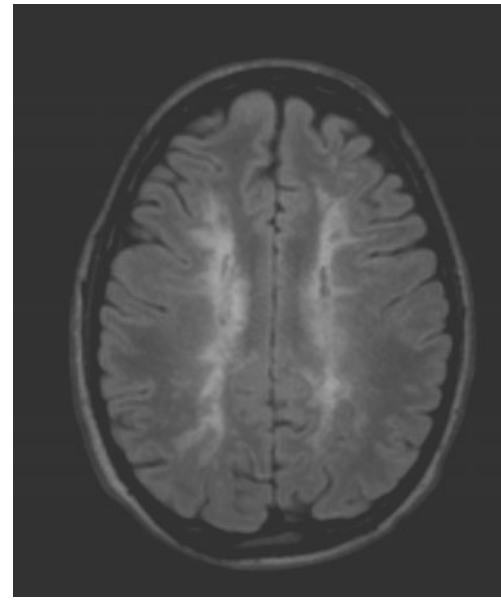

Figure 8–4. Fluid attenuated inversion recovery (FLAIR) MRI scan of a 20-year-old man who took one methadone pill given to him by a friend for stomach pain and did not awaken the next morning. He came out of a coma 9 days later but developed postanoxic leukoencephalopathy. After 3 months, he began to recover, and he resumed work after 6 months. Mild spasticity in the legs remained after 3 years, but otherwise he was functioning well.

HYPOXIA-INDUCIBLE FACTORS AND GENE EXPRESSION

Hypoxia may be severe, as in cardiac arrest, or it may be mild and chronic. Living at high altitude, suffering from sleep apnea, or having poor brain perfusion secondary to cardiovascular disease all initiate a molecular response to compensate for the reduced levels of oxygen. Hypoxia initiates a large number of

changes in transcription factors. Some of the proteins produced in response to the lack of oxygen participate in the disruption of tissue, preparing dead cells for removal or recycling; others initiate repair processes that increase the number of blood vessels and lead to new cell growth. Hypoxia-inducible factors (HIF) are central to an understanding of the mechanisms involved in the response of the brain to oxygen.[17]

The HIF molecular complex is composed of two protein subunits: HIF-1β/ARNT (aryl hydrocarbon receptor nuclear translocator), which is constitutively expressed, and HIF-1α, which is not present in normal cells but is induced under hypoxic conditions. The HIF-1α subunit is continuously synthesized and degraded under normoxic conditions, while it accumulates rapidly following exposure to low oxygen tensions. The ubiquitin-proteasome system proteolytically destroys HIF-1α under normoxic conditions, which maintains its normal low level.[18]

The α subunit of HIF-1α is a target for prolyl hydroxylation by HIF prolyl-hydroxylase, which makes HIF-1α a target for degradation by an E3 ubiquitin ligase, leading to quick degradation by the proteasome (Figure 8–5). E3 ubiquitin ligase is a protein that, in combination with an E2 ubiquitin-conjugating enzyme, causes the attachment of ubiquitin to a lysine on a target protein via an isopeptide bond; the E3 ubiquitin ligase targets specific protein substrates for degradation by the proteasome. Polyubiquitination marks proteins for degradation by the proteasome, which occurs only under normoxic conditions. With hypoxia HIF prolyl-hydroxylase is inhibited, since it utilizes oxygen as a cosubstrate.[19]

At normal tissue oxygen tension, O_2 is bound to a hemoprotein oxygen sensor (S·Heme). When oxygen levels drop, oxygen dissociates, causing a change in the sensor that triggers a signaling cascade involving protein phosphorylation. This leads to activation of a hypothetical regulator (Factor X) and increased expression of the HIF-1α and -1β subunits. The HIF-1 α/β heterodimer binds and activates expression of various genes, including those encoding glycolytic enzymes (for anaerobic metabolism), vascular endothelial growth factor (VEGF; for angiogenesis), inducible nitric oxide synthase and heme oxygenase-1 (for production of vasodilators), erythropoietin (EPO; for erythropoiesis), and possibly tyrosine hydroxylase (for dopamine production to increase breathing). These genes help the cell survive the low-oxygen environment and act to restore normal oxygen levels. Some targets of HIF-1α are induced in most hypoxic cells, while others, like EPO, are only induced in specific tissues and hence also require tissue-specific regulators.[20]

Tumor cells exist in a hypoxic environment and HIF plays a major role in tumor growth, which is regulated by the effect of HIF on p53, which suppresses the production of HIF-1α. The tumor suppressor gene has multiple roles in promoting apoptosis and preventing cancer cell growth (Figure 8–6). The anticancer mechanisms of p53 include (1) activation of DNA repair proteins when DNA has sustained

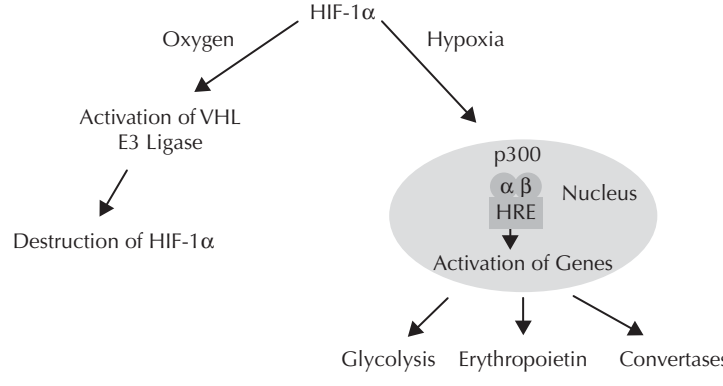

Figure 8–5. Mechanism of HIF-1α induction of other genes. When oxygen is present, the HIF molecule is degraded by E3 ligase. Under anaerobic conditions, HIF-1α joins with HIF-1β to form a dimer (αβ). This dimer activates an HIF-responsive element (HRE) in many genes. VHL is von Hippel-Lindau.

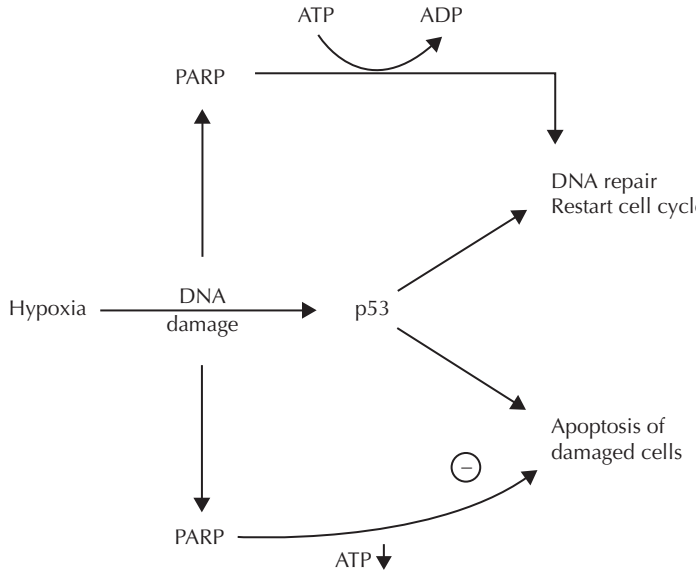

Figure 8–6. Hypoxia initiates DNA damage in the nucleus. Poly-adenosine diphosphate (ADP)-ribose polymerase (PARP) is activated in an attempt to repair the DNA, but when the hypoxia is prolonged, there is a depletion of adenosine triphosphate that causes apoptosis rather than repair.

damage; (2) induction of growth arrest by holding the cell cycle at the G1/S regulation point on DNA damage recognition (if it holds the cell there long enough, the DNA repair proteins will have time to correct the damage and the cell will be allowed to continue the cell cycle); and (3) initiation of apoptosis if the DNA damage proves to be irreparable. Hypoxia-inducible factor-1α acts together with p53 to stabilize it, resulting in cell death.[21]

Another important gene that is induced by HIF-1α is the convertase, *fur*. Furin is the protein produced by the *fur* gene; it has a number of actions, including establishment of new blood vessels and endoproteolytic cleavage of multiple growth factors, such as transforming growth factor-β1, platelet-derived growth factor, and insulin-like growth factor. Furin is the activator of membrane-bound type 1 matrix metalloproteinase (MT1-MMP; MMP-14.[22] When the *fur* gene leads to increased expression of furin, it initiates the cascade that activates MMP-2; furin activates MMP-14, and MMP-14 activates MMP-2. Since both MMP-14 and MMP-2 are constitutive MMPs, they are the first responders in the early stages of an ischemic insult.[23] When furin is induced, it leads to a number of important actions.

INTERMITTENT HYPOXIA IS A STRONG STIMULUS FOR HIF

Acute hypoxia transiently prevents the degradation of HIF-1α, limiting the effects of the activation of HIF-responsive genes. When the hypoxic stimulus is intermittent, prolonged activation of HIF occurs, which can lead to persistence of the inflammatory pathways, promoting cardiovascular and cerebrovascular diseases.[24] Patients with obstructive sleep apnea have repeated episodes of reduced oxygen during the night. Sleep-disordered breathing with recurrent apnea (periodic cessation of breathing) results in chronic intermittent hypoxia, which leads to cardiovascular and respiratory pathology. The molecular mechanisms underlying the intermittent hypoxia-evoked cardiorespiratory comorbidities have not been fully delineated, but several lines of evidence implicate the apnea in the vascular damage. In one study, mice with heterozygous deficiency of HIF-1α failed to develop cardiorespiratory responses to chronic intermittent hypoxia. Hypoxia-inducible-1α protein expression and HIF-1α transcriptional activity were induced by intermittent hypoxia in PC12 cells exposed to either aerobic conditions (20% O_2) or 60 cycles of intermittent hypoxia (30 seconds at

1.5% O_2 followed by 5 minutes at 20% O_2). Intermittent hypoxia-induced HIF-1α accumulation is due to increased generation of reactive oxygen species (ROS) by reduced nicotinamide adenine dinucleotide phosphate (NADPH) oxidase. Reactive oxygen species-dependent Ca^{2+} signaling pathways involving phospholipase Cγ (PLCγ) and protein kinase C activation are required for intermittent hypoxia-evoked HIF-1α accumulation.[25]

VASCULAR COGNITIVE IMPAIRMENT

Vascular disease is a major cause of intellectual loss in the elderly, which is projected to increase dramatically in the next 50 years as populations worldwide increase in age. Early studies on cerebral blood flow that were done prior to the introduction of CT and MRI showed that patients with vascular dementia had multiple strokes, and the term *multi-infarct dementia* (MID) was popular.[26] As interest in AD developed, emphasis shifted to the buildup of amyloid plaques and neuronal tangles as a major cause of memory loss from neurodegenerative causes and interest in vascular causes of dementia waned. This situation changed dramatically with the introduction first of CT and later, even more, with availability and routine use of MRI. Patients thought to have a degenerative form of dementia due to the progressive course rather than a series of stroke-like events were found to have extensive white matter damage on MRI highly suggestive of ischemic insults. Emphasis shifted to understanding the role of vascular disease of the small vessels as an important cause of dementia. Another dilemma arose from the finding in suspected vascular disease patients of subtle forms of intellectual loss different from the primary memory loss in AD patients. New terms were proposed to classify these patients. It was realized that both large and small vessel disease could lead to vascular dementia, but that in the early stages of the illness, the type of cognitive impairment more frequently involved the inability to complete sequential tasks or perform executive functions. New ways of testing for cognitive impairment and more refined definitions, utilizing clinical information and biomarkers, were clearly a priority. In 2006 a National Institutes of Health-sponsored consensus conference adopted the term *vascular cognitive impairment* (VCI), which is now used to describe patients with all forms of vascular disease related to intellectual loss.[27,28]

Earlier classification schemes had little difficulty defining multiple infarcts as a cause of dementia. These patients had strokes with intellectual loss associated with the ischemic events and had a characteristic stepwise progression, allowing the diagnosis of MID to be readily made.[29] However, problems were encountered when the illness followed a progressive course and overlapped with other neurodegenerative disorders, such as AD and frontotemporal dementia. Vascular diseases were heterogeneous in clinical phenotypes and pathology, leading to a multiplicity of diseases labeled as VCI, which has impeded research and treatment of this condition (Table 8–2).

As studies accumulated, using MRI to screen large populations and correlating the imaging studies with those of pathological investigators, the importance of small vessel disease became evident. The term *cerebral small vessel disease* refers to a group of pathological processes that affect the small arteries, arterioles, venules, and capillaries of the brain.[30] Common causes of small vessel disease are hypertension, diabetes mellitus, cerebral amyloid angiopathy, and the aging process. The cardinal feature of small vessel disease is changes in the deep white matter, which are ascribed to ischemic injury, but other causes are possible. Because of the need to identify such changes in making the diagnosis of VCI, MRI has taken on a critical role in the evaluation of these patients, but it has also created confusion because of the frequent finding of changes in the white matter in otherwise healthy elderly persons

Table 8–2 **Vascular Cognitive Impairment**

Large vessel disease (multi-infarct dementia)
Emboli from the heart, carotids, and vertebral arteries
Thromboses
Small vessel disease
Lacunar strokes (état lacunar)
Subcortical ischemic vascular disease (Binswanger's disease)

over the age of 65. History, neurological and neuropsychological testing, MRI, and several biomarkers using more elaborate MR testing and cerebrospinal fluid studies have improved the classification.

Small vessel disease results in lacunar infarcts in deep white matter and basal ganglia that can be widespread and result in état lacunar, or a lacunar state, a condition characterized by numerous small infarcts in the basal ganglia associated with memory loss, disorientation, and convulsions, along with cerebellar ataxia, hemiplegia, pure sensory stroke, dysarthria, and clumsy hand syndrome. The lacunar state can cause symptoms of Parkinson's disease.

WHITE MATTER HYPERINTENSITIES ON MRI AND BINSWANGER'S DISEASE

In 1894, Otto Binswanger, who was a student of Alzheimer, reported a novel form of demyelination related to cerebrovascular disease, which he termed *encephalitis subcorticalis chronica progressiva*. Alzheimer named the new disease entity *Binswanger's disease* (BD). In the days prior to CT and MRI, few patients were reported with BD, and all involved pathological studies.[31] With the routine use of CT scanning, it became possible to see the changes in the white matter that appeared as areas of white matter attenuation around the ventricles. Autopsy studies verified that the lesions in the white matter seen on CT were due to vascular demyelination of the type described originally by Binswanger.[32,33] Diagnosis of BD became possible during life by the characteristic changes on the CT scan and the clinical symptoms. Initially, the diagnosis was made from the radiological findings, causing otherwise asymptomatic individuals being told that they had BD. By 1981 this practice was widespread, and this obscure disease was frequently diagnosed. An editorial that year in the medical journal *The Lancet* described this as an "epidemic" of BD and warned against making the diagnosis on the basis of a CT scan.[34] When MRI because available and showed greater white matter changes than CT, the situation was not improved. The first report of BD using MRI described 23 patients; 8 patients presented with vague, nonspecific symptoms and had no neurologic deficits.[35] This indicated the problems in relying on radiological studies to diagnose BD. These problems were confirmed in several studies done shortly after the introduction of MRI in large cohorts of normal elderly individuals, which showed that up to 30% of them had moderate changes in white matter.[36,37] Thus, use of the radiological changes in the white matter on MRI for the diagnosis of BD should be avoided.

Large autopsy series have demonstrated that the most common form of vascular disease causing cognitive impairment is arteriolosclerosis of small vessels[38–40] (Figure 8–7). These changes are usually due to hypertension, diabetes mellitus, hyperlipidemia, and other causes of vascular disease. Chronic hypertension stiffens the walls of the small blood vessels, which become fibrotic. With time, arteriolosclerosis of the vessels impairs blood flow to the watershed areas of the deep white matter. At this stage, the small blood vessels may form a thrombus and produce a lacunar stroke, which may be silent. Alternatively, the fibrotic vessels may initiate a remodeling process that recruits inflammatory cells, such as microglia and macrophages. These cells attempt to repair the damaged vessels but may also secrete toxic proteases and free radicals that damage the blood vessels and the surrounding cells. A number of causes may result in damage to the blood vessels and inflammation.

Small vessel disease is a pathological finding that is diagnosed by a radiological change. This has created controversy as to how best to classify these patients. Using MRI alone is useful for showing lacunas in the basal ganglia, large strokes in the cortical regions, and extensive white matter lesions. Most likely the underlying pathological substrates for each of these changes will have both similarities and differences. For example, a small hypertensive vessel in the basal ganglia can develop a thrombosis and produce a lacunar stroke. This stroke may be isolated to that region. Thrombosis of a similar vessel in the deep white matter may lead to a change in that region referred to as a *silent stroke*, although the pathological basis for the two lesions is the same. Some patients have symmetric lesions in the deep white

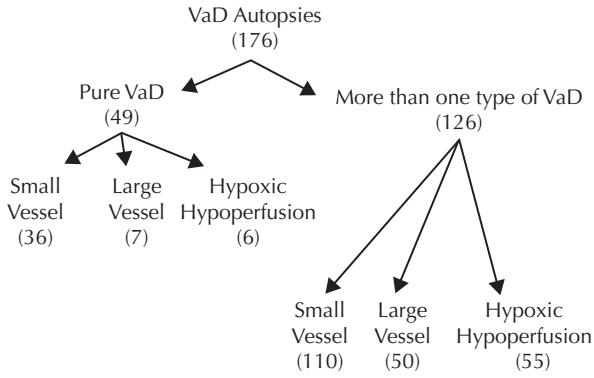

Figure 8–7. Autopsy series of patients with vascular dementia (VaD). Of the 176 autopsied patients, 49 had pure VaD and 126 had more than one type of dementia. Most had small vessel disease regardless of whether they had one or more types of VaD. (From Ref. 39.)

matter, which do not directly follow a vascular pattern but rather suggest hypoxic hypoperfusion involving a watershed region. In addition, patterns of BBB disruption that can be seen in the deep white matter suggest that vasogenic edema may be a cause. Finally, the finding of inflammatory cells around hypertensive or otherwise damaged blood vessels raises the possibility that an inflammatory response is taking place.

Several terms are used to describe the suspected underlying pathology and to suggest a common etiology. The general term used to describe the changes seen in the white matter is *white matter hyperintensities*; this is a nonspecific term, and the etiology may be ischemic, inflammatory, autoimmune, or normal aging. Thus, it is of little diagnostic value. When there are lacunas in the basal ganglia alone, the condition can be described as a *lacunar state*. If there are also extensive changes in the deep white matter without evidence of cortical strokes, these patients are described as having *subcortical ischemic vascular disease* or BD. In the late stages of BD there may be cortical strokes. In an occasional patient there is hydrocephalus, and the diagnosis of normal pressure hydrocephalus is made. To further confound the nomenclature, patients with BD can have pathological changes consistent with AD and the term *mixed dementia* (MD) is used to describe them. In some patients, separating those with BD from those with AD is a challenge. Knowing the mode of onset of the illness and using biomarkers to be described later can be helpful.

Clinical findings are important in making the diagnosis of BD.[41] These patients represent an important subgroup of those with VCI because they have a progressive disease that will be more amenable to clinical trials than the patients with sporadic strokes, in whom the natural history is less predictable.[42] Clinical symptoms of BD include gait disturbance, which is often the earliest finding; subtle mental changes including problems with information processing referred to as *executive dysfunction*; apathy; and depression (Table 8–3). Generally, focal findings suggestive of a small stroke are present, including hyperreflexia and hemiparesis. Hypertension is the major cause of fibrotic changes in the blood vessels. Arterioles that supply the deep white matter are mainly affected. Arteriolosclerosis of these vessels has several adverse consequences: (1) blood flow is limited by the reduced caliber of the blood vessels; (2) loss of resilience of the vessels prevents vasodilatation under hypoxic conditions; (3) the risk of small strokes is increased; and (4) inflammatory cells are activated by the fibrotic vessels. External factors can increase the vulnerability

Table 8–3 **Clinical Features of BD**

Hypertension, diabetes mellitus, hyperlipidemia
Gait disturbance
Cognitive impairment (executive dysfunction)
Apathy, depression, anxiety
Focal neurological findings (hyperreflexia, hemiparesis)
Large white matter hyperintensities

of the deep white matter, which is the primary site of involvement in patients with hypertensive small vessel disease. Lesions in the brain white matter are often found bilaterally and in both periventricular and deep regions of the white matter. They often progress slowly in a symmetrical fashion that eventually involves all of the white matter except the U-fibers at the borders of the cortex; this pattern has been suggested to produce incomplete infarction and silent strokes.[43,44]

Deep white matter is vulnerable to hypoxic injury because of the dual supply from the cortical arteries feeding the white matter from above and the arteries at the base of the brain feeding the subcortical white matter from below. Infarcts due to loss of blood flow affect the regions between the major circulations, resulting in border zone region infarctions (Figure 8–8). Contrast-enhanced x-rays using colloidal barium sulfate provide an excellent way to visualize cerebral arteries. Using this method, De Reuck showed that the periventricular regions of the brain are watershed regions that are vulnerable to reduced blood flow (Figure 8–9). Medullary arteries supply blood to the periventricular regions that comes from the cortical surface, and the middle cerebral artery branches to the caudate as it forms the choroidal arteries of the caudate.[45]

The pathological changes in VCI are similar for large vessel and small vessel strokes in that there are ischemic changes with gliosis and reactive changes in the tissues consistent with infarctions of various ages. When the small vessel form predominates and mainly involves the white matter, several pathological features are unique: deep white matter shows a pattern of extensive gliosis with few oligodendrocytes, demyelination is seen on myelin stains, blood vessels are fibrotic, and around the blood vessels are inflammatory cells (Table 8–4). Macrophages and pericytes in the vicinity of the blood vessels contain stromelysin-1 (MMP-3). Reactive astrocytes, which replace the oligodendrocytes in the white matter, contain MMP-2. Microglial cells are present in the regions of demyelination[46] (Figure 8–10). Because the brain's vasculature has few anastomoses, certain vascular territories are more vulnerable than others to drops in blood pressure. Blood vessels that supply deep structures such as the subcortical and periventricular white matter are derived from the surface of the brain. This makes the periventricular and subcortical white matter particularly sensitive to reductions in cerebral blood flow as well as oxygen levels. Areas between major blood vessels can be damaged by a sudden fall in blood pressure, such as occurs in a cardiac arrest. These watershed regions lead to damage in a pattern between the major vessels.

Damaged blood vessels lead to vasogenic edema, which interferes with delivery of oxygen to the edematous white matter.[47] Disruption of the BBB on MRI occurs in patients with

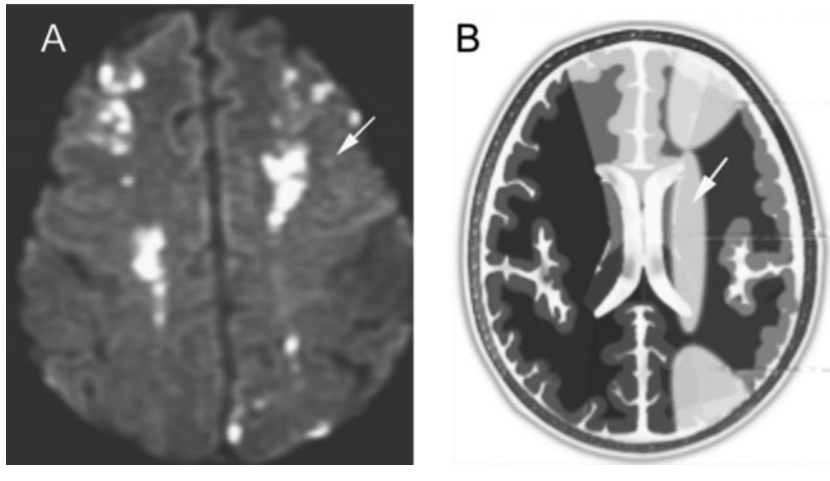

Figure 8–8. (**A**) T2-weighted MRI scan showing white matter lesions due to watershed or border zone infarcts (Arrow). Note the sparing of the anterior and posterior circulations and the involvement of the middle cerebral. (**B**) A drawing of the regions (light gray with arrow) involved in border zone infarctions.

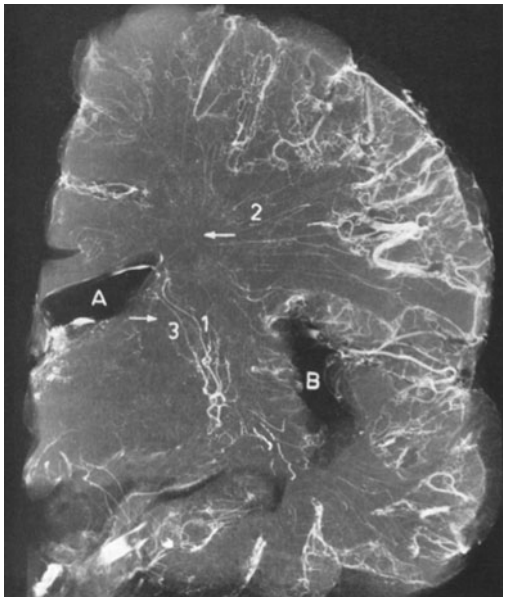

Figure 8–9. Brain injected with x-ray contrast agent to show distribution of arterial supple to the deep white matter. Coronal section through the body of the lateral ventricle. The external branches of the lateral striatal arteries (1) with their ventriculofugal end branches in the white matter at the external angle of the lateral ventricle (2) from the middle and anterior cerebral arteries. Medial branches of the middle striatal arteries (3) with ventriculofugal end branches in the caudate nucleus. Arrows indicate the direction of flow (A and B indicate the ventricles). (From Ref. 71.)

diabetes,[48] lacunar strokes,[49,50] BD,[51] and AD.[52] Quantification of the permeability of the BBB using dynamic contrast-enhanced MRI and the Patlak plot graphical method of analysis has shown extensive disruption of the BBB in VCI patients. The patterns of vessel leakage suggest that it is occurring in the center of the lesions and is less extensive than the white matter changes[53] (Figure 8–11). This pattern differs from the vascular leakage seen with multiple sclerosis lesions, where there is often enhancement around the edge of the lesion.

Measurements of MMPs in the cerebrospinal fluid (CSF) of patients with VCI showed a reduction in the latent form of MMP-2. Blood samples collected along with the CSF were used to determine the amount of the MMPs coming from blood in a fashion similar to that used in multiple sclerosis for measurements of the IgG index. The levels of the MMP-2 index were lower in the VCI than in control CSF obtained during spinal anesthesia. In addition, the levels of active MMP-3 were increased. Comparison of the MMP-2 levels with the albumin index, an independent marker of BBB disruption, shows a significant correlation between the fall in MMP-2 index and the increase in albumin index, indicating an association between the MMPs and the opening of the BBB[54] (Figure 8–12).

One explanation of the changes in the white matter is that a state of partial infarction exists.[43] Incomplete infarcts could occur when there is a drop in blood pressure or a reduction in oxygen. The brain is vulnerable when patients undergo surgery and during periods of low oxygen. Lack of oxygen during periods of sleep apnea is a possible factor. In spite of the common occurrence of white matter changes on MRI in the elderly, the etiology of the progressive changes in BD remains to be determined (Table 8–4). A possible scenario for the development of BD is shown in Figure 8–13. Initiation of an inflammatory reaction is due either to reduced oxygen or to remodeling of the blood vessels by macrophages, with damage to the myelin as a secondary effect.

Animal studies support an inflammatory mechanism for the demyelination. In contrast to multiple sclerosis, the loss of myelin appears to be a nonimmunological process. Animal models of VCI show myelin damage. Bilateral carotid artery occlusion (BCAO) in the rat causes a hypoxic hypoperfusion that is proposed to be a model for VCI.[55] After 3 days of BCAO, vasogenic edema, increased MMP activity, and vascular damage are seen in the white matter.[56] Damage to the white matter can be induced in mice by placing small metal coils around the carotid artery to create carotid artery stenosis. Using the bilateral carotid stenosis model, the

Table 8–4 Possible Etiologies of WMHs in BD

Silent strokes in the deep white matter
Disruption of the BBB with vasogenic edema in the white matter
Inflammation around damaged blood vessels with bystander Demyelination
Hypoxic hypoperfusion due to cardiac arrest, surgery, congestive heart failure, etc.
Intermittent hypoxia secondary to sleep apnea with hypoxia
Amyloid angiopathy

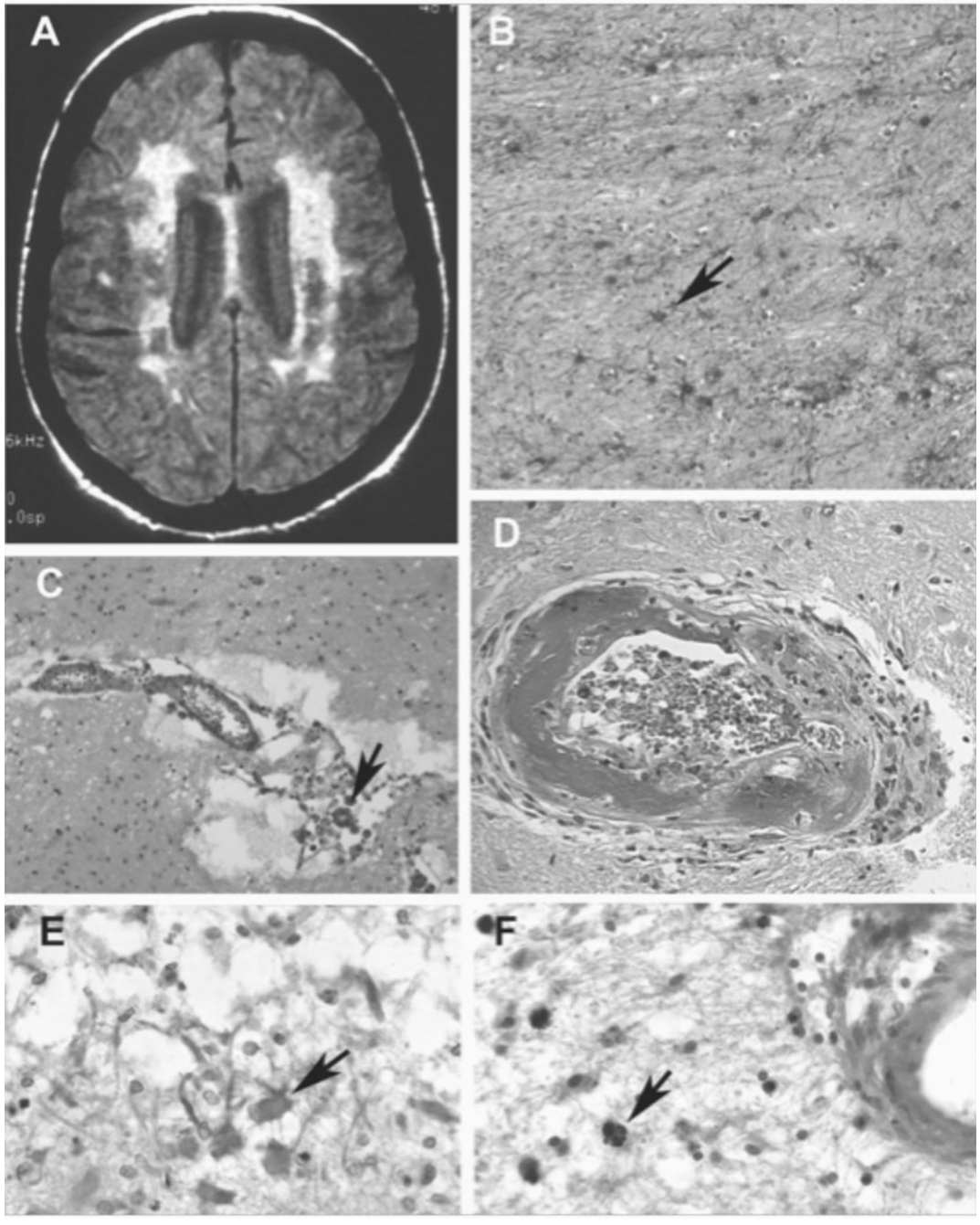

Figure 8–10. An MRI scan and pathological material from a BD patient with the small vessel hypertensive disease. (**A**) An MRI scan demonstrating the extensive white matter lesions seen in the periventricular region. The scan was made with a fluid attenuated inversion recovery scan (FLAIR) that suppresses water in the CSF space (black) and reveals the water in the tissue. (**B**) White matter shows gliosis with loss of myelin and oligodendrocytes. The arrow shows an astrocyte immunostained with glial fibrillary acidic protein, which is a marker for reactive astrocytes. (**C**) A fibrotic blood vessel surrounded by inflammatory macrophages. The arrow indicates a macrophage. (**D**) A blood vessel exposed to long-term hypertension showing damage to the wall and eosinophilic deposits. (**E**) Matrix metalloproteinase-2 in reactive astrocytes (arrow). (**F**) An MMP-3-positive macrophage around a fibrotic blood vessel in a white matter demyelinated region (arrow). (From Ref. 46; See also the color insert.)

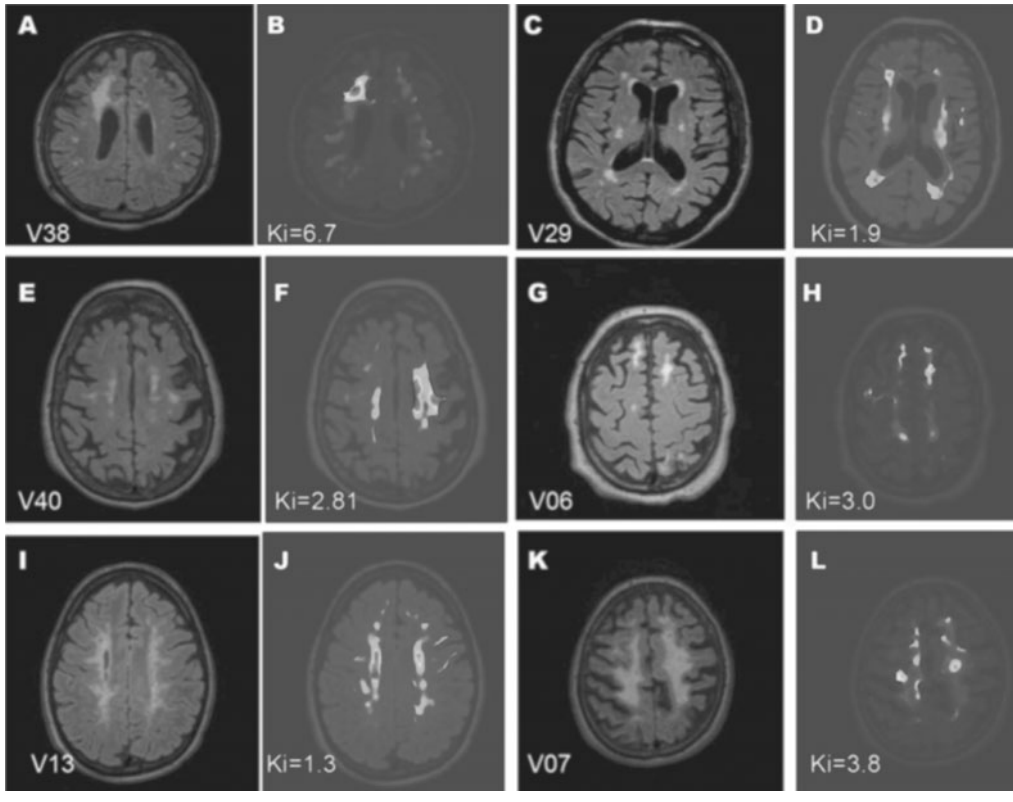

Figure 8–11. Representative FLAIR and permeability images of the brains of six VCI patients with increased permeability. (**A,B**) Permeability and FLAIR maps. The WMHs are in the frontal white matter of the centrum semiovale, without involvement of the cortex. The corresponding permeability map in B has regions of moderately increased permeability (light blue) and high permeability (red). (**C-D, E-F, G-H, I-J, K-L**) Other pairs of FLAIR and related permeability images showing regions of increased permeability. (From Ref. 53; See also the color insert.)

disruption of the BBB in the white matter was shown to be caused by MMP-2 since it was attenuated in the MMP-2 knockout mouse.[57]

AD, VASCULAR DISEASE, AND THE AMYLOID HYPOTHESIS

The importance of the interaction between vascular disease and AD was first observed in a longitudinal study of nuns in one large religious order whose members agreed to undergo neurological and neuropsychological testing and to donate their brains for pathological studies. The investigators found that those with both vascular disease and AD at autopsy had the greatest risk of dementia.[58] Other researchers have observed similar connections.[59] The characteristic findings in AD are plaques formed with amyloid and tangles derived from dying neurons.[60] Deposition of amyloid that has been improperly processed is thought to be a major factor in the pathophysiology of AD.

Amyloid precursor protein (APP), the building block for the amyloid found in the brain, has a transmembrane component and an extracellular component. A group of enzymes called *secretases* are involved in the degradation of the APP molecule. The normal pathway involves cleavage by α-secretase, producing a soluble APP component that can be broken down for clearance. Pathological accumulation of amyloid occurs when a fragment of the full APP molecule, $A\beta_{1-42}$ (Aβ42), is formed. The processing of Aβ42 that leads to fibril formation does not begin with the normal cleavage of APP by α-secretase to form a soluble APP fragment, but instead with β-secretase forming a fragment of APP that can be further processed

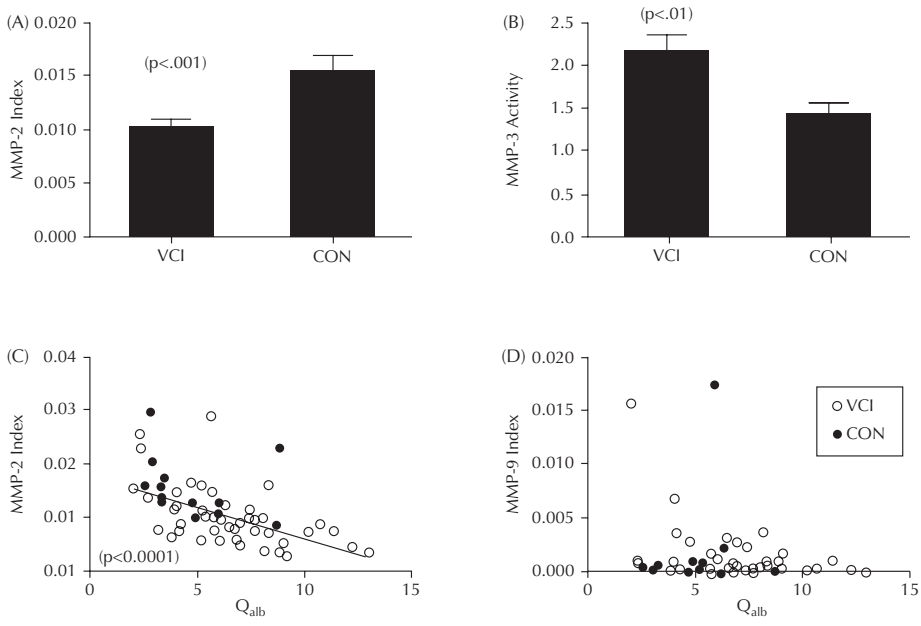

Figure 8–12. Cerebrospinal fluid values for the MMP-2 index and MMP-3 activity. (**A**) The MMP-2 index for VCI patients and controls. The MMP-2 index for the VCI group was significantly lower than that of the controls. (B) The MMP-3 activity is increased compared to controls ($p < .01$). Significance levels are shown in parentheses. (**C**) The MMP-2 index values for all VCI patients (open circles) and controls (black dots) are plotted against the albumin index (Q_{alb}). There is a significant negative correlation ($p < .0001$). (**D**) The MMP-9 index plotted similarly failed to show a correlation. (From Ref. 54.)

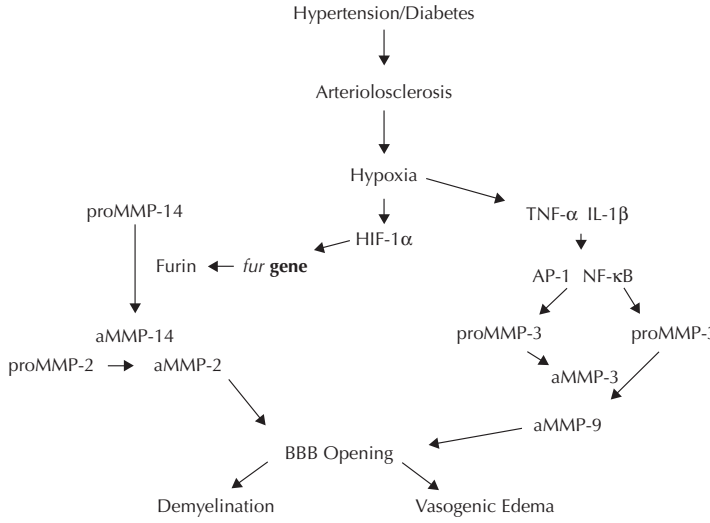

Figure 8–13. A schematic of a possible mechanism for vascular demyelination in the BD type of VCI. Hypertension, diabetes mellitus, and other diseases that damage blood vessels can initiate the process by leading to thrombosis with hypoxia/ischemia or by inducing inflammation. Hypoxia secondary to hypoperfusion may be a cause. There is an increase in HIF-1α, which turns on cassettes of genes involved in both types of injury, such as the *fur* gene and VEGF and TGF-β, which are important in repair. Furin leads to the activation of MMP-2 through MT-MMP. Matrix metalloproteinase-2 can disrupt the tight junction proteins and open the BBB, creating edema, but it also can directly attack myelin. In addition, MMP-2 activates endothelin-1, which acts through calcium metabolism in the small muscles to cause vasoconstriction. The latter effect aggravates the hypoxia. On the repair side, VEGF and angiopoietin-2 (ang2) act through the secretion of MMPs to cause angiogenesis and neurogenesis.The latter effect aggravates the hypoxia. AP-1, activator protein-1; aMMP, active MMP; NF-kB, nuclear factor-kappa B; IL-1 is interleukin-1; BBB is blood-brain barrier; TNF is tumor necrosis factor; BD is Binswanger's disease; VCI is vascular cognitive impairment; HIF is hypoxia inducible factor; VEGF is vascular endothelial growth factor; and TGF is transforming growth factor; MT-MMP is membrane-type metalloproteinase. (From Ref. 73.)

to Aβ42 by γ-secretase. A disintegrin and metalloproteinase 10 (ADAM10; tumor necrosis factor-α converting enzyme [TACE]) is a possible candidate for the α-secretase.[61] The amyloid hypothesis of AD postulates that when Aβ42 builds up in the interstitial fluid due to lack of enzymatic breakdown of the molecule, the insoluble fibrils turn into neuritic plaques.

Amyloid stimulates production of MMPs with the activation of microglia and astrocytes. When astrocytes are exposed to Aβ40 they secrete MMP-2, MMP-3, and MMP-9.[62] An inflammatory response contributes to neuronal death.[63] MMP-3 appears in hippocampal neurons, around amyloid plaques in cortex, and in the interstitium of white matter.[64] Although plasma levels of MMP-9 are increased in AD,[65] there is no elevation of MMPs in the CSF in AD.[66] Cleavage of the Aβ42 by proteases, possibly MMPs, results in a form that is more readily cleared from the brain (Figure 8–14).

A transgenic mouse with a gene from a familial form of AD, namely, the APP/presenilin gene, was found to have increased MMP-2 and MMP-9 in astrocytes around amyloid plaques.[67] *Mmp-2* and *mmp-9* knockout mice had higher levels of Aβ, and treatment with the MMP inhibitor, GM6001, increased Aβ in a transgenic mouse overexpressing the Swedish variant of the APP gene (*APPsw*). In a subsequent study, the same investigators showed that MMP-9 is able to degrade the fibrillary form of Aβ.[68] These studies suggest that MMP-9 can contribute to the ongoing clearance of soluble and fibrillary Aβ.

Zlokovic and colleagues have advocated for a role of vascular disease in AD based on studies showing diminished cerebrovascular function,

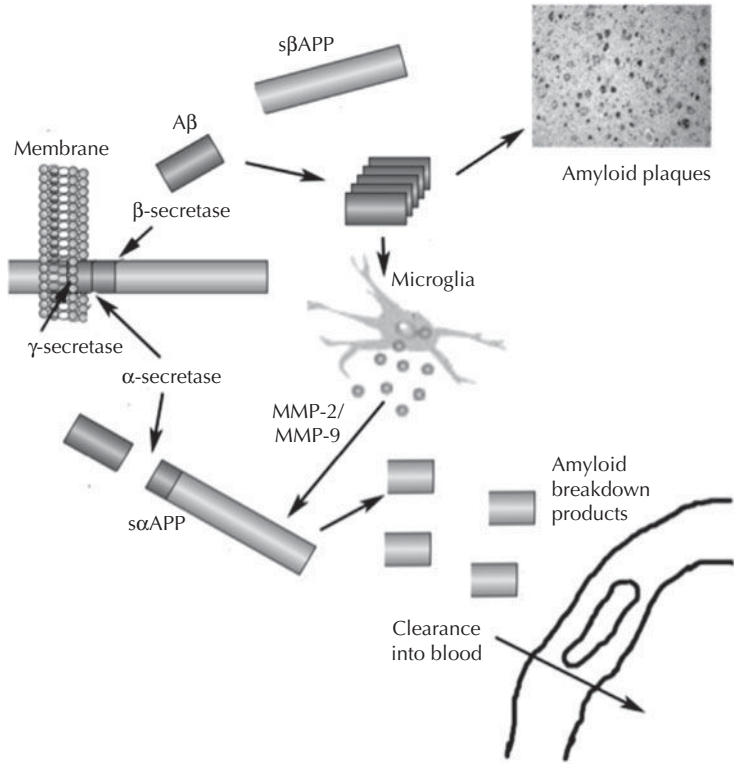

Figure 8–14. The MMPs and ADAMs are involved in the processing of amyloid precursor protein (APP). When β-secretase cleaves the APP molecule close to the membrane, a soluble fragment of APP is produced, sαAPP, which can be further metabolized by MMPs and cleared from the brain. However, if β-secretase initiates the cleavage and γ-secretase participates, then the Aβ molecule is formed. The most prevalent form of Aβ is Aβ(1–40); a smaller amount of Aβ(1–42) is formed, but this form can clump into fibrils that accumulate in amyloid plaques. The MMPs aid in the removal of amyloid from the brain across the BBB to enter the blood. Microglia are activated by amyloid, Aβ, and are the likely source of the MMP-9. sβAPP, soluble amyloid precursor protein. (From Ref. 46.)

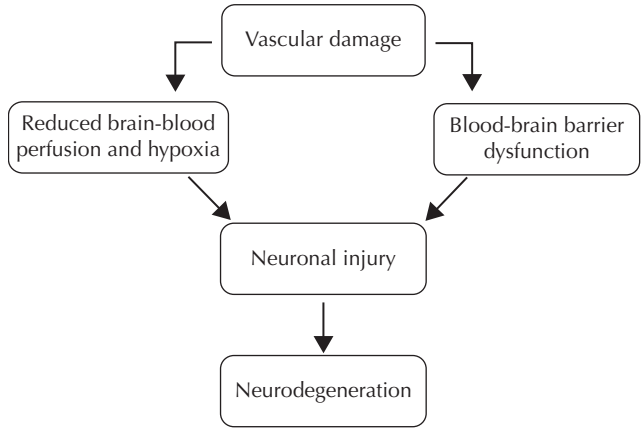

Figure 8–15. Vascular damage can result in reduced blood perfusion of the brain and hypoxia from one end and BBB dysfunction from the other. The BBB breakdown might facilitate the accumulation in the brain of potentially toxic serum proteins. Both reduced blood perfusion of the brain and BBB disruption might contribute to secondary neuronal injury and the development of neurodegenerative changes. (From Ref. 69.)

including reduced blood flow, breakdown of the BBB, or both, which has been associated with or shown to precede neurodegenerative disease.[69] Growing evidence from epidemiological, neuroimaging, pathological, and experimental studies suggest that reductions in brain microcirculation and blood flow might precede cognitive decline. When blood vessels are damaged and there is reduced blood perfusion of the brain, along with brain hypoxia and/or BBB dysfunction, these changes may lead to neurodegenerative changes rather than vice versa. This would cause an accumulation of Aβ through its faulty clearance.[70] If Aβ begins to accumulate in the brain, it can amplify the neurovascular dysfunction through the development of amyloid angiopathy, increasing blood flow dysfunction and vascular-mediated neuronal injury and neurodegeneration (Figure 8–15).

REFERENCES

1. Hinchey J, Chaves C, Appignani B, et al. A reversible posterior leukoencephalopathy syndrome [see comments]. *N Eng J Med*. 1996;334:494–500.
2. Rossen R, Kabat H, Anderson JP. Acute arrest of cerebral circulation in man. *Arch Neurol Psychiatry*. 1943; 50:510–528.
3. Longstreth WT Jr, Inui TS, Cobb LA, et al. Neurologic recovery after out-of-hospital cardiac arrest. *Ann Intern Med*. 1983;98:588–592.
4. Levy DE, Bates D, Caronna JJ, et al. Prognosis in nontraumatic coma. *Ann Intern Med*. 1981;94: 293–301.
5. Rosenberg GA, Johnson SF, Brenner RP. Recovery of cognition after prolonged vegetative state. *Ann Neurol*. 1977;2:167–169.
6. Levy DE, Sidtis JJ, Rottenberg DA, et al. Differences in cerebral blood flow and glucose utilization in vegetative versus locked-in patients. *Ann Neurol*. 1987;22:673–682.
7. Jennett B, Plum F. Persistent vegetative state after brain damage: a syndrome in search of a name. *Lancet*. 1972;1:734–737.
8. Schiff ND, Rodriguez-Moreno D, Kamal A, et al. FMRI reveals large-scale network activation in minimally conscious patients. *Neurology*. 2005;64:514–523.
9. Fins JJ, Schiff ND, Foley KM. Late recovery from the minimally conscious state: ethical and policy implications. *Neurology*. 2007;68:304–307.
10. Sotaniemi KA. Brain damage and neurological outcome after open-heart surgery. *J Neurol Neurosurg Psychiatry*. 1980;43:127–135.
11. Tufo HM, Ostfeld AM, Shekelle R. Central nervous system dysfunction following open-heart surgery. *JAMA*. 1970;212:1333–1340.
12. Furlan AJ, Breuer AC. Central nervous system complications of open heart surgery. *Stroke*. 1984;15: 912–915.
13. Nevin M, Adams S, Colchester ACF, et al. Evidence for involvement of hypocapnia and hypoperfusion in aetiology of neurological deficit after cardiopulmonary bypass. *Lancet*. 1987;2:1493–1495.
14. McKhann GM, Selnes OA, Grega MA, et al. Subjective memory symptoms in surgical and nonsurgical coronary artery patients: 6-year follow-up. *Ann Thorac Surg*. 2009;87:27–34.
15. Selnes OA, Grega MA, Bailey MM, et al. Cognition 6 years after surgical or medical therapy for coronary artery disease. *Ann Neurol*. 2008;63:581–590.
16. Protass LM. Delayed postanoxic encephalopathy after heroin use. *Ann Intern Med*. 1971;74:738–739.
17. Semenza GL. Vascular responses to hypoxia and ischemia. *Arterioscler Thromb Vasc Biol*. 2010;30: 648–652.

18. Salceda S, Caro J. Hypoxia-inducible factor 1alpha (hif-1alpha) protein is rapidly degraded by the ubiquitin-proteasome system under normoxic conditions. Its stabilization by hypoxia depends on redox-induced changes. *J Biol Chem*. 1997;272: 22642–22647.
19. Semenza GL. Hydroxylation of hif-1: oxygen sensing at the molecular level. *Physiology* (*Bethesda*). 2004;19: 176–182.
20. Guillemin K, Krasnow MA. The hypoxic response: huffing and hifing. *Cell*. 1997;89:9–12
21. Halterman MW, Miller CC, Federoff HJ. Hypoxia-inducible factor-1alpha mediates hypoxia-induced delayed neuronal death that involves p53. *J Neurosci*. 1999;19:6818–6824.
22. Yana I, Weiss SJ. Regulation of membrane type-1 matrix metalloproteinase activation by proprotein convertases. *Mol Biol Cell*. 2000;11:2387–2401.
23. Heo JH, Lucero J, Abumiya T, et al. Matrix metalloproteinases increase very early during experimental focal cerebral ischemia. *J Cereb Blood Flow Metab*. 1999;19:624–633.
24. Garvey JF, Taylor CT, McNicholas WT. Cardiovascular disease in obstructive sleep apnoea syndrome: the role of intermittent hypoxia and inflammation. *Eur Respir J*. 2009;33:1195–1205.
25. Yuan G, Nanduri J, Khan S, et al. Induction of hif-1-alpha expression by intermittent hypoxia: involvement of nadph oxidase, ca^{2+} signaling, prolyl hydroxylases, and mtor. *J Cell Physiol*. 2008;217:674–685.
26. Hachinski VC, Lassen NA, Marshall J. Multi-infarct dementia. A cause of mental deterioration in the elderly. *Lancet*. 1974;2:207–210.
27. Hachinski V, Iadecola C, Petersen RC, et al. National Institute of Neurological Disorders and Stroke–Canadian Stroke Network Vascular Cognitive Impairment Harmonization Standards. *Stroke*. 2006;37:2220–2241
28. Bowler JV. Modern concept of vascular cognitive impairment. *Br Med Bull*. 2007;83:291–305.
29. Chui HC, Victoroff JI, Margolin D, et al. Criteria for the diagnosis of ischemic vascular dementia proposed by the State of California Alzheimer's Disease Diagnostic and Treatment Centers. *Neurology*. 1992;42:473–480.
30. Pantoni L. Cerebral small vessel disease: from pathogenesis and clinical characteristics to therapeutic challenges. *Lancet Neurol*. 2010;9:689–701.
31. Olszewski J. Subcortical arteriosclerotic encephalopathy: review of the literature on the so-called Binswanger's disease and presentation of 2 cases. *World Neurol*. 1962;3:359–375.
32. Rosenberg GA, Kornfeld M, Stovring J, et al. Subcortical arteriosclerotic encephalopathy (Binswanger): computerized tomography. *Neurology*. 1979;29:1102–1106.
33. Goto K, Ishii N, Fukasawa H. Diffuse white-matter disease in the geriatric population. A clinical, neuropathological, and ct study. *Radiology*. 1981;141:687–695.
34. Binswanger's encephalopathy. *Lancet*. 1981;1:923.
35. Kinkel WR, Jacobs L, Polachini I, et al. Subcortical arteriosclerotic encephalopathy (Binswanger's disease). Computed tomographic, nuclear magnetic resonance, and clinical correlations. *Arch Neurol*. 1985;42: 951–959.
36. Awad IA, Spetzler RF, Hodak JA, et al. Incidental subcortical lesions identified on magnetic resonance imaging in the elderly. I. Correlation with age and cerebrovascular risk factors. *Stroke*. 1986;17:1084–1089.
37. Hunt AL, Orrison WW, Yeo RA, et al. Clinical significance of mri white matter lesions in the elderly. *Neurology*. 1989;39:1470–1474.
38. Esiri MM, Wilcock GK, Morris JH. Neuropathological assessment of the lesions of significance in vascular dementia. *J Neurol Neurosurg Psychiatry*. 1997;63: 749–753.
39. Andin U, Gustafson L, Brun A, et al. Clinical manifestations in neuropathologically defined subgroups of vascular dementia. *Int J Geriatr Psychiatry*. 2006;21: 688–697.
40. Gold G, Giannakopoulos P, Herrmann FR, et al. Identification of Alzheimer and vascular lesion thresholds for mixed dementia. *Brain*. 2007;130:2830–2836.
41. Caplan LR. Binswanger's disease—revisited [review]. *Neurology*. 1995;45:626–633.
42. Erkinjuntti T, Inzitari D, Pantoni L, et al. Research criteria for subcortical vascular dementia in clinical trials [in process citation]. *J Neural Transm Suppl*. 2000;59:23–30.
43. Brun A, Englund E. A white matter disorder in dementia of the Alzheimer type: a pathoanatomical study. *Ann Neurol*. 1986;19:253–262.
44. Vermeer SE, Hollander M, Van Dijk EJ, et al. Silent brain infarcts and white matter lesions increase stroke risk in the general population: the Rotterdam Scan Study. *Stroke*. 2003;34:1126–1129.
45. De Reuck J. The human periventricular arterial blood supply and the anatomy of cerebral infarctions. *Eur Neurol*. 1971;5:321–334.
46. Rosenberg GA. Matrix metalloproteinases and their multiple roles in neurodegenerative diseases. *Lancet Neurol*. 2009;8:205–216.
47. Feigin I, Popoff N. Neuropathological changes late in cerebral edema: the relationship to trauma, hypertensive disease and Binswanger's encephalopathy. *J Neuropathol Exp Neurol*. 1963;22:500–511.
48. Starr JM, Wardlaw J, Ferguson K, et al. Increased blood-brain barrier permeability in type II diabetes demonstrated by gadolinium magnetic resonance imaging. *J Neurol Neurosurg Psychiatry*. 2003;74:70–76.
49. Wardlaw JM, Doubal F, Armitage P, et al. Lacunar stroke is associated with diffuse blood-brain barrier dysfunction. *Ann Neurol*. 2009;65:194–202.
50. Topakian R, Barrick TR, Howe FA, et al. Blood-brain barrier permeability is increased in normal-appearing white matter in patients with lacunar stroke and leucoaraiosis. *J Neurol Neurosurg Psychiatry*. 2010;81:192–197.
51. Hanyu H, Asano T, Tanaka Y, et al. Increased blood-brain barrier permeability in white matter lesions of Binswanger's disease evaluated by contrast-enhanced mri. *Dement Geriatr Cogn Disord*. 2002;14:1–6.
52. Starr JM, Farrall AJ, Armitage P, et al. Blood-brain barrier permeability in Alzheimer's disease: a case-control mri study. *Psychiatry Res*. 2009;171:232–241.
53. Taheri S, Gasparovic C, Shah NJ, et al. Quantitative measurement of blood-brain barrier permeability in human using dynamic contrast-enhanced mri with fast t(1) mapping. *Magn Reson Med*. 2011;65:1036–1042.
54. Candelario-Jalil E, Thompson J, Taheri S, Grossetete M, Adair J, Edmonds E, Prestopnik J, Wills J, Rosenberg G. Matrix metalloproteinases are associated with increased blood-brain barrier

opening in vascular cognitive impairment. *Stroke*. 2011;42:1345–1350.
55. Tomimoto H, Ihara M, Wakita H, et al. Chronic cerebral hypoperfusion induces white matter lesions and loss of oligodendroglia with DNA fragmentation in the rat. *Acta Neuropathol* (*Berl*). 2003;106: 527–534.
56. Sood R, Yang Y, Taheri S, et al. Increased apparent diffusion coefficients on mri linked with matrix metalloproteinases and edema in white matter after bilateral carotid artery occlusion in rats. *J Cereb Blood Flow Metab*. 2009;29:308–316.
57. Nakaji K, Ihara M, Takahashi C, et al. Matrix metalloproteinase-2 plays a critical role in the pathogenesis of white matter lesions after chronic cerebral hypoperfusion in rodents. *Stroke*. 2006;37:2816–2823.
58. Snowdon DA, Greiner LH, Mortimer JA, et al. Brain infarction and the clinical expression of Alzheimer disease. The Nun Study [see comments]. *JAMA*. 1997;277:813–817.
59. Esiri MM, Nagy Z, Smith MZ, et al. Cerebrovascular disease and threshold for dementia in the early stages of Alzheimer's disease [letter]. *Lancet*. 1999;354: 919–920.
60. LaFerla FM, Green KN, Oddo S. Intracellular amyloid-beta in Alzheimer's disease. *Nat Rev Neurosci*. 2007;8:499–509.
61. Buxbaum JD, Liu KN, Luo Y, et al. Evidence that tumor necrosis factor alpha converting enzyme is involved in regulated alpha-secretase cleavage of the Alzheimer amyloid protein precursor. *J Biol Chem*. 1998;273:27765–27767.
62. Deb S, Gottschall PE. Increased production of matrix metalloproteinases in enriched astrocyte and mixed hippocampal cultures treated with beta-amyloid peptides. *J Neurochem*. 1996;66:1641–1647.
63. Selkoe DJ. Biochemistry and molecular biology of amyloid beta-protein and the mechanism of Alzheimer's disease. *Handb Clin Neurol*. 2008;89:245–260.
64. Yoshiyama Y, Asahina M, Hattori T. Selective distribution of matrix metalloproteinase-3 (mmp-3) in Alzheimer's disease brain. *Acta Neuropathol* (*Berl*). 2000;99:91–95.
65. Lorenzl S, Albers DS, Relkin N, et al. Increased plasma levels of matrix metalloproteinase-9 in patients with Alzheimer's disease. *Neurochem Int*. 2003;43:191–196.
66. Adair JC, Charlie J, Dencoff JE, et al. Measurement of gelatinase b (mmp-9) in the cerebrospinal fluid of patients with vascular dementia and Alzheimer disease. *Stroke*. 2004;35:e159-e162.
67. Yin KJ, Cirrito JR, Yan P, et al. Matrix metalloproteinases expressed by astrocytes mediate extracellular amyloid-beta peptide catabolism. *J Neurosci*. 2006;26:10939–10948.
68. Yan P, Hu X, Song H, et al. Matrix metalloproteinase-9 degrades amyloid-beta fibrils in vitro and compact plaques in situ. *J Biol Chem*. 2006;281:24566–24574.
69. Zlokovic BV. Neurodegeneration and the neurovascular unit. *Nat Med*. 2010;16:1370–1371.
70. Deane R, Wu Z, Sagare A, et al. Lrp/amyloid beta-peptide interaction mediates differential brain efflux of abeta isoforms. *Neuron*. 2004;43:333–344.
71. De Reuck J, Crevits L, De Coster W, et al. Pathogenesis of Binswanger chronic progressive subcortical encephalopathy. *Neurology*. 1980;30:920–928.
72. Rosenberg GA, Sullivan N, Esiri MM. White matter damage is associated with matrix metalloproteinases in vascular dementia. *Stroke*. 2001;32:1162–1168.
73. Rivera S, Khrestchatisky M, Kaczmarek L, et al. Metzincin proteases and their inhibitors: foes or friends in nervous system physiology? *J Neurosci*. 2010;30:15337–15357.

Chapter 9

Effects of Altitude on the Brain

INTRODUCTION

The concentration of ambient oxygen is maintained at 21%, but the amount of oxygen in the air that is breathed depends on the altitude. As the altitude increases and the atmospheric pressure is reduced, the amount of oxygen is also reduced, reaching dangerously low levels on the highest mountains in the world. Hypobaric hypoxia initiates a series of reactions to compensate for the reduced oxygen content of the air. Acute reductions in oxygen cause a constellation of cerebral symptoms that includes initially headache, ataxia, and short-term memory impairment, and can progress to cerebral edema with papilledema, coma, and death. Acute mountain sickness (AMS) is the first stage of this sequence of events. Most patients with severe cerebral symptoms have high-altitude pulmonary edema (HAPE). The life-threatening high-altitude cerebral edema (HACE) is seen with rapid ascent to over 6000 m. Air travel has increased the number of individuals exposed to hypobaric hypoxia at the summits of mountains such as Mount Everest (8848 m) and Kilmanjaro (5895 m). Exposure to high altitudes after coming from sea level leads to a high incidence of AMS, with smaller but significant numbers of people developing HAPE and HACE.

GENETIC TOLERANCE TO ALTITUDE

Remarkable compensatory mechanisms occur in individuals exposed for long periods of time to low-oxygen environments. Humans are able to live at extreme altitudes by acclimating to the lack of oxygen. Genetic differences have been found that contribute to the acclimatization. Around 5000 to 7000 years ago, Han Chinese living at sea level diverged from Tibetans living on the high plateau of the Himalayas above 4300 m, providing a unique situation in which to attempt to identify the genetic differences between the two populations. Tibetans, who live at very high altitudes, have a distinctive suite of physiological traits that enable them to tolerate environmental hypoxia, which they acquired thousands of years ago when they separated from the Han Chinese living at lower altitudes. Genome-wide scans from the two populations reveal positive selection in several regions that contain genes whose products

are likely involved in high-altitude adaptation. One of the molecules identified as important in adaptation to living at high altitude is Egl nine homolog 1 (EGLN1), which is also known as prolyl hydroxylase domain-containing protein 2 (PHD2) or hypoxia-inducible factor prolyl hydroxylase 2 (HIF-PH2), and is an enzyme that in humans is encoded by the *EGLN1* gene. Positively selected haplotypes of (EGLN1) and peroxisome-proliferator-activated (PPARA) were significantly associated with the decreased hemoglobin phenotype that is unique to this highland population. In spite of the extremes of altitude, Tibetans tolerate hypoxic conditions that would otherwise cause illness. They have acquired a number of mechanisms for adaptation. Investigators identified EGLN1 and endothelial PAS domain-containing protein 1 (EPAS1), which are both in the hypoxia-inducible factor (HIF) pathway. Three additional loci, EDNRA (endothelin receptor type A), PTEN (phosphatase and tensin homolog), and PPARA, that are also associated with HIF activity were found. Paradoxically, the increased activity in the HIF pathway leads to a reduction in hemoglobin levels. The investigators proposed that this prevented polycythemia and conferred a protective effect.[1]

EGLN1 is a mammalian HIF prolyl hydroxylase involved in the ubiquitination and removal of HIF. Ubiquitination is a posttranslational modification carried out by a set of three enzymes: E1, E2, and E3. When EGLN1 is blocked by a peptide, the HIF molecule is stabilized. Treatment of cells with one such compound, FG-0041, led to the accumulation of transcriptionally active HIF.[2] Stabilization of HIF through inhibition of the HIF prolyl hydroxylase might be therapeutically beneficial in diseases characterized by acute or chronic ischemia because prolonged stabilization of HIF might lead to increased angiogenesis through the elaboration of HIF target genes such as vascular endothelial growth factor (VEGF) and platelet-derived growth factor subunit B (PDGF B). While this is theoretically interesting, the prolonged activity of HIF as a therapy remains speculative.

Humans living at 5000 m are breathing half of the oxygen available at sea level. Chronic exposure to low-oxygen conditions causes compensatory changes that include hyperventilation, tachycardia, erythropoietin-induced polycythemia, and increased cerebral blood flow (CBF).[3] Hypoxia can be induced in animals by the substitution of nitrogen for oxygen. Reducing the oxygen content of the inspired air from 30% to 10% lowers arterial oxygen from 90 to 30 mmHg. The neurological consequences of increasing altitude are shown in Table 9–1. The effects of the different altitudes are shown for several ranges: high (1500–3500 m), very high (3500–5500 m), and extreme (>5500 m). The partial pressure of oxygen (pO_2), and the neurological consequences of exposure to these pressure changes, are shown in the table. These neurological consequences vary greatly from person to person and with the rate of ascent. Barometric pressure falls from 760 mm Hg at sea level with an inspired pO_2 of 149 mm

Table 9–1 **Relationship of Altitude, pO2, and Symptoms**

Altitude, m	pO_2 (FIO_2)	Symptoms
0–1000	95 (21)	None
1000–2000	70 (15)	Commercial aircraft at this altitude
2000–3000	60 (14)	Complex reaction time slows AMS and HACE possible
3000–5000	35 (9)	Learning and special memory impaired
5000–7000	30 (7)	Memory retrieval impaired MRI changes, including white matter hyperintensities
>7000		MRI shows brain atrophy Hallucinations Loss of consciousness possible

Source: Modified from Ref. 3.

Hg to 253 mm Hg at the top of Mount Everest at 8848 m with an inspired pO_2 of 43 mm Hg, or 29% of the value at sea level.[4]

AMS AND HIGH-ALTITUDE PULMONARY EDEMA

Acute mountain sickness is common when a person living at sea level travels to a mountainous region. Minimal symptoms may occur while visiting a location at a moderately high elevation, such as Denver or Albuquerque, which are both about 1 mile (1600 m) high. While these cities are at moderate altitudes, the nearby mountains reach heights of over 3000 m (Figure 9–1). Headache, shortness of breath, and fatigue may occur in the first day or two of the visit, but generally they are only briefly present. Venturing to higher elevations, such as driving to the top of a nearby mountain, which can range from 3000 to 4000 m, can lead to more severe and prolonged symptoms. Above 3000 m sleep patterns may be disturbed, fatigue more pronounced, and headache prolonged. Tourists to several high-altitude cities in Latin America, such as Cusco, Peru, which is 3395 m above sea level and Quito, Equador, at 2850 m, may require supplemental oxygen to overcome the headache, ataxia, and fatigue that can last for several days. Sleeping at these high altitudes can lead to sleep disturbances. However, even at these altitudes, acclimatization occurs spontaneously over several days.

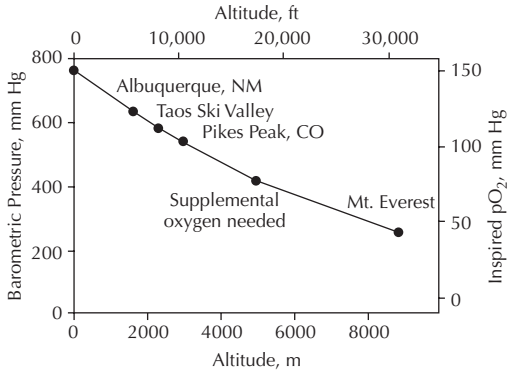

Figure 9–1. Effect of increasing altitude on barometric pressure and inspired pO_2. At sea level, the pressure is 760 mm Hg and the inspired oxygen level is normal. At Mount Everest the inspired oxygen level is less than 50 mm Hg, below the point at which supplemental oxygen is needed.

More serious symptoms can occur in susceptible individuals. High-altitude pulmonary edema, which may be a harbinger of HACE, generally is seen only above 3500 m. There is difficulty breathing, which is made worse by physical exertion. Pulmonary edema increases the intracranial pressure by interfering with venous drainage of blood from the brain. This increased intracranial pressure may contribute to the development of HACE.

HIGH-ALTITUDE CEREBRAL EDEMA

Airplane travel has made access to mountains possible, and a growing number of individuals are trekking at extreme altitudes in the mountains above 6500 m in the Himalayas of Southeast Asia and the Andes of Latin America. Many of the peaks in the Himalayas are over 7000 m, which is higher than Aconcagua (6962 m) in the Andean mountain range of Argentina, the highest peak in the Western Hemisphere. Preparation for these trips requires understanding the symptoms and treatment of AMS, HAPE, and HACE. Trekking in the Himalayas often begins from Pheriche at an altitude of 4243 m (Figure 9–2). Mountainous regions in the western United States, such as Pikes Peak (4300 m) in Colorado, are only 70 miles from Denver. The ability to go from sea level in a day to the top of Pikes Peak by car or train increases the risk of AMS. Although only 31st in height in Colorado, it is the most visited mountain in North America and the second most visited in the world after Japan's Mount Fuji.

In individuals with HACE, the condition is usually preceded by either AMS and/or HAPE. It is estimated to occur in 0.5% to 1.0% of trekkers above 4500 m.[3] An early report described 34 Indian soldiers who developed HACE after being taken rapidly up to 5867 m from sea level; they had elevated cerebrospinal fluid (CSF) pressure, papilledema, ataxia, and other signs of HACE.[5] The syndrome is characterized by confusion, psychiatric changes, ataxia of gait, and loss of consciousness.

Two major factors are thought to be involved in AMS and HACE.[3,4] One factor is the effect of hypoxia on blood vessels. The increased

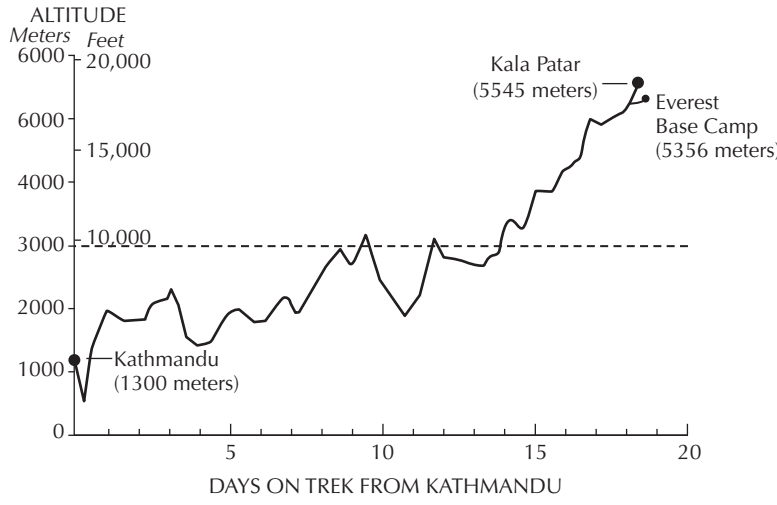

Figure 9–2. Changes in elevation experienced by trekkers in the Himalayas. Depending on the time available, the trek may begin at Kathmandu or Pheriche. The base camp for the ascent of Mount Everest is at 5356 m. (Adapted from ref. 23).

CBF leads to an increase in intravascular pressure causing vasogenic edema with vessel wall damage. The second factor is the disruption of the Na^+/K^+ adenosine triphosphatase (ATPase) pump due to the hypoxic conditions, which leads to cytotoxic edema. Both the vasogenic and cytotoxic edema raise the intracranial pressure and impede venous outflow, adding another possible factor.

As the oxygen content of the air is reduced, there is a compensatory hyperventilation. The partial pressures of oxygen and carbon dioxide are lowered. Since hypoxia causes vasodilatation and hypocapnic vasconstriction, the combined effects initially balance each other and there are no dramatic changes. However, as the level of oxygen falls and exertion becomes extreme, dangerous levels of hypocapnia develop. The vasoconstriction results in a reduction of blood flow to the brain. In an experiment conducted at a research camp on Mount Everest, it was discovered that breathing into a bag to increase the concenetration of CO_2 to 3% to 5% relieved high-altitude symptoms. This increased the feeling of well-being and improved brain oxygenation.[6]

An important consequence of the acute reduction in pCO_2 is a respiratory alkalosis. As the pH of the blood and CSF increases, a compensatory loss of bicarbonate from the CSF returns the brain pH to normal. This increase in brain and blood pH with the accompanying alkalosis, in turn, inhibits the hyperventilatory response. However, this compensatory mechanism is overcome by the exertional hyperventilation of exercise at extreme altitudes. Hyperventilatilation maintains the pO_2 at 35 mm Hg, which is called the *defense zone* since it is the lowest the oxygen level. In this situation, pCO_2 can drop below 10 mm Hg with vasocontriction reducing CBF.

In addition to the disruption of the blood vessels that occurs under the hypoxic condition, cell swelling, or cytotoxic edema, results from failure of the Na^+/K^+ ATPase pumps that maintain cell integrity. The profound effects of reduced CBF and hypoxia release chemical mediators implicated in the neuroinflammatory response. Free radical formation directly damages vessel basement membranes, amplifying both vasogenic and cytotoxic edema. An important consequence is the failure to remove HIF-1α, resulting in the upregulation of VEGF and erythropoietin, which are produced in an effort to improve blood flow but also contribute to basement membrane damage and vasogenic edema.

Local hyperkalemia triggers calcium-mediated nitric oxide release, which acts on vessel smooth muscle to cause vasodilatation. Adenosine, which is released from neurons, contributes to vasodilatation. Finally, the vasodilatation may activate the trigeminovascular system, causing headache.[7]

COGNITIVE CONSEQUENCES OF HYPOBARIC HYPOXIA

While even brief loss of oxygen can result in cell death of the vulnerable large neurons in the hippocampus, Purkinje cells in the cerebellum, and certain layers of the cortex, less dramatic consequences of reduced oxygen over longer periods of time can be damaging to brain cells. The lack of oxygen content at extreme altitudes that can be reached by experienced mountain climbers can permanently damage brain cells unless supplemental oxygen is used. Even with additional oxygen, there is a danger of milder forms of brain injury than those seen with the full syndrome of HACE.

Mild reductions in oxygen level are reported to impair the ability to learn a complex task.[8] At 5000 m, where the alveolar oxygen falls to around 40 mm Hg, short-term memory can be affected.[9] West and colleagues performed experiments on mountain climbers on Mount Everest.[10] As the level of oxygen in the inspired air falls, compensatory hyperventilation ensues. The pCO_2 falls as low as 10 mm Hg, which causes alkalosis and vasoconstriction. One mechanism to compensate for the effects of the combination of cold and low oxygen is a shift in the oxygen dissociation curve to the left, allowing a greater oxygen-carrying capacity. Normally, at an atmospheric pressure of 760 mm Hg and 20% oxygen, alverolar gas has a pO_2 of about 100 mm Hg and a similar arterial blood gas level. At high altitude, the barometric pressure is lower and the inspired oxygen is reduced. Mountain climbers on Mount Everest had an alveolar pO_2 of 35 mm Hg at 7000 m and a remarkable pCO_2 of 7.5 mm Hg with an arterial pH of 7.7.[10] Under these conditions, psychometric tests showed impairment of learning, memory, and expression of verbal material.[11] Impairments in finger-tapping speed persisted in climbers tested 12 months later. Persistent impairment in memory has been reported in mountain climbers who have climbed to extreme altitudes; five of eight men who reached 8000 m without supplemental oxygen showed subtle defects in concentration, short-term memory, and ability to shift concepts.[12] These changes lasted for months, with loss of cognitive skills tested with the Stroop color chart and the card-sorting tests. Another factor that may impact the performance on cognitive tests is an anxiety disorder that is common among trekkers to high altitudes.[13]

IMAGING OF THE BRAIN AT HIGH ALTITUDE

An important advance in the study of high-altitude pathology is the use of magnetic resonance imaging (MRI) to document subtle changes in brain volume and brain edema. The imaging studies are performed in simulated hypoxic environments or in regions where there is an MRI facility in reasonable proximity to the mountains, such as Denver, which is close to Pikes Peak.

Simulation of an ascent to 4572 m was performed in nine volunteers who were exposed to hypobaric hypoxia for 32 hours in an attempt to simulate the conditions that cause AMS. The investigators calculated brain volumes from three-dimensional MRI data sets and T2 decay rates in the white matter. They demonstrated significant brain swelling after 32-hour hypobaric hypoxia exposure, with a volume increase of 5.8% (71.3 mL) for gray matter but no significant effect on white matter. The reversible brain volume changes were similar to those in patients with diffuse brain edema or increased cerebral blood volume.[14]

Hackett and colleagues studied nine patients with HACE after mountain climbing or skiing; the MRI scans in seven of these patients demonstrated increased T2 signal in the corpus callosum, particularly in the splenium, with additional involvement in the centrum semiovale[15] (Figure 9–3). Gray matter was normal, and the abnormalities resolved in four patients who had a repeat MRI scan; all seven patients recovered. The MRI pattern with reversible white matter edema in HACE suggested vasogenic edema, but the investigators could not exclude some cytotoxic edema. This important study implicates a primary disturbance in the cerebral blood vessels with breakdown of the blood-brain barrier (BBB), leading to interference with white matter metabolic activity and cytotoxic edema.

Retinal hemorrhage may occur in individuals exposed to hypobaric hypoxia. More seriously, MRI has demonstrated small regions of bleeding in the brain. Similar findings were

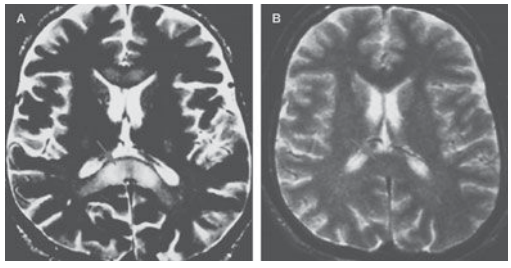

Figure 9–3. (**A**) Axial T2-weighted MR image of a patient with high-altitude cerebral edema demonstrating high signal in the splenium (arrow) and slightly increased signal in the centrum semiovale. (**B**) Axial T2-weighted MR image of the same patient demonstrating complete resolution of abnormal signals 11 months later (arrow). (From Ref. 15.)

seen in an autopsy study of seven trekkers who died in the Himalayas and whose deaths were related to high altitude. They had HAPE and HACE with edema of the lungs and brain that led to thromboses and hemorrhage. Most of the men were middle-aged. Some began their trek soon after flying to high altitude before becoming acclimatized, and some remained at high altitude or climbed even higher despite the development of vomiting, breathlessness, and exhaustion. In one case, death occurred despite prompt recognition and treatment of symptoms by administration of oxygen and swift evacuation to low altitude.[16]

HIFS AND SLEEP DISORDERS IN AMS

Chronic hypoxia leads to slower changes in brain chemistry that can either accelerate AMS or aid in preventing it. When the rate of acclimatization is sufficiently slow, adaptation occurs through a shift in the cassette of genes that is driven by HIF-1α. Exposure to hypoxic conditions over an extended period of time in animals leads to the buildup of HIF-1α. Following an increase in HIF-1α, the brain initiates angiogenesis through the release of VEGF and erythropoietin. While growth of blood vessels is advantageous in that the new vessels can carry more oxygen, there is a period during which the newly formed vessels exhibit increased permeability that contributes to the cerebral edema. Increased levels of hemoglobin provide additional oxygen under these circumstances, but can produce polycythemia with accompanying complications.

Expression of HIF-1α has been studied in rat brain during chronic hypoxia. Under normoxic conditions, the investigators found low levels of HIF-1α protein by Western blot analysis, levels that were not detectable by the less sensitive immunohistochemistry. They measured HIF-1α and HIF-1β expression during adaptation to hypobaric hypoxia (0.5 atm) in rat cerebral cortex. Western blot analysis indicated that HIF-1α rapidly accumulated during the onset of hypoxia and did not fall to normal for 21 days despite the continuous low arterial oxygen tension. Immunostaining showed that neurons, astrocytes, ependymal cells, and possibly endothelial cells were the cell types expressing HIF-1α. Genes with hypoxia-responsive elements were activated under these conditions, as evidenced by elevated VEGF and glucose transporter-1 mRNA levels. A second hypoxic challenge (8% oxygen) in the 21-day-adapted rats caused HIF-1α to reaccumulate. The investigators concluded that the angiogenesis and vascular remodeling with metabolic changes triggered during prolonged hypoxia are capable of restoring normal tissue oxygen levels.[17]

Acute hypoxia increases HIF-1α transiently, but sustained elevation of HIF-1α has been observed during intermittent hypoxia. Sleep-disordered breathing with recurrent apnea (periodic cessation of breathing) results in chronic intermittent hypoxia, which leads to heart, lung, and brain pathology. The molecular mechanisms underlying intermittent hypoxia have been studied in mice with heterozygous deficiency of HIF-1α, who do not develop cardiorespiratory responses to chronic intermittent hypoxia. Hypoxia-inducible factor-1α protein expression and HIF-1 transcriptional activity are induced by intermittent hypoxia in PC12 cells. The investigators showed that intermittent hypoxia-induced HIF-1α accumulation was due to increased generation of reactive oxygen species (ROS) by reduced nicotinamide adenine dinucleotide phosphate (NADPH) oxidase along with ROS-dependent Ca^{2+} signaling pathways involving phospholipase C and protein kinase C activation.[18]

Sleep disorders are common at high altitude. At moderate elevations, vivid dreams occur, and frequent awakenings can be experienced.

One study reported that 60% of people rapidly reaching 3500 m have recurrent awaking during the night.[19] Burgess and colleagues performed 13-channel polysomnography on 14 subjects (8 males, 6 females aged 36 ± 10 years) who were studied at six different altitudes from sea level to 5050 m over 12 days on a trekking route in the Nepal Himalayas. The investigators quantified AMS by the Lake Louise score. They observed desaturation during sleep associated with AMS.[20] In a second study, they tested the hypothesis that isobaric hypoxia would cause obstructive sleep apnea to switch to central sleep apnea. Five adult men with moderate obstructive sleep apnea underwent overnight polysomnography at three altitudes, 60, 610, and 2750 m, with the highest altitude simulated in a normobaric hypoxic chamber. Moderately severe obstructive sleep apnea at sea level (60 m) was completely replaced by severe central sleep apnea at the simulated altitude of 2750 m.[21]

TREATMENT OF ALTITUDE ILLNESSES

Prophylactic treatment with the carbonic anhydrase inhibitor, acetazolamide, is beneficial for prevention of the initial symptoms of AMS. Doses of 125–250 mg twice a day are generally well tolerated. Blocking the activity of carbonic anhydrase has multiple beneficial effects on fluid balance. Acetazolamide causes a renal diuresis of bicarbonate that produces acidosis. It reduces the production of CSF, which provides relief of increased intracranial pressure in persons with idiopathic increased intracranial pressure.[22] Steroids may be used in individuals who are unable to tolerate acetazolamide: treatment with 8 mg dexamethasone to start and 4 mg every 6 hours can be used in HACE. Steroids probably act on altitude sickness by decreasing the release of cytokines and preserving the integrity of the BBB. It is important that individuals with HAPE and HACE be transported as quickly as possible to lower altitudes. In some cases, oxygen may be delivered in specially designed bags that are large enough to accommodate the patient. Delay in treatment may cause permanent brain damage from the cerebral edema.

Cerebral perfusion is preserved or increased in the early stages of hypoxia. However, as the compensatory hyperventilation lowers arterial pCO_2, vasoconstriction develops. Furthermore, the heart is sensitive to hypoxia; in severe hypoxia, cardiac output falls, and hypotension augments the damage from hypoxia. The combination of hypoxia and hypotension is thus an additional factor to take into account when assessing the extent of permanent injury to cells.

REFERENCES

1. Simonson TS, Yang Y, Huff CD, et al. Genetic evidence for high-altitude adaptation in tibet. *Science*. 2010;329:72–75.
2. Ivan M, Haberberger T, Gervasi DC, et al. Biochemical purification and pharmacological inhibition of a mammalian prolyl hydroxylase acting on hypoxia-inducible factor. *Proc Natl Acad Sci USA*. 2002;99:13459–13464.
3. Wilson MH, Newman S, Imray CH. The cerebral effects of ascent to high altitudes. *Lancet Neurol*. 2009;8:175–191.
4. West JB. The physiologic basis of high-altitude diseases. *Ann Intern Med*. 2004;141:789–800.
5. Singh I, Khanna PK, Srivastava MC, et al. Acute mountain sickness. *N Engl J Med*. 1969;280:175–184.
6. Harvey TC, Raichle ME, Winterborn MH, et al. Effect of carbon dioxide in acute mountain sickness: a rediscovery. *Lancet*. 1988;2:639–641.
7. Moskowitz MA. The 2006 Thomas Willis Lecture: the adventures of a translational researcher in stroke and migraine. *Stroke*. 2007;38:1645–1651.
8. Ernsting J. The effects of hypoxia upon human performance and the electroencephalogram. *Int Anesthesiol Clin*. 1966;4:245–259.
9. Crow TJ, Kelman GR. Effect of mild acute hypoxia on human short-term memory. *Br J Anaesth*. 1971;43:548–552.
10. West JB. 1984 Armstrong Lecture. Hypoxic man: lessons from extreme altitude. *Aviat Space Environ Med*. 1984;55:1058–1062.
11. West JB. Do climbs to extreme altitude cause brain damage? *Lancet*. 1986;2:387–388.
12. Regard M, Oelz O, Brugger P, et al. Persistent cognitive impairment in climbers after repeated exposure to extreme altitude. *Neurology*. 1989;39:210–213.
13. Fagenholz PJ, Murray AF, Gutman JA, et al. New-onset anxiety disorders at high altitude. *Wilderness Environ Med*. 2007;18:312–316.
14. Morocz IA, Zientara GP, Gudbjartsson H, et al. Volumetric quantification of brain swelling after hypobaric hypoxia exposure. *Exp Neurol*. 2001;168:96–104.
15. Hackett PH, Yarnell PR, Hill R, et al. High-altitude cerebral edema evaluated with magnetic resonance imaging: clinical correlation and pathophysiology. *JAMA*. 1998;280:1920–1925.

16. Dickinson J, Heath D, Gosney J, et al. Altitude-related deaths in seven trekkers in the Himalayas. *Thorax*. 1983;38:646–656.
17. Chavez JC, Agani F, Pichiule P, et al. Expression of hypoxia-inducible factor-1alpha in the brain of rats during chronic hypoxia. *J Appl Physiol*. 2000;89: 1937–1942.
18. Yuan G, Nanduri J, Khan S, et al. Induction of hif-1alpha expression by intermittent hypoxia: involvement of nadph oxidase, Ca^{2+} signaling, prolyl hydroxylases, and mtor. *J Cell Physiol*. 2008;217:674–685.
19. Jafarian S, Gorouhi F, Taghva A, et al. High-altitude sleep disturbance: results of the Groningen Sleep Quality Questionnaire survey. *Sleep Med*. 2008;9:446–449.
20. Burgess KR, Johnson P, Edwards N, et al. Acute mountain sickness is associated with sleep desaturation at high altitude. *Respirology*. 2004;9:485–492.
21. Burgess KR, Cooper J, Rice A, et al. Effect of simulated altitude during sleep on moderate-severity osa. *Respirology*. 2006;11:62–69.
22. Basnyat B, Gertsch JH, Holck PS, et al. Acetazolamide 125 mg bd is not significantly different from 375 mg bd in the prevention of acute mountain sickness: the Prophylactic Acetazolamide Dosage Comparison for Efficacy (pace) trial. *High Alt Med Biol*. 2006;7:17–27.
23. Editorial, See Nuptse and die, Lancet. 1976; 2(7996: 1177–1179).

Chapter 10

Brain Edema

INTRODUCTION

Cerebral edema is a final common pathway for many brain insults and is often the proximate cause of death due to brain herniation. Enlargement in any of the three compartments of blood, cerebrospinal fluid (CSF), or brain tissue causes an increase in intracranial pressure (ICP) with shifting of the contents. Although enlargement of the blood space leads to an increase in CSF pressure and may cause headaches, it is not life-threatening. By contrast, enlargement of the CSF space by obstruction of the outflow pathways for the ventricles can lead to downward herniation. Most threatening, however, is the enlargement of the brain tissue space, which can occur with cell swelling, blood vessel breakdown, or mass lesions such as an intracranial bleed or a brain tumor. When the tissue itself enlarges in the absence of a mass lesion, one of the three types of cerebral edema, cytotoxic, vasogenic, or interstitial, is present.[1,2] While the definitions provide useful constructs, the distinction between the different types of edema is generally blurred because of the overlap among them.

Brain swelling is poorly tolerated because of the limitations imposed by the bony cavity of the skull. While a reasonable amount of tissue swelling can be tolerated in other tissues of the body, the restrictions imposed by the bony structures and the dense dura mater of the falx cerebri and tentorium are life-threatening. Herniation is a serious consequence of brain tissue displacement by mass lesions and hydrocephalus. Increased ICP without a mass or hydrocephalus does not cause herniation. Even in hydrocephalus, if the pressure is evenly distributed throughout the ventricular system, as occurs in communicating hydrocephalus, there is no threat of herniation. Major sites of herniation include the area beneath the falx, across the tentorium, downward shift of cerebellar tonsils through the foramen magnum, and central movement compressing the supratentorial area downward, shifting the brainstem (Table 10–1).

While minor shifts of the brain can be tolerated, especially in elderly patients with brain atrophy, downward pressure on brainstem structures tears the small pontine, perforating vessels that branch off the basilar artery. Tears in the pontine perforating arteries result in hemorrhages in the pons. These so-called *Duret's hemorrhages* are generally a signal of irreversible damage, and if they disrupt the

Table 10–1 **Types and Consequences of Herniation**

Herniation	Regions of Brain Affected	Consequences of Herniation
Cingulate or subfalcial	Cingulate gyrus pushed under the falx	Compression of the anterior cerebral artery with infarction
Central	Downward displacement of the hemispheres or basal ganglia	Compression of brain tissue through the tentorial notch with rostral caudal movement of the brainstem
Uncal	Temporal lobe masses press brain tissue against the tentorium	Ipsilateral midbrain peduncle flattened, and third nerve and posterior cerebral artery compressed

periaqeductal gray, except in rare cases they cause brain death[3] (Figure 10–1).

Cytotoxic edema is by definition cellular swelling. As the cell swells in the constrained space, the extracellular space is reduced, restricting diffusion of interstitial fluid. The most common cause of cytotoxic edema is hypoxic injury secondary to cerebral ischemia. Diffusion-weighted images (DWIs) obtained with magnetic resonance imaging (MRI) show the restricted diffusion within minutes after its development, making DWI an excellent early diagnostic tool for stroke[4] (Figure 10–2). The DWI remains positive for 1 to 2 weeks after a stroke, but the intensity of the signal begins to fade as the edema resolves. Diffusion-weighted imaging is an excellent marker to show an ischemic region, which is essential in patients with white matter lesions because these lesions obscure the normal T2-weighted image signal that is seen in stroke. Occasionally, a DWI-negative stroke will be found, and the cause of the stroke-like findings is not apparent. Some patients with symptoms of transient ischemic attack (TIA) have DWI positivity consistent with a stroke. In one study, 20 of

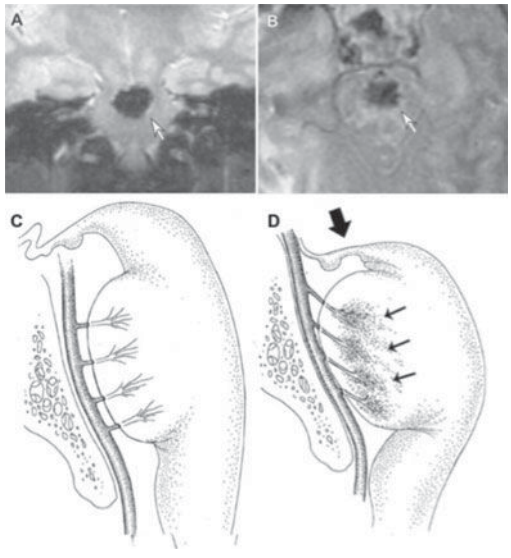

Figure 10–1. Coronal multiplanar gradient echo imaging sequence (**A**) and axial fluid attenuated inversion recovery (FLAIR) sequence (**B**) demonstrating blood in the pons (arrows). (**C**) Sagittal schematic views of the basilar artery and brainstem before (left) and after (right) cerebral herniation. In a normal brainstem, the basilar perforating arteries penetrate the pons in a perpendicular fashion. (**D**) With downward herniation (large arrow), the basilar artery remains fixed by the circle of Willis and the caudal shift of the pons results in stretching and rupture of small pontine perforating vessels, which leads to a Duret hemorrhage (arrows). (From Ref. 3.)

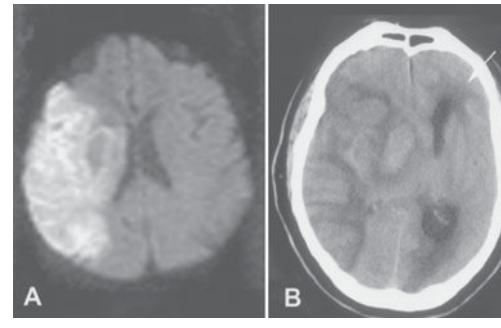

Figure 10–2. (**A**) Diffusion-weighted MRI scan of a patient with large middle cerebral artery stroke. There is involvement of the entire vessel territory with possibly some hemorrhage in the basal ganglia. The image was made within hours of the infarction, and there is minimal compression of the ventricles. (**B**) A CT scan performed 3 days after the infarction shows the massive shift of the midline structures away from the evolving mass lesion. Compression of the CSF outflow tracts causes the hydrocephalus with interstitial edema in the white matter adjacent to the ventricles (arrow).

42 TIA patients (48%) showed focal abnormalities on DWI and apparent diffusion coefficient (ADC) imaging. Those with positive MRI scans had a TIA symptom duration that was significantly longer (7.3 hours) than that of MRI-negative TIA patients (3.2 hours). Thus, in general, MRI is excellent for the early diagnosis of stroke. It has been shown to be as good as computed tomography (CT) for the detection of blood, which is essential for the use of tissue plasminogen activator (tPA) within the 3 hour therapeutic window. Ideally, MRI would be the optimal imaging method to guide tPA treatment because it provides a positive image of the early stroke, while CT provides little evidence of early stroke since it is most likely negative until hours later, depending on the size of the stroke. However, relatively few medical centers providing tPA treatment use MRI because it is rarely available on an emergent basis.

Vasogenic edema occurs in hypertensive crisis and in masses that appear as foreign tissue to the brain. Massive edema is seen around metastatic lesions. Brain tumors that have abnormal blood vessels, such as glioblastoma multiforme and metastases, cause marked vasogenic edema. Meningiomas have extensive vasogenic edema. Tumors that have a tissue structure similar to that of normal brain, such as low-grade gliomas and oligodendrogliomas, produce less brain edema. As with stroke, MRI is far superior to CT for detection of vasogenic edema except when the edema is extensive. In the case of metastatic lesions, many more tumors are seen with MRI than with CT, and the use of contrast agents, such as gadolinium-diethylenetriaminepentaacetic acid (DTPA) further enhances the ability to detect lesions.

When vasogenic edema causes the leakage of excess fluid across damaged blood vessels, the spaces between cells are enlarged, in contrast to the loss of extracellular space in cytotoxic edema. The result is striking images on fluid attenuated inversion recovery (FLAIR) and T2-weighted MRI that correspond to the white matter. Increased diffusion results from the enlargement of the extracellular space, resulting in loss of signal on DWI and an increase in the ADC. Finally, interstitial edema is used to describe the movement of water out of the ventricle transependymally into the adjacent white matter (Figure 10–3).

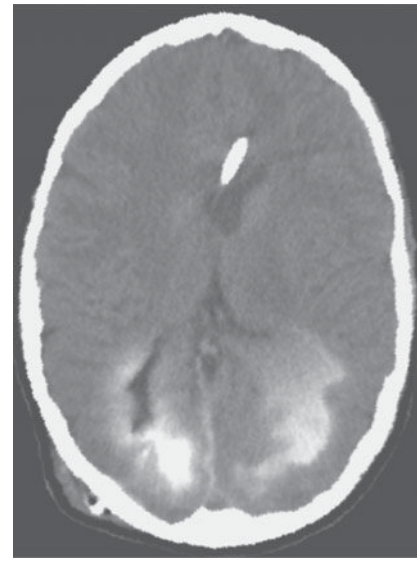

Figure 10–3. Computed tomograph of patient with hydrocephalus treated with a shunt seen in the frontal horn of the cerebral ventricle. A contrast agent was injected, and it can be seen extravasating into the posterior regions by transependymal absorption of CSF. (Courtesy of Blain Hart, M.D.)

Transependymal movement of CSF occurs primarily in hydrocephalus, which is the main cause of interstitial edema. Because there is excess fluid in the tissues around the ventricles, particularly in the white matter regions, the MRI signal is bright on T2-weighted images. Another imagining sequence, FLAIR, shows tissue water as a hyperintense signal while suppressing the water in the ventricle. While the T2-weighted image blurs the distinction between water in the ventricle and water in the tissue, since both have hyperintense signals, FLAIR easily separates one from the other.

A number of insults lead to brain swelling. These include ischemia, hypoxia, infection, and noninfectious inflammation. Table 10–2 lists the major causes of each type of edema. Movement of water within the brain is determined by hydrostatic and osmotic gradients. Osmotic pressure is a major force in the movement of water between compartments in the brain. For example, when vasogenic edema develops because of damage to the blood vessels, proteins that are normally in the vascular space cross the blood-brain barrier (BBB). The water that follows the proteins swells the extracellular spaces and moves in the white matter. When blood pressure is acutely increased,

Table 10–2 **Types of Cerebral Edema**

Types	Pathology	Causes	Treatments
Vasogenic	Widened extracellular space in white matter; damaged BBB	Brain tumors, brain metastases, cerebral abscesses, hypertensive encephalopathy, neuroinflammation	Dexamethasone; osmotic treatment
Cytotoxic	Swollen cells with decreased extracellular space	Cerebral ischemia, hypoxia, toxins	Hypertonic solutions used, but are unproven
Interstitial	Transependymal fluid movement	Hydrocephalus	Shunt to remove excess fluid from the brain

there is movement of water and some proteins into the brain. The increased water and protein in the extracellular space prevent oxygen from reaching cells, and hypoxic conditions are created that induce cytotoxic edema. By the time the insult has evolved, both types of edema may be present.

Vasogenic edema occurs in trauma, ischemia, hypertension, or infections. Blood vessels begin to leak when the basal lamina is damaged and the tight junction proteins are degraded. Once the tight junctions are disrupted, fluid and toxic substances from the blood can enter the brain. Normal concentrations of electrolytes in the blood have damaging effects when they enter the brain. Because of the ease of movement between fiber tracts, white matter is the site of fluid bulk flow in vasogenic insults.[5] An example is eclampsia, which causes damage primarily to the posterior regions of the brain; these patients have disturbances of vision. After the blood pressure is restored to normal, the vasogenic edema disappears and function is restored. Vasogenic edema differs from cytotoxic edema in that resolution can lead to complete recovery of function, whereas in cytotoxic edema the membrane is damaged through energy loss and recovery is unlikely or, if it occurs, progress is very slow.

ROLE OF AQUAPORINS IN BRAIN EDEMA

Erythrocyte membranes are more permeable to water than expected from water diffusion through a lipid bilayer. This provided the first experimental evidence of the existence of molecules that acted as pores in the membrane. Discovery of aquaporins (AQPs), a family of at least 13 members of small membrane-spanning proteins, confirmed the existence of such pores. Aquaporins assemble in cell membranes as homotetramers.[6] Each monomer is approximately 30 kDa, and six α-helical domains with cytosolically oriented amino and carboxy termini surround the water pore. Aquaporins act as passive pores, allowing water movement in both directions along hydrostatic and osmotic gradients[7,8] (Figure 10–4).

Of the AQP family members, AQP4 is the main one expressed in the brain. Expression of AQP4 is dense at the borders between brain parenchyma and major fluid compartments, including astrocytic foot processes, glia limitans, ependymal cells, and subependymal astrocytes, where it acts to control water flow into and out of the brain[9] (Figure 10–5). Aquaporin-1

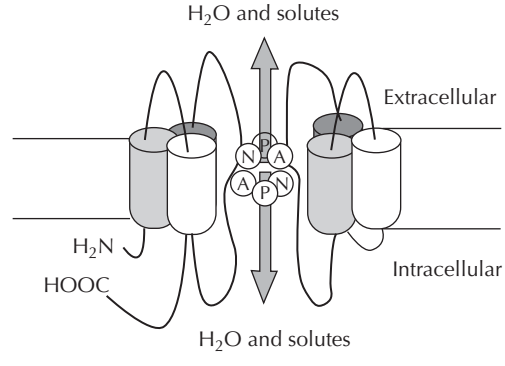

Figure 10–4. Schematic representation of the common AQP structure. The AQPs are formed by two tandem repeats of three membrane-spanning α-helices. Two connecting loops, each containing an Asparagine-Proline-Alanine (NPA) motif, are supposed to form a pore in plasma membrane. (From Ref. 11.) HOOC, dicarboxylic acid and H_2N is an amino group.

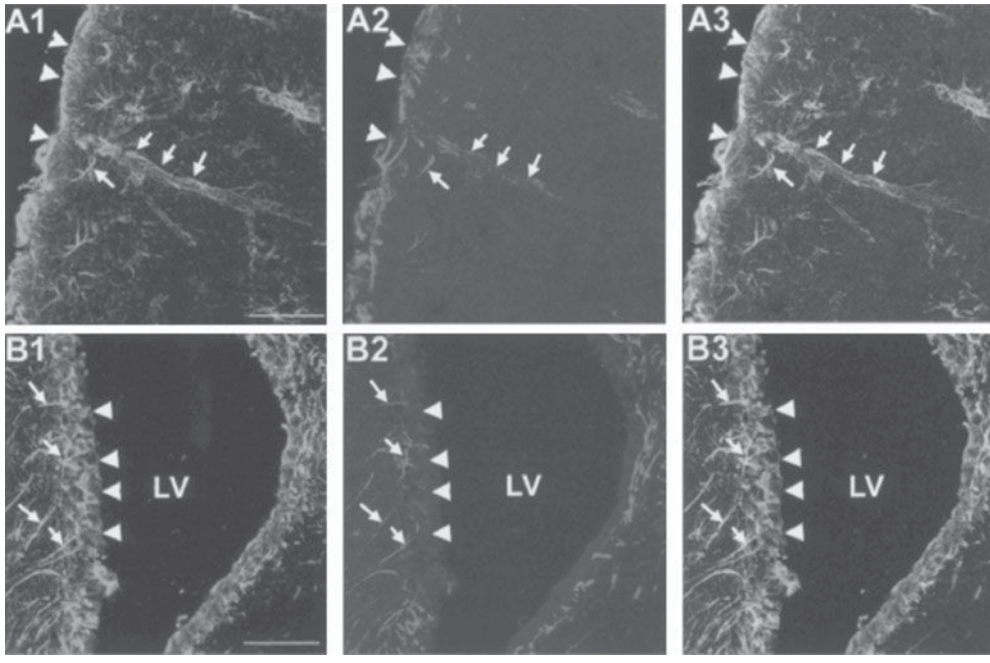

Figure 10–5. Confocal pictures of anti-GFAP (glial fibrillary acidic protein) and anti-AQP9 in two mouse brain regions: parietal cortex (**A1, A2, A3**) and lateral septum (**B1, B2, B3**). (**A1–A3**) Confocal pictures of anti-GFAP labeling (green, **A1**) and anti-AQP9 labeling (red, **A2**) and superposition of both forms of labeling (**A3**) in parietal cortex. Arrowheads and arrows indicate colocalization between anti-GFAP (A1) and anti-AQP9 (**A2**) on glia limitans (arrowheads) and on astrocytes in parietal cortex (arrows). This colocalization is yellow on the superposed picture (**A3**), suggesting that AQP9 is present on glia limitans (arrowheads) and on astrocytes in cortex (arrows). (**B1–B3**) The double labeling between anti-GFAP (green, **B1**) and anti-AQP9 (red, B2) and the superposition of both forms of labeling (B3) show the presence of AQP9 in the lateral septum. Arrows indicate colocalization between anti-GFAP (**B1**) and anti-AQP9 (**B2**), suggesting the presence of AQP9 on astrocytes in septum. Arrowheads indicate the ependymal cells of the lateral ventricle (LV), which are not labeled by anti-AQP9. This result suggests that AQP9 is not expressed by ependymal cells in mouse brain. (From Ref. 11; See also the color insert.)

is expressed in the apical membrane of the choroid plexus and plays an important role in CSF formation. Another member of the family, AQP9, appears in neurons according to a study using mice with a targeted deletion of the AQP9 gene.[10]

Aquaporin-4 is one of the most abundant molecules at the brain-blood interface and has been shown to play an important role in edema associated with many brain pathologies.[11,12] In a clinically relevant model of ischemic stroke, AQP4 knockout mice had decreased cerebral edema and an improved outcome. In AQP4-deficient mice, brain tissue water content and swelling of pericapillary astrocytic foot processes were significantly reduced in comparison with wild-type controls.[13] Similarly, in a model of water intoxication, AQP4-null mice displayed decreased brain water content and a significant improvement in survival.[13,14] Significantly reduced brain edema after cerebral ischemia and water intoxication has been reported in α-syntrophin-deficient mice, which have reduced AQP4 expression in astrocyte foot processes.[15,16] Transgenic mice overexpressing endothelin-1 in astrocytes showed more BBB disruption with increased water accumulation and brain edema, possibly because of elevated AQP4 expression in astrocytic endfeet following temporary focal cerebral ischemia.

Deletion of AQP4 reduces edema in models in which cytotoxic edema is the predominant pathophysiological mechanism. However, in conditions in which vasogenic edema is significant, AQP4 deletion exacerbates brain edema.[14] Aquaporin-4 function has been demonstrated to be of great importance in

the clearance of extracellular fluid and the resolution of vasogenic edema.[17,18] Deletion of AQP4 results in increased brain swelling in vasogenic edema because of impaired removal of excess brain water through glial limitans and ependymal barriers. Mice deficient in AQP4 have higher ICP and brain water content after continuous intraparenchymal fluid infusion. In a freeze-injury model of vasogenic brain edema, AQP4-deficient mice had a remarkably worse clinical outcome, higher ICP, and greater brain water content. Similarly, in a brain tumor edema model involving stereotactic implantation of melanoma cells, tumor growth was comparable in wild-type and AQP4-deficient mice. However, the AQP4-deficient mice had higher ICP and corresponding accelerated neurological deterioration. Results from these studies indicate that AQP4-mediated transcellular water movement is crucial for fluid clearance in vasogenic brain edema.

Together, these studies emphasize the importance of AQPs in water flux and brain edema formation and suggest that AQPs are potential targets for drug development. In addition to providing control of brain water balance, AQPs participate in cell migration and neuronal excitability.[9] The complex involvement of AQPs in multiple aspects of brain function, and the opposite role of AQPs in cytotoxic and vasogenic edema, will require greater understanding before AQPs can be considered targets of therapy.

A novel role was recently found for AQP4 in neuromyelitis optica (NMO), or Devic's syndrome. Originally thought to be a variant of multiple sclerosis (MS), NMO has a unique antibody that separates patients. Clinically, NMO presents as optic neuritis combined with lesions in the upper cervical cord that span at least three segments. Pathologically, there is inflammation with necrosis rather than the demyelination seen in MS.[19] Treatment with agents that suppress inflammation, such as azathioprine, are more effective than drugs used to treat MS. The NMO-IgG antibodies that bind to blood vessels are characteristic of the illness. Aquaporin-4 is the main target of the NMO-IgG antibody. Neuromyelitis optica is the first inflammatory demyelinating disorder of the central nervous system to have a defined autoantigen.[7]

ROLE OF NEUROINFLAMMATION IN THE FORMATION OF VASOGENIC EDEMA

Oxidative Stress and Brain Edema

Free radicals, which are formed during normal metabolism, contribute to cell death as part of the neuroinflammatory response. Reactive oxygen species (ROS) and nitric oxide (NO) are involved in brain damage. Nitric oxide is formed by three enzymes: endothelial nitric oxide synthase (eNOS), neuronal nitric oxide (nNOS), and inducible nitric oxide (iNOS). Nitric oxide formed in blood vessels plays an essential role in normal vasodilation, and knockout of eNOS exacerbates injury after stroke.[20] Both nNOS and iNOS contribute to tissue injury by amplifying the inflammatory pathways, and knockout mice lacking one of the other of these genes have smaller strokes.[21]

Nitric oxide is a free radical with both beneficial and deleterious actions during ischemia/reperfusion.[22] Excessive NO generation by nNOS is cytotoxic.[23] By contrast, eNOS knockouts develop larger infarcts because NO of endothelial origin promotes survival by improving blood flow during ischemia.[24] However, excessive production of NO by eNOS during reperfusion may contribute to ischemic brain injury via the formation of peroxynitrite, the product of the reaction between NO and the superoxide radical. In a model of transient focal ischemia in the mouse, superoxide and peroxynitrite formation was particularly intense in microvessels and the astrocytic endfoot processes surrounding them. There was colocalization of sites with peroxynitrite formation and vascular injury, as shown by increased Evans blue leakage and matrix metalloproteinase -9 (MMP-9) labeling, suggesting an association between peroxynitrite and microvascular injury. Nonselective NOS inhibition has been shown to significantly reduce brain edema, BBB disruption, and infarct size in experimental stroke.

While ROS and NO are not necessarily toxic by themselves, when they are combined into a compound called *peroxynitrate*, they become highly toxic to the cell. Electron transport in the mitochondria is an important source of the

ROS that result from oxidative phosphorylation. In reperfusion injury, the reintroduction of oxygen to an ischemic region leads to production of ROS. Amino acid metabolism in the presence of oxygen forms NO through the action of the three NOSs.

Free radical formation is an important contributor to cell death and brain injury in many neurological diseases and an important determinant in brain edema. Shortly after brain damage by hypoxia/ischemia, hemorrhage, or trauma, excessive production of ROS occurs; at the same time, there is an impairment of antioxidant protective mechanisms, which leads to oxidative stress.[25]

During cerebral ischemia, ROS contribute to cytotoxic edema by perturbing the functioning of plasma membrane ion transport systems such as Na^+-K^+-ATPase, Ca^{2+}-ATPase, and the Na^+-Ca^{2+} exchanger. The proposed mechanisms underlying ion transport modulation by ROS include peroxidation of membrane phospholipids, oxidation of sulfhydryl groups located on the ion transport proteins, and oxidative protein modification.[26] Oxidative stress triggers the release of mediators known to be responsible for cytotoxic cell swelling, such as K^+ ions, glutamate, lactic acid, and arachidonic acid.

Oxidative stress damages endothelial cells of the BBB and contributes to vasogenic edema. Incubation of endothelial cells with ROS-generating systems increases the permeability of endothelial monolayers. The superoxide radical ($O_2^{\cdot-}$) has been identified as the primary ROS involved in increased vascular permeability and edema formation in global and focal cerebral ischemia, cold-induced brain lesions, and brain tumors.[27] Scavenging $O_2^{\cdot-}$ radicals using recombinant superoxide dismutase (SOD) or polyethylene glycol-SOD reduce ischemia-induced BBB injury and vasogenic edema. Treatment of ischemic rats with encapsulated SOD in biodegradable poly (D,L-lactide co-glycolide) nanoparticles (SOD-NPs) maintained BBB integrity, thereby preventing edema and reducing oxidative injury following reperfusion; ultimately, this resulted in protection of neurons from apoptosis.[28] Further evidence emphasizing the important role of ROS formation in brain edema development comes from transgenic animals overexpressing antioxidant enzymes. Brain water content and infarct size are significantly reduced after transient focal cerebral ischemia in transgenic mice overexpressing the human Cu,Zn-SOD (SOD1) compared with nontransgenic controls.[29] These SOD1-overexpressing mice also have reduced vasogenic edema and infarction after cold-trauma brain injury.[30]

Hyperglycemia increases oxidative stress and MMP-9 expression/activity, exacerbating BBB breakdown and dramatically increasing edema formation after ischemia-reperfusion injury in the rat.[31] Heterozygous *SOD1* transgenic rats, carrying human *SOD1* genes with a four- to six-fold increase in Cu/Zn-SOD activity, showed a significant reduction in hyperglycemia-induced Evans blue leakage, vasogenic edema, and MMP-9 activation after experimental ischemia compared with control nontransgenic rats.

Transgenic mice overexpressing the intracellular form of glutathione peroxidase (GPx1) displayed reduced infarct size and decreased edema formation compared with nontransgenic mice at 24 hours of reperfusion following 1 hour of middle cerebral artery occlusion. Absence of GPx1 exacerbates cerebral ischemia-reperfusion injury, as shown by larger infarct volumes, increased activation of MMP-9, and dramatic disruption of the BBB in GPx1-null mice compared with wild-type controls.[32]

The gp^{91phox} (Nox2)-containing NADPH oxidase is an important source of ROS during cerebral ischemia. Deletion of gp^{91phox} confers protection against ischemic stroke in mice; gp^{91phox}-null mice showed less BBB breakdown, brain edema, and lesion volume after stroke compared with wild-type mice.[33] In another study, intracerebral injection of collagenase produced less bleeding in gp^{91phox}-null mice than in wild-type mice. Brain edema formation, neurological deficit, and a high mortality rate were observed in wild- type but not in gp^{91phox} knockout mice.[34] These studies suggest that formation of ROS by NADPH oxidase plays a central role in BBB injury and edema in stroke and intracerebral hemorrhage.

Free radicals interact with proteases to amplify the tissue damage. In reperfusion injury models, the reintroduction of oxygen and white blood cells to the hypoxic tissue results in an increase in free radical formation. Permanent occlusion of an artery restricts the reoxygenation of infarcted tissues; less damage is evident in the infarct and the surrounding penumbra. Free radicals activate proteases, which are present in a latent state until acted upon by other proteases or free radicals.

Although activation is observed for proteases in the presence of free radicals, the underlying mechanisms are not well understood.[35]

Arachidonic Acid and Brain Edema

Experimental evidence indicates that cyclooxygenase (COX) modulates BBB permeability in neuroinflammatory conditions, ischemia, and hemorrhage. The COX inhibitor, KBT-3022, prevented brain edema induced by bilateral carotid occlusion and recirculation in gerbils.[36] In the collagenase model of intracerebral hemorrhage, the brain water content of rats treated with the COX-2 inhibitor, celecoxib, decreased both in lesioned and nonlesioned hemispheres in a dose-dependent manner, accompanied by reduced perihematomal cell death.[37] Delayed damage to the BBB and vasogenic edema, which follow ischemic stroke, were significantly diminished by administration of the COX-2 inhibitor, nimesulide.[38] Inhibition of COX activity with indomethacin prevented BBB damage following intracerebral administration of tumor necrosis factor-α (TNF-α) in the rat. Indomethacin significantly reduced TNF-α-induced MMP-9 and MMP-3 expression and activity and attenuated free radical formation.[38]

Vascular Endothelial Growth Factor and Angiopoietins

Vascular endothelial growth factor (VEGF) and angiopoietins are families of vascular-specific growth factors that regulate blood vessel growth, maturation, and function.[39] Vascular endothelial growth factor, the predominant angiogenic growth factor, triggers endothelial cell proliferation, migration, and increased vascular permeability due to the formation of nascent vessels, which essentially consist of immature endothelium with few pericytes and little mature matrix.[40] The angiopoietins, Ang-1 and Ang-2, modulate in different ways the actions of VEGF in angiogenesis. In particular, Ang-1 and its endothelial receptor, Tie2, mediate the maturation and stabilization of the VEGF-induced vasculature by promoting the recruitment of pericytes to the abluminal surface of the newly generated vascular bed, increasing the structural integrity of blood vessels. In contrast, Ang-2, a natural antagonist of Ang-1, is associated with both initial angiogenesis and capillary destabilization. An increase in the expression of Ang-2 in the presence of VEGF promotes vessel sprouting and increased vascular permeability.

Vascular endothelial growth factor is an angiogenic factor that induces increased permeability of the BBB, leading to the formation of edema following ischemia/hypoxia. Ang-1 blocks the BBB permeability effect of VEGF by modulation of MMP activity. In ischemia, VEGF enhances BBB damage and MMP-9 activity; Ang-1 counteracts both effects, suggesting a synergistic angiogenic effect of Ang-1 and VEGF in the brain. This suggests that Ang-1 and VEGF could be used early to promote the formation of mature neovessels without inducing side effects on BBB permeability.[41] Vascular endothelial growth factor is associated with endothelial proliferation and neovascularization, suggesting that VEGF promotes angiogenesis and repair following stroke. However, new vessels lack a fully mature BBB and are consequently leaky. In addition, VEGF directly increases the permeability of the BBB via the synthesis/release of NO and subsequent activation of soluble guanylate cyclase.

Vascular endothelial growth factor caused a loss of occludin and zona occludens-1 (ZO-1) from the endothelial cell junctions, suggesting that VEGF increases BBB permeability by reducing occludin expression and disrupting ZO-1 and occludin organization, which leads to tight junction disassembly.[42] Blood-brain barrier disruption, resulting from loss of tight junctions and activation of MMPs, is associated with edema formation in ischemic stroke.

CLINICAL CONDITIONS ASSOCIATED WITH BRAIN EDEMA

The consequences of brain edema depend on the amount of tissue involved, the effect on ICP, and the threat of herniation. Small lesions, such as limited edema around a metastatic lesion or an early abscess, may have little clinical impact. By contrast, a large middle cerebral artery stroke with massive edema may block CSF flow, resulting in unilateral hydrocephalus and herniation. When the edema is generalized and the ICP is massively increased, as can

occur with head trauma, there is a threat of secondary ischemia due to loss of CBF. Cerebellar infarctions and cerebellar hemorrhages can obstruct the outflow of CSF through the fourth ventricle, causing acute hydrocephalus. In cerebellar hemorrhage, CT is adequate to show the large hematoma, but cerebellar infarction often requires MRI (Figure 10–6). Both hemorrhage and infarction of the cerebellum, when they compress the brainstem and cause hydrocephalus, require surgery. Large masses in the hemispheres can also compress the CSF outflow pathways and cause contralateral hydrocephalus with transependymal absorption (Figure 10–7).

Brain tumors cause brain edema through several mechanisms. Highly vascular tumors often have vessels with leaky BBB, and both the mass lesion and the vasogenic edema produce the pathological changes. In the case of metastatic tumors, which can act like foreign objects, there is swelling in the tissue around the mass from disruption of the BBB and cellular function. The resulting edema around the metastatic tissue fans out into the white matter in finger-like projections. Generally, there are multiple masses due to metastatic lesions and one lesion in primary tumors. In some tumors, such as low-grade astrocytomas, which have tissue characteristics close to those of normal brain tissue, relatively little edema accompanies the mass.

A different pattern is seen in the cerebral edema occurring with ischemia/hypoxia. The lesions evolve over time, as described above. The early energy failure causes cellular swelling with cytotoxic edema. This can occur within minutes, as shown in DWI studies in animals.

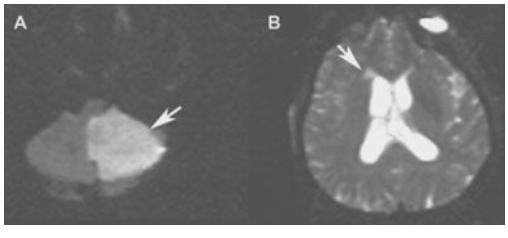

Figure 10–6. Cerebellar infarct with secondary hydrocephalus and transependymal fluid movement (interstitial edema). (**A**) Initial DWI with cerebellar infarct in the territory of the left posterior inferior cerebellar artery. (**B**) Echo-planar T2 axial image shows enlargement of the ventricles prior to surgery for hydrocephalus. The arrow shows transependymal movement of fluid.

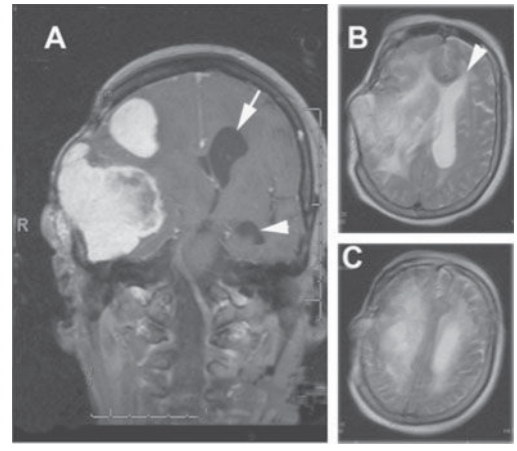

Figure 10–7. (**A**) Large mass on the right (R) with signs of earlier surgery. Pressure on the aqueduct caused enlargement of the lateral ventricle on the left (arrow), which included the temporal horn (arrowhead). (**B**) Transpendymal absorption of CSF is seen (arrowhead). (**C**) Diffuse edema is seen in both hemispheres.

The cell swelling compresses the extracellular space, constricting water diffusion, which appears on diffusion-weighted MRI as a hyperintense region with a corresponding dark area on the ADC scan.

An inflammatory response occurs in autoimmune processes such as MS, involving infiltration by circulating white blood cells, primarily T cells, with venules being the site of inflammation. Characteristic lesions in MS patients appear in the region of the corpus callosum, where the veins fan out like fingers at a 90° angle. Involvement of the veins in the corpus callosum is referred to as *Dawson's fingers*.[43] While the myelinated fibers are the site of most of the injury, recent evidence suggests that eventually the axons are damaged in MS.[44] Loss of myelin leads to expression of excess numbers of sodium channels. Glutamate channels are activated with calcium overload. The denuded axons with excess sodium and glutamate channels are more vulnerable to minor forms of hypoxia, making it possible that edema as part of a hypoxia-related injury occurs in the white matter.[45]

IMAGING BRAIN EDEMA

Cerebral edema has a characteristic appearance on CT and MRI. In CT the x-rays pass

more easily through the edematous tissue due to the higher water content; images of edematous areas are attenuated and appear as a dark area on the scan..Brain tissue water content is inversely correlated with x-ray attenuation and can thus be measured with CT. Several different MRI techniques have been developed to measure abnormalities in water mobility and water content of tissues. Diffusion-weighted imaging (DWI) and diffusion tensor imaging (DTI) have been developed to measure the changes in water mobility in cerebral tissues. Diffusion-weighted imaging measures the one-dimensional distribution of water diffusion. The result of DWI imaging is represented as an apparent diffusion coefficient (ADC) map.

Diffusion tensor imaging can be used to reconstruct a map of the fiber tracts based on the general direction of the three-dimensional diffusion vectors. Tissue water diffusion is determined by the presence and orientation of barriers to translational motion. The measured ADC values can vary, depending on the direction in which the diffusion-sensitive gradients are applied. The ADC is direction-dependent, which makes it possible to visualize the pattern of water movement. Diffusion leads to an elliptical shape of the probability, with the longest axis aligned along the fiber direction. It is possible to characterize the diffusion ellipsoid with six parameters that are organized in a tensor called a *diffusion tensor*. Six diffusion constants along six independent axes are measured. Having tensor data, DTI measures three diffusion properties: (1) magnitude, (2) direction, and (3) anisotropy of water molecule in tissues. When DTI was used in a mouse model of traumatic brain injury, at every time point it was more sensitive to injury than conventional MRI, and relative anisotropy distinguished injured from control mice with no overlap between groups.

Diffusion tensor imaging measures the three-dimensional distribution of water. Two important parameters, fractional anisotropy (FA) and mean diffusivity (MD), are calculated from DTI images to represent the diffusion abnormalities[46] (Figure 10–8). The effects of edema on DTI measurements include increased MD and decreased FA. This pattern of DTI measures is a general hallmark of many diseases and injury processes, which limits the specificity of DTI measurements.

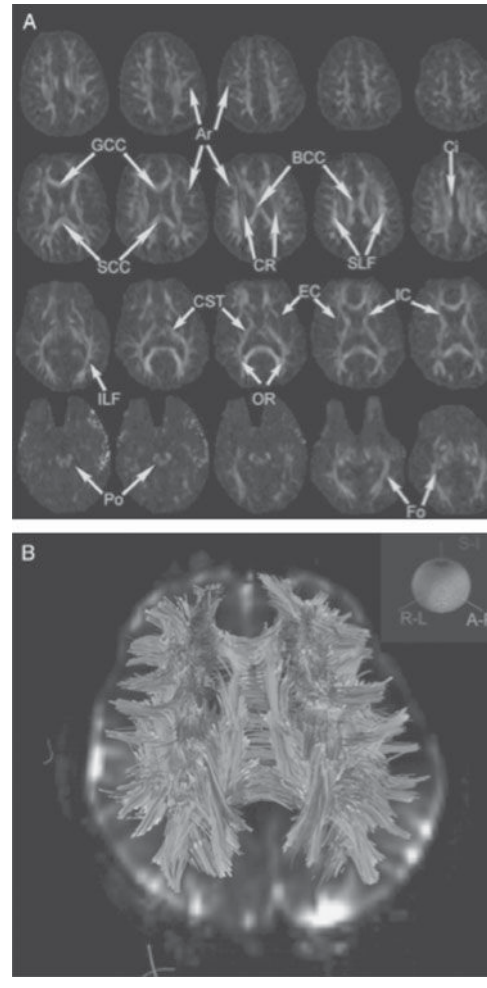

Figure 10–8. This multislice echo-planar imaging/diffusion tensor imaging (EPI-DTI) color map comes from a healthy volunteer at 7 T following a field map dewarping processing. (**A**) Fiber bundles are visualized, including the pons (Po), forceps (Fo), optic radiation (OR), genu, splenum and body of the corpus callosum (GCC/SCC/BCC), corticospinal tract (CST), internal and external capsules (IC/EC), corona radiata (CR), cingulum bundle (Ci), inferior and superior longitudinal fasciculi (ILF/SLF), and arcuate fibers (Ar). Some fiber groups in lateral subcortical regions are less conspicuous, perhaps due to lower coil sensitivity (arrows indicate labeled regions). (**B**) Tractography results in the midbrain region of this acquisition, highlighting many of the same fiber bundles in three dimensions. (From Ref. 46; See also the color insert.)

An important event in the pathophysiological cascade that leads to infarction following ischemia is the net movement of water from the extracellular space into the intracellular compartment without an increase in total water content in the affected zone. Because of the

lack of change in water, the T2-weighted image remains normal at this stage. When endothelial cells break down, leading to vasogenic edema, there is an increase in total water content, which produces a bright signal on the T2-weighted image.

Susceptibility differences between tissues have been used as a new type of MR contrast by susceptibility-weighted imaging (SWI).[47] Susceptibility-weighted imaging is a fully velocity-compensated, high-resolution, three-dimensional gradient-echo sequence that uses magnitude and filtered-phase information, both separately and in combination with each other, to create new sources of contrast.[48] In SWI, there is a mixture of spin density, T1, T2*, CSF suppression, and susceptibility sensitivity. The SWI images reveal regions of edema identical to those seen on FLAIR images because of short relaxation time (TR) and comparatively longer echo time (TE); however, SWI does not reveal a low signal in CSF because of the low flip angle. Diffusion-weighted imaging highlights the edematous regions affected by stroke, while SWI shows changes in oxygen saturation along with other sources of susceptibility. Therefore, SWI demonstrates the affected vascular territory in stroke. The hypothesis is that the deoxyhemoglobin content of small vessels is increased over their normal values due to slower or restricted flow, making these vessels visible.

TREATMENT OF BRAIN EDEMA AND HYPOXIC/ISCHEMIC INJURY

A large number of studies in animals have tested potential treatments for cerebral edema. Although many have been shown to work in animal studies, treatment of cerebral edema in humans has been extremely difficult to study, and in spite of multiple studies, convincing evidence of efficacy is lacking for many of the currently used treatments. In a recent review of several decades of studies, no agent met vigorous criteria for efficacy. Based on uncontrolled studies, many centers perform decompressive craniectomies to treat massive ischemic edema. While several uncontrolled studies indicate that lives can be saved, this conclusion should be considered provisional until properly controlled trials are conducted.[49] A controlled trial has been done in patients with traumatic brain injury. A total of 155 adults with severe diffuse traumatic brain injury and intracranial hypertension that was refractory to first-tier therapies were randomly assigned to undergo either bifrontotemporoparietal decompressive craniectomy or standard care. Patients in the craniectomy group, compared with those in the standard-care group, had less time with ICP above the treatment threshold, fewer interventions for increased ICP, and fewer days in the intensive care unit (ICU). However, patients undergoing craniectomy had worse scores on the Extended Glasgow Outcome Scale than those receiving standard care and a greater risk of an unfavorable outcome. The study concluded that in adults with severe diffuse traumatic brain injury and refractory intracranial hypertension, early bifrontotemporoparietal decompressive craniectomy decreased ICP and the length of stay in the ICU, but it was associated with more unfavorable outcomes.[50] A similar controlled trial is needed for ischemic brain edema.

Why have the treatment efforts lagged so far behind the rapid advances in understanding the underlying molecular mechanisms and successes in the treatment of animal models of brain edema? One obvious reason is the difficulty in identifying patients with similar lesions who can be entered into controlled studies. Obtaining consent for experimental treatments in poorly responsive patients raises ethical questions about patient protection. Another factor confounding efforts to study treatments for brain edema is that the number of patients with severe edema seen at any one center is generally too small to conduct a randomized study, making costly multicenter studies necessary. Finally, long-term follow-up is necessary to adequately test a new treatment, and many of the studies are short-term.

Because of a lack of evidence-based treatment protocols, current practice, which is empirical, has influenced the treatment of cerebral edema. The two treatments most commonly used are osmotic agents and steroids. The key to the treatment of cerebral edema, which remains largely empirical, is accurate identification of the type of injury. In cytotoxic edema, for example, mannitol and hypertonic saline provide short-term relief to control life-threatening increases in ICP. Another example is the use of a short course of high-dose

steroids to reduce the inflammatory response and vasogenic edema. A common mistake is to use steroids for the treatment of cytotoxic edema in stroke; a large number of studies have documented the futility of steroid treatment in stroke, and they are countraindicated in the treatment of edema secondary to stroke or hemorrhage. In fact, systemic complications of corticosteroids can worsen the condition of patients with intracerebral hemorrhage.[51]

Hypertonic solutions are used to reduce the water content of brain tissue. The first such agent was urea. It is no longer used because it was a small molecule and could enter the brain, where it caused a rebound in CSF pressure.[52] Mannitol is currently the agent of choice for osmotic treatment of brain edema. Initially, it was used in doses of 3 g/kg, which caused marked alterations in the level of serum electrolytes, permitting the use of only one or two doses. More recently, it was found that low doses of mannitol (0.25–1.0 g/kg) are as effective as higher doses without affecting the electrolytes. Noninfarcted regions are mainly affected by the hypertonic solutions rather than the infarcted hemisphere.[53] Mannitol also changes the rheological characteristics of the blood and may have an antioxidant effect. Prolonged administration of mannitol results in an electrolyte imbalance that may override its benefit, and it must be carefully monitored. More recently, hypertonic saline has been advocated for the treatment of cerebral edema.[12] Studies in animals have shown that it lowers ICP, and studies in humans are being done.

Most treatments have been directed at controlling the secondary consequences of brain edema rather than treating the underlying causes. Although not directly aimed at the edema itself, reducing the blood and CSF volumes is used to lower the ICP. Blood volume can be reduced with hyperventilation, which lowers carbon dioxide. However, excessive hyperventilation can cause vasoconstriction and ischemia. Reduction of the CSF volume can be done mechanically by placing a drainage catheter into one of the ventricles, which may be difficult if the cerebral ventricles are compressed by the edema. Agents that reduce the production of CSF, such as acetazolamide or diuretics, may be used, but they are of marginal benefit.

Edema surrounding brain tumors, particularly metastatic brain tumors, responds dramatically to treatment with high doses of dexamethasone, which can be given to control the brain swelling as radiation or surgical treatment is planned. The corticosteroid closes the BBB rapidly. Hence, it is important to obtain contrast-enhanced MRI or CT scans before treatment with corticosteroids; otherwise, enhancement of the lesion may be missed. High doses of corticosteroids have been shown to be effective in brain edema secondary to inflammation in MS; the steroids act by closing the BBB, which can be seen on contrast-enhanced MRI.[54] The opening of the BBB is associated with elevated levels of the proinflammatory cytokine, TNF-α. Inflammatory lesions, such as those that occur in acute attacks of MS, respond well to high-dose methylprednisolone.[55,56] Treatment with 1 g/day of methylprednisolone for 3 to 5 days reduces the inflammatory changes in the blood vessels during an acute exacerbation.[55] Dramatic reduction in enhancement on MRI may be seen after treatment. However, the effect is lost after several months. High- dose steroids reduce the MMP-9 in the brain, as reflected in the CSF, preserving the integrity of the BBB.[57]

Treatment of edema surrounding an intracerebral hemorrhage has recently been intensively studied because of the side effect of hemorrhagic transformation in patients treated with tPA. As in studies of edema secondary to ischemia, a large number of animal studies have documented the use of various agents to reduce edema secondary to hemorrhage. An initial study of recombinant activated factor VII, which enhances clot formation, showed reduction of hemorrhage growth.[58] However, a subsequent study failed to confirm the results of the first one because of a high rate of thrombotic complications, and the use of factor VII remains uncertain.[59]

Except for tPA in the first 3 hours after stroke, no therapy has been shown to be effective. In the absence of effective treatments, efforts are directed at prevention. Treatment of hypertension, diabetes, hyperlipidemia, and coagulopathies and aspirin are accepted preventive measures. Surgeries for carotid stenosis when the symptomatic artery has an occlusion greater than 70% have been shown in a controlled study to be beneficial, but they carry the risk of restenosis.[60,61] Anticoagulation for atrial fibrillation is effective, but the age

limit is controversial. Reduction of edema by hyperosmolar agents, improvement in CBF with hemodilution, and blockade of calcium uptake by calcium entry blockers have not proven useful. Superficial temporal artery to middle cerebral artery bypass was another surgical procedure that was performed for many years without a controlled trial. When the trial was finally done, the procedure was not found to be better than medical treatment for stroke. In a few conditions, such as Moyamoya syndrome, where the blood flow to the brain is compromised, the procedure is thought to be helpful. This is an excellent example of why it is important to conduct controlled trials prior to general use of surgical procedures, particularly if the procedure is very costly and unproven.

MULTIPLE DRUGS FOR TREATMENT OF ISCHEMIA

Complex interrelationships between elements of the molecular cascades of injury and repair have thwarted attempts to find unitary treatments for ischemic and traumatic brain injury. We have learned not only that the individual molecules that are potential targets of treatment are involved, but also that the time at which they are expressed in the molecular cascades of injury is critical. Most of the major molecules have evolved dual functions with an early detrimental effect balanced by a later beneficial one. The challenge of future studies will be to develop paradigms for multiple drug studies that are based on the duality of the natural process. One possible scenario for ischemia could involve the use of agents to reduce the early disruption of the BBB by proteases, an intermediate agent to reduce the inflammatory response, and finally, an agent to enhance angiogenesis and neurogenesis. Such a theoretical scheme is shown in Figure 10–9.

We have described a large number of molecular reactions in the cell cytoplasm, nucleus, and extracellular matrix. They begin and end at different times in the injury cascade. At one point in the cycle these reactions damage tissues, at another they participate in the removal of debris, and over time they contribute to repair. Determining when to inhibit a particular reaction requires an intimate understanding of the stage of the process, the type of injury, and the age and other conditions of the organism. This complexity has confounded studies of novel treatments in the field of stroke and brain injury, and at this time only tPA has U.S.

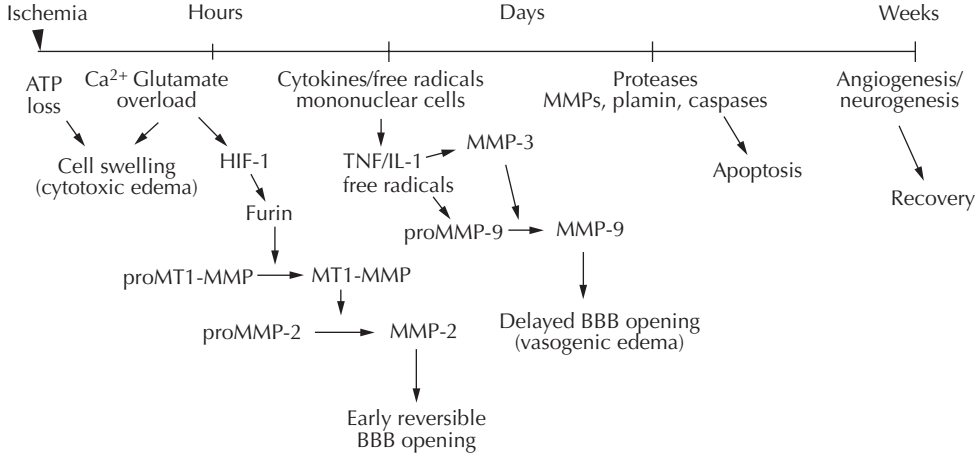

Figure 10–9. Molecular cascade involved in cerebral edema. The time course of events is depicted at the top of the drawing, beginning with the initiating ischemic event and progressing over several weeks. In the first hours there is energy failure, with Ca^{2+} and glutamate entering the cells. The cell swelling produces cytotoxic edema, HIF-1α is activated, and MT1-MMP activates the constitutively expressed MMP-2. Reversible opening of the BBB occurs. After 24 to 48 hours, there is formation of a second group of molecules that turn on cassettes of genes. The cytokines include tumor necrosis factor-α (TNF-α) and interleukin-1β (IL-1β), which activate transcription factors to induce MMP-3 and MMP-9. The second wave of MMPs leads to irreversible damage to the BBB with delayed vasogenic edema. Induction of caspases occurs in the nucleus, and apoptosis takes place. Finally, angiogenesis and neurogenesis participate in the recovery.

Food and Drug Administration approved for the treatment of stroke.

Investigators have puzzled over numerous treatments that work in animal models and fail in the clinic. There are many agents that are currently in the pipeline or actively being tested, but none are approved. One of the major problems is the use of a single animal and a single time point. Proving that drugs block damage at 24 to 48 hours may have little relevance to long-term recovery. A second major impediment to success is the use of a single sex for studies and young animals for stroke studies to test treatments that will be used mainly in elderly individuals. A third factor is the genetic influences in different animal strains and in humans. Spontaneously hypertensive rats (SHR) have a slightly higher incidence of strokes, but modification of the genes further to produce SHR stroke-prone rats increases greatly the likelihood that a stroke will occur. Which of these is the best model in which to test new drugs is unclear; most likely, all of them will be needed. In addition, several species will be needed for testing new agents. Finally, there is the issue of whether to use a permanent occlusion model or one that includes reperfusion. Should the focus of the study be on the early events or on the later recovery phase? Will different drugs be needed at different stages, for persons with different genetic backgrounds, and for both sexes and different ages? Such questions are not trivial. In fact, the early failure of so many studies was caused by an overzealous investigator convincing an industrial sponsor that the short-term animal studies were sufficient to lead to a large clinical trial.

Many investigators are convinced that the current approach to the problem of moving drugs from the laboratory to clinical practice needs radical rethinking. Testing in multiple species is needed. Multiple time periods need to be studied. Different stroke and injury models need to be included, and the variations in sex and age must be carefully balanced. With this more complex approach, more work prior to a clinical trial will be necessary, but targeting drugs that have been more thoroughly tested will reduce the major costs involved in clinical trials.

Treatment in the recovery phase offers opportunities beyond the limited time frame of the acute injury. Angiogenesis and neurogenesis begin within the first week after an injury and continue for several weeks. The same molecular events that amplify the injury are often involved in this phase. Angiogenesis initially leads to a blood vessel that has not completely formed tight junctions and could be contributing to edema formation.[62] An example of the dual nature of growth factors is VEGF. Released under the influence of HIF in the early stages of an injury, VEGF is a key molecule in the formation of new vessels. It also contributes to the early opening of the BBB, and while it is acting, vessels remain permeable. Thus, it is not considered a good target for treatment except at the early stages, and how this will affect the later recovery phase becomes a major problem.

Astrocytes secrete growth factors that contribute to the survival of neurons and oligodendrocytes, but they also form a glial scar that restricts axonal growth. Microglia are major players in early tissue destruction by secreting potent enzymes that remove debris from an injury site; later, they contribute to the healing process in ways that are just beginning to be understood. It appears that as the extracellular matrix undergoes remodeling, microglia provide essential growth factors to facilitate that process. In addition, they release proteases that are essential for matrix remodeling. These proteases, if released in the white matter, attack myelin, causing bystander demyelination, but curbing the delayed inflammatory response may impede recovery.

Taking into account the dual nature of the inflammatory response in the design of treatment trials provides a unique challenge. When does the beneficial aspect of inflammation replace the detrimental phase? What part of the initial inflammatory phase should be contained, and how can the later benefits of inflammation be preserved and augmented? Answers to these important questions are beginning to emerge from studies of the natural course of the illness.

As the injury begins, the influx of calcium turns on a number of genes that participate in the full spectrum of injury and recovery. If the calcium levels remain elevated for an extended period of time, irreversible apoptotic events are initiated. Levels of calcium remain elevated by excessive extracellular levels of glutamate. Intact astrocytes take up the excess glutamate as long as they are viable. Protective mechanisms can be overwhelmed at this early stage, laying the foundation for later cell death. If the

cell survives this initial insult caused by loss of ATPase, increase of glutamate extracellularly, and increase of calcium and sodium intracellularly, the surviving astrocytes and microglia release the next wave of cytokines and growth factors that begin tissue repair.

At this stage, free radicals and proteases, which had participated in the cleanup, take on a new role as the repair process begins. Initial injury to the synapses, which occurs during ischemia, has the potential to reverse.[63] Loss of synapses most likely is an important mechanism for the cognitive impairment that results from injury.[64]

Neurons are highly vulnerable to ischemic/hypoxic injury, dying early by necrosis and later by apoptosis. Other cellular elements are less vulnerable. Astrocytes can survive on stores of glycogen, and endothelial cells have a higher tolerance of ischemia. In the core of the injury cell death is extensive, and within several days, masses of macrophages are found in the regions of the dead cells. It is likely that factors secreted by the microglia/macrophages contribute to the astroglial scar that walls off the dead cells. New vessels grow into the core region in much the same way as they do into any wound. Proteases acting in conjunction with free radicals clear the path for the growing vessels. Tight junction proteins are released from astrocytes to aid in creating competent vessels. Scar tissue forms a wall of astrocytes around the lesion.

At some stage, depending on the age of the patient, migration of cells toward the site of the lesion takes place. Some of these are pluripotential stem cells that will grow into mature cells.[65,66] Many laboratories are attempting to find ways to augment the growth of these cells or to introduce new ones to take over the function of those that are damaged. Still in an infant phase, stem cell biology holds the promise of restorative function, although it is still many years away from clinical use.

Recovery after stroke occurs most rapidly in the first month, with slower progress in the second and third months. Even up to 1 to 2 years after the initial insult, some recovery of function can occur. Most often these are younger patients with traumatic brain injury. Occasionally, an individual in a prolonged, minimally conscious state for several years regains some function. Such cases are rare and result in individual case reports, but they show the ongoing plasticity of the brain.[67]

REFERENCES

1. Klatzo I. Presidental address. Neuropathological aspects of brain edema. *J Neuropathol Exp Neurol*. 1967;26:1–14.
2. Fishman RA. Brain edema. *N Engl J Med*. 1975;293: 706–711.
3. Stiver SI, Gean AD, Manley GT. Survival with good outcome after cerebral herniation and duret hemorrhage caused by traumatic brain injury. *J Neurosurg*. 2009;110:1242–1246.
4. Moseley ME, Cohen Y, Mintorovitch J, et al. Early detection of regional cerebral ischemia in cats: comparison of diffusion- and T2-weighted mri and spectroscopy. *Magn Reson Med*. 1990;14:330–346.
5. Rosenberg GA, Kyner WT, Estrada E. Bulk flow of brain interstitial fluid under normal and hyperosmolar conditions. *Am J Physiol*. 1980;238:F42-F49.
6. Agre P, Kozono D. Aquaporin water channels: molecular mechanisms for human diseases. *FEBS Lett*. 2003;555:72–78.
7. Jarius S, Paul F, Franciotta D, et al. Mechanisms of disease: aquaporin-4 antibodies in neuromyelitis optica. *Nat Clin Pract Neurol*. 2008;4:202–214.
8. Verkman AS. Aquaporins: translating bench research to human disease. *J Exp Biol*. 2009;212:1707–1715.
9. Tait MJ, Saadoun S, Bell BA, et al. Water movements in the brain: role of aquaporins. *Trends Neurosci*. 2008;31:37–43.
10. Mylonakou MN, Petersen PH, Rinvik E, et al. Analysis of mice with targeted deletion of aqp9 gene provides conclusive evidence for expression of aqp9 in neurons. *J Neurosci Res*. 2009;87:1310–1322.
11. Badaut J, Lasbennes F, Magistretti PJ, et al. Aquaporins in brain: distribution, physiology, and pathophysiology. *J Cereb Blood Flow Metab*. 2002;22:367–378.
12. Zeynalov E, Chen CH, Froehner SC, et al. The perivascular pool of aquaporin-4 mediates the effect of osmotherapy in postischemic cerebral edema. *Crit Care Med*. 2008;36:2634–2640.
13. Manley GT, Fujimura M, Ma T, et al. Aquaporin-4 deletion in mice reduces brain edema after acute water intoxication and ischemic stroke. *Nat Med*. 2000;6:159–163.
14. Zador Z, Bloch O, Yao X, et al. Aquaporins: role in cerebral edema and brain water balance. *Prog Brain Res*. 2007;161:185–194.
15. Amiry-Moghaddam M, Otsuka T, Hurn PD, et al. An alpha-syntrophin-dependent pool of aqp4 in astroglial end-feet confers bidirectional water flow between blood and brain. *Proc Natl Acad Sci USA*. 2003;100: 2106–2111.
16. Amiry-Moghaddam M, Xue R, Haug FM, et al. Alpha-syntrophin deletion removes the perivascular but not endothelial pool of aquaporin-4 at the blood-brain barrier and delays the development of brain edema in an experimental model of acute hyponatremia. *FASEB J*. 2004;18:542–544.
17. Papadopoulos MC, Manley GT, Krishna S, et al. Aquaporin-4 facilitates reabsorption of excess fluid in vasogenic brain edema. *FASEB J*. 2004;18: 1291–1293.
18. Papadopoulos MC, Saadoun S, Binder DK, et al. Molecular mechanisms of brain tumor edema. *Neuroscience*. 2004;129:1011–1020.

19. Mandler RN, Davis LE, Jeffery DR, et al. Devic's neuromyelitis optica: a clinicopathological study of 8 patients. *Ann Neurol*. 1993;34:162–168.
20. Endres M, Laufs U, Liao JK, et al. Targeting enos for stroke protection. *Trends Neurosci*. 2004;27:283–289.
21. Iadecola C, Zhang F, Xu S, et al. Inducible nitric oxide synthase gene expression in brain following cerebral ischemia. *J Cereb Blood Flow Metab*. 1995;15: 378–384.
22. Gursoy-Ozdemir Y, Bolay H, Aribas O, et al. Role of endothelial nitric oxide generation and peroxynitrite formation in reperfusion injury after focal cerebral ischemia. *Stroke*. 2000;31(8):1974–1980; discussion 1981.
23. Huang Z, Huang PL, Panahian N, et al. Effects of cerebral ischemia in mice deficient in neuronal nitric oxide synthase. *Science*. 1994;265:1883–1885.
24. Huang Z, Huang PL, Ma J, et al. Enlarged infarcts in endothelial nitric oxide synthase knockout mice are attenuated by nitro-l-arginine. *J Cereb Blood Flow Metab*. 1996;16:981–987.
25. Chan PH, Fishman RA, Wesley MA, et al. Pathogenesis of vasogenic edema in focal cerebral ischemia. Role of superoxide radicals. *Adv Neurol*. 1990;52:177–183.
26. Kourie JI. Interaction of reactive oxygen species with ion transport mechanisms. *Am J Physiol*. 1998;275:C1-C24.
27. Heo JH, Han SW, Lee SK. Free radicals as triggers of brain edema formation after stroke. *Free Radic Biol Med*. 2005;39:51–70.
28. Reddy MK, Labhasetwar V. Nanoparticle-mediated delivery of superoxide dismutase to the brain: an effective strategy to reduce ischemia-reperfusion injury. *FASEB J*. 2009;23:1384–1395.
29. Kinouchi H, Epstein CJ, Mizui T, et al. Attenuation of focal cerebral ischemic injury in transgenic mice overexpressing cuzn superoxide dismutase. *Proc Natl Acad Sci USA*. 1991;88:11158–11162.
30. Chan PH, Epstein CJ, Li Y, et al. Transgenic mice and knockout mutants in the study of oxidative stress in brain injury. *J Neurotrauma*. 1995;12:815–824.
31. Kamada H, Yu F, Nito C, et al. Influence of hyperglycemia on oxidative stress and matrix metalloproteinase-9 activation after focal cerebral ischemia/reperfusion in rats: relation to blood-brain barrier dysfunction. *Stroke*. 2007;38:1044–1049.
32. Wong CH, Bozinovski S, Hertzog PJ, et al. Absence of glutathione peroxidase-1 exacerbates cerebral ischemia-reperfusion injury by reducing post-ischemic microvascular perfusion. *J Neurochem*. 2008;107: 241–252.
33. Kahles T, Luedike P, Endres M, et al. Nadph oxidase plays a central role in blood-brain barrier damage in experimental stroke. *Stroke*. 2007;38:3000–3006.
34. Tang J, Liu J, Zhou C, et al. Role of nadph oxidase in the brain injury of intracerebral hemorrhage. *J Neurochem*. 2005;94:1342–1350.
35. Jian LK, Rosenberg GA. Matrix metalloproteinases and free radicals in cerebral ischemia. *Free Radic Biol Med*. 2005;39:71–80.
36. Yamamoto N, Yokota K, Yamashita A, et al. Effect of kbt-3022, a new cyclooxygenase inhibitor, on experimental brain edema in vitro and in vivo. *Eur J Pharmacol*. 1996;297:225–231.
37. Chu K, Jeong SW, Jung KH, et al. Celecoxib induces functional recovery after intracerebral hemorrhage with reduction of brain edema and perihematomal cell death. *J Cereb Blood Flow Metab*. 2004;24: 926–933.
38. Candelario-Jalil E, Gonzalez-Falcon A, Garcia-Cabrera M, et al. Post-ischaemic treatment with the cyclooxygenase-2 inhibitor nimesulide reduces blood-brain barrier disruption and leukocyte infiltration following transient focal cerebral ischaemia in rats. *J Neurochem*. 2007;100:1108–1120.
39. Thurston G. Complementary actions of vegf and angiopoietin-1 on blood vessel growth and leakage. *J Anat*. 2002;200:575–580.
40. Ballabh P, Xu H, Hu F, et al. Angiogenic inhibition reduces germinal matrix hemorrhage. *Nat Med*. 2007;13:477–485.
41. Valable S, Montaner J, Bellail A, et al. Vegf-induced bbb permeability is associated with an mmp-9 activity increase in cerebral ischemia: both effects decreased by ang-1. *J Cereb Blood Flow Metab*. 2005;25: 1491–1504.
42. Wang W, Dentler WL, Borchardt RT. Vegf increases bmec monolayer permeability by affecting occludin expression and tight junction assembly. *Am J Physiol Heart Circ Physiol*. 2001;280:H434-H440.
43. Dawson JW. The histology of disseminated sclerosis. *Trans R Soc Edin*. 1916;50:517–525.
44. Trapp BD, Bo L, Mork S, et al. Pathogenesis of tissue injury in ms lesions. *J Neuroimmunol*. 1999;98:49–56.
45. Trapp BD, Stys PK. Virtual hypoxia and chronic necrosis of demyelinated axons in multiple sclerosis. *Lancet Neurol*. 2009;8:280–291.
46. Sigmund EE, Gutman D. Diffusion-weighted imaging of the brain at 7 t with echo-planar and turbo spin echo sequences: preliminary results. *Magn Reson Imaging*. 2011;29:752–765.
47. Haacke EM. Susceptibility weighted imaging (swi). *Z Med Phys*. 2006;16:237.
48. Mittal S, Wu Z, Neelavalli J, et al. Susceptibility-weighted imaging: technical aspects and clinical applications, part 2. *AJNR Am J Neuroradiol*. 2009;30: 232–252.
49. Rabinstein AA. Treatment of cerebral edema. *Neurologist*. 2006;12:59–73.
50. Cooper DJ, Rosenfeld JV, Murray L, et al. Decompressive craniectomy in diffuse traumatic brain injury. *N Engl J Med*. 2011;364:1493–1502.
51. Qureshi AI, Tuhrim S, Broderick JP, et al. Spontaneous intracerebral hemorrhage. *N Engl J Med*. 2001;344:1450–1460.
52. Pappius HM, Dayes LA. Hypertonic urea: its effect on the distribution of water and electrolytes in normal and edematous brain tissues. *Arch Neurol*. 1965;13: 395–402.
53. Videen TO, Zazulia AR, Manno EM, et al. Mannitol bolus preferentially shrinks non-infarcted brain in patients with ischemic stroke. *Neurology*. 2001;57: 2120–2122.
54. Noseworthy JH, Lucchinetti C, Rodriguez M, et al. Multiple sclerosis. *N Engl J Med*. 2000;343:938–952.
55. Kermode AG, Thompson AJ, Tofts P, et al. Breakdown of the blood-brain barrier precedes symptoms and other mri signs of new lesions in multiple sclerosis. Pathogenetic and clinical implications. *Brain*. 1990;113:1477–1489.
56. Broom KA, Anthony DC, Blamire AM, et al. Mri reveals that early changes in cerebral blood volume precede blood-brain barrier breakdown and overt

pathology in ms-like lesions in rat brain. *J Cereb Blood Flow Metab*. 2005;25:204–216.
57. Rosenberg GA, Dencoff JE, Correa N Jr, et al. Effect of steroids on csf matrix metalloproteinases in multiple sclerosis: relation to blood-brain barrier injury. *Neurology*. 1996;46:1626–1632.
58. Mayer SA, Brun NC, Begtrup K, et al. Efficacy and safety of recombinant activated factor VII for acute intracerebral hemorrhage. *N Engl J Med*. 2008;358:2127–2137.
59. Mayer SA, Davis SM, Skolnick BE, et al. Can a subset of intracerebral hemorrhage patients benefit from hemostatic therapy with recombinant activated factor VII? *Stroke*. 2009;40:833–840.
60. Barnett HJ, Taylor DW, Eliasziw M, et al. Benefit of carotid endarterectomy in patients with symptomatic moderate or severe stenosis. North American symptomatic carotid endarterectomy trial collaborators. *N Engl J Med*. 1998;339:1415–1425.
61. Bonati LH, Ederle J, McCabe DJ, et al. Long-term risk of carotid restenosis in patients randomly assigned to endovascular treatment or endarterectomy in the Carotid and Vertebral Artery Transluminal Angioplasty Study (cavatas): long-term follow-up of a randomised trial. *Lancet Neurol*. 2009;8:908–917.
62. Teng H, Zhang ZG, Wang L, et al. Coupling of angiogenesis and neurogenesis in cultured endothelial cells and neural progenitor cells after stroke. *J Cereb Blood Flow Metab*. 2008;28:764–771.
63. Zhang S, Boyd J, Delaney K, et al. Rapid reversible changes in dendritic spine structure in vivo gated by the degree of ischemia. *J Neurosci*. 2005;25:5333–5338.
64. Szklarczyk A, Lapinska J, Rylski M, et al. Matrix metalloproteinase-9 undergoes expression and activation during dendritic remodeling in adult hippocampus. *J Neurosci*. 2002;22:920–930.
65. Wang L, Zhang ZG, Zhang RL, et al. Matrix metalloproteinase 2 (mmp2) and mmp9 secreted by erythropoietin-activated endothelial cells promote neural progenitor cell migration. *J Neurosci*. 2006;26:5996–6003.
66. Kokovay E, Li L, Cunningham LA. Angiogenic recruitment of pericytes from bone marrow after stroke. *J Cereb Blood Flow Metab*. 2006;26:545–555.
67. Cramer SC. Brain repair after stroke. *N Engl J Med*. 2010;362:1827–1829.

Chapter 11

Intracerebral Hemorrhage

INTRODUCTION

Intracerebral hemorrhage (ICH) is the least frequent of the three major types of stroke, but it is the most deadly.[1] Occurring in 10% to 15% of patients with stroke, ICH is the major cause of death and disability.[2] Neuroimaging with computed tomography (CT) and magnetic resonance imaging (MRI) has dramatically changed the way we view a hemorrhagic mass lesion. Both CT and MRI show sites of bleeding and allow the sequence of events leading up to the formation of a mass lesion to be readily visualized. Prior to the development of modern neuroimaging methods, intracranial bleeding was considered a devastating illness with dramatic symptoms. Computed tomography scans reveal that many patients thought to have small thromboses because of the limited nature of the symptoms actually have small bleeds. In the pre-CT era, the cause of the hemorrhage rarely was resolved, even at autopsy, because the large hemorrhages obscured the mechanisms at the onset of the insult.

The hemorrhagic mass is due either to the rupture of a blood vessel or the breakdown of tissue after a cerebral infarction. Two major theories grew out of early pathological studies to explain the occurrence of an ICH. One involved the rupture of an aneurysmal dilatation on a blood vessel damaged by hypertension, while the other was that the infarcted tissue had undegone hemorrhagic transformation. This controversy was resolved when CT scanning revealed a group of patients with early development of a large mass most likely due to a vessel rupture, which we now refer to as a *primary ICH*. By contrast, in some stroke patients, the initial CT scan shows no blood, but over several hours to days, a mottled pattern of bleeding is seen, indicating that the infarcted tissue has undergone hemorrhagic transformation.

Nontraumatic hemorrhages are most commonly due to hypertensive damage to the blood vessels with bleeding from the small perforating vessels in the basal ganglia.[4] The three main sites of ICH are the basal ganglia, the cerebellum, and the pons. When those sites are involved, the ICH is generally due to hypertensive damage to the vessel wall. In addition to hypertensive small vessel disease, other clinical causes of ICH include vascular malformations, tumors that bleed, blood dyscrasias, coagulation defects, and amyloid angiopathy.[5] Intracranial bleeding outside the main sites of hypertensive bleeds suggests one of these causes: vascular malformations can bleed in any location in the brain; cavernous hemagiomas and amyloid angiopathy can have numerous microbleeds, which can be visualized by susceptibility-weighted MRI (T2* echo gradient).

New definitions of ICH emerged that take into account the underlying etiology and the rapidity of the emergence of the mass lesion. When the accumulation of blood is rapid and the mass lesion is seen on the initial CT scan, the term *primary ICH* is often used. However, when the hemorrhage begins as a region of infarct and subsequently evolves into a mass lesion, the term *secondary ICH* is used. This secondary hemorrhage implies that the hemorrhagic mass begins as an ischemic injury, progresses through a stage of bleeding, and results in a mass lesion, a process that is best defined as hemorrhagic transformation. Serial CT scans have demonstrated growth of the lesion over time.[6]

HISTORY OF ICH

In the 1800s, Durand-Fardell proposed that ICH originated in a previously disorganized brain substance[7] (Table 11–1). Early pathologists observed red blood cells outside intact blood vessels, which were termed *ball hemorrhages*; they appeared to exit blood vessels by "walking across" them, or diapedesis. Bouchard, working with Charcot, observed dilatations of the small hypertensive vessels in the basal ganglia and proposed that there were aneurysms on these arteries that ruptured. This remained a dominant theory of the origin of ICH up to the present (Figure 11–1). More recently, Fisher and Adams proposed that cardioembolic strokes have an increased likelihood of undergoing hemorrhagic transformation than thromboses based on a series of autopsy cases.[8] They studied 373 brains with vascular occlusion. Sixty-six had hemorrhagic transformation, with all but three having a source of emboli. The investigators also noted that the emboli lodged in a proximal artery gave rise to bland infarctions, while those with hemorrhagic transformation had emboli in distal branches, suggesting that a large embolus had broken up and fragments had lodged distal to the bleeding areas. They concluded that the "fragmentation of the embolic material . . . exposes the necrotic tissue to the full forces of arterial blood pressure with resulting hemorrhages from damaged capillaries." Thus, tissue distal to the occlusion was preserved from ICH, while reperfusion of the infarcted regions resulted in hemorrhagic transformation.

Figure 11–1. An original drawing of the aneurysmal dilatation on a artery that is thought to be the site of bleeding in basal ganglia hemorrhages. The drawing is from the frontispiece of the book *The Miliary Aneurysms of Charcot and Bouchard*. From Charcot J-M, *Clinical Lectures on Senile and Chronic Diseases*, [translated by WS Tuke]. London: The New Sydenham Society; 1881.

Table 11–1 **Landmarks in the Development of Early ICH Concepts**

Cruveilhier (1829) separated ICH into aneurysm and vessel breakdown
Rochoux (1814) and Durand-Fardell (1854) described diapedesis ('jumping across')-damaged vessels
Virchow (1857), Charcot (1881), and Bouchard (1866) described rupture of miliary aneurysms
Rosenblath (1927) related bleeding to an enzymatic substance (German: "stuff")

MOLECULAR MECHANISMS IN ICH

Computed tomography scans performed very early after the onset of symptoms revealed a group of patients who had no bleeding seen on the initial scan; however, subsequent scans showed a well-developed mass lesion, suggesting rapid conversion of the infarcted tissues into a hemorrhagic mass.[9] In a prospective MRI study of 200 patients with cardioembolic stroke, 41 had CT-proven supratentorial infarcts due to cardiogenic embolism; MRI 3 weeks after the stroke in 35 of these 41 patients showed hemorrhagic transformation in 68.6%, suggesting that hemorrhagic transformation is common in medium-sized and large cardioembolic infarcts.[10] In a study of 103 patients who were excluded from treatment with tissue plasminogen activator because of bleeding on CT, enlargement of the initial hemorrhage occurred in 26% within the first hour, while 38% had an increase in the size of the hemorrhage by 20 hours, and those patients who demonstrated enlargement of the mass had a greater likelihood of undergoing clinical deterioration.[11] Irregular hematoma shape and density heterogeneity, reflecting active multifocal bleeding or a variable bleeding time course, predicted ICH growth; large ICHs were significantly more irregular in shape, were heterogeneous in density, and had greater growth.[6]

The size of the hemorrhagic mass further contributes to the pathophysiology since larger masses cause greater damage, not only from increased levels of toxic blood products, but also due to the increased compression exerted on the tissues surrounding the lesion. Recently, it has been argued that small bleeds may actually protect brain tissue because of preconditioning of the brain to blood components, while large bleeds lead to secondary damage.[12] Studies in experimental animals using a variety of methods to induce ischemia with reperfusion implicate reperfusion in blood-brain barrier (BBB) disruption with hemorrhage, which follows a pattern of biphasic opening.[13] Hemorrhagic transformation is often seen 48 to 72 hours after a large region of cerebral ischemia develops. Occasionally, hemorrhage into the reperfused region is seen after endarterectomy (Figure 11–2). Whether this is due to the pressure on the blood vessel wall that is suddenly exerted when the blockage is removed or to infarction during the operative procedure is uncertain. Fortunately, bleeding after endarterectomy is a rare event.

The injury cascade results in the activation of genes responsible for the production and activation of various proteolytic enzymes. Several proteases are involved in the fibrinolytic and coagulation systems, such as urokinase- and tissue-type plasminogen activators (uPA and tPA). These proteases are important in both normal and pathological processes, including clot lysis, angiogenesis, and remodeling of the extracellular matrix. The plasminogen activators interact with the matrix metalloproteinases (MMPs) to induce a variety of toxic effects on brain cells and blood vessels.[14] The MMPs and

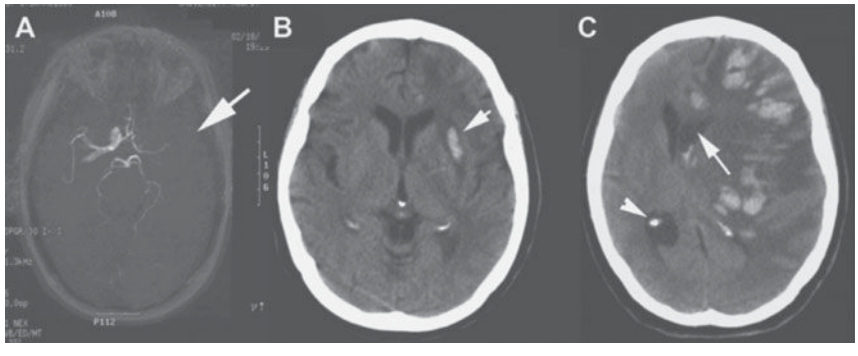

Figure 11–2. Hemorrhagic transformation after carotid endarterectomy. (**A**) Axial view of an arteriogram showing the lack of filling on the left side of the brain (arrow). (**B**) Five days after surgery, a small bleed is seen in the left basal ganglia (arrow). (**C**) Seven days after surgery, extensive bleeding is seen in the region of the small bleed. There is a shift of the ventricles due to the mass effect (arrow) and dilatation of the opposite temporal horn from compression of the aqueduct of Sylvius (arrowhead).

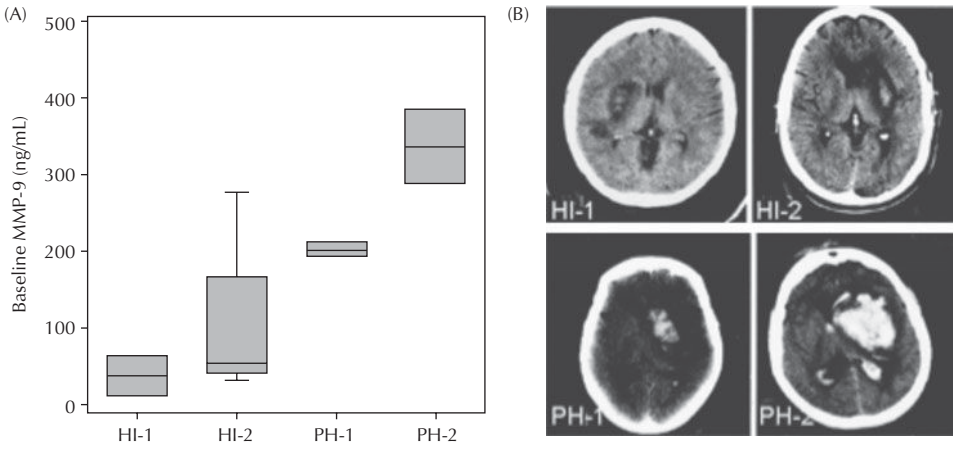

Figure 11–3. Correlation of levels of plasma MMP-9 and extent of ICH. HI is hemorrhagic transformation and PH is parenchymal hemorrhage. HI-1 is minimal hemorrhagic transformation and HT-2 is more extensive transformation. PH-1 indicates a small ICH, while PH-2 denotes extensive bleeding. The graph to the left shows the levels of MMP-9 measured in the blood. There was a dramatic increase in MMP-9 levels corresponding to the size of the intracranial bleeding. (Modified from Ref. 15.)

thrombin are the two proteases that have been most extensively studied in ICH. In patients with cardioembolic stroke, elevation of MMP-9 predicts hemorrhagic transformation and parenchymal hemorrhage[15] (Figure 11–3).

Ischemia with reperfusion leads to fibrinogen, complement, and thrombin entry into the brain across a compromised BBB, initiating an extravascular coagulation cascade. Toxic products from serum and lysed red blood cells, such as the coagulation cascade enzymes, thrombin and plasmin, induce secondary edema and amplify the inflammatory response.[16] As a result, hemorrhagic areas may consolidate into a mass lesion, and the blood products further facilitate the formation of cerebral edema.

Several blood products have been implicated in the secondary inflammatory response that leads to cerebral edema and BBB damage. The coagulation cascade enzymes, thrombin and plasmin, are pleuripotential molecules that act on cells directly and indirectly by activation of other proteases. Injection of thrombin into the brain produces a focal increase in brain water content (Figure 11–4). Thrombin stimulates the production of hypoxia-inducing factor-1α (HIF-1α) and induces the tumor suppressor gene, p53, which promotes apoptosis.[17] In addition to proteases, free radicals are thought to be involved in the hemorrhagic injury. The evidence of free radical involvement is indirect and comes from studies showing that free radical scavengers and spin trap agents reduce the bleeding and improve function in animal models.[18]

CLINICAL ASPECTS OF INTRACRANIAL BLEEDING

Chronic hypertension produces a small vessel vasculopathy characterized by lipohyalinosis, fibrinoid necrosis, and development of

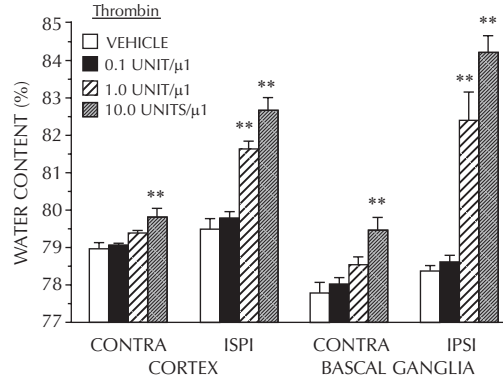

Figure 11–4. Bar graph depicting the water content (percentage of wet weight) in the cortex and basal ganglia contralateral (CONTRA) and ipsilateral (IPSI) to the site of intracerebral injection of 10 μL solutions of 0, 0.1, 1, and 10 U/μL of thrombin. The values shown are expressed as the mean ± standard error of the mean. ** $p < .01$. (From Ref. 46.)

Charcot-Bouchard aneurysms, affecting penetrating arteries throughout the brain including lenticulostriates, thalamoperforators, paramedian branches of the basilar artery, superior cerebellar arteries, and anterior inferior cerebellar arteries. Predilection sites for intracerebral hemorrhage include the basal ganglia, pons, and cerebellum. Intraventricular hemorrhage occurs in one-third of intracerebral hemorrhage patients from extension of thalamic ganglionic bleeding. Isolated intraventricular hemorrhages infrequently arise from subependymal structures including the germinal matrix in newborns, arteriovenous malformations, and cavernous angiomas. Premature infants are at risk of intraventricular hemorrhages from the germinal matrix, which can cause secondary hydrocephalus.

Pathological changes can occur in the vessels without hypertension. Amyloid deposits in the vessel wall can occur with aging or with forms of familial amyloid angiopathy. Often the amyloid-damaged vessels are seen in the occipital regions. Bleeding around the vessels leads to hemosiderin deposits that can be seen on MRI susceptibility-weighted sequences (T2* gradient echo). These small regions of bleeding have been named *microbleeds*; they are variable in number. Microbleeds seen on MRI represent only a small fraction of those seen in the brain at autopsy. Because of the tendency of these vessels to bleed, some neurologists are concerned about the use of antiplatelet agents, which may increase the risk of bleeding; anticoagulants are not recommended. When intracranial bleeding takes place in the occipital regions, amyloid angiopathy should be suspected. Lobar hemorrhages in younger patients are mainly due to arteriovenous malformations or cavernous hemangiomas. Rarely, an intracranial bleed is due to blood dyscrasia. Children with leukemia are at risk of ICH. Cancer patients with coagulation defects that reduce platelet levels or cause disseminated intravascular clotting are at greater risk for ICH. Tumors can bleed and present as a primary ICH; metastatic melanomas, metastatic tumors from the kidney, hemangioblastic meningiomas, and rapidly growing glioblastomas can outgrow their vascular supply, resulting in bleeding.

When an aneurysm on the middle cerebral artery located in the Sylvian fissure ruptures, it can appear to be an ICH, but the mass is outside the parenchyma, pressing on the surrounding tissue, making it similar to a subdural hematoma. This is a surgical emergency that requires evacuation of the extraparenchymal mass and repair of the aneurysm (Figure 11–5). Other surgically remedial intracerebral hemorrhages are those in the posterior fossa due to cerebellar hemorrhage, which have either compressed the fourth ventricle, causing hydrocephalus, or have damaged the brainstem (Figure 11–6).

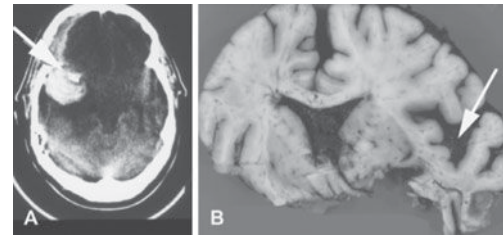

Figure 11–5. Patient with bleed secondary to a middle cerebral artery aneurysm in the Sylvian fissure. (**A**) A CT scan showing the round-appearing bleed with a dense calcified aneurysm (arrow). (**B**) Postmortem brain section demonstrating the location of the blood outside the brain, producing a subdural-like compression of the tissue that appears as an intraparenchymal mass (arrow). The extraparenchymal aspect of the mass was mistaken for a primary ICH; the patient was not operated on and subsequently died.

Magnetic resonance imaging is as sensitive as CT in identifying blood in ICH. In one multicenter study of acute stroke within 6 hours

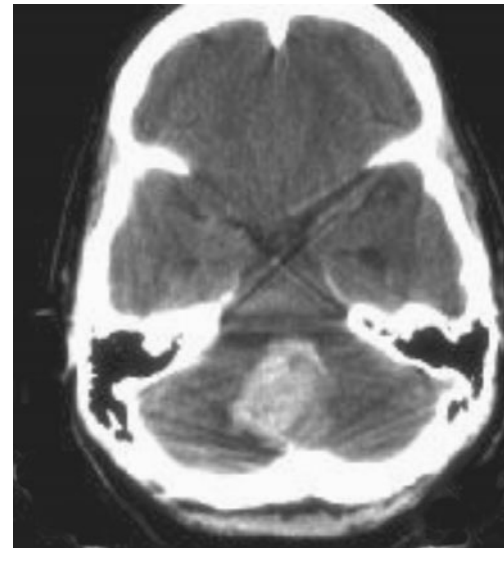

Figure 11–6. Computed tomographic image from patient with large cerebellar hemorrhage that compresses the brainstem.

of onset, gradient-echo MRI was as accurate as CT for the identification of acute hemorrhage and more accurate for the identification of chronic hemorrhage.[19] Blood has characteristic appearances on both imaging modalities at each stage (acute, subacute, and chronic), and it is important to be familiar with the appearance of various types of intracranial hemorrhage on CT and MRI and their clinical implications. The MR signal characteristics of intracranial hemorrhage are determined by the paramagnetic effects of the breakdown products of hemoglobin, the magnetic field strength, and the pulse sequence[20] (Table 11–2). The breakdown products of hemoglobin have different oxidation states of iron, producing different magnetic properties. Oxygenated hemoglobin, which has no unpaired electrons and is diamagnetic, is present in the hyperacute stage, and the hematoma is isointense or hyperintense on T1-weighted MRI and hyperintense on T2-weighted MRI owing to the hemoglobin content. Deoxyhemoglobin has few unpaired electrons and is paramagnetic; consequently, in the acute stage, the hemorrhage is isointense or hypointense on T1-weighted MRI and hypointense on T2-weighted MRI. Methemoglobin is paramagnetic and confined to the intracellular compartment, with a magnetic gradient between those of the intracellular and extracellular compartments, appearing hyperintense on T1-weighted MRI and hypointense on T2-weighted MRI. In the late subacute stage, when methemoglobin is released by lysis of the red blood cells, the magnetic gradient between the intracellular and extracellular compartments is lost, and hemorrhage is hyperintense on T1-weighted and T2-weighted MRI. Hemosiderin is found in the chronic phase; it has many unpaired electrons and is superparamagnetic, making the hemorrhage hypointense on T1-weighted and T2-weighted MRI.

Gradient recall MRI has the ability to detect not only acute and chronic hematomas but also old, clinically silent cerebral microbleeds. Microbleeds are generally defined as punctate, homogeneous, rounded, hypointense lesions in the parenchyma that are smaller than 5–10 mm (Figure 11–7). Pathological studies have shown that microbleeds seen with gradient recall echo MRI usually correspond to hemosiderin-laden macrophages adjacent to small vessels and are indicative of previous extravasation of blood. Microbleeds have been seen in up to 80% of patients with primary intracerebral hemorrhage, 21%–26% of patients with ischemic stroke, and 5%–6% of asymptomatic or healthy elderly individuals. Hypertension, cerebral amyloid angiopathy, getting older, and, less commonly, cerebral autosomal dominant arteriopathy with silent infarcts and leukoaraiosis (CADASIL) have been identified as important risk factors for microbleeds.[21]

Table 11–2 **Changes in MRI Patterns Seen in the Stages of Blood Formation After ICH**

	CT	T1-Weighted MRI	T2-Weighted MRI	MRI FLAIR	GRE MRI
Hyperacute (<12 hours)	Hyperdense	Isointense or mildly hyperintense	Hyperintense	Hyperintense	Hypointense rim
Acute (12 hours to 2 days)	Hyperdense	Isointense or hypointense	Hypointense	Hypointense	Hypointense rim that gradually progresses to the center
Early subacute (2–7 days)	Hyperdense	Hyperintense	Hypointense	Hypointense	Hypointense
Late subacute (8 days to1 month)	Isodense	Hyperintense	Hyperintense	Hyperintense	Hypointense
Chronic (>1 month)	Hypodense	Isointense or hypointense	Hypointense	Hypointense	Slit-like hyperintense or isointense core surrounded by a hypointense rim

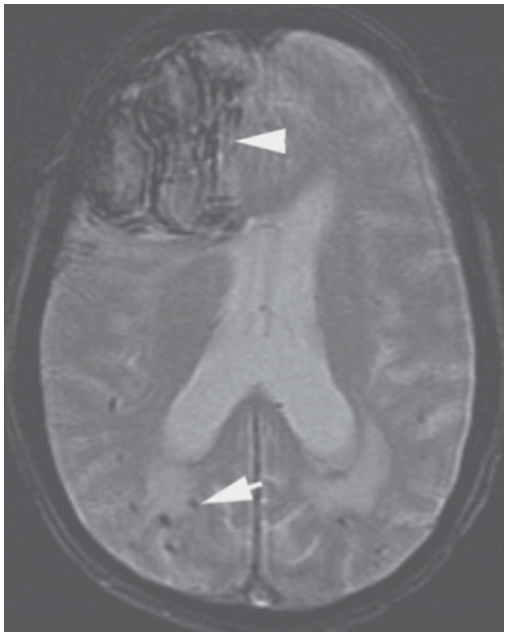

Figure 11–7. T2* gradient echo MRI image of a patient with microbleeds (arrow) and a large ICH in the frontal region (arrowhead). There are white matter hyperintensities around the posterior horns of the lateral ventricle, which are thought to increase the risk of ICH from amyloid angiopathy.

Except for several isolated instances when surgical evacuation of a large intracranial collection of blood is indicated, such as cerebellar hemorrhages larger than 3 cm and causing hydrocephalus and/or brainstem compression, and lobar hemorrhages due to arteriovenous malformations or ruptured aneurysms, the current treatment options for ICH are mainly supportive. In spite of many trials of surgical treatments dating from the 1960s to the present, there is no evidence that removing a hemorrhagic mass is beneficial.[22]

Cerebellar hemorrhage is a life-threatening condition and one of the few stroke syndromes that benefits from surgery. Fisher et al. described the clinical features of cerebellar hemorrhage and the cardinal features of ataxia, cranial nerve palsies, and hemiparesis that indicated brainstem compression and signaled the need for surgery for a potentially life-threatening situation.[23] This remarkable paper appeared before the introduction of CT and MRI, when the decision to operate to remove a possible mass lesion in the posterior fossa had to be made quickly and accurately if death was to be prevented. More recently, the use of CT and MRI has removed some of the uncertainty in the diagnosis, but the diagnosis can be difficult, particularly when a single symptom, such as vertigo, is the only warning of the mass in the cerebellum, and the treatment is still controversial. The key to successful treatment is twofold: (1) suspicion of a cerebellar bleed based on the sequence of events, as revealed by the history rather than reliance on the examination alone, and (2) the correct choice of imaging modalities. Even with the most careful history, neurological examination, and MRI scan with attention to the posterior fossa, criteria for selection of patients for surgery and timing of the surgery differ among neurosurgeons.

Following Fisher et al.'s report, several large series of patients showed the treacherous course of the illness, with death occurring either rapidly from early brainstem compression or after a delay due to the consequences of the mass impinging on the brainstem from below and the hydrocephalus distorting the brainstem from above.[24] The typical patient with cerebellar hemorrhage is hypertensive. At the onset, there is a severe headache followed shortly by difficulty walking due to the cerebellar lesion. An interval of 24 to 48 hours separates the initial symptoms from the second phase, in which the growing mass presses on the brainstem, causing sixth and seventh cranial nerve palsies. As the mass progressively enlarges and the tissue destruction causes edema, the brainstem is compressed and hemiparesis occurs. Without surgical removal of the mass, death may result in 24 to 72 hours. Occasionally, the progression to death is prolonged, but the presence of a large posterior mass, which causes hydrocephalus, has a very high mortality rate without surgery.

Treatment of cerebellar hemorrhage in humans remains controversial in spite of the passage of over 50 years since the initial reports on surgical treatment. Large masses with signs of brainstem compression require urgent ventriculostomy and surgical removal of the mass. When the patient has a mass less than 3 cm and is stable, the threat of deterioration is difficult to judge. Some neurosurgeons favor removal of the mass before the patient deteriorates, while others prefer to watch the patient carefully and intervene when deterioration begins. With the ability to visualize the mass and the hydrocephalus with CT, the watchful waiting approach is generally favored. Some neurosurgeons prophylactically place a catheter in the ventricle to prevent the development of hydrocephalus.

Table 11–3 **Animal Models for ICH**

Method	Advantages	Disadvantages
Cerebral infarction with induced hypertension	Close to the clinical condition	Difficult to reproduce
Autologous blood injection	Causes a mass effect and blood toxicity	Maximal at onset without evolution of lesion
Multiple carotid emboli	Closest to hemorrhagic transformation	Sites of bleeding randomly distributed
Bacterial collagenase	Multifocal bleeding sites evolve into a hemorrhagic mass	Foreign product present in early stages

Little is understood about the mechanisms involved in the growth of the mass lesion after an intracerebral bleed. Several studies have shown an increase in size that occurs over 12 to 24 hours.[25] The impact of the hemorrhage on the surrounding tissue has been extensively studied in supratentorial bleeds but not in cerebellar hemorrhages. The supratentorial mass does not appear to exert sufficient pressure on the surrounding tissues to restrict cerebral blood flow,[26] but the toxic molecules released by the breakdown of blood products, particularly thrombin, seem to have a deleterious effect.[27]

In addition to the disappointing results of surgical trials in supratentorial ICH, medical treatments have proven elusive. A large clinical trial was done in an attempt to control the growth of the hemorrhage using recombinant factor VIIa (rFVIIa), a serine protease that acts in conjunction with tissue factor to control bleeding in hemophiliacs who have a deficiency in this coagulation cascade component. An initial trial of rFVIIa in ICH was reported to be successful,[28] but a subsequent trail failed to confirm the results of the first trial.[29] The Cochrane Review analyzed all published and unpublished randomized, controlled trials evaluating hemostatic drugs in ICH.[30] A total of 1398 patients within 4 hours of ICH onset were included: 975 subjects received rFVIIa, two epsilon-aminocaproic acid, and 423 received placebo. The primary endpoints were mortality and dependence at 90 days. There was no significant difference in the risk of death (18.5% vs. 19.4% for placebo, RR 0.85) and no difference in the combination of death or dependence (49.6% vs. 51.7%, RR 0.91). There was also no significant difference in thromboembolic events (8.5% vs. 6.2%, RR 1.37). In spite of the apparent finding of no adverse effects, the conclusion was that available data do not support the use of rFVIIa for the treatment of spontaneous ICH.

PATHOPHYSIOLOGY OF ICH: EVIDENCE FROM ANIMAL STUDIES

Several animal models have been used to study the effect of different drugs and surgical intervention on supratentorial ICH (Table 11–3). These studies have focused on strategies to reduce the damage from tissue compression by the mass lesion and the toxicity of the blood products.[31] Two models are generally accepted in studies of ICH: (1) direct injection of autologous blood, which models the mass effect and includes the toxicity of the blood products, and (2) injection of bacterial collagenase, which causes breakdown of multiple small blood

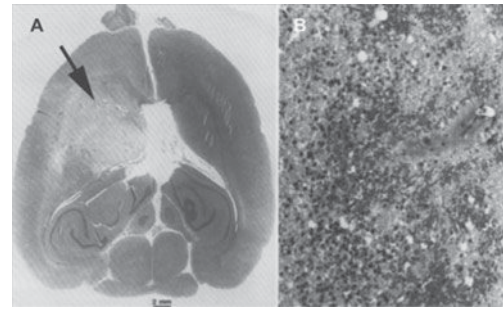

Figure 11–8. Photomicrographs of histological changes in the caudate nucleus of a rat 48 hours after infusion of 0.5 unit of bacterial collagenase. (**A**) A large hemorrhagic lesion in the caudate protrudes into the lateral ventricle (arrow). (**B**) Infiltrate of polymorphonuclear leukocytes at the periphery of the lesion (hematoxylin and eosin stain, x229). (From Ref. 33.)

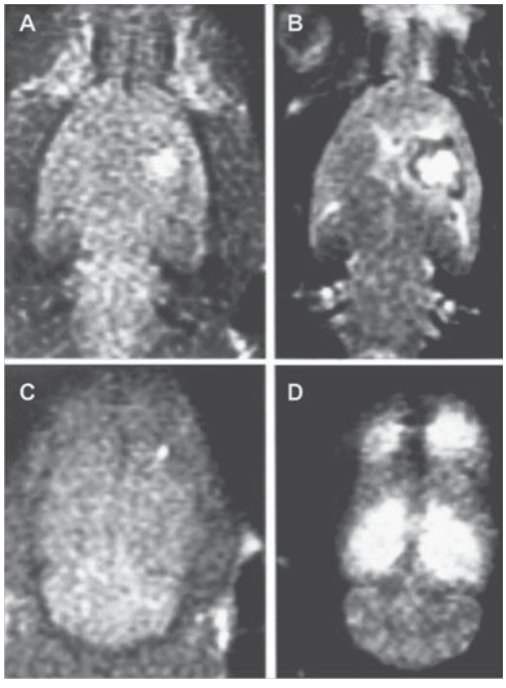

Figure 11–9. (**A**) T1-weighted and (**B**) T2-weighted MRI images 24 hours after bacterial collagenase injection. The lesion is bright on both images due to the paramagnetic effect and increased water, respectively. (**C**) T1-weighted image of a horizontal slice taken higher in the brain. (**D**) T2-weighted image of the top of the brain from the same region as in C showing the edema in both posterior hippocampal regions. (From Ref. 3.)

vessels in the region of injection, producing a mass lesion that grows over time, simulating more closely the natural history of ICH.[32]

Bacterial collagenase produces a dose-dependent hemorrhagic mass when directly injected into the brain. Most studies have been done with the enzyme injected into the basal ganglia. Collagenase attacks the type IV collagen in the basal lamina around the cerebral blood vessels, causing bleeding. Histological studies show multiple ball hemorrhages around blood vessels shortly after collagenase injection. With time the multiple sites form into a mass lesion[33] (Figure 11–8). Magnetic resonance imaging shows the lesion size and the edema in the rat after collagenase injection (Figure 11–9). Gradual resolution of the mass lesion with absorption and cyst formation takes place over 3 to 4 weeks. Behavioral studies show a concomitant improvement over several weeks as the blood is resorbed.

After several hours, there is production of endogenous matrix metalloproteinases (MMPs).[34] Continued damage is caused by the MMPs, which amplify the injury initiated by the bacterial product. The primary MMPs involved in the secondary damage are the gelatinases, 72 kDa type IV collagenase (MMP-2) and 92 kDa type IV collagenase (MMP-9). Less well studied, but important in inflammatory protease production, is stromelysin-1 (MMP-3), a major product of macrophage/microglia activation.[35] Both brain cells and invading white blood cells are the sources of the MMPs. Neutrophils contain MMP-9 in an active form that is packaged in packets released at the site of inflammation, but the contribution of MMP-9 from neutrophils and from brain cells is controversial.[36] Other white blood cells and brain cells induce MMPs through activation of inflammatory cascades.

Drugs that block the inflammatory response around the hematoma have been tested in models of ICH. Minocycline, a tetracycline derivative with anti-inflammatory effects that blocks the action of MMPs, reduces the injury after intracerebral hemorrhage in the rat (Figure 11–10).[1] Hydroxymates, which are potent inhibitors of the MMPs through their binding to the active zinc site in the molecule, are effective in reducing edema in the rat model of ICH.[37] The hydroxymate MMP inhibitor, GM6001, reduced hemorrhage size and improved the outcome in a mouse model of ICH using the collagenase-induced hemorrhage model[38] (Figure 11–11). A recent study showed that both direct injection of minocycline into the hemorrhage and systemic administration were superior to systemic delivery.[39]

EXTRAPOLATION OF EXPERIMENTAL RESULTS TO TREATMENTS FOR ICH

The complexity of the molecular cascades involved in the formation of a hemorrhagic mass is slowly beginning to emerge from the wealth of experimental studies (Figure 11–12). There are numerous feedforward and feedback loops analogous to the situation in ischemia. Nontraumatic hemorrhages evolve from multiple large regions of hemorrhagic transformation via multiple mechanisms. Assuming

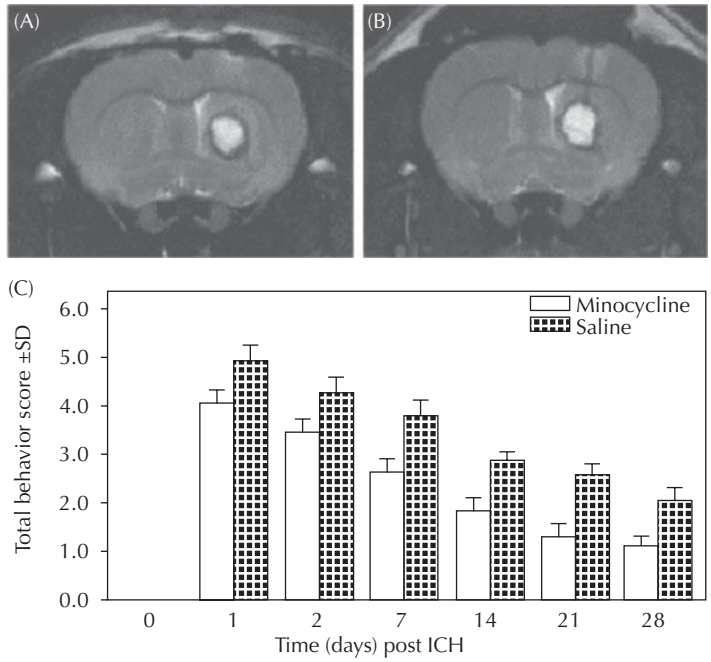

Figure 11–10. Neuroimaging and neurobehavioral abnormalities after ICH induction. Untreated (**A**) and minocycline-treated (**B**) animals with ICH did not differ in the size of the T2-weighted lesion on day 1 after ICH induction. In contrast, minocycline treatment improved neurobehavioral performance (**C**) after ICH induction, with a trend beginning on day 1 but reaching statistical significance on day 7, which was maintained until day 28 after ICH (single asterisk, $p < .05$; double asterisk, $p < .01$). SD = standard deviation.[1]

that there is tissue infarction with hemorrhagic transformation possibly related to reperfusion, the reactive oxygen species and nitric oxide are important early in the process, occurring after the formation of immediate early genes (*c-fos/c-jun*) and cytokines such as tumor necrosis factor-α (TNF-α) and interleukin-β (IL-1β). These cytokines initiate an inflammatory response, which results in an increase in MMP-9 through activation of the activator protein-1 (AP-1) and nuclear factor-κB (NF-κB) gene promoter regions by the proto-oncogenes (*c-fos/c-jun*) and cytokines. Latent stromelysin-1 (MMP-3) is also produced. Activation of proMMP-3 occurs by plasmin and contributes to the activation of proMMP-9. There is production of H1F-1α and p53, the tumor suppressor, which promotes cell death but most likely also has long-term beneficial effects. Expression of tissue- and urokinase-plasminogen activator (tPA/uPA) leads to production of plasmin. Microglia contribute to the inflammatory response after activation by ischemia and tPA.

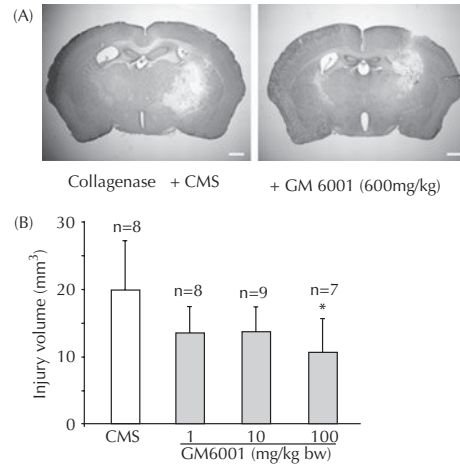

Figure 11–11. Bacterial collagenase-induced ICH in mouse brain. A broad-spectrum MMP inhibitor, GM6001, reduced the injury volume after ICH. (**A**) Coronal sections were collected 3 days after ICH induction and stained for Luxol fast blue/Cresyl violet. Left: control mice; right: GM6001 (100 mg/kg)-treated mice. (**B**) GM6001-treated mice had smaller injury volumes than control mice ($n = 7–9$/group, $^*p < .05$). Values are means ± SD. Scale bar, 1 mm. (From Ref. 48.)

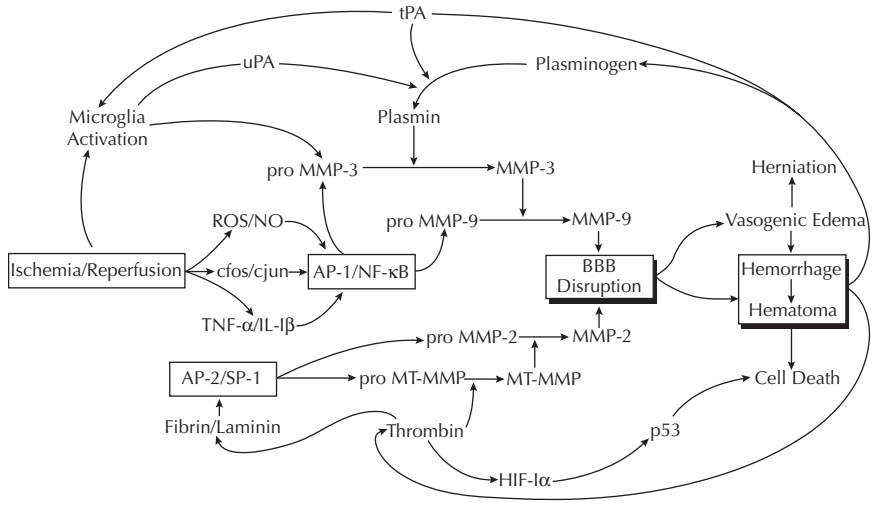

Figure 11–12. The complex feedforward and feedback loops are shown for the substances involved in the evolution of an ICH (see text for explanation). (From Ref. 32.)

Table 11–4 **Agents Shown to Improve Various Outcome Measures in Collagenase-Induced ICH**

Agent	Action	Reference
Atrial natriuretic peptide	Reduced posterior edema	40
BB-1101, GM6001 (MMP inhibitors)	Reduced posterior edema	37, 38
PBN*; NXY-059† (free radical scavengers)	Improved behavioral outcome	41
Citicoline	Improved function and decreased infarct size	42
ORF4-PE (TNF-α antisense)	Behavioral improvement	43
GABA agonist	Temporary improvement	44
zVADfmk (caspase inhibitor)	Decreased TUNEL-positive cells	45
Tauroursodeoxycholic acid	Reduced lesion volume	46
Atorvastatin (HMG-CoA reductase inhibitor)	Reduced edema, inflammation, and cell death	47
Tufts in fragment 1–3 macrophage/microglial inhibitory factor (MIF)	Reduced injury volume and improved functional recovery	48
Neural stem cell transplantation (intraveneous)	Behavioral improvement	49
Minocycline	Decreased glial activation and apoptosis with improved functional recovery	50
AMPA receptor antagonist	Behavioral improvement	51
Constraint-induced movement therapy and focused rehabilitation	Improved functional recovery	52
Memantine (glutamate inhibitor)	Reduced hemorrhage volume and improved recovery	53
Argatroban (thrombin inhibitor)	Reduced brain edema	54

*PBN: spin-trap: α-phenyl-*N*-tert-butyl nitrone.
†NXY-059: disodium 4-[(tert-butylimino) metyl] benzene –1, 3-disulfonate *N*-oxide.
GABA, gamma-aminobutyric acid; HMG, 3-hydroxy-3-methyl-glutaryl; AMPA, α-amino-3-hydroxy-5-4-isoxazolepropionic acid.

Translating the results of the experimental studies in rodents and other animals into treatments for patients with ICH has been a challenge because of the complexity and interactions of the molecular cascades involved in the formation and progression of ICH. The ability to study animals lacking specific genes has challenged researchers to develop models of ICH in the mouse. Both autologous blood and bacterial collagenase have been used successfully in mice to model ICH. Behavioral tests are more readily performed in the rat, but can be done as well in the smaller mouse models and the larger pig models.

In the long run, the search for effective treatments for this devastating disorder will come from multiple sources. Treatment options may come from improvements in surgical methods with more precise selection of appropriate groups of patients. Agents will be developed for the control of neuroinflammation in ischemic models and hemorrhagic transformation (HT) when more studies are done. With improvements in the MMP inhibitors or the derivates of tetracycline, such as doxycycline and minocycline, which block the metalloproteinases, novel treatments may be available. The development of agents to control the free radicals is another potential therapeutic route. Chelation of iron reduces the secondary damage from the iron released by the red blood cells. The growing number of potential treatments for ICH will require several years of testing (Table 11–4), but the promise of finding useful agents to ameliorate the consequences of ICH will make the effort worthwhile.

REFERENCES

1. Power C, Henry S, Del Bigio MR, et al. Intracerebral hemorrhage induces macrophage activation and matrix metalloproteinases. *Ann Neurol*. 2003;53:731–742.
2. Qureshi AI, Mendelow AD, Hanley DF. Intracerebral haemorrhage. *Lancet*. 2009;373:1632–1644.
3. Brown MS, Kornfeld M, Mun-Bryce S, et al. Comparison of magnetic resonance imaging and histology in collagenase-induced hemorrhage in the rat. *J Neuroimaging*. 1995;5:23–33.
4. Grotta JC. Current medical and surgical therapy for cerebrovascular disease. *N Engl J Med*. 1987;317: 1505–1516.
5. Caplan LR. Intracerebral haemorrhage. *Lancet*. 1992; 339:656–658.
6. Barras CD, Tress BM, Christensen S, et al. Density and shape as ct predictors of intracerebral hemorrhage growth. *Stroke*. 2009;40:1325–1331.
7. Roman GC. From UBOs to Binswanger's disease. Impact of magnetic resonance imaging on vascular dementia research. *Stroke*. 1996;27:1269–1273.
8. Fisher M, Adams RD. Observations on brain embolism with special reference to the mechanism of hemorrhagic infarction. *J Exp Neurol Neuropathol*. 1951;10:92–96.
9. Bogousslavsky J, Regli F, Uske A, et al. Early spontaneous hematoma in cerebral infarct: is primary cerebral hemorrhage overdiagnosed? *Neurology*. 1991;41: 837–840.
10. Hornig CR, Bauer T, Simon C, et al. Hemorrhagic transformation in cardioembolic cerebral infarction. *Stroke*. 1993;24:465–468.
11. Brott T, Broderick J, Kothari R, et al. Early hemorrhage growth in patients with intracerebral hemorrhage. *Stroke*. 1997;28:1–5.
12. Keep RF, Xi G, Hua Y, et al. The deleterious or beneficial effects of different agents in intracerebral hemorrhage: think big, think small, or is hematoma size important? *Stroke*. 2005;36:1594–1596.
13. Kuroiwa T, Ting P, Martinez H, et al. The biphasic opening of the blood-brain barrier to proteins following temporary middle cerebral artery occlusion. *Acta Neuropathol*. 1985;68:122–129.
14. Cuzner ML, Opdenakker G. Plasminogen activators and matrix metalloproteases, mediators of extracellular proteolysis in inflammatory demyelination of the central nervous system. *J Neuroimmunol*. 1999;94:1–14.
15. Montaner J, Molina CA, Monasterio J, et al. Matrix metalloproteinase-9 pretreatment level predicts intracranial hemorrhagic complications after thrombolysis in human stroke. *Circulation*. 2003;107:598–603.
16. Lee KR, Colon GP, Betz AL, et al. Edema from intracerebral hemorrhage: the role of thrombin. *J Neurosurg*. 1996;84:91–96.
17. Jiang Y, Wu J, Hua Y, et al. Thrombin-receptor activation and thrombin-induced brain tolerance. *J Cereb Blood Flow Metab*. 2002;22:404–410.
18. Lapchak PA, Araujo DM, Song D, et al. Effects of the spin trap agent disodium- [tert-butylimino)methyl] benzene-1,3-disulfonate n-oxide (generic nxy-059) on intracerebral hemorrhage in a rabbit large clot embolic stroke model: combination studies with tissue plasminogen activator. *Stroke*. 2002;33(6):1665–1670.
19. Kidwell CS, Chalela JA, Saver JL, et al. Comparison of mri and ct for detection of acute intracerebral hemorrhage. *JAMA*. 2004;292:1823–1830.
20. Kidwell CS, Wintermark M. Imaging of intracranial haemorrhage. *Lancet Neurol*. 2008;7:256–267.
21. Greenberg SM, Vernooij MW, Cordonnier C, et al. Cerebral microbleeds: a guide to detection and interpretation. *Lancet Neurol*. 2009;8:165–174.
22. Kirkman MA, Mahattanakul W, Gregson BA, et al. The effect of the results of the stich trial on the management of spontaneous supratentorial intracerebral haemorrhage in newcastle. *Br J Neurosurg*. 2008;22: 739–746; discussion 747.
23. Fisher CM, Picard EH, Polak A, et al. Acute hypertensive cerebellar hemorrhage: diagnosis and surgical treatment. *J Nerv Ment Disord*. 1965;140:38–57.
24. Ott KH, Kase CS, Ojemann RG, et al. Cerebellar hemorrhage: diagnosis and treatment. A review of 56 cases. *Arch Neurol*. 1974;31:160–167.
25. Broderick JP, Diringer MN, Hill MD, et al. Determinants of intracerebral hemorrhage growth: an exploratory analysis. *Stroke*. 2007;38:1072–1075.

26. Powers WJ, Zazulia AR, Videen TO, et al. Autoregulation of cerebral blood flow surrounding acute (6 to 22 hours) intracerebral hemorrhage. *Neurology*. 2001;57:18–24.
27. Hua Y, Keep RF, Gu Y, et al. Thrombin and brain recovery after intracerebral hemorrhage. *Stroke*. 2009;40:S88-S89.
28. Mayer SA, Brun NC, Begtrup K, et al. Recombinant activated factor VII for acute intracerebral hemorrhage. *N Engl J Med*. 2005;352:777–785.
29. Mayer SA, Brun NC, Begtrup K, et al. Efficacy and safety of recombinant activated factor VII for acute intracerebral hemorrhage. *N Engl J Med*. 2008;358: 2127–2137.
30. Al-Shahi Salman R. Haemostatic drug therapies for acute spontaneous intracerebral haemorrhage. *Cochrane Database Syst Rev*. 2009:CD005951.
31. Xi G, Keep RF, Hoff JT. Mechanisms of brain injury after intracerebral haemorrhage. *Lancet Neurol*. 2006;5:53–63.
32. Rosenberg GA, Grossetete M, Mun-Bryce S. Experimental models in intracerebral hemorrhage. *Handb Clin Neurol*. 2008;92:307–324.
33. Rosenberg GA, Mun-Bryce S, Wesley M, et al. Collagenase-induced intracerebral hemorrhage in rats. *Stroke*. 1990;21:801–807.
34. Rosenberg GA, Dencoff JE, McGuire PG, et al. Injury-induced 92-kda gelatinase and urokinase expression in rat brain. *Lab Invest*. 1994;71:417–422.
35. Gurney KJ, Estrada EY, Rosenberg GA. Blood-brain barrier disruption by stromelysin-1 facilitates neutrophil infiltration in neuroinflammation. *Neurobiol Dis*. 2006;23:87–96.
36. Maier CM, Hsieh L, Yu F, et al. Matrix metalloproteinase-9 and myeloperoxidase expression: quantitative analysis by antigen immunohistochemistry in a model of transient focal cerebral ischemia. *Stroke*. 2004;35:1169–1174.
37. Rosenberg GA, Navratil M. Metalloproteinase inhibition blocks edema in intracerebral hemorrhage in the rat. *Neurology*. 1997;48:921–926.
38. Wang J, Tsirka SE. Neuroprotection by inhibition of matrix metalloproteinases in a mouse model of intracerebral haemorrhage. *Brain*. 2005;128:1622–1633.
39. Xue M, Mikliaeva EI, Casha S, et al. Improving outcomes of neuroprotection by minocycline: guides from cell culture and intracerebral hemorrhage in mice. *Am J Pathol*. 2010;176:1193–1202.
40. Rosenberg GA, Scremin O, Estrada E, et al. Arginine vasopressin V1-antagonist and atrial natriuretic peptide reduce hemorrhagic brain edema in rats. *Stroke*. 1992;23:1767–1773.
41. Peeling J, Yan HJ, Chen SG, et al. Protective effects of free radical inhibitors in intracerebral hemorrhage in rat. *Brain Res*. 1998;795:63–70.
42. Clark W, Gunion-Rinker L, Lessov N, et al. Citicoline treatment for experimental intracerebral hemorrhage in mice. *Stroke*. 1998;29:2136–2140.
43. Mayne M, Ni W, Yan HJ, et al. Antisense oligodeoxynucleotide inhibition of tumor necrosis factor-alpha expression is neuroprotective after intracerebral hemorrhage [in process citation]. *Stroke*. 2001;32: 240–248.
44. Lyden PD, Jackson-Friedman C, Lonzo-Doktor L. Medical therapy for intracerebral hematoma with the gamma-aminobutyric acid-A agonist muscimol. *Stroke*. 1997;28:387–391.
45. Matsushita K, Meng W, Wang X, et al. Evidence for apoptosis after intercerebral hemorrhage in rat striatum. *J Cereb Blood Flow Metab*. 2000;20:396–404.
46. Rodrigues CM, Sola S, Nan Z, et al. Tauroursodeoxycholic acid reduces apoptosis and protects against neurological injury after acute hemorrhagic stroke in rats. *Proc Natl Acad Sci USA*. 2003;100:6087–6092.
47. Jung KH, Chu K, Jeong SW, et al. Hmg-coa reductase inhibitor, atorvastatin, promotes sensorimotor recovery, suppressing acute inflammatory reaction after experimental intracerebral hemorrhage. *Stroke*. 2004;35:1744–1749.
48. Wang J, Tsirka SE. Tuftsin fragment 1–3 is beneficial when delivered after the induction of intracerebral hemorrhage. *Stroke*. 2005;36:613–618.
49. Jeong SW, Chu K, Jung KH, et al. Human neural stem cell transplantation promotes functional recovery in rats with experimental intracerebral hemorrhage. *Stroke*. 2003;34:2258–2263.
50. Power C, Henry S, Del Bigio MR, et al. Intracerebral hemorrhage induces macrophage activation and matrix metalloproteinases. *Ann Neurol*. 2003;53:731–742.
51. Terai K, Suzuki M, Sasamata M, et al. Amount of bleeding and hematoma size in the collagenase-induced intracerebral hemorrhage rat model. *Neurochem Res*. 2003;28:779–785.
52. DeBow SB, Davies ML, Clarke HL, et al. Constraint-induced movement therapy and rehabilitation exercises lessen motor deficits and volume of brain injury after striatal hemorrhagic stroke in rats. *Stroke*. 2003;34:1021–1026.
53. Lee ST, Chu K, Jung KH, et al. Memantine reduces hematoma expansion in experimental intracerebral hemorrhage, resulting in functional improvement. *J Cereb Blood Flow Metab*. 2006;26:536–544.
54. Nagatsuna T, Nomura S, Suehiro E, et al. Systemic administration of argatroban reduces secondary brain damage in a rat model of intracerebral hemorrhage: histopathological assessment. *Cerebrovasc Dis*. 2005;19:192–200.
55. Lee KR, Betz AL, Keep RF, et al. Intracerebral infusion of thrombin as a cause of brain edema. *J Neurosurg*. 1995;83:1045–1050.

Chapter 12

Autoimmunity, Hypoxia, and Inflammation in Demyelinating Diseases

INTRODUCTION

Multiple sclerosis (MS) is an autoimmune central nervous system demyelinating disease that affects mainly young women.[1] It is generally accepted to be an autoimmune disorder with demyelination due to T cells. However, in spite of much research, the etiology remains uncertain, and the initiating factors and the reason for the relapsing-remitting course are unclear. Demyelinating plaques grow from venules, producing characteristic patterns of myelin damage on magnetic resonance imaging (MRI). Perivenule inflammation is mainly composed of T cells and macrophages.[2] Acute attacks with relapses occur in an unpredictable manner in the early stages of the illness, with a highly variable pattern of disease ranging from mild attacks with few residual symptoms to fulminant disease leading to death. After years of a relapsing-remitting course, the disease generally enters a secondary progressive phase; only a few patients have a primary progressive form of the illness without relapses.

Early pathologists showed the relationship of blood vessels to areas of demyelination, and acute pathology was often seen in the preantibiotic era. With better treatment, including antibiotics for infection, bladder care, and rehabilitation, fewer patients died during the acute phase of the illness, and the inflammation involving the blood vessels was less frequently seen at autopsy. Instead, the major pathological change in the brain was that of sclerotic plaques. Absence of the acute changes in the blood vessels resulted in the emphasis on the chronic neurodegenerative aspects of the illness rather than on the inflammatory ones. With the introduction of MRI into clinical practice, a major shift in conceptualization of the pathophysiology of MS occurred, with a revisiting of the original concepts of blood vessel inflammation.

Diagnosis of MS is made from the history and the neurological examination. Characteristic changes are seen on MRI and in the cerebrospinal fluid (CSF) that have reduced much of the uncertainty in the diagnosis. While the clinical

evaluation is made easier by the new diagnostic methods, a more confusing picture is emerging from careful pathological studies, which have benefited from worldwide collaboration between multiple centers. These large studies are revealing a heterogeneous disease with several types of pathological changes leading to demyelination and oligodendrocyte death, which remain the hallmarks of the illness.

Although the etiology underlying the demyelination remains uncertain, it is recognized that inflammation is prominent in the relapsing and remitting form of the illness. This inflammatory response is mediated by invading leukocytes. It results in the destruction of myelin by free radicals and proteases, and apoptosis of oligodendrocytes from hypoxic injury. Many factors contribute to the complex molecular cascades triggered by infection, trauma, and other factors. Magnetic resonance imaging studies have led to a revival of the original concept that the disease process involves damage to the cerebral blood vessels with opening of the blood-brain barrier (BBB).

Early pathological studies published in 1916 by Dawson showed inflammatory cells clustered around veins in the center of the demyelinated plaque. He wrote: "A study of a series of sections shows that the plaques are deposited in relation to the distribution of the veins and to the walls of the ventricles."[3] Demyelinated areas were seen surrounding the veins that fanned out from the central veins of the cerebral ventricles, giving the appearance of finger-like lesions, which have became known as *Dawson's fingers* (Figure 12–1). Other early studies confirmed the importance of an inflamed blood vessel in the etiology of MS. In 1937 Putnam and Adler showed that fibrosed vessels with thromboses were centrally located in plaques.[4] By carefully reconstructing serial brain sections from MS patients, they showed that fibrin deposits surrounded the inflamed vessels. These early studies led to the theory that vascular disease contributed to the pathophysiology of MS, which was supported by hematological studies of changes in fibrinogen in the blood of MS patients.

For many years after the discovery of the experimental allergic encephalomyelitis (EAE) model and the parallel increase in knowledge in the fields of virology and immunology, the search for an immunological basis of the disease shifted the interest of researchers away from vascular disease with inflammation to an autoimmune etiology. However, with the introduction of MRI with gadolinium enhancement into patient studies, the pendulum swung back as serial contrast-enhanced MRI revealed a surprising number of enhancing lesions, which often failed to correlate with the clinical symptoms. Not only were a large number of enhancing lesions seen on the initial scans, but those present were observed to disappear in subsequent scans, while new enhancing lesions appeared. Investigators could not necessarily correlate disease symptoms with the appearance or disappearance of the enhancing lesions.[5]

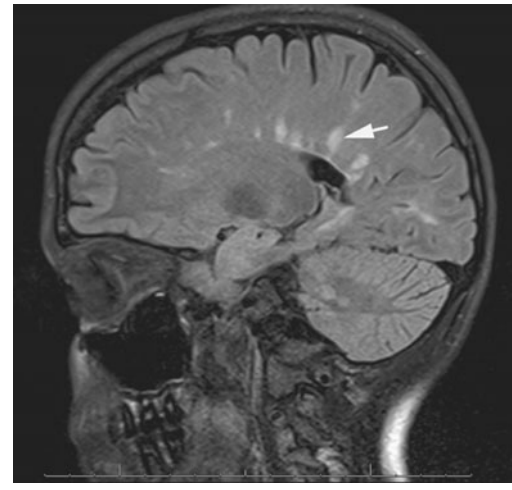

Figure12–1. Sagittal FLAIR MRI image from 17 year old patient with multiple sclerosis. Perivenular lesions in MS called *Dawson's fingers* because they were first described by him and they fan out from the ventricles in a finger-like pattern. (arrow). (Courtesy of Elaine Edmonds, MD, PhD)

Correlation of venous pathology with MS lesions is possible with MR venography, which takes advantage of the difference between oxygenated and deoxygenated blood to visualize venous blood. In most MS lesions, venograms show a vein in the center of the lesions (Figure 12–2). This pattern is not specific for MS; a similar pattern with venule involvement occurs with hypoxic ischemic white matter lesions. However, in contrast to MS lesions, these white matter lesions show no relationship to the shape and location of the veins.[6]

A study using 7T MRI showed that T2*-weighted images can reliably identify all patients with clinically definite MS. Small

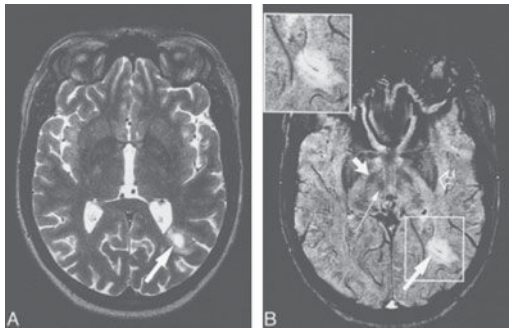

Figure 12–2. (**A**) Axial T2-weighted image and (**B**) corresponding contrast-enhanced MR venogram with a magnified image shown in the boxed area. The lesion at the left occipital horn (long wide arrow) is hypointense. The MR venogram shows a vein with its course corresponding to the form of the lesion. Note the susceptibility artifacts in the frontal regions and the low intensity of the globus pallidus (open arrow), substantia nigra (short wide arrow), and red nucleus (thin arrow). (From Ref. 6.)

venules in the center of lesions are visualized using T2*-weighted MRI because of the paramagnetic effect of deoxyhemoglobin. These patients have more than 40% of the MS lesions in a perivenous location, while in those without clinical MS, less than 40% of the lesions appear perivenous[7] (Figure 12–3).

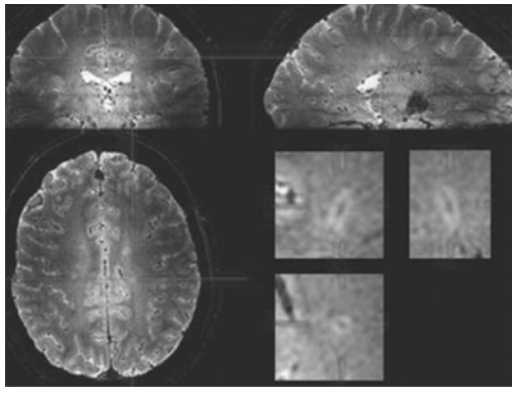

Figure 12–3. The 7 T T2*-weighted images were viewed in orthogonal planes. For each lesion, the presence or absence of a central vein was noted. Veins were counted if they (1) could be visualized in at least two perpendicular planes, (2) appeared linear in at least one plane, and (3) were completely surrounded by hyperintense signal in at least one plane (to avoid the inclusion of adjacent rather than central veins). Lesions were classified as perivenous if they contained one or more central veins. The proportion of perivenous lesions in patients with MS (mean 80%, range 53%–100%) was consistently much higher than in subjects without MS (mean 16%, range 0%–34%). The perivenous lesion appearance was equally common in patients with clinically isolated syndrome, relapsing-remitting MS, primary progressive MS, and secondary progressive MS. (From Ref. 7; See also the color insert.)

HETEROGENEITY OF THE PATHOLOGICAL FINDINGS IN MS

To overcome the heterogeneous nature of MS and the relatively few patients that had been autopsied at each center, a group of neuropathologists pooled data from 51 biopsies and 32 autopsies from active MS lesions. These patients had a variable clinical course, and differing neuroradiological appearance of the lesions, susceptibility gene loci, and response to therapy. Analyzing the pathology of the lesions from the various centers with similar immunological and neurobiological markers, they found four different patterns of demyelination. They classified the patients on the basis of myelin protein loss, geography and extension of plaques, patterns of oligodendrocyte destruction, and immunopathological evidence of complement activation. With the use of all of the findings, two dominant patterns emerged for the original four types. Patterns I and II showed close similarities to T-cell-mediated or T-cell plus antibody-mediated autoimmune encephalomyelitis, respectively. The other patterns (III and IV) were highly suggestive of a primary oligodendrocyte dystrophy, reminiscent of virus- or toxin-induced demyelination rather than autoimmunity[8] (Figure 12–4).

T cells are of several types and participate in both the initiation of the inflammatory response and its suppression (Figure 12–5). Inflammation in MS brains is characterized by the presence of T helper 1 (Th1) cells. These Th1 cells activate macrophages, leading to secretion of toxic cytokines, which cause demyelination and axonal injury. In the four patterns described by Lucchinetti and colleagues, type I demyelination is induced by macrophages (Table 12–1). Demyelinating antibodies in conjunction with complement produce pattern II. Other T cells contribute to the myelin damage. T helper 2 (Th2) cells may modify the outcome of the lesions. Pattern III involves degenerative changes in distal oligodendrocyte processes, in particular those of periaxonal oligodendrocytes, which undergo apoptosis and myelin loss. On rare occasions, pattern IV is seen; this consists of primary degeneration of oligodendrocytes followed

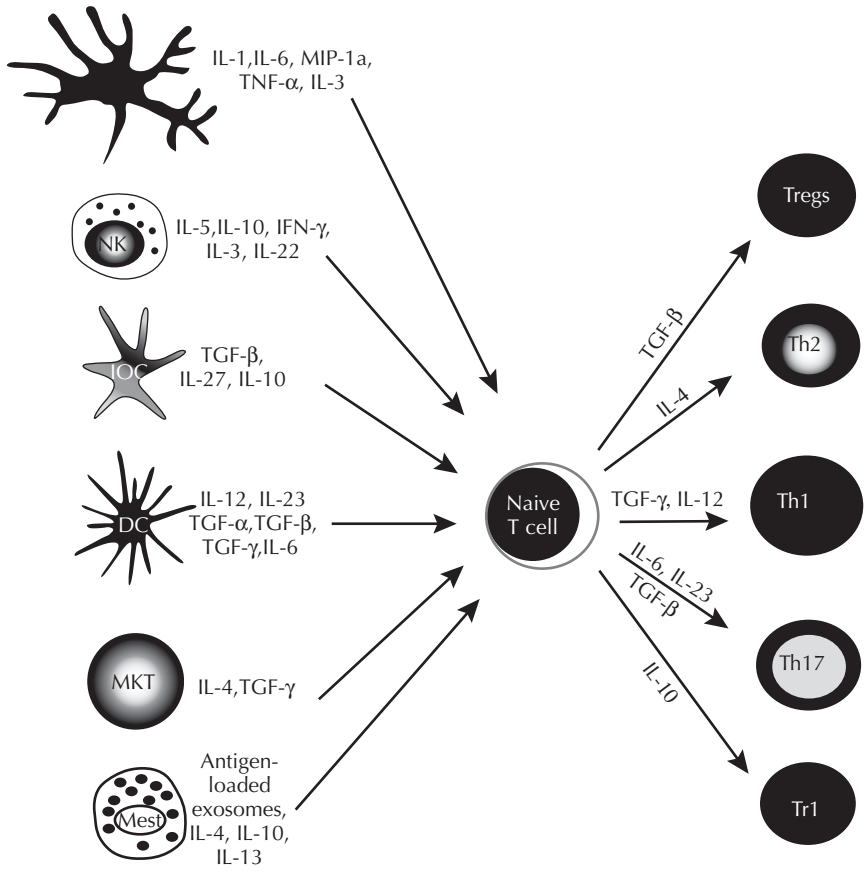

Figure 12–4. Potential contribution of cytokines secreted by innate immune cells in MS and their role in T-cell differentiation: effector or regulatory T cells. Inflammatory cytokines secreted by innate immune cells lead to differentiation of effector T- cell populations such as Th1, Th2, and Th17 involved either in mediating inflammation or in immunomodulation. By contrast, anti-inflammatory cytokines secreted by innate immune cells play an important role in induction of regulatory T cells that are capable of mediating tolerance during disease (From Ref. 11.).

by myelin destruction. Cytokines secreted by either endogenous or hematogenous macrophages and microglia, such as tumor necrosis factor-α (TNF-α), act in conjunction with reactive oxygen intermediates and antibodies against myelin oligodendrocyte glycoprotein (anti-MOG) or galactocerebroside (anti-GC). An important component of the inflammatory-mediated attack on the myelinated fibers is bystander axonal injury with acute destruction of myelin sheaths. In the active phase of demyelination, axonal injury is likely to be induced by macrophage toxins or by the direct effects of cytotoxic T cells. The chronic axonal injury observed in inactive plaques may be caused by a lack of trophic support by glial cells, such as oligodendrocytes, but could also involve inflammatory mediators, produced by macrophages, that persist in most active chronic lesions.

In pattern III, actively demyelinating lesions show preferential loss of myelin-associated glycoprotein and apoptotic-like oligodendrocyte destruction, whereas other myelin proteins remain well preserved. This is a form of primary "dying-back" oligodendrogliopathy beginning in the most distal periaxonal oligodendrocyte processes. A similar pattern of oligodendrogliopathy was present in some cases of virus encephalitis and all lesions of acute white matter stroke. Prominent nuclear expression of hypoxia inducible factor-1α (HIF-1α) was seen in various cell types, including oligodendrocytes, suggesting that a hypoxia-like tissue injury may play a pathogenetic role in a subset of inflammatory demyelinating brain lesions.[9]

In another study of active MS lesions, rather than CD4 T-cell-dependent macrophage activation directed against a myelin

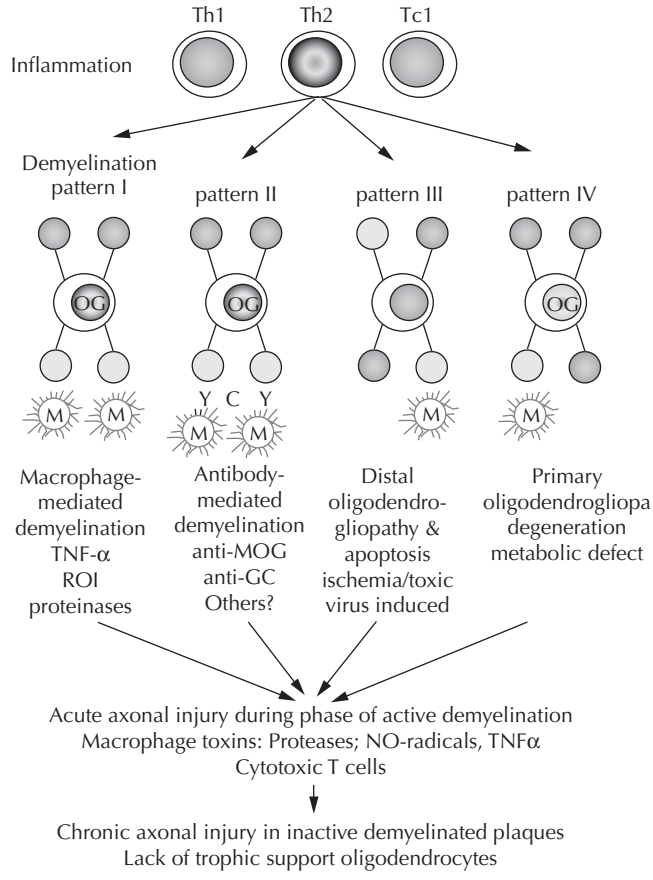

Figure 12–5. Summary of the pathogenetic mechanisms involved in the formation of MS lesions. Inflammation: evidence indicates that Th1 cells have a role in inducing inflammatory reactions in the central nervous system. Proinflammatory cytokines released from Th1 cells activate macrophages, which are responsible for the majority of demyelination and axonal injury. In addition, however, Th2 cells and cytotoxic cells may modify the outcome of the lesions. Demyelination: myelin sheaths and oligodendrocytes (OG) can be destroyed, possibly by different mechanisms in different individuals. This results in distinctly different patterns of demyelination in active lesions. Demyelination may be induced by macrophages (M) and/or their toxic products (resulting in pattern I); by specific demyelinating antibodies and complement (C, resulting in pattern II); by degenerative changes in distal processes, in particular those of periaxonal oligodendrocytes (distal oligodendrogliopathy), followed by apoptosis (resulting in pattern III); or by primary degeneration of oligodendrocytes followed by myelin destruction (resulting in pattern IV). Possible mediators of myelin and oligodendrocyte destruction include TNF-α, reactive oxygen intermediates (ROI), and anti-MOG and anti-GC. Axonal injury: axonal injury follows acute destruction of myelin sheaths. In the active phase of demyelination, axonal injury is likely to be induced by macrophage toxins or by the direct effects of cytotoxic T cells. The chronic axonal injury observed in inactive plaques may be caused by a lack of trophic support by glial cells, such as oligodendrocytes, but could also involve inflammatory mediators, produced by macrophages, that persist in most active chronic lesions. (From Ref. 78.)

or oligodendrocyte antigen, which is generally thought to be the mechanism causing myelin destruction in MS, the investigators identified oligodendrocyte loss and apoptosis in the absence of infiltrating lymphocytes. Areas with demyelination, which were filled with lipid macrophages and regenerating oligodendrocytes, showed large numbers of T cells, B cells, and immunoglobulin G (IgG)-positive plasma cells. Lesions in two exceptionally early cases contained relatively few T and B cells and no IgG-positive plasma cells. The authors concluded that early loss of oligodendrocytes suggests that plaque formation has some basis other than destructive cell-mediated immunity directed against a myelin or oligodendrocyte antigen.[10] They argued against the schema of four pathological types and suggested a single

Table 12–1 **Essential Characteristics of Different Patterns of Demyelination in MS**

Patterns of Demyelination	Pathology	Putative Mechanisms
(I) Macrophage mediated	Perivenous distribution of lesions; radial expansion of the lesions; inflammatory infiltrates composed of T cells and macrophages; activated macrophages and microglia associated with degenerating myelin	T-cell-mediated inflammation with macrophage/microglia activation; demyelination induced by macrophage toxins
(II) Antibody mediated	Lesions similar to those in I for additional deposition of immunoglobulin and activated complement at sites of active myelin destruction	T-cell-mediated inflammation with macrophage/microglia activation; complement-mediated lysis of antibody-targeted myelin
(III) Distal oligodendrogliopathy	Inflammation by T cells and macrophages; small vessel vasculitis with endothelial cell damage and microvessel thrombosis; degeneration of distal oligodendrocyte processes, followed by oligodendrocyte apoptosis and demyelination	T-cell-mediated small vessel vasculitis with secondary ischemic damage of the white matter
(IV) Primary oligodendrocyte damage with secondary demyelination	Lesions similar to those in (I), but prominent oligodendrocyte degeneration in a small rim of periplaque white matter	T-cell-mediated inflammation with macrophage/microglia activation; demyelination induced by macrophage toxins on a background of metabolically impaired oligodendrocytes; genetic defect of oligodendrocytes?

pathophysiological process, involving oligodendrocytes' apoptosis by hypoxic injury, perhaps modified in part by genetic factors in individual cases.[11] The number of pathological processes is difficult to ascertain with certainty because of the rarity of finding an ultra-early lesion and the need to use autopsy material from many patients with chronic disease. Furthermore, current laboratory models of MS are based on an immunological process, while the ultra-early pathology raises the possibility of some novel process underlying new lesion formation in MS.[12]

Multiple sclerosis has a number of possible mechanisms involved in myelin injury and oligodendrocyte regeneration. While a direct genetic link has not been found, there are several candidate genes in families with multiple members with the disease. The potential environmental factors also remain speculative, with the leading candidates including infections and metabolism factors. Any mechanism for disruption of the BBB can potentially initiate the immunological process or cause a relapse. When the BBB is damaged, sensitized T cells from the systemic circulation can enter the central nervous system. Matrix metalloproteinases (MMPs) degrade the extracellular matrix and facilitate migration of immune cells. Once the T cells have entered the brain, they can release cytokines, which can attack the oligodendrocyte and lead to its death. Injury to the myelin membrane results in axons that are no longer able to transmit action potentials efficiently within the central nervous system. There are several possible mechanisms of repair of the myelin membrane, including resolution of the inflammatory response followed by remyelination; spread of sodium channels from the nodes of Ranvier to cover denuded axon segments and restore conduction; antibody-mediated remyelination; and remyelination resulting from the proliferation, migration, and differentiation of resident oligodendrocyte precursor cells.[1]

PROTEASES IMPLICATED IN MS PATHOLOGY

Several proteases in the brains of MS patients can attack myelin. Lysosomal enzymes were identified in inflammatory cells. Phospholipase A attacks membrane lipid components, such as lysolecithin, which has cytolytic action on myelin membranes. Acid and neutral proteases have been detected in the CSF of patients with MS. Neutral proteases were shown to attack the structure of the myelin molecule. Stimulated macrophages secreted proteases that attacked myelin.[13] The active substance in the macrophage supernatant was found to be plasmin, which was shown to disrupt myelin basic protein in frozen specimens of tissue. Similarly, there was myelin breakdown in fresh tissue when both complement and plasmin were added. Animal studies in EAE showed a beneficial response to treatment with agents that interfered with the action of plasmin.[14] Fibrin films placed on the surface of tissues from MS patients showed lytic regions suggestive of fibrinolysis by plasmin.[15]

Matrix metalloproteinases are increased in the CSF and brains of MS patients. During an acute exacerbation of MS, MMP-9 is elevated in CSF.[16] The MMPs attack myelin and break it into myelin basic protein fragments.[17] The MMP-9 comes from the brain compartment, which was convincingly demonstrated in studies that measured MMP-9 levels in the blood and CSF, indexing the MMP-9 to albumin in both compartments by analogy with the IgG index used in the diagnosis of MS.[18]

Treatment of animals with EAE with MMP inhibitors reduces the severity of the illness.[19] Direct inhibitors of MMPs have not been tested in the treatment of MS patients. However, a tetracycline derivative, minocycline, which has anti-inflammatory actions, including inhibition of MMPs, benefited patients with MS in an uncontrolled clinical trial involving a small number of subjects.[20,21] Minocycline suppresses production of MMP-9 but also has other effects on the inflammatory response, including inhibiting the microglia response, making it difficult to determine its mechanism of action.

In the test tube, myelin can be degraded into immunogenic fragments of myelin basic protein (MBP) by the addition of MMPs.[22,23] Furthermore, MMP-7 knockout mice displayed reduced inflammation and white blood cell entry into the brain as well as across an in vitro cell culture system, suggesting that MMP-7 may contribute to the inflammatory response.[24] Several broad-spectrum MMP inhibitors, such as BB-1101 and GM6001, improve function and reduce weight loss in EAE.[25]

While the expression of the classic MBP transcripts is restricted to myelin-forming cells, splice variants of MBP, called *Golli-MBP*, can be generated by a membrane-bound MMP, MMP-25, to create similar immunogenic peptides. Autoactivation of two proconvertases (PCs), furin and PC2, activates MMP-25 in macrophages, leading to immunogenic MBP fragments that are presented in the major histocompatibility complex on the cell surface. This results in T-cell activation and homing to the brain, MBP attack, and inflammation that increases macrophage infiltration and the activation of multiple MMPs, thereby contributing to further MBP destruction.[26]

Immunomodulation with β-interferon reduces MMPs, as does treatment with the anti-inflammatory agent minocycline; however, minocycline causes only a minor reduction in disease severity.[27] In contrast, short-term use of high-dose steroids (e.g., methylprednisolone), commonly used in acute MS flares, dramatically reduces elevated MMP-9 levels in CSF (Figure 12–6) and corresponds with closure of the leaky BBB, likely by blocking the proinflammatory activator protein-1 (AP-1) sites in the MMP-9 promoter[28] (Figure 12–7).

Treatment of inflammation is beneficial in the early stages of an injury, but it may block essential molecular mechanisms in the repair process and slow recovery. Oligodendrocytes grow by secreting MMPs at the ends of the processes, which, similarly to the growing blood vessels, allow the processes to extend.[29] Such a mechanism may be important in repair. Mice lacking MMP-9 have impairment in myelin formation after lysolecithin-induced demyelination. Macrophages and oligodendrocyte progenitors express NG2, a specific chondroitin sulfate proteolglycan (CSPG) family member. Impairment in myelin formation may be explained by the failure to clear the accumulation of NG2, an inhibitory protolglycan that retards the maturation and differentiation of oligodendrocytes that are required for remyelination.[30]

A novel model of MS in the mouse has recently been introduced that overexpresses

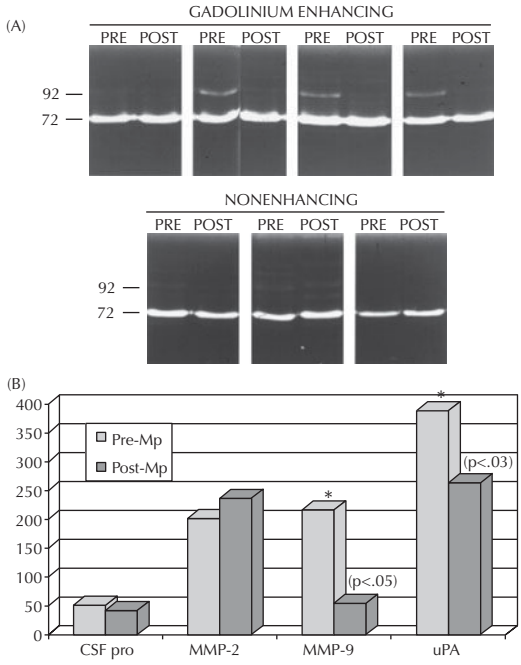

Figure 12–6. (**A**) Gelatin-substrate zymograms (upper) of CSF from MS patients with gadolinium-enhancing lesions on MRI. Pre- and posttreatment CSF samples for individual patients are shown. Molecular weights were determined from human HT1080 cells that constitutively express MMP-2 (72 kDa) and MMP-9 (92 kDa). Lower zymograms from patients without enhancement on MRI. Low levels of MMP-9 were seen in both the pre- and posttreatment gels. (**B**) Relative lysis zones for MMP-9 for pre- and posttreatment values for patients with enhancing lesions. Levels of MMP-9 before (Pre-MP) and after (Post-MP) treatment with high-dose methylprednisolone were significantly reduced as shown by means and standard errors. Urokinase plasminogen activator (uPA) was significantly decreased by MP. The asterisk shows the statistically significant differences between before- and after-treatment values, with the significance level given in parentheses. (From Ref. 28.)

DM20 (ND4). These mice have a slowly demyelinating process that begins at around the fourth month of life and causes early death.[31] Unexpectedly, the investigators found elevated mRNA levels of MMP-3 prior to the onset of overt disease but no elevation in MMP-9. The other MMPs, including MMP-11, -2, and -9, failed to show an increase in mRNA levels. MMP-13 showed a small increase. The increase in MMP-3 was confirmed at the protein level by Western blot analysis. When the investigators crossbred a DM20-overexpressing mouse with a tissue inhibitor of metalloproteinase-1 (TIMP-1) transgenic mouse, the resulting

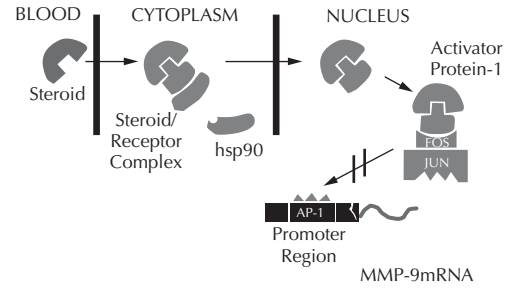

Figure 12–7. Hypothetical mechanism involved in the inhibition of MMP-9 production with steroids. The steroid (far left) enters the brain across the BBB. Once within the cytoplasm, the steroid joins the receptor complex with heat shock protein-90 (hsp90). The complex enters the nucleus, attaches to the *fos/jun* proto-oncogene, and blocks the AP-1 promoter regions to reduce the transcription of MMP-9 mRNA.

hybrid had a milder clinical course than the DM20 strain alone, and there was reduced expression of MMP-3.[32]

BBB DISRUPTION IN MS

Free radicals contribute to the disruption of the extracellular matrix and the opening of the BBB. Nitrogen free radicals are produced in the site of inflammation. Cocultures of neurons and microglia that have been stimulated with the inflammatory-inducing agents, interferon gamma and lipopolysaccharide, lead to the death of the neurons.[33] Dexamethasone reduces cell death by blocking the production of nitric oxide through inhibition of the gene that produces inflammatory nitric oxide synthetase. The mechanism of steroid action involves interfering with the steroid receptor and blocking the action of the c-fos/c-jun dimer at the AP-1 site, as described earlier. These cell studies have been paralleled in humans by showing that the contrast enhancement in both CT and MRI can be drastically attenuated with high-dose steroids.

In the relapsing and remitting form of MS, there is active inflammation around venules. The triggering event that initiates the attack on the venule remains elusive, but it is recognized that exacerbations can be started by multiple factors, including viral infection and trauma. Often the initiating event is not found. Searches have been carried out to identify the

antigen that could be the cause of an autoimmune attack, but none has been found. While hereditary factors are important, the manner in which they increase susceptibility is unclear.

Most of the research has focused on the relapsing-remitting form of MS; little is known about the primary progressive form of the disease. Pathological studies show less inflammatory activity around blood vessels in the primary progressive form than in the relapsing-remitting and secondary progressive forms. Pathological studies show that the blood vessels become hypertrophic, with thickening of the collagenous material around the blood vessel.[34] Fewer enhancing regions are seen on gadolinium-DTPA (diethylenetriaminepentaacetic acid) MRI in the primary progressive form than in the relapsing-remitting form, but serum proteins are found in the brain, suggesting a subtle lesion of the BBB below the threshold for visualization with gadolinium. The primary progressive form of MS is similar clinically to the secondary progressive form, which has more of an inflammatory response around the blood vessels than is seen in the primary progressive form. The differences in pathological findings in the various forms of MS have led some investigators to question whether they are due to one disease process. Multiple forms of MS have been described based on MRI findings and at autopsy.[35]

DEVIC'S NEUROMYELITIS OPTICA

Neuromyelitis optica (NMO), also known as *Devic's disease*, has clinical features that resemble MS and acute disseminated encephalomyelitis (ADE). However, patients have relapses and remissions in NMO and a monophasic course in ADE. Neuromyelitis optica is a pathologically separate entity with necrosis of the spinal cord rather than demyelination.[36] An antibody to aquaporin-4 (AQP4) was discovered in the serum of patients with NMO; it localizes to several regions that affect water balance, such as astrocytic endfeet and glial limitans. The antibody has been developed into a diagnostic test that has greatly facilitated the diagnosis of NMO and aided the ability to separate NMO from MS, which are similar clinically but have different underlying pathology and require different treatments. Since NMO has an antibody that is thought to produce the symptoms, it is classified as an autoimmune disease that can be treated with steroids, plasmapheresis, and immunosuppressants, which have all been shown to be useful in NMO treatment but are of limited effectiveness in the treatment of MS.

Diagnostic criteria are based on clinical findings, characteristic images on MRI ,and the detection of AQP4 antibodies in the blood. In 2004 a protein was detected in the serum of NMO patients, which was shown to react with AQP4 and provided a diagnostic test to aid in the diagnosis of Devic's disease.[37] Some patients with NMO may be seronegative for NMO-IgG, while some patients with NMO-IgG may not fulfill the clinical criteria for NMO. Thus, serological testing is now an important part of the diagnostic procedure, and seropositive and seronegative cases are described in a manner similar to that of myasthenia gravis.

The diagnosis of Devic's disease requires the presence of two absolute criteria plus at least two of three supportive criteria. The absolute criteria are optic neuritis and acute myelitis. Supportive criteria include two of the following three: (1) a brain MRI scan that does not meet the criteria for MS at disease onset; (2) a spinal cord MRI scan with a contiguous T2-weighted signal abnormality extending over three or more vertebral segments, indicating a relatively large lesion in the spinal cord; and (3) NMO-IgG seropositive status.[38]

Neuromyelitis optica-IgG is a clinically validated serum biomarker that distinguishes relapsing central nervous system inflammatory demyelinating disorders related to NMO from multiple sclerosis (Table 12–2). This autoantibody targets astrocytic AQP4 water channels. Clinical, radiological, and immunopathological data suggest that NMO-IgG might be pathogenic. Brains with NMO have depletion of AQP4, usually without associated myelin loss. There are focal vasculocentric deposits of IgG, IgM, and complement, prominent edema, and inflammation.[36]

Exposure of astrocytes to NMO patient serum and active complement compromises the membrane integrity of central nervous system-derived astrocytes. Aquaporin-4 is endocytosed, with concomitant loss of Na^+-dependent glutamate transport and loss of the excitatory amino acid transporter 2 (EAAT2), which exists in astrocytic membranes as a macromolecular

Table 12–2 **Clinical Characteristics and NMO-IgG Seropositivity Rates in NMO and MS in 102 Patients**

				High-Risk Syndromes	
	NMO (n = 45)	MS (n = 22)	p	Recurrent optic neuritis (n = 8)	Recurrent transverse myelitis (n = 27)
			Demography		
Male/female	7 (16%)/38 (84%)	6 (27%)/16 (73%)	0.3271	1 (13%)/7 (87%)	9 (33%)/18 (67%)
Median age at onset, years (IQR)	41 (30–50)	32 (28–38)	0.0092	43 (25–51)	42 (37–53)
White (% of those recorded)	32 (76%)	18 (95%)	0.1481	7 (100%)	17 (68%)
			Clinical Features		
Bilateral optic neuritis	30 (67%)	9 (41%)	0.0447	7 (88%)	n/a
Bilateral simultaneous optic neuritis	16 (36%)	4 (18%)	0.1444	1 (13%)	n/a
Severe attack-related weakness	32 (71%)	3 (14%)	<0.0001	n/a	15 (56%)
			Imaging and CSF		
Initial MRI brain normal (% of those tested)	31 (77%)	9 (47%)	0.0309	7 (88%)	17 (71%)
Initial MRI brain does not meet multiple sclerosis criteria (% of those tested)	38 (84%)	14 (64%)	0.0953	7 (88%)	23 (85%)
MRI spinal cord lesion >3 segments (% of those tested)	42 (98%)	3 (15%)	<0.0001	0	26 (100%)
CSF OB or raised lgG index (% of those tested)	4 (17%)	8 (67%)	0.0074	0	2 (13%)
NMO lgG detected	33 (73%)	2 (9%)	<0.0001	2 (25%)	14 (52%)

CSF = cerebrospinal fluid. p values compare patients with NMO with those with index symptoms of optic neuritis and myelitis (subsequently diagnosed with MS).
n/a = not applicable.
Source: From Ref. 76.

complex with AQP4. Binding of NMO-IgG to astrocytic AQP4 initiates several potentially neuropathogenic mechanisms: complement activation, AQP4 and EAAT2 downregulation, and disruption of glutamate homeostasis.[39]

NONIMMUNOLOGICAL PROCESSES IN DEMYELINATION

Proteolytic demyelination can occur after nonimmunological stimuli. Many neutral proteases have been shown to attack the myelin molecule. These enzymes are released into the extracellular space, where they can be activated. An example of a nonimmunological demyelinating process was demonstrated in animals that had been injected peripherally with purified protein derivative and subsequently had an intraventricular challenge with the same antigen. There was widespread demyelination.[40] The source of the demyelinating factors was shown to be macrophages that had been attracted to the sensitized regions, where they released neutral proteases that caused the demyelination. This process was called *bystander demyelination* to distinguish it from an antigen-driven response. In vitro studies showed that macrophages collected from the peritoneum could be stimulated to release the proteolytic enzyme, plasmin, which was shown to be involved in the breakdown of MBP in the presence of complement.[13] A delayed hypersensitivity reaction due to intracerebral injection of Bacillus Calmette-Guerin with a peripheral challenge led to the MMP-mediated opening of the BBB, and synthetic inhibitors of MMPs blocked the injury to the BBB.[41] Evidence for an effect of the MMPs on myelin came from the direct injection of MMPs into the white matter, which resulted in axonal damage that could be blocked by MMP inhibitors.[42]

Axonal damage is now recognized to be important in MS. Hypoxia may play an important role in both the apoptotic death of oligodendrocytes[10] and the energy failure leading to axonal damage.[43] While the mechanism of axonal damage in MS is uncertain, there is accumulating evidence to support a role for energy failure secondary to hypoxic injury. One possible mechanism involves mitochondrial damage and calcium. In this scenario, the increased energy demand of impulse conduction along excitable demyelinated axons and reduced axonal adenosine triphosphate production induces hypoxia in demyelinated axons. The chronic necrosis of axons damages mitochondria, with Na^+ influx through voltage-gated Na^+ channels and axonal α-amino-3-hydroxy-5-methyl-4-isoxazolepropionic acid (AMPA) receptors, release of toxic Ca^{2+} from the axoplasmic reticulum, overactivation of ionotropic and metabotropic axonal glutamate receptors, and activation of voltage-gated Ca^{2+} channels, ultimately leading to excessive stimulation of Ca^{2+}-dependent degradative pathways.[43]

In acute MS lesions in humans, the leakage of plasma proteins into the brain was demonstrated with stains for complement.[44] Vessel wall damage was found in all acute plaques, and intramural deposition of complement was seen on smooth muscle components. Macrophages infiltrated the region of the plaques, and the blood vessels showed damage to the type IV collagen and laminin, suggesting disruption of the basal lamina. These actions suggested that humoral, immune-mediated damage to the myelin was unlikely, but that the myelin was damaged as an innocent bystander rather than as a specific target for the inflammatory reactions. In a study of primary and secondary progressive forms of MS, the majority of the demyelinated plaques were of the chronic, inactive type, with few oligodendrocytes and fibrous gliosis, suggesting a late stage of the illness.[34] Thickened, hyalinized blood vessel walls were commonly seen. The secondary progressive MS group showed a larger number of active lesions containing macrophages with digested myelin degradation products than the primary progressive group. The investigators concluded that the pathological findings showed unequivocally that primary progressive MS was an inflammatory disease.

Two reports have identified MMPs in acute and chronic MS. In one study, tissue was available from an acute case of MS, which could be frozen for immunostaining. In this tissue, the macrophages in active MS lesions expressed MMPs, including MMP-1, -2, -3, and -9.[45] Another study of acute and chronic MS lesions found MMP-7 and MMP-2 but failed to find MMP-3.[46] Levels of mRNA have been studied by quantitative reverse transcriptase polymerase chain reaction from regions of normal-appearing white matter and MS lesions. Increased levels of mRNA for MMP-2, -3, -8,

and -9 were detected in the regions with lesions, and mRNA for MMP-9 was elevated in normal-appearing tissues.[47] Immunohistochemistry showed MMP-9 in blood vessels in both normal and abnormal tissues. Levels of TIMPs were similar in control and MS patients, suggesting an imbalance between the proteases and their inhibitors. Since mRNA levels for several of the MMPs were elevated in the tissues but not in the cells in the CSF, an endogenous source was suggested for the MMPs. Matrix metalloproteinases have been identified in the CSF of patients with MS. Gelatin-substrate zymography has shown that latent MMP-2 is a normal constituent of the CSF. In many neuroinflammatory conditions, zymography and enzyme-linked immunosorbent assay have detected MMP-9. In bacterial meningitis, where large numbers of neutrophils are present, they are a major source of the enzyme. However, in patients with MS, when the CSF levels of MMP-9 are markedly elevated, generally only a small number of white blood cells are present, and more likely brain cells are the major source for the MMP-9.

Agents that block the action of the MMPs reduce transport across the artificial membranes.[48] Interferon-β, which is used in the treatment of MS, decreases the movement of white blood cells by blocking the release of the MMPs.[49] The MMPs have been found to be elevated in the blood of patients with MS, particularly during the acute phase of the illness, and there is a correlation between the levels in the blood and an acute attack of MS.[50] Levels of serum MMPs fall during treatment with interferon-β, and mRNA for the MMPs from blood-derived leukocytes is reduced by such treatment.[51]

EAE AND THE PATHOGENESIS OF MS

A model of demyelination in the monkey was first published in 1935. Rivers and Schwentker injected monkeys with homologous brain tissue.[52] The model was refined by Kabat and colleagues, who added Freund's complete adjuvant to enhance the response.[53] Animals with EAE have a mononuclear infiltrate of lymphocytes and macrophages around small blood vessels. In contrast to MS, EAE is a monophasic illness that primarily involves the blood vessels, with demyelination limited to the immediate vicinity of the inflamed vessels. The lesions of EAE are similar to those seen in acute disseminated encephalomyelitis, which is often found in postviral or postvaccination syndromes. Experimental allergic encephalomyelitis resembles an early stage of an acute MS attack since the inflammation occurs around the blood vessels and the damage to the white matter grows around the vessels. In the early stages of an acute MS attack, white blood cells adhere to blood vessels and release proteolytic enzymes that facilitate the entrance of the cells into the brain across the inflamed veins. The MMPs are important in the penetration of circulating white blood cells into the brain. Amplification of the inflammation occurs due to the release of cytokines by the infiltrating and resident cells.

Inflammation causes the opening of the BBB and is one of the initial events in the acute MS lesion. Fibrin and fibrinogen are found in the walls of the vessels involved in the acute inflammation. In the EAE model, the deposition of fibrinogen is an early event that impacts the inflammatory cascade characterizing EAE. In rats sensitized to whole spinal cord or MBP, perivascular fibrin deposits corresponded with the occurrence of clinical paralytic signs, but neither paralytic signs nor fibrin deposition were temporally related to perivascular cellular infiltrates. Treatment with ancrod, a polypeptide derived from the venom of *Agkistrodon rhodostoma*, caused a severe hypofibrinogenemia with inhibition of fibrin deposition and attenuation of the paralysis without influencing the cellular infiltrates. Increasing neurovascular permeability and accumulation of edema fluid secondary to activation of the clotting cascade were proposed to be responsible for the clinical abnormalities characterizing EAE; cellular infiltrates constituted an independent immune response.[54]

In EAE, inflammatory T lymphocytes cross the BBB after being sensitized by the peripheral injection of MBP in Freund's adjuvant. In the early stages of EAE, disruption of the BBB has been shown by studies with radioisotopes.[55] Fibrin is deposited in the inflamed vessels, and agents that break down the fibrin, such as snake venom, reduce the injury.[54] Damage to the wall of the blood vessel initiates a repair process. Myelin fragments are phagocytized by

macrophages. Plasmin/plasminogen is upregulated to participate in the remodeling of the damaged tissues. Proteases released by the macrophages, however, perpetuate the injury by causing bystander demyelination.

When brain tissue is permeable to blood proteins, extravascular fibrin deposition occurs and correlates with sites of inflammatory demyelination and axonal damage. Depleting fibrin in TNF transgenic mouse models of MS (TgK21 and Tg6074) by crossing the TgK21 strain into a fibrin-deficient background produced a TgK21*fib*$^{-/-}$ mouse. The fibrin-depleted transgenic mouse showed decreased inflammation and less expression of major histocompatibility complex class I antigens, reduced demyelination, and a lengthened life span compared with TgK21 mice. Fibrin depletion, using the snake venom ancrod, in Tg6074 mice also delayed the onset of inflammatory demyelination. The investigators concluded that fibrin regulates the inflammatory response in neuroinflammatory diseases.[56]

Since its inception as a model of MS, numerous drugs have been tested on animals with EAE. Although many have been shown to be efficacious in the animals, few have been successfully developed as therapies for human patients. One of the drugs that were shown to affect the course of EAE was the MMP inhibitor, GM6001. Using the EAE model, disruption of the BBB and clinical symptoms in the animals were reduced by inhibitors to the MMPs.[57] Rats with EAE show the expression of mRNA for MMP-3, MMP-7, and MMP-9, while MMP-2 and membrane-type-MMP are constitutively expressed. Immunohistochemistry of rats with EAE shows MMP-9 in blood vessels and neutrophils and MMP-7 in macrophages.[58]

While EAE is used as a model for the pathological processes that occur in MS, the primary site of the injury lies in the blood vessels. Secondarily, the myelin is attacked by proteases released during either the initial entry of the white blood cells into the brain or by macrophage products formed as part of the remodeling and repair process. It could be argued from the MRI studies, which show permeability changes in the early stages of the acute MS attack, that the blood vessels are the primary site and that the attack on the myelin is secondary in the human disease. If that is the case, then the relevance of the EAE model increases.

Ultra-small particles of iron oxide (USPIOs), which accumulate in phagocytic cells, have been used as contrast agents for MRI. The USPIOs are taken up by the macrophages and, after entering the brain, produce a paramagnetic effect that identifies their presence. In an MRI study in rats with EAE, the particles were shown to infiltrate into the brain.[59] However, enhancement with gadolinium-DTPA appeared at the onset of illness on day 9, while the USPIOs were best seen at the height of the illness on day 14. This provides convincing evidence that changes in the BBB precede the infiltration of monocytes into the brain. The iron particles were shown histologically to be inside the microglia/macrophages with iron stains.

There has been considerable debate about the relevance of the EAE model for the human disease because of its monophasic course and intense monocytic infiltration around the blood vessels. The demonstration of inflammation on MRI in the early stages of MS, and the observation that the enhancement on MRI can precede the development of clinical symptoms, have greatly increased interest in the role of inflammation and the BBB in acute MS. With the rekindling of interest in inflammation in MS, the EAE model has taken on new significance.

MODERN APPROACHES TO THE TREATMENT OF MS

With the introduction of interferons the modern era of immunomodulatory treatment of MS began. Several agents, including interferon beta-1a, interferon beta-1b, glatiramer acetate, and natalizumab, are beneficial in relapsing-remitting MS.. Interferon beta-1b (Betaseron) was the first agent approved by the U.S. Food and Drug Administration (FDA) for use in MS. A dose of 8 million international units (MIU) administered subcutaneously every other day produced a significant reduction in relapse rate with long-term benefits. Efficacy is compromised in some patients who develop neutralizing antibodies to the drug.

An intramuscular form, interferon beta-1b, is available. The INCOMIN study showed that interferon beta-1b was superior to interferon beta-1a, with more patients remaining relapse-free and fewer new lesions appearing on MRI.[60]

Another study comparing both agents found them to be similar, leaving open the question of which agent is superior.[61] Interferon beta-1a (Avonex) is given by weekly intramuscular injection of 6 million units (30 μg). A newer interferon beta-1a (Rebif) was shown in the PRISM trial to also reduce the number of relapses, but it had a higher rate of neutralizing antibody production.[62]

Use of the interferons is associated with significant side effects. Reactions at the injection site are common, as are flu-like symptoms. Treatment with nonsteroidal anti-inflammatory agents can control these symptoms. Elevated levels of alanine aminotransferase suggests hepatic injury in patients, but liver failure is rare. The development of neutralizing antibodies limits the effectiveness of the interferons. The rates of development of these antibodies differ, depending on the type of interferon. Antibody formation was highest over 18 months in Betaseron (31%), Rebif (15%), and Avonex (2%).[63]

The serendipitous discovery that a polymer composed of four amino acids that are antigenically similar to MBP reduced the incidence of EAE led to the development of Glatiramer acetate (copolymer).[64] Treatment with copolymer in MS patients significantly reduced the number of new T2 lesions. Copolymer has an effect similar to that of the interferons and does not lead to the development of neutralizing antibodies. Many studies comparing copolymer to various interferons showed the similarity of the agents.

Several oral medications are being tested, but only one has FDA approval. These agents generally act to reduce white blood cell transport into brain. Fingolimod (Gilenya), a sphingosine-1-phosphate-receptor modulator that prevents lymphocyte egress from lymph nodes, showed clinical efficacy and improvement on imaging in a phase 2 study involving patients with MS. This trial showed the superior efficacy of oral fingolimod with respect to relapse rates and MRI outcomes in patients with MS compared with intramuscular interferon beta-1a. However, there were several fatal infections in patients taking fingolimod, and studies lasting for more than 1 year are needed to assess the safety and efficacy of treatment beyond 1 year.[65]

Natalizumab (Tysabri) is a humanized monoclonal antibody against the cellular adhesion molecule α4-integrin that is used in the treatment of MS. It is administered by intravenous infusion every 28 days. The drug reduces the ability of inflammatory immune cells to attach to and pass through the BBB. Natalizumab has proven effective in treating the symptoms and preventing relapse, vision loss, and cognitive decline and significantly improving the quality of life for persons with MS. Natalizumab was approved in 2004 by the FDA. It was subsequently withdrawn from the market by its manufacturer after it was linked with three cases of the rare neurological condition progressive multifocal leukoencephalopathy when administered in combination with interferon beta-1a.[66,67]

EPILOGUE: SYNTHESIS AND FUTURE DIRECTIONS

White matter hyperintensities are commonly identified on MRI and are associated with a wide variety of pathological processes. The fact that they are nonspecific and common limits the use of MRI in diagnosis and emphasizes the need for correlation with the clinical history and neurological examination. The common occurrence of white matter hyperintensities in elderly patients further reduces the diagnostic value of MRI alone. In spite of the ubiquitous nature of white matter hyperintensities and their prevalence in the elderly, hypoxic/ischemic injury is the main cause of injury in pathological states, making them a useful biomarker for hypoxia. In a study of white matter lesions in the elderly, the lesions were visualized postmortem with MRI and correlated histologically with molecular markers of hypoxic injury. The investigators found pathological evidence of BBB disruption and hypoxia. Severe myelin loss and increased microglia were present in periventricular and deep subcortical lesions compared with nonlesional aged brain. Clasmatodendritic astroglia, immunoreactive for the serum protein fibrinogen, were present, suggesting extravasation of serum proteins. Data from that study suggested that dysfunction of the BBB contributed to the pathogenesis of some cerebral white matter lesions associated with aging.[68] Another study from the same group linked the white matter lesions with the presence of hypoxia. The investigators showed that periventricular

lesions were associated with loss of the ependymal lining, and that in deep subcortical lesions there was arteriolosclerosis as well as capillary endothelial and microglial activation compared with normal white matter. Immunoreactivity for HIF-1α and HIF-2α was elevated along with other hypoxia-regulated proteins, including MMP-7, and neuroglobin, which is a member of the vertebrate globin family involved in cellular oxygen homeostasis. The severity of congophilic amyloid angiopathy was associated with increased HIF-1α expression. The data support a hypoxic environment within white matter hyperintensities. Persistent HIF expression may result from failure of normal adaptive mechanisms. White matter ischemia appears to be a common feature of the aging brain.[69]

Studies of multiple types of white matter lesions from autopsy material from patients with MS, encephalitis, and acute and chronic stroke show the importance of hypoxia in the inflammatory response that results in demyelination[9] (Figure 12–8). Acute MS studies indicate that pattern III due to hypoxic injury to the oligodendrocytes resulting in apoptosis has pathological similarities with ischemic injury to the white matter. While multiple pathologies are clearly involved, the final common pathway of injury appears to be inflammation triggered by hypoxia with activation of capillary endothelial cells and microglia, recruitment of macrophages, and release of proteases and free radicals. The result is an attack on the BBB and the myelinated fibers that perpetuates the hypoxic environment and contributes

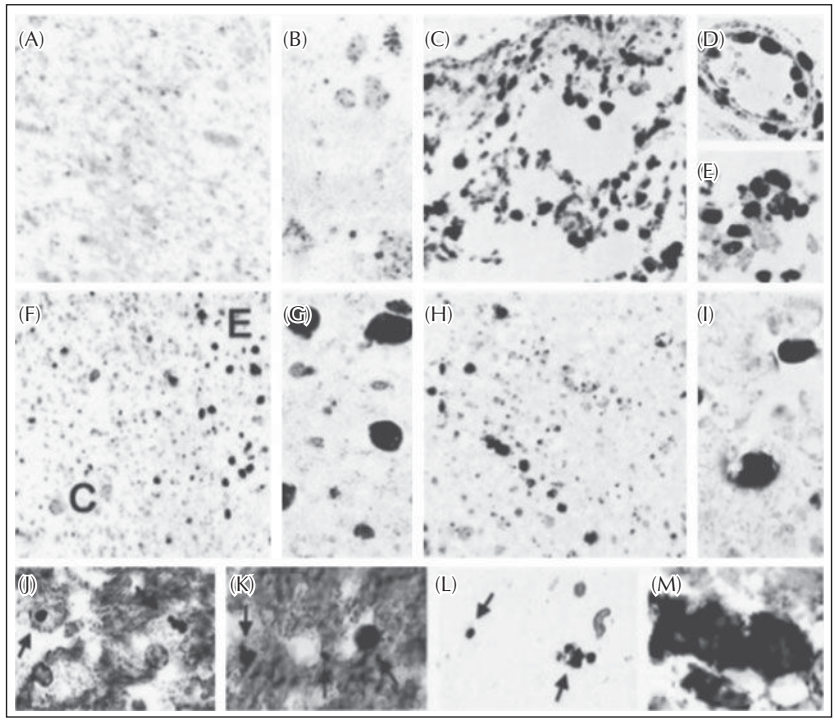

Figure 12–8. Immunocytochemical detection of HIF-lα in brain lesions. (**A,B**) White matter of the control brain showing some immunoreactivity in lipofuscin granules but absence of staining of nuclei. (**C–E**) Acute ischemic lesion of a stroke patient showing abundant expression of HIF-lα in nearly all cell nuclei, including glia cells, macrophages, and endothelial cells. (**F,G**) Active MS lesion with MAG loss showing a high density of nuclei with HIF-lα expression at the active plaque edge (**EI; C**): inactive plaque center. (**H,I**) Active lesion in a case of cytomegalovirus encephalitis with MAG loss with profound expression of HIF-lα in cell nuclei. (**J–M**) White matter, acute ischemic lesion of a stroke patient. (**J,K**) Immunocytochemistry for MOG and nuclear counterstaining with hematoxylin shows numerous oligodendrocytes with condensation of chromatin and nuclear fragmentation (arrows). (**I**) Cells with nuclear condensation and fragmentation in the lesions are stained by in situ end labeling for visualization of DNA fragmentation (arrows). (**M**) Double labeling of an oligodendrocyte in the infarct edge with HIF-lα (brown) and 2',3'-cyclic nucleotidase 3'-phosphodiesterase (CNPase; blue). Magnifications: **A**, ×11160; **B**, ×790; **C**, ×388; **D**, e, **G**, **J-I**, ×990; **F**, ×246; **H**, ×308; **M**, ×1800. (From Ref. 9; See also the color insert.)

to the progressive damage. This concept shifts the emphasis away from the immunological causes of demyelination and opens an interesting new approach, namely, the reduction of inflammation, BBB damage, and proteolysis, which is similar to the approach used in the studies being done to promote neuroprotection in stroke. Another implication of the role of hypoxia rather than immunological mechanisms is that the model for immunology of MS, EAE, provides information only on the early stages of the lesions, which are dominated by the presence of T lymphocytes. This may explain why many agents that are effective in EAE models fail in clinical trials.

Hypoxia is recognized as the key factor in cell death from stroke, but the role of hypoxia in demyelinating diseases has waxed and waned with advocates. Inflammatory opening of the BBB with vasogenic edema in the white matter may cause tissue hypoxia. Since stroke and MS have multiple pathologies, which often are not apparent from the clinical examination, use of neuroimaging and biochemical measures aids in identifying the underlying pathological process. In stroke, the key to diagnosis is use of the diffusion-weighted imaging sequence, which was a major advance in the diagnosis of stroke. In MS, the use of fluid attenuated inversion recovery sequences in the imaging of white matter improves the diagnosis of the disease, and enhancement of the meninges is helpful in identifying an infection in the subarachnoid space.

Combining multiple modalities improves the ability to identify the underlying pathological process. A well-known example of the multimodal approach is the use of the clinical examination; MRI changes in white matter suggestive of venule involvement, such as Dawson's fingers and CSF biomarkers including elevation of IgG and MBP; and identification of oligoclonal bands in the CSF of MS patients. The major distinction between an ischemic pathological process and one driven by immunological factors is the timing of the disruption of the BBB. When the insult is initiated by an ischemic event, there is initial loss of oxygen and depletion of tissue energy stores. Neurons are the primary site of injury, with swelling of the cells leading to cytotoxic edema and shrinkage of the extracellular space. Diffusion is restricted and the diffusion-weighted image, which reflects the slowed movement of water in the extracellular space, produces the increased signal on the diffusion-weighted image. As the ischemic injury proceeds from the initial energy depletion phase to the inflammatory phase, there is disruption of the BBB with vasogenic edema, as well as secondary damage to the white matter that actually began at the initial stages of hypoxia but was not fully manifest until late in the process.

Demyelinating lesions in MS begin very differently. Initially, the BBB is disrupted by some insult, which could be an autoimmune cell sensitized to myelin fragments, a viral infection, head trauma, or possibly extreme stress. All of these factors and others are postulated to be important in initiating the MS attack. Once the T cells and B cells are inside the BBB, they initiate the inflammatory response that leads to conversion of the T cells into Th1 and Th2 cells, linking with major histocompatibility complexes and antigen-presenting cells to release toxic cytokines that attack myelin. Thus, the MS disease process is an extrinsically driven one, while ischemia/hypoxia is an intrinsically mediated damaging process (Figure 12–9).

Attempts to create one coherent explanation of the diverse pathological processes in MS are likely to fail. A signaling event begins the pathological process. For reasons that remain to be discovered, the state of the venules in the brain changes to a proinflammatory condition. This could be due to a viral infection or some other insult in a person with a susceptible genetic makeup. Regardless of the initiating event, there is an influx of mononuclear cells facilitated by the release of proteases that attack the extracellular matrix around the blood vessels, allowing the lymphocytes, particularly the T lymphocytes, to cross the barrier provided by the tight junctions and the basal lamina. Once lodged within the brain, the activated lymphocytes secrete substances that attack white blood cells and aggravate the injury. At this early stage, the predominant cells are the neutrophils and the lymphocytes. As the acute inflammation is suppressed to limit the extent of the damage, the macrophages wait to begin the long, complicated repair process (Figure 12–10). While the final common pathway for damaging the oligodendrocytes to produce the white matter damage is similar in ischemic injury, there is an early hypoxia-driven activation of intrinsic macrophages and microglia that results in the production of proteases and free radicals, the

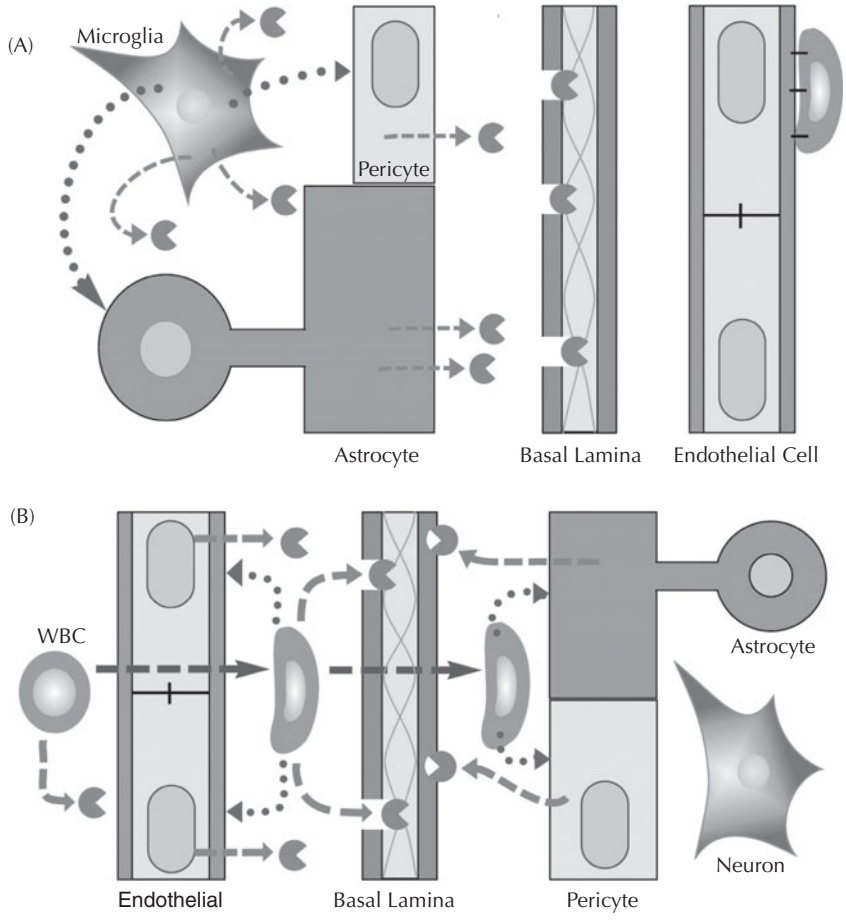

Figure 12–9. (**A**) Hypoxia/ischemia-initiated inflammation leads to activation of the intrinsic pathway of BBB damage through activation of astrocytes, microglia, and pericytes by the oxygen loss. (**B**) Initial attack on the BBB by autoimmune cells disrupts the basal lamina and allows the white blood cells to infiltrate. Inside the brain, the white blood cells proceed to damage cells by immune and inflammatory mechanisms.

execution substances that attack the myelin and lead to the death of the oligodendrocytes.

Treatments to enhance the recovery phase offer opportunities beyond the limited time frame of the acute injury. Angiogenesis and neurogenesis begin within the first week after an injury and continue for several weeks in stroke, and remyelination from oligodendrocyte precursors probably begins soon after the acute MS attack. The same molecular events that amplify the injury are often involved in recovery. Angiogenesis initially leads to a blood vessel that has not completely formed tight junctions and could be contributing to edema formation.[70] An example of the dual nature of growth factors is vascular endothelial growth factor (VEGF). Released under the influence of HIF in the early stages of an injury, VEGF is a key molecule in the formation of new vessels. It also contributes to the early opening of the BBB, and while it is acting, vessels remain permeable. Astrocytes secrete growth factors that contribute to survival of neurons and oligodendrocytes, but they also form a glial scar that restricts axonal growth. Microglia are major players in the early tissue destruction by secreting potent enzymes that remove debris from an injury site; later, they contribute to the healing process in ways that are just beginning to be understood. It appears that as the extracellular matrix undergoes remodeling, microglia provide essential growth factors to facilitate that process. In addition, they release proteases that are essential for matrix

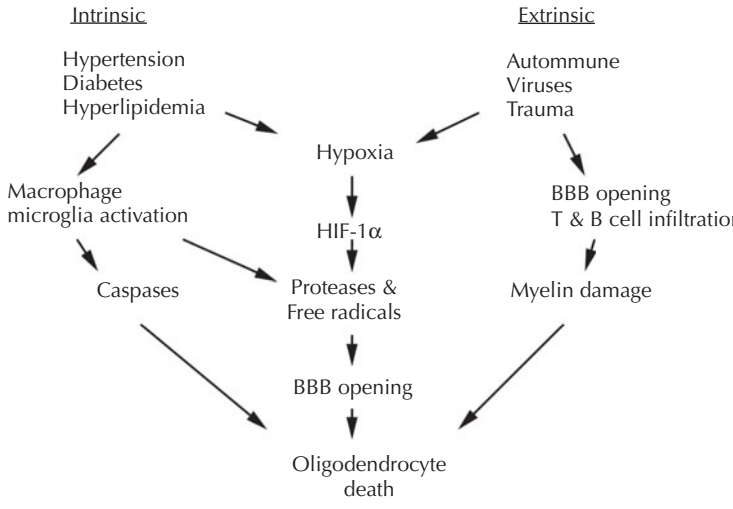

Figure 12–10. Schematic diagram showing the central role of hypoxia in the inflammatory-mediated death of the oligodendrocytes. In the intrinsic pathway, blood vessels are damaged by hypertension and arteriolosclerosis. This leads to activation of intrinsic macrophages that attempt to remodel the blood vessels but, in doing so, release proteases and free radicals that secondarily open the BBB and participate in the death of the oligodendrocytes. Caspases are also released by the hypoxia and directly cause apoptosis of the oligodendrocytes. In the extrinsic pathway, the invading cells secrete MMPs to cross the BBB, and the opening of the barrier is the initial event in the injury cascade. T and B cells form immune complexes with macrophages and antigen presenting cells to attack myelin and oligodendrocytes.

remodeling. These proteases, if released in the white matter, attack myelin, causing bystander demyelination, but curbing the delayed inflammatory response may impede recovery.

Taking into account the dual nature of the inflammatory response in the design of treatment trials provides a unique challenge. When does the beneficial phase of inflammation replace the detrimental phase? What part of the initial inflammatory phase should be contained, and how can the later benefits of inflammation be preserved and augmented? As the recovery begins, reformation of synapses occurs. Initial injury to the synapses, which occurs during ischemia, has the potential to reverse.[71] Loss of synapses most likely is an important mechanism for cognitive impairment that results from injury.[72]

At some stage, depending on the age of the patient, migration of cells toward the site of the lesion takes place. Some of these are pluripotenial stem cells that will grow into mature cells.[73,74] Many laboratories are attempting to find ways to augment the growth of these cells or to introduce new ones to take over the function of those that are damaged. Recovery after stroke occurs most rapidly in the first month, with slower progress in the second and third months. Even up to 1 to 2 years after the initial insult, some recovery of function can occur. Most often this involves younger patients with traumatic brain injury, but it also is seen in older individuals, which shows the potential for ongoing plasticity of the brain.[75]

REFERENCES

1. Noseworthy JH, Lucchinetti C, Rodriguez M, et al. Multiple sclerosis. *N Engl J Med*. 2000;343:938–952.
2. Prineas JW, Wright RG. Macrophages, lymphocytes, and plasma cells in the perivascular compartment in chronic multiple sclerosis. *Lab.Invest*. 1978;38: 409–421.
3. Dawson JW. The histology of disseminated sclerosis. *Trans R Soc Edin*. 1916;50:517–525.
4. Putnam TJ, Adler A. Vascular architecture of the lesions of multiple sclerosis. *Arch Neurol Psychiatry*. 1937;38:1–15.
5. Miller DH, Rudge P, Johnson G, et al. Serial gadolinium enhanced magnetic resonance imaging in multiple sclerosis. *Brain*. 1988;111:927–939.
6. Tan IL, van Schijndel RA, Pouwels PJ, et al. MR venography of multiple sclerosis. *AJNR Am J Neuroradiol*. 2000;21:1039–1042.
7. Tallantyre EC, Dixon JE, Donaldson I, et al. Ultra-high-field imaging distinguishes ms lesions from asymptomatic white matter lesions. *Neurology*. 2011;76: 534–539.
8. Lucchinetti C, Bruck W, Parisi J, et al. Heterogeneity of multiple sclerosis lesions: implications for the

pathogenesis of demyelination. *Ann Neurol*. 2000;47: 707–717.
9. Aboul-Enein F, Rauschka H, Kornek B, et al. Preferential loss of myelin-associated glycoprotein reflects hypoxia-like white matter damage in stroke and inflammatory brain diseases. *J Neuropathol Exp Neurol*. 2003;62:25–33.
10. Henderson AP, Barnett MH, Parratt JD, et al. Multiple sclerosis: distribution of inflammatory cells in newly forming lesions. *Ann Neurol*. 2009;66:739–753.
11. Gandhi R, Laroni A, Weiner HL. Role of the innate immune system in the pathogenesis of multiple sclerosis. *J Neuroimmunology*. 2010;221:7–14.
12. Barnett MH, Prineas JW. Relapsing and remitting multiple sclerosis: pathology of the newly forming lesion. *Ann Neurol*. 2004;55:458–468.
13. Cammer W, Bloom BR, Norton WT, et al. Degradation of basic protein in myelin by neutral proteases secreted by stimulated macrophages: a possible mechanism of inflammatory demyelination. *Proc Natl Acad Sci USA*. 1978;75:1554–1558.
14. Brosnan CF, Cammer W, Norton WT, et al. Proteinase inhibitors suppress the development of experimental allergic encephalomyelitis. *Nature*. 1980;285: 235–237.
15. Hirsch HE, Blanco CE, Parks ME. Fibrinolytic activity of plaques and white matter in multiple sclerosis. *J Neuropathol Exp Neurol*. 1981;40:271–280.
16. Gijbels K, Masure S, Carton H, Opdenakker G. Gelatinase in the cerebrospinal fluid of patients with multiple sclerosis and other inflammatory neurological disorders. *J Neuroimmunol*. 1992;41:29–34.
17. Chandler S, Cossins J, Lury J, et al. Macrophage metalloelastase degrades matrix and myelin proteins and processes a tumour necrosis factor-alpha fusion protein. *Biochem Biophys Res Commun*. 1996;228:421–429.
18. Liuzzi GM, Trojano M, Fanelli M, et al. Intrathecal synthesis of matrix metalloproteinase-9 in patients with multiple sclerosis: implication for pathogenesis. *Mult Scler*. 2002;8:222–228.
19. Hewson AK, Smith T, Leonard JP, et al. Suppression of experimental allergic encephalomyelitis in the Lewis rat by the matrix metalloproteinase inhibitor ro31–9790. *Inflammation Research*. 1995;44:345–349
20. Metz LM, Zhang Y, Yeung M, et al. Minocycline reduces gadolinium-enhancing magnetic resonance imaging lesions in multiple sclerosis. *Ann Neurol*. 2004;55:756.
21. Yong VW, Giuliani F, Xue M, et al. Experimental models of neuroprotection relevant to multiple sclerosis. *Neurology*. 2007;68:S32-S37; discussion S43-S54.
22. Chandler S, Coates R, Gearing A, et al. Matrix metalloproteinases degrade myelin basic protein. *Neurosci Lett*. 1995;201:223–226.
23. Opdenakker G, Van den Steen PE, Van Damme J. Gelatinase b: a tuner and amplifier of immune functions. *Trends Immunol*. 2001;22:571–579.
24. Buhler LA, Samara R, Guzman E, et al. Matrix metalloproteinase-7 facilitates immune access to the cns in experimental autoimmune encephalomyelitis. *BMC Neurosci*. 2009;10:17.
25. Clements JM, Cossins JA, Wells GM, et al. Matrix metalloproteinase expression during experimental autoimmune encephalomyelitis and effects of a combined matrix metalloproteinase and tumour necrosis factor-alpha inhibitor. *J Neuroimmunol*. 1997;74:85–94.
26. Shiryaev SA, Remacle AG, Savinov AY, et al. Inflammatory proprotein convertase-matrix metalloproteinase proteolytic pathway in antigen-presenting cells as a step to autoimmune multiple sclerosis. *J Biol Chem*. 2009;284:30615–30626.
27. Yong VW, Zabad RK, Agrawal S, et al. Elevation of matrix metalloproteinases (mmps) in multiple sclerosis and impact of immunomodulators. *J Neurol Sci*. 2007;259:79–84.
28. Rosenberg GA, Dencoff JE, Correa N Jr, et al. Effect of steroids on csf matrix metalloproteinases in multiple sclerosis: relation to blood-brain barrier injury. *Neurology*. 1996;46:1626–1632.
29. Oh LY, Larsen PH, Krekoski CA, et al. Matrix metalloproteinase-9/gelatinase b is required for process outgrowth by oligodendrocytes. *J Neurosci*. 1999;19: 8464–8475.
30. Larsen PH, Wells JE, Stallcup WB, et al. Matrix metalloproteinase-9 facilitates remyelination in part by processing the inhibitory ng2 proteoglycan. *J Neurosci*. 2003;23:11127–11135.
31. Mastronardi FG, Mak B, Ackerley CA, et al. Modifications of myelin basic protein in dm20 transgenic mice are similar to those in myelin basic protein from multiple sclerosis. *J Clin Invest*. 1996;97: 349–358.
32. D'Souza CA, Mak B, Moscarello MA. The up-regulation of stromelysin-1 (mmp-3) in a spontaneously demyelinating transgenic mouse precedes onset of disease. *J Biol Chem*. 2002;277:13589–13596.
33. Golde S, Coles A, Lindquist JA, et al. Decreased inos synthesis mediates dexamethasone-induced protection of neurons from inflammatory injury in vitro. *Eur J Neurosci*. 2003;18:2527–2537.
34. Revesz T, Kidd D, Thompson AJ, et al. A comparison of the pathology of primary and secondary progressive multiple sclerosis. *Brain*. 1994;117:759–765.
35. Wingerchuk DM, Weinshenker BG. Neuromyelitis optica. *Curr Treat Options Neurol*. 2008;10:55–66.
36. Roemer SF, Parisi JE, Lennon VA, et al. Pattern-specific loss of aquaporin-4 immunoreactivity distinguishes neuromyelitis optica from multiple sclerosis. *Brain*. 2007;130:1194–1205.
37. Wingerchuk DM, Lennon VA, Lucchinetti CF, et al. The spectrum of neuromyelitis optica. *Lancet Neurol*. 2007;6:805–815.
38. Wingerchuk DM, Lennon VA, Pittock SJ, et al. Revised diagnostic criteria for neuromyelitis optica. *Neurology*. 2006;66:1485–1489.
39. Hinson SR, Roemer SF, Lucchinetti CF, et al. Aquaporin-4-binding autoantibodies in patients with neuromyelitis optica impair glutamate transport by down-regulating eaat2. *J Exp Med*. 2008;205: 2473–2481.
40. Wisniewski HM, Bloom BR. Primary demyelination as a nonspecific consequence of a cell-mediated immune reaction. *J Exp Med*. 1975;141:346–359.
41. Matyszak MK, Perry VH. Delayed-type hypersensitivity lesions in the central nervous system are prevented by inhibitors of matrix metalloproteinases. *J Neuroimmunol*. 1996;69:141–149.
42. Newman TA, Woolley ST, Hughes PM, et al. T-cell- and macrophage-mediated axon damage in the absence of a cns-specific immune response: involvement of metalloproteinases. *Brain*. 2001;124:2203–2214.

43. Trapp BD, Stys PK. Virtual hypoxia and chronic necrosis of demyelinated axons in multiple sclerosis. *Lancet Neurol*. 2009;8:280–291.
44. Gay D, Esiri M. Blood-brain barrier damage in acute multiple sclerosis plaques. An immunocytological study. *Brain*. 1991;114:557–572.
45. Maeda A, Sobel RA. Matrix metalloproteinases in the normal human central nervous system, microglial nodules, and multiple sclerosis lesions. *J Neuropathol Exp Neurol*. 1996;55:300–309.
46. Anthony DC, Ferguson B, Matyzak MK, et al. Differential matrix metalloproteinase expression in cases of multiple sclerosis and stroke. *Neuropathol Appl Neurobiol*. 1997;23:406–415.
47. Lindberg RL, De Groot CJ, Montagne L, et al. The expression profile of matrix metalloproteinases (mmps) and their inhibitors (timps) in lesions and normal appearing white matter of multiple sclerosis. *Brain*. 2001;124:1743–1753.
48. Leppert D, Waubant E, Galardy R, et al. T cell gelatinases mediate basement membrane transmigration in vitro. *J Immunol*. 1995;154:4379–4389.
49. Stuve O, Dooley NP, Uhm JH, et al. Interferon beta-1b decreases the migration of T lymphocytes in vitro: effects on matrix metalloproteinase-9. *Ann Neurol*. 1996;40:853–863.
50. Waubant E, Goodkin DE, Gee L, et al. Serum mmp-9 and timp-1 levels are related to mri activity in relapsing multiple sclerosis [see comments]. *Neurology*. 1999;53:1397–1401.
51. Galboiz Y, Shapiro S, Lahat N, et al. Matrix metalloproteinases (mmps) and their tissue inhibitor (timps) as markers of disease subtype and response to interferon-beta therapy in relapsing and secondary progressive multiple sclerosis patients. *Ann Neurol*. 2001;50(4):443–451.
52. Rivers TM, Schwentker FF. Encephalomyelitis accompanied by myelin destruction experimentally produced in monkeys. *J Exp Med*. 1935;61:689–702.
53. Kabat EA, Wolf AP, Bezer AE. The rapid production of acute disseminated encephalomyelitis in rhesus monkeys by injection of heterologous and homologous brain tissue with adjuvants. *J Exp Med*. 1947;85:117–129.
54. Paterson PY. Experimental allergic encephalomyelitis: role of fibrin deposition in immunopathogenesis of inflammation in rats. *Fed Proc*. 1976;35:2428–2434.
55. Leibowitz S, Kennedy L. Cerebral vascular permeability and cellular infiltration in experimental allergic encephalomyelitis. *Immunology*. 1972;22:859–869.
56. Akassoglou K, Adams RA, Bauer J, et al. Fibrin depletion decreases inflammation and delays the onset of demyelination in a tumor necrosis factor transgenic mouse model for multiple sclerosis. *Proc Natl Acad Sci USA*. 2004;101:6698–6703.
57. Liedtke W, Cannella B, Mazzaccaro RJ, et al. Effective treatment of models of multiple sclerosis by matrix metalloproteinase inhibitors. *Ann Neurol*. 1998;44: 35–46.
58. Kieseier BC, Kiefer R, Clements JM, et al. Matrix metalloproteinase-9 and -7 are regulated in experimental autoimmune encephalomyelitis. *Brain*. 1998;121: 159–166.
59. Floris S, Blezer EL, Schreibelt G, et al. Blood-brain barrier permeability and monocyte infiltration in experimental allergic encephalomyelitis. *Brain*. 2004; 127:616–627.
60. Durelli L, Verdun E, Barbero P, et al. Every-other-day interferon beta-1b versus once-weekly interferon beta-1a for multiple sclerosis: results of a 2-year prospective randomised multicentre study (incomin). *Lancet*. 2002;359:1453–1460.
61. Koch-Henriksen N, Sorensen PS, Christensen T, et al. A randomized study of two interferon-beta treatments in relapsing-remitting multiple sclerosis. *Neurology*. 2006;66:1056–1060.
62. Kappos L, Traboulsee A, Constantinescu C, et al. Long-term subcutaneous interferon beta-1a therapy in patients with relapsing-remitting ms. *Neurology*. 2006;67:944–953.
63. Bertolotto A, Malucchi S, Sala A, et al. Differential effects of three interferon betas on neutralising antibodies in patients with multiple sclerosis: a follow-up study in an independent laboratory. *J Neurol Neurosurg Psychiatry*. 2002;73:148–153.
64. Teitelbaum D, Webb C, Meshorer A, et al. Protection against experimental allergic encephalomyelitis. *Nature*. 1972;240:564–566.
65. Cohen JA, Barkhof F, Comi G, et al. Oral fingolimod or intramuscular interferon for relapsing multiple sclerosis. *N Engl J Med*. 2010;362:402–415.
66. Goodin DS, Cohen BA, O'Connor P, et al. Assessment: the use of natalizumab (Tysabri) for the treatment of multiple sclerosis (an evidence-based review): report of the Therapeutics and Technology Assessment Subcommittee of the American Academy of Neurology. *Neurology*. 2008;71:766–773.
67. Kappos L, Bates D, Edan G, et al. Natalizumab treatment for multiple sclerosis: updated recommendations for patient selection and monitoring. *Lancet Neurol*. 2011;10:745–758.
68. Simpson JE, Fernando MS, Clark L, et al. White matter lesions in an unselected cohort of the elderly: astrocytic, microglial and oligodendrocyte precursor cell responses. *Neuropathol Appl Neurobiol*. 2007;33:410–419.
69. Fernando MS, Simpson JE, Matthews F, et al. White matter lesions in an unselected cohort of the elderly: molecular pathology suggests origin from chronic hypoperfusion injury. *Stroke*. 2006;37:1391–1398.
70. Teng H, Zhang ZG, Wang L, et al. Coupling of angiogenesis and neurogenesis in cultured endothelial cells and neural progenitor cells after stroke. *J Cereb Blood Flow Metab*. 2008;28:764–771.
71. Zhang S, Boyd J, Delaney K, et al. Rapid reversible changes in dendritic spine structure in vivo gated by the degree of ischemia. *J Neurosci*. 2005;25:5333–5338.
72. Szklarczyk A, Lapinska J, Rylski M, et al. Matrix metalloproteinase-9 undergoes expression and activation during dendritic remodeling in adult hippocampus. *J Neurosci*. 2002;22:920–930.
73. Wang L, Zhang ZG, Zhang RL, et al. Matrix metalloproteinase 2 (mmp2) and mmp9 secreted by erythropoietin-activated endothelial cells promote neural progenitor cell migration. *J Neurosci*. 2006;26: 5996–6003.
74. Kokovay E, Li L, Cunningham LA. Angiogenic recruitment of pericytes from bone marrow after stroke. *J Cereb Blood Flow Metab*. 2006;26:545–555.
75. Cramer SC. Brain repair after stroke. *N Engl J Med*. 2010;362:1827–1829.

76. Lennon VA, Wingerchuk DM, Kryzer TJ, et al. A serum autoantibody marker of neuromyelitis optica: distinction from multiple sclerosis. *Lancet*. 2004;364: 2106–2112.
77. Adams CW, Abdulla YH, Torres EM, et al. Periventricular lesions in multiple sclerosis: their perivenous origin and relationship to granular ependymitis. *Neuropathol Appl Neurobiol*. 1987;13(2): 141–152.
78. Lassmann H, Bruck W, Lucchinetti C. Heterogeneity of multiple sclerosis pathogenesis: implications for diagnosis and therapy. *Trends Mol Med*. 2001;7: 115–121.

Index

This page intentionally left blank

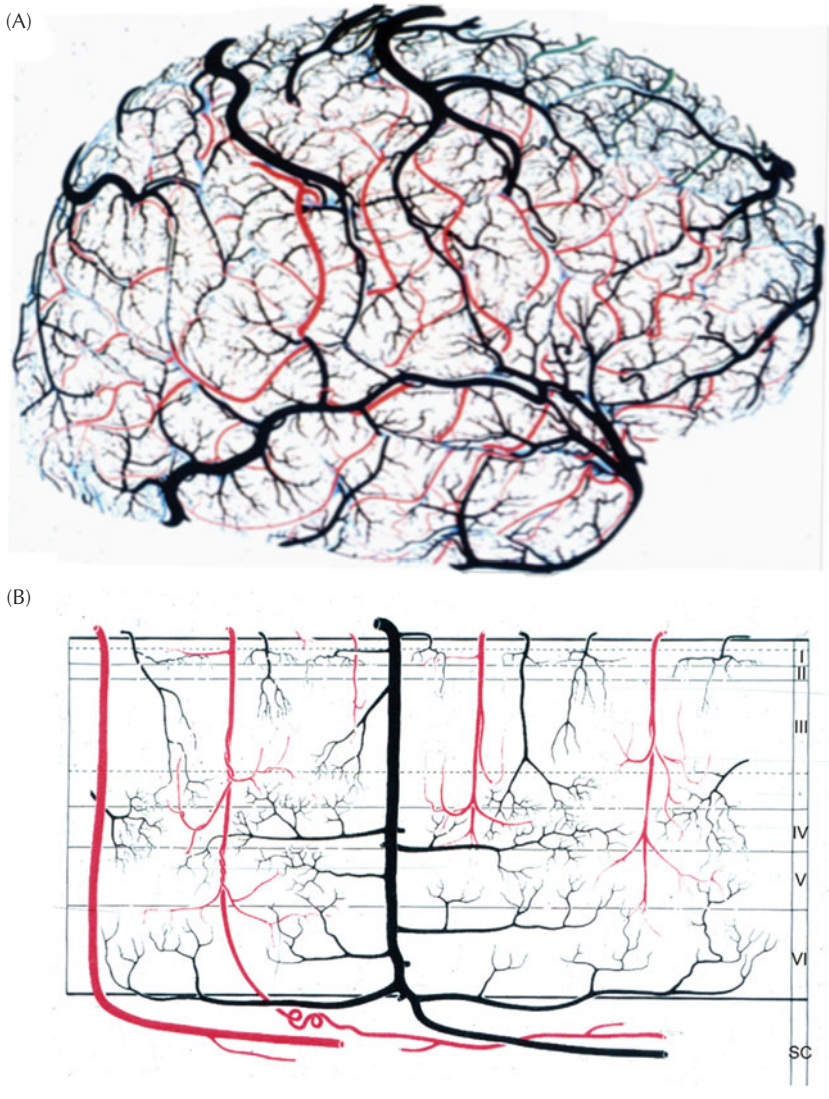

Figure 1–7. Blood vessels in the human brain. (**A**) Brain vasculature on the surface of the brain. Red plastic fills the arteries and blue plastic fills the veins. There are no anastomoses of the arteries and the veins since the arteries are end arteries. (**B**) This schematic drawing demonstrates that the arteries pass from the surface to the deep white matter, traversing the six layers of the cortex. Arterioles give off branches as the arteries pass through the cortex. The capillaries that join the arterioles and the veins are not seen. (From Ref. 31)

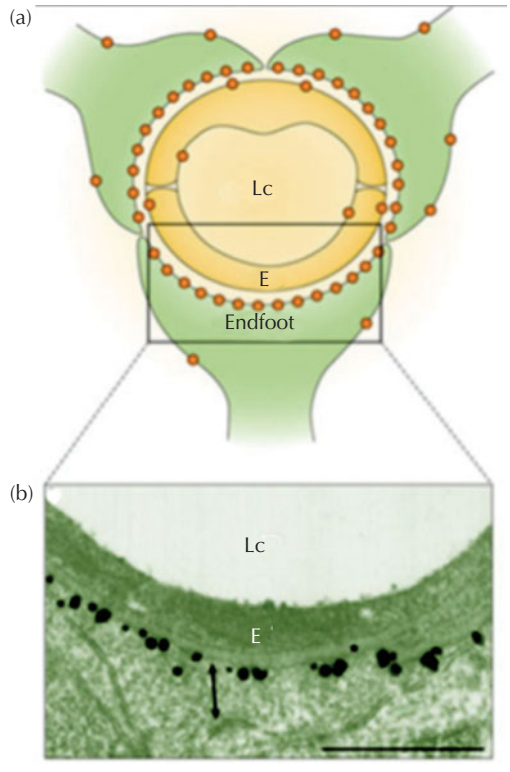

Figure 2–8. Drawing showing the expression pattern of AQP4 around brain microvessels. The concentration of AQP4 is high in the perivascular endfeet membrane domains that face the vessels and drops to low levels as soon as the membrane loses contact with the basal lamina. Endothelial cells express AQP4 at their adluminal as well as abluminal membranes but at much lower levels than the astrocytic endfeet. (**B**) An electron micrograph (corresponding to the box in (**A**) shows strong AQP4 immunogold labeling in the perivascular membrane of an astrocytic endfoot. (The endothelial AQP4 was not evident at this level of labeling sensitivity.) Asterisk, basal lamina; E, endothelium; Endfoot, astrocyte endfoot; Lc, capillary lumen. The arrow indicates the two membrane domains of the endfoot. Scale bar, 0.5 m. (From Ref. 83)

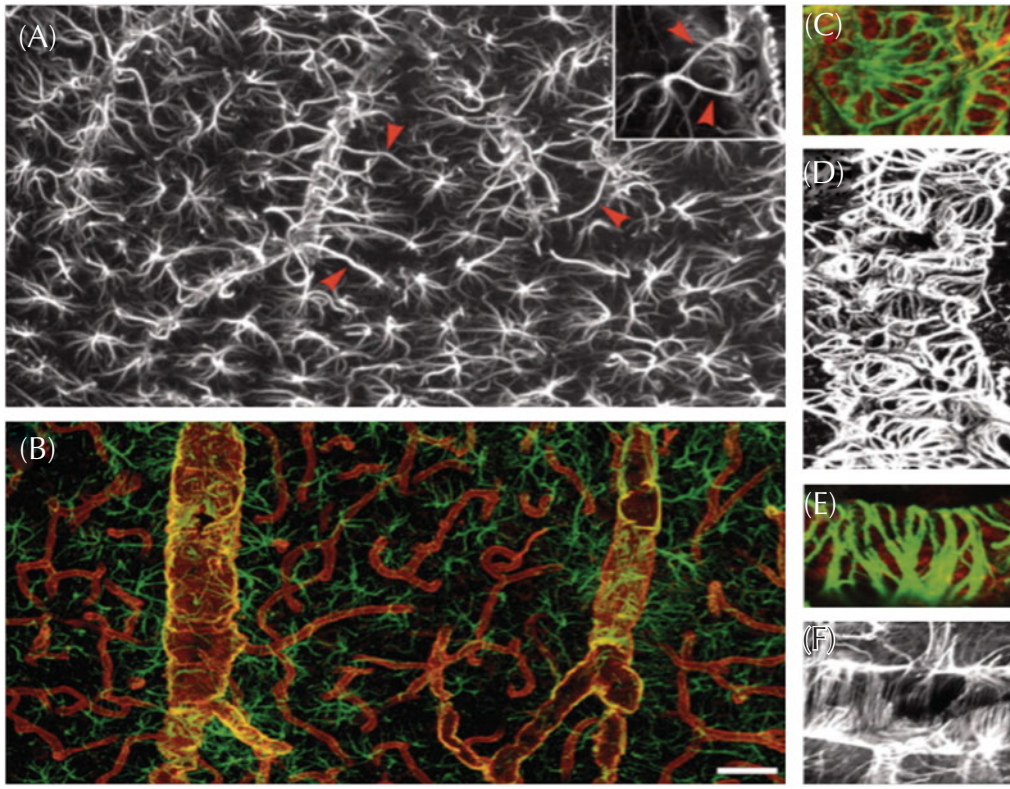

Figure 3–4. Not all vascular astrocytic endfoot processes are GFAP positive. (**A**) Glial fibrillary acidic protein immunolabeling of astrocytes in cortex. Individual astrocytes are star-shaped and distributed symmetrically, with minimal contact with neighboring astrocytes. Vascular processes differ from other processes by being straight, unbranched, and of wide diameter (arrowheads). The surfaces of large to medium-sized vessels were densely covered by GFAP-positive astrocytic endfeet. Inset: An astrocyte with two vascular processes. (**B**) Double immunolabeling of AQP-4 (red) and GFAP (green). Aquaporin-4 immunolabeling reveals that the entire network of vessels, including capillaries, is covered by astrocytic processes, albeit GFAP negative. Smaller vessels and capillaries are mostly GFAP negative but display intense labeling against the astrocyte-specific channel AQP-4. The AQP-4 labeling reveals continuous coverage by astrocytic endfeet. (**C–F**) Examples of the organization of GFAP in astrocytic endfeet around larger vessels. **C** and **D** display examples of wagon-wheel or rosette formation of GFAP filaments in the vascular endfeet, whereas **E** and **F** are examples on parallel arrays running perpendicular to the length of the vessel. C and E are double labeled against GFAP (green) and AQP-4 (red), whereas **D** and **F** are stained against GFAP only. Scale bar: inset, 40 μm; A, 10 μm; B, 60 μm; C, E, 5 μm; D, F, 30 μm. (From Ref. 51)

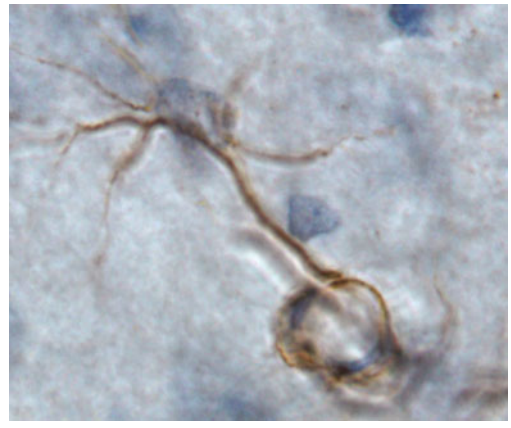

Figure 3–12. An astrocyte is shown that has been immunostained with MMP-2 (brown). The endfoot is seen encircling a small blood vessel. Relatively little immunostaining is seen in the cell body.

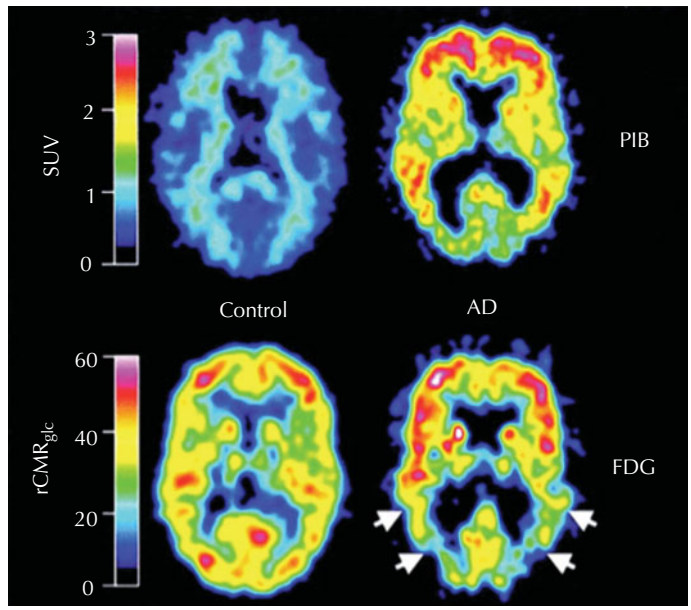

Figure 6–3. Pittsburgh Compound-B standardized uptake value (SUV) images demonstrate a marked difference between PIB retention in Alzheimer's disease (AD) patients and healthy control (HC) subjects. Positron emission tomography images of a 67-year-old HC subject (left) and a 79-year-old AD patient (AD6; mini-mental status examination (MMSE) = 21; right). Top: SUV PIB images summed over 40 to 60 minutes. Bottom: ^{18}Fluorodeoxyglucose regional cerebral metabolic rate for glucose(^{18}FDG rCMRglc) images (mol/min/100 mL). The left column shows lack of PIB retention throughout the gray matter of the HC subject (top left) and normal ^{18}FDG uptake (bottom left). Nonspecific PIB retention is seen in the white matter (top left). The right column shows high PIB retention in the frontal and temporoparietal cortices of the AD patient (top right) and a typical pattern of ^{18}FDG hypometabolism present in the temporoparietal cortex (arrows; bottom right) along with a preserved metabolic rate in the frontal cortex. The PIB and ^{18}FDG scans were obtained within 3 days of each other. (From Ref. 15)

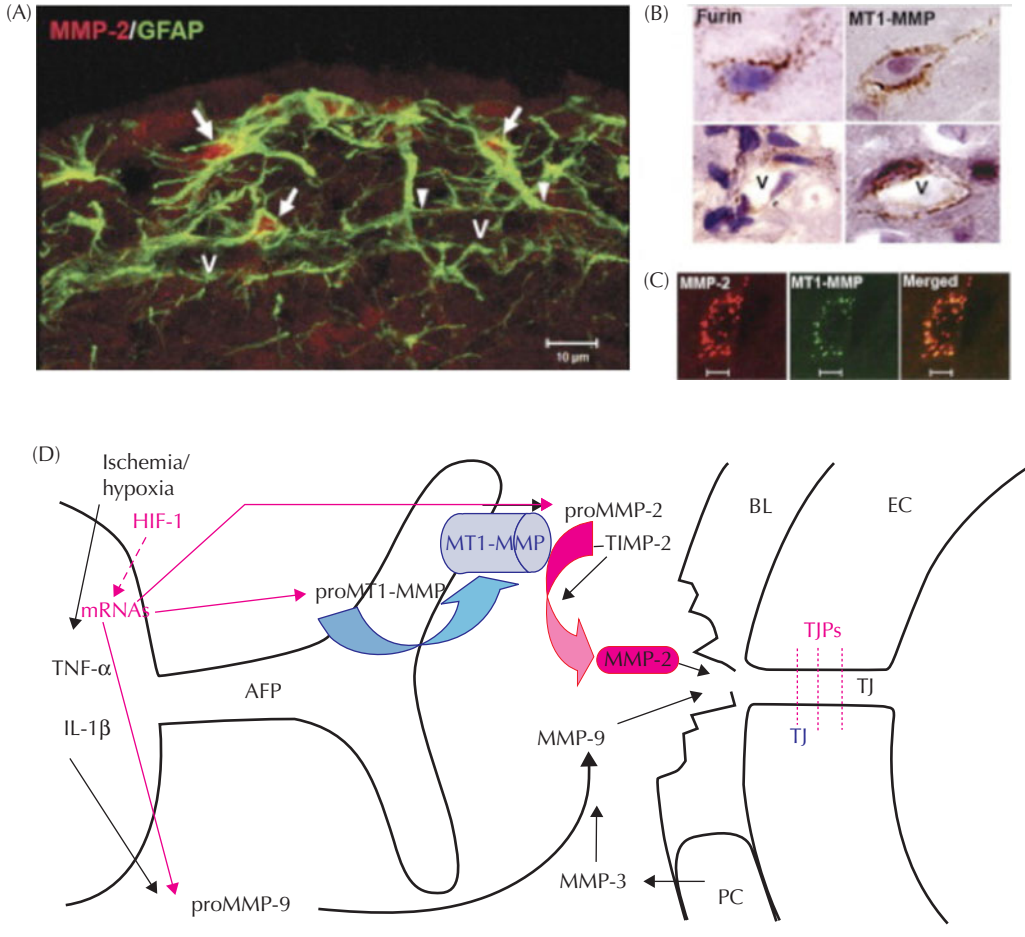

Figure 7–11. (**A**) Confocal immunohistochemistry shows GFAP-positive astrocytes around a vessel (V) that express MMP-2 (arrows) in intact rat brain tissue. The arrowheads indicate the astrocyte endfeet around the vessel. (**B**) Expression of furin and MT1-MMP in brain cells and around vessels (V). (**C**) Confocal images show the colocalization of MMP-2 and MT1-MMP immunohistochemistry in brain cells. (**D**) Schematic drawing showing that the activation of MMP-2 occurs through the action of the trimolecular complex during the early opening of the BBB in 3 hours of reperfusion after 90 minutes of MCAO. In the astrocytic foot processes (AFP), MT1-MMP joins with TIMP-2 to activate proMMP-2 in a spatially constrained manner close to the basal lamina (BL). In the BL are the pericytes (PC). The endothelial cells (ECs) have tight junctions (TJ). The activated MMP-2 has direct access to the portion of the BL beneath the AFP, and components of the BL are degraded. The manner in which this disruption of the BL leads to increased permeability is unclear since the role of the BL in maintaining the integrity of the blood vessel is uncertain. (From Ref. 96)

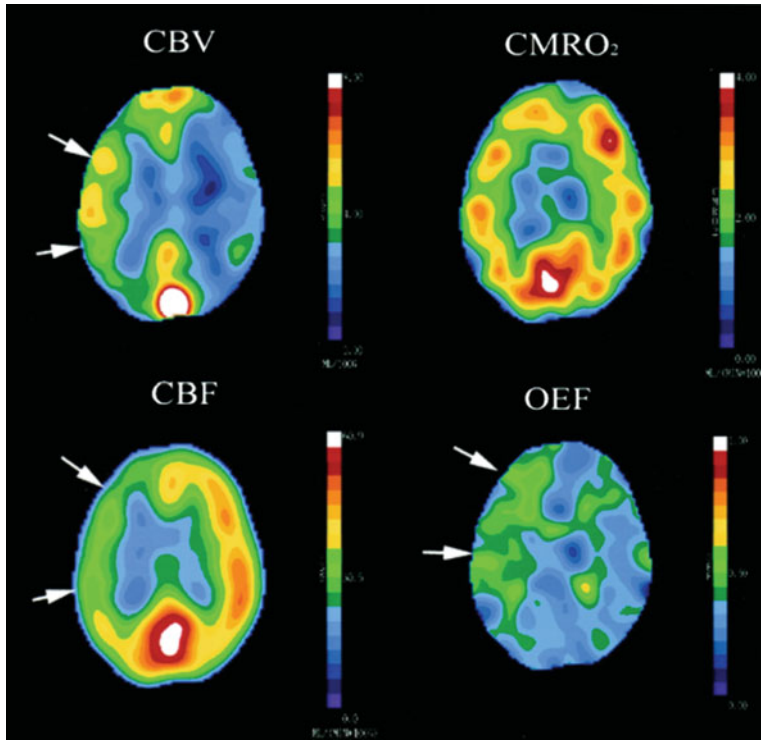

Figure 7–13. Stage 2 haemodynamic failure. Increased CBV indicates autoregulatory vasodilation (CBV, arrows). This is insufficient to maintain flow, however, and flow falls (CBF, arrows). In this situation, the brain can increase the fraction of oxygen extracted from the blood (OEF, arrows) in order to maintain normal oxygen metabolism ($CMRO_2$) and brain function. (From Ref. 90)

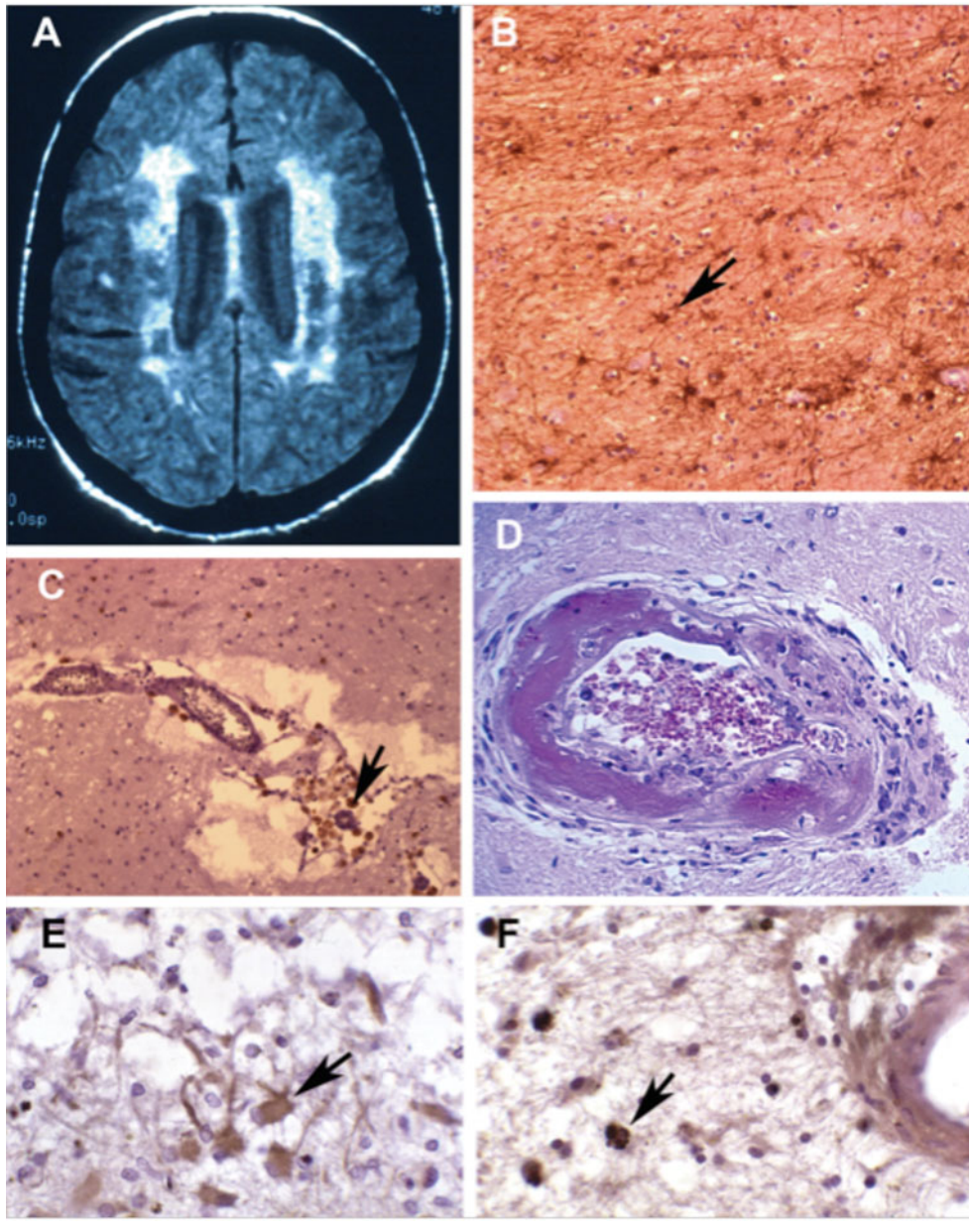

Figure 8–10. An MRI scan and pathological material from a BD patient with the small vessel hypertensive disease. (**A**) An MRI scan demonstrating the extensive white matter lesions seen in the periventricular region. The scan was made with a fluid attenuated inversion recovery scan (FLAIR) that suppresses water in the CSF space (black) and reveals the water in the tissue. (**B**) White matter shows gliosis with loss of myelin and oligodendrocytes. The arrow shows an astrocyte immunostained with glial fibrillary acidic protein, which is a marker for reactive astrocytes. (**C**) A fibrotic blood vessel surrounded by inflammatory macrophages. The arrow indicates a macrophage. (**D**) A blood vessel exposed to long-term hypertension showing damage to the wall and eosinophilic deposits. (**E**) Matrix metalloproteinase-2 in reactive astrocytes (arrow). (**F**) An MMP-3-positive macrophage around a fibrotic blood vessel in a white matter demyelinated region (arrow). (From Ref. 46)

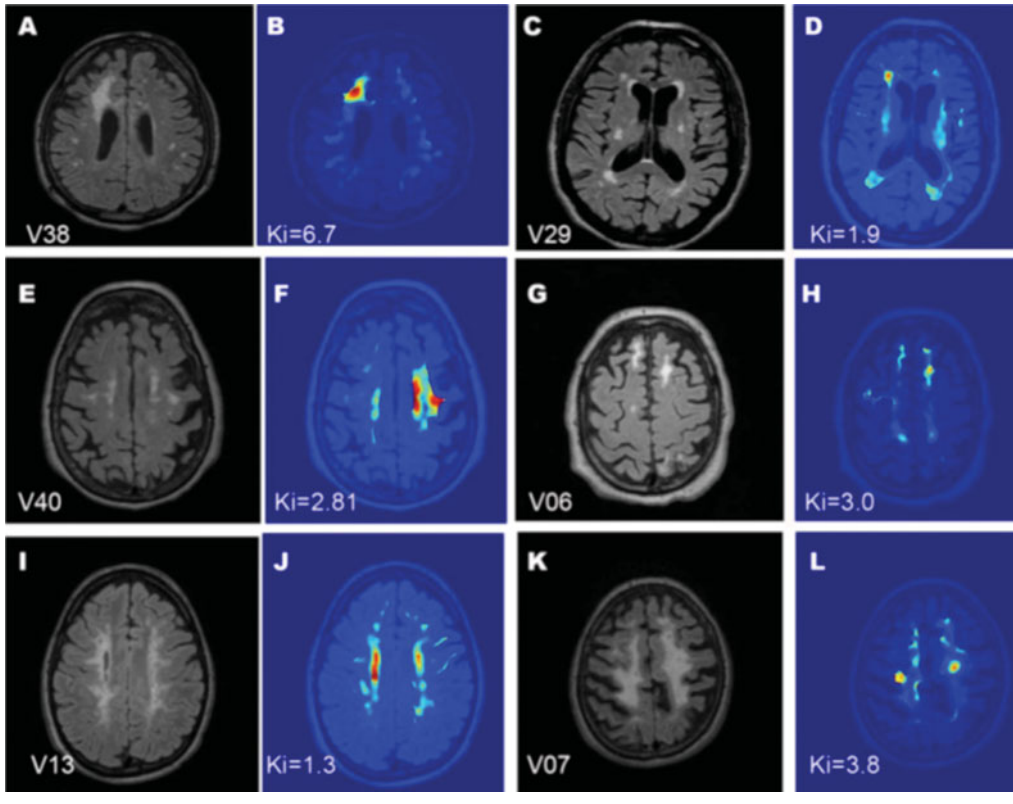

Figure 8–11. Representative FLAIR and permeability images of the brains of six VCI patients with increased permeability. (**A,B**) Permeability and FLAIR maps. The WMHs are in the frontal white matter of the centrum semiovale, without involvement of the cortex. The corresponding permeability map in B has regions of moderately increased permeability (light blue) and high permeability (red). (**C-D, E-F, G-H, I-J, K-L**) Other pairs of FLAIR and related permeability images showing regions of increased permeability. (From Ref. 53)

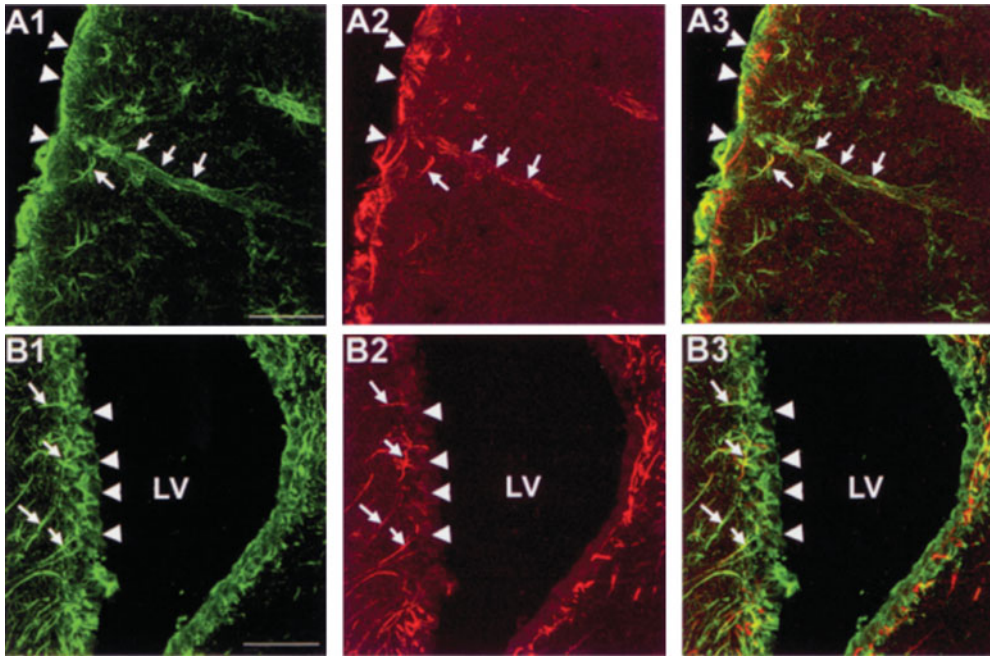

Figure 10–5. Confocal pictures of anti-GFAP (glial fibrillary acidic protein) and anti-AQP9 in two mouse brain regions: parietal cortex (**A1, A2, A3**) and lateral septum (**B1, B2, B3**). (**A1–A3**) Confocal pictures of anti-GFAP labeling (green, **A1**) and anti-AQP9 labeling (red, **A2**) and superposition of both forms of labeling (**A3**) in parietal cortex. Arrowheads and arrows indicate colocalization between anti-GFAP (A1) and anti-AQP9 (**A2**) on glia limitans (arrowheads) and on astrocytes in parietal cortex (arrows). This colocalization is yellow on the superposed picture (**A3**), suggesting that AQP9 is present on glia limitans (arrowheads) and on astrocytes in cortex (arrows). (**B1–B3**) The double labeling between anti-GFAP (green, **B1**) and anti-AQP9 (red, B2) and the superposition of both forms of labeling (B3) show the presence of AQP9 in the lateral septum. Arrows indicate colocalization between anti-GFAP (**B1**) and anti-AQP9 (**B2**), suggesting the presence of AQP9 on astrocytes in septum. Arrowheads indicate the ependymal cells of the lateral ventricle (LV), which are not labeled by anti-AQP9. This result suggests that AQP9 is not expressed by ependymal cells in mouse brain. (From Ref. 11)

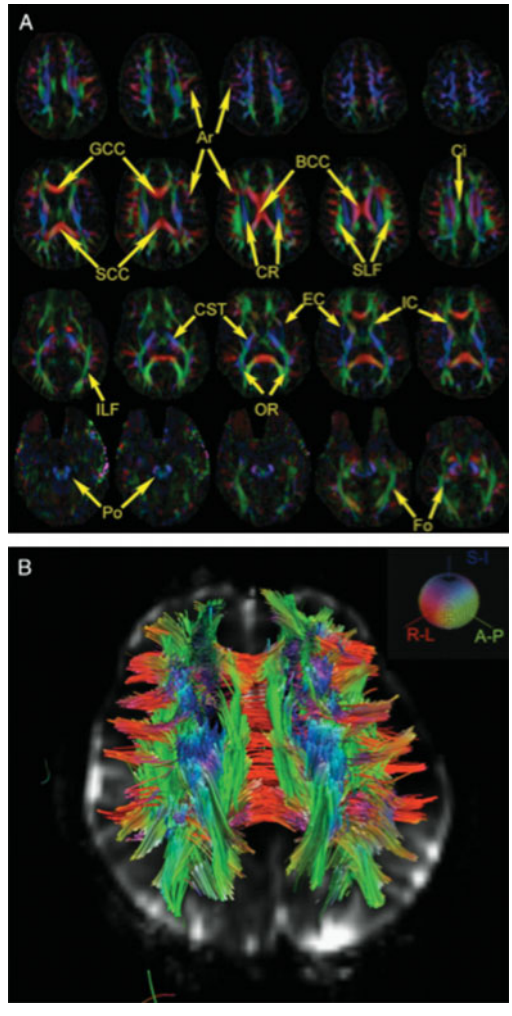

Figure 10–8. This multislice (EPI-DTI) color map comes from a healthy volunteer at 7 T following a field map dewarping processing. (**A**) Fiber bundles are visualized, including the pons (Po), forceps (Fo), optic radiation (OR), genu, splenum and body of the corpus callosum (GCC/SCC/BCC), corticospinal tract (CST), internal and external capsules (IC/EC), corona radiata (CR), cingulum bundle (Ci), inferior and superior longitudinal fasciculi (ILF/SLF), and arcuate fibers (Ar). Some fiber groups in lateral subcortical regions are less conspicuous, perhaps due to lower coil sensitivity. (**B**) Tractography results in the midbrain region of this acquisition, highlighting many of the same fiber bundles in three dimensions. (From Ref. 46)

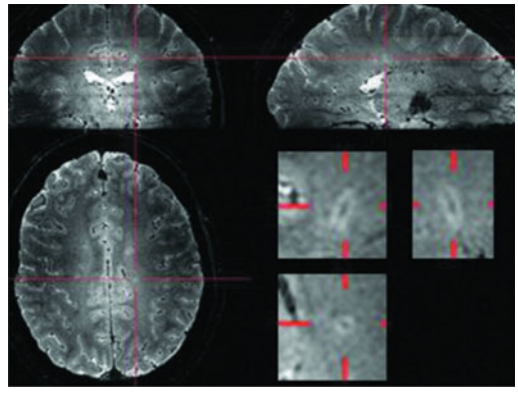

Figure 12–3. The 7 T T2*-weighted images were viewed in orthogonal planes. For each lesion, the presence or absence of a central vein was noted. Veins were counted if they (1) could be visualized in at least two perpendicular planes, (2) appeared linear in at least one plane, and (3) were completely surrounded by hyperintense signal in at least one plane (to avoid the inclusion of adjacent rather than central veins). Lesions were classified as perivenous if they contained one or more central veins. The proportion of perivenous lesions in patients with MS (mean 80%, range 53%–100%) was consistently much higher than in subjects without MS (mean 16%, range 0%–34%). The perivenous lesion appearance was equally common in patients with clinically isolated syndrome, relapsing-remitting MS, primary progressive MS, and secondary progressive MS. (From Ref. 7)

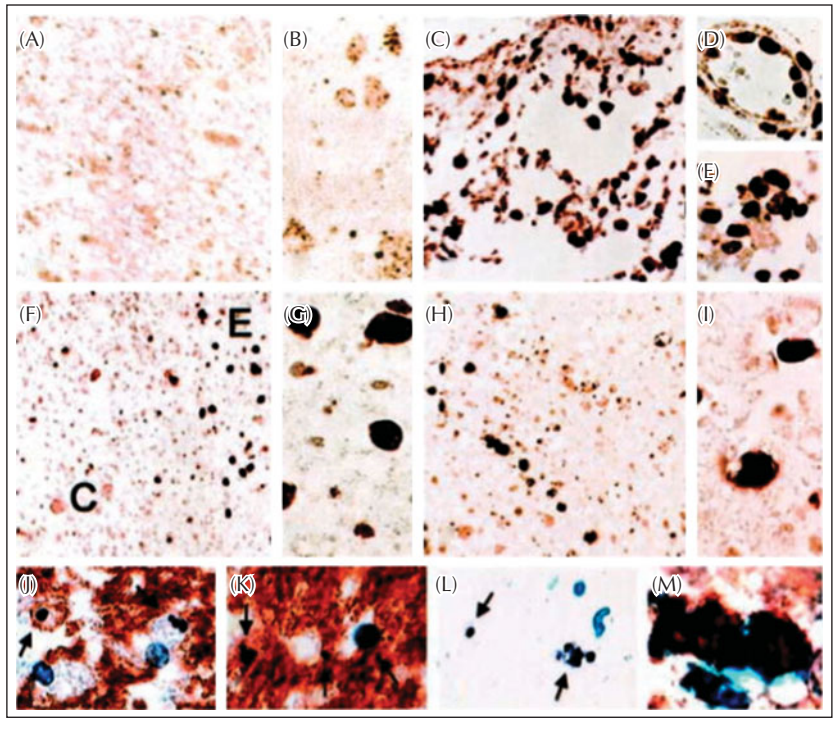

Figure 12–8. Immunocytochemical detection of HIF-lα in brain lesions. (**A,B**) White matter of the control brain showing some immunoreactivity in lipofuscin granules but absence of staining of nuclei. (**C–E**) Acute ischemic lesion of a stroke patient showing abundant expression of HIF-lα in nearly all cell nuclei, including glia cells, macrophages, and endothelial cells. (**F,G**) Active MS lesion with MAG loss showing a high density of nuclei with HIF-lα expression at the active plaque edge (**EI; C**): inactive plaque center. (**H,I**) Active lesion in a case of cytomegalovirus encephalitis with MAG loss with profound expression of HIF-lα in cell nuclei. (**J–M**) White matter, acute ischemic lesion of a stroke patient. (**J,K**) Immunocytochemistry for MOG and nuclear counterstaining with hematoxylin shows numerous oligodendrocytes with condensation of chromatin and nuclear fragmentation (arrows). (**I**) Cells with nuclear condensation and fragmentation in the lesions are stained by in situ end labeling for visualization of DNA fragmentation (arrows). (**M**) Double labeling of an oligodendrocyte in the infarct edge with HIF-lα (brown) and 2',3'-cyclic nucleotidase 3'-phosphodiesterase (CNPase; blue). Magnifications: **A**, ×11160; **B**, ×790; **C**, ×388; **D**, e, **G**, **J-I**, ×990; **F**, ×246; **H**, ×308; **M**, ×1800. (From Ref. 9)